



**Rocketdyne Division**  
**Rockwell International**

6633 Canoga Avenue  
Canoga Park, California 91304

R-9049

LINEAR TEST BED  
FINAL REPORT  
VOLUME II: TEST BED NO. 2

27 March 1974

Contract NAS8-25156

**PREPARED BY**

Rocketdyne Engineering  
Canoga Park, California

**APPROVED BY**

*J. R. Johnson*  
R. Johnson  
Program Manager  
Saturn Engines

(NASA-CR-120183) LINEAR TEST BED.  
VOLUME 2: TEST BED NO. 2 Final Report  
(Rocketdyne) 208 p HC \$13.50 CSCL 14B

N74-19893

G3/11 Unclas  
34958



Frontispiece. Test Bed No. 2 in Mainstage

R-9049

iii/iv

ENDING PAGE BLANK NOT REPRODUCED

CONTENTS

Introduction . . . . .	1
Summary . . . . .	3
Concept Selection . . . . .	9
Design and Fabrication . . . . .	15
Thrust Frame . . . . .	16
Combustor . . . . .	18
Nozzle . . . . .	22
Turbine Exhaust Manifold . . . . .	25
Thrust Chamber Assembly . . . . .	31
Flexible Ducting . . . . .	33
Combustion Wave Ignition System . . . . .	37
Electrical Control System . . . . .	37
Purge and Drain System . . . . .	47
Facility Modifications - Delta-2B, SSFL . . . . .	49
Test Bed Installation and Checkout . . . . .	51
System Operation and Performance . . . . .	53
Test Summary . . . . .	53
Engine Start . . . . .	53
Engine Cutoff . . . . .	67
Ignition System Operation . . . . .	81
Ignition Detection System . . . . .	84
Mainstage Performance . . . . .	84
Thrust Chamber Performance . . . . .	84
Secondary Flow Effects . . . . .	83
Base Pressure Trends . . . . .	96
Thrust Vector Control Studies . . . . .	99
Dynamic Hinging . . . . .	99
Static Hinging . . . . .	99
Thrust Chamber Hardware Durability . . . . .	117
Nozzle Durability . . . . .	117
End Fence Durability . . . . .	118

Turbine Exhaust Manifold and Hot-Gas Seal Durability . . . . . 118  
Combustor Durability . . . . . 121  
References . . . . . 129  
Appendix A  
Breadboard Thrust Chamber Test Bed Thrust Vector Control Study . . . . . A-1

## ILLUSTRATIONS

Frontispiece. Test Bed No. 2 in Mainstage . . . . .	iii
1. Advanced Breadboard Concepts Incorporating Thrust Vector Control . . . . .	4
2. General Arrangement, End View . . . . .	5
3. General Arrangement, Top View . . . . .	6
4. Test Bed No. 2 Installed in the Delta-2B Test Facility . . . . .	13
5. Linear Engine Test Bed No. 2 Schematic . . . . .	14
6. Test Bed No. 2 - Thrust Chamber Segment Igniter Port Design . . . . .	19
7. Test Bed No. 2 - Thrust Chamber Segment Primary and Secondary Copper Plating, Interior Nickel Plating . . . . .	20
8. Backup Machined Liner Segment Design . . . . .	23
9. Test Bed No. 2 Thrust Chamber Added Nozzle, H <sub>2</sub> Collection, and Dump Manifold . . . . .	26
10. Turbine Exhaust Manifold, Test Bed No. 2 . . . . .	27
11. Test Bed No. 2 Thrust Chamber Tested Positions of Nozzle Banks . . . . .	32
12. Flexible Ducting Configuration . . . . .	34
13. Internal Configuration of the Hot-Gas Bypass Bellows Assembly . . . . .	35
14. LOX/Fuel Pump Discharge Flex Joint . . . . .	36
15. Turbine Exhaust Flex Joint . . . . .	38
16. Test Bed No. 2 Triaxial Combustion Wave Ignition System . . . . .	39
17. Triaxial Combustion Wave Element . . . . .	40
18. Test Bed No. 2 Combustion Wave Manifolding and Valve Arrangement . . . . .	41
19. Test Bed No. 2 Premixed With Miniaturized Spark System . . . . .	42
20. Combustion Wave Ignition System Spark Igniter Unit . . . . .	43
21. Test Bed No. 2 Start Sequence . . . . .	45
22. Test Bed No. 2 Cutoff Sequence . . . . .	46
23. Start Model Chamber Pressure . . . . .	61
24. Start Model Thrust Chamber Mixture Ratio. . . . .	62
25. Start Model Fuel Turbopump H vs Q . . . . .	63
26. Start Model Pump Discharge Pressures . . . . .	64

27.	Start Model Fuel Injection and Chamber Gas-Side Wall Temperatures . . . . .	65
28.	Linear Test Bed No. 2 Start Sequence, Combustion Wave Ignition System . . . . .	66
29.	Main Thrust vs Time . . . . .	68
30.	Chamber Pressure vs Time . . . . .	69
31.	Fuel Turbine Inlet Pressure vs Time . . . . .	70
32.	Fuel Turbine Inlet Temperature vs Time . . . . .	71
33.	Cutoff Model Chamber Pressure and Fuel Turbine Inlet Pressure vs Time . . . . .	73
34.	Cutoff Model Mixture Ratio vs Time . . . . .	74
35.	Cutoff Model Fuel Pump Flow Coefficient vs Time . . . . .	75
36.	Linear Test Bed Program, No. 2 Test Bed Cutoff Sequence . . . . .	76
37.	No. 2 Test Bed Cutoff, Main Thrust vs Time . . . . .	77
38.	No. 2 Test Bed Cutoff, Typical Chamber Pressure vs Time . . . . .	78
39.	No. 2 Test Bed Cutoff, Turbine Inlet Pressure vs Time . . . . .	79
40.	No. 2 Test Bed Cutoff, Typical Fuel Injection Temperature . . . . .	80
41.	Test Bed No. 2 Low-Power Level Start Sequence . . . . .	82
42.	Linear Engine Test Bed No. 1, $W/P_c$ vs Accumulated Run Time . . . . .	89
43.	Linear Engine Test Bed No. 1, Characteristic Velocity Efficiency vs Mixture Ratio . . . . .	91
44.	Linear Engine Test Bed No. 1 and 2, $\eta_{c^*}$ vs MR . . . . .	92
45.	Linear Engine Site Performance Parameters . . . . .	94
46.	Linear Engine Test Beds, Secondary Flow Effect . . . . .	95
47.	Linear Engine Average Base Pressures . . . . .	97
48.	Test Bed No. 2 Dynamic Hinging Gimbal Actuator . . . . .	100
49.	Test Bed No. 2 Dynamic Hinging at $\pm 16$ Degrees . . . . .	101
50.	Linear Engine Test Bed No. 2 Stating Hinging Tests, $F/P_c$ vs $P_c/P_a$ . . . . .	103
51.	Equations for Calculation of Linear Thrust Chamber Resultant Force Angle . . . . .	105

52.	+17½°, -5° Static Hinging Configuration, Test Bed No. 2 . . . . .	106
53.	Equation for Calculation of Linear Engine Equivalent Gimbal Angle . . . . .	107
54.	Linear Engine Test Bed No. 2 Static Hinging Tests ( $F/P_c$ vs $P_c/P_a$ ) . . . . .	108
55.	Test Bed No. 2 Engine Thrust vs Chamber Pressure . . . . .	115
56.	Test Bed No. 2 Thrust Vector Analysis . . . . .	116
57.	Posttest Condition of Turbine Exhaust Manifold Base, Test Bed No. 2 . . . . .	119
58.	Posttest Condition of Turbine Exhaust Manifold Inlet, Test Bed No. 2 . . . . .	120
59.	Test Bed No. 2 Chamber Conditions vs Accumulated Duration . . . . .	123
60.	Test Bed No. 2 Thrust Chamber Estimated Average Peak Wall Temperature vs Accumulated Duration . . . . .	124
61.	Test Bed No. 2 Thrust Chamber Heat Flux Parameter vs Accumulated Duration . . . . .	125
62.	Test Bed No. 2 Thrust Chamber Calculated Segment Mixture Ratio vs Accumulated Erosion Severity . . . . .	127

TABLES

1. Summary of Test Bed No. 2 Combustor H <sub>2</sub> Embrittlement Protection . . . . .	21
2. Purge Systems Sequence of Operation . . . . .	48
3. Linear Test Bed Program, Test Bed No. 2 Test Summary, Ignition and Start . . . . .	54
4. Combustion Wave Igniter Mixture Ratios and Flows . . . . .	83
5. Linear Test Bed No. 2 Mainstage Performance . . . . .	85
6. Test and Calculated Data for Linear Engine . . . . .	109
7. Linear Test Bed No. 2 Thrust Vector Data . . . . .	110
8. Thrust Vector Control Data . . . . .	115

## INTRODUCTION

The Linear Test Bed program objectives were to design, fabricate, and evaluation test advanced aerospike test beds that employ the segmented combustor concept. The program started in April 1970 with the release of a work statement by NASA, and was finished in October 1973 with the successful completion of 29 tests on test bed No. 2.

Test bed No. 1 explored the feasibility of the segmented combustor concept. The control system, ignition system, basic sequencing, and operating procedures were developed and system performance and durability were demonstrated on test bed No. 1. Advanced thrust vector control concepts, thrust vector optimization techniques were developed and demonstrated on test bed No. 2.

This report (Volume II) describes the complete program conducted on test bed No. 2 including concept selection, design analysis, design, fabrication, and testing of test bed No. 2.

## SUMMARY

Test bed No. 2 consists of 10 combustors welded in banks of 5 to 2 symmetrical tubular nozzle assemblies, an upper stationary thrust frame, a lower thrust frame which can be hinged, a power package, a triaxial combustion wave ignition system, a pneumatic control system, pneumatically actuated propellant valves, a purge and drain system, and an electrical control system. An isometric drawing and two views of the general arrangement of test bed No. 2 are shown in Fig. 1 through 3. The power package consists of the Mark 29-F fuel turbopump, the Mark 29-0 oxidizer turbopump, a gas generator assembly, and propellant ducting.

The system, designated as a linear aerospike system, was designed to demonstrate the feasibility of the concept and to explore technology related to thrust vector control, thrust vector optimization, improved sequencing and control, and advanced ignition systems.

The propellants are liquid oxygen/liquid hydrogen. The system was designed to operate at 1200-psia chamber pressure at an engine mixture ratio of 5.5. With 10 combustors, the sea level thrust is 95,000 pounds.

The thrust chamber assembly consists of 10 combustors, 2 nozzle assemblies, a turbine exhaust base manifold, and the supporting rib structure and tie linkages. The combustors are made from precision investment case NARloy (silver-copper alloy) with the combustor coolant channels cast into the lines. Nickel is electrodeposited to the outside of the liner to provide coolant channel closeout and for structural purposes. Aluminum backup structures are then bolted to each side of the combustor to provide the structural support required for hot firing. The nozzles are bounded at each end by water-cooled fences 9 inches high. The fences are provided to contain the expanding combustion gases, to direct all gas flow downward, and prevent gas spillage over the side of the nozzle.

The upper and lower thrust frames are welded tubular structures designed to support the thrust chamber and power package and to transmit thrust through the hinge axis and, from there, into the test stand structure.

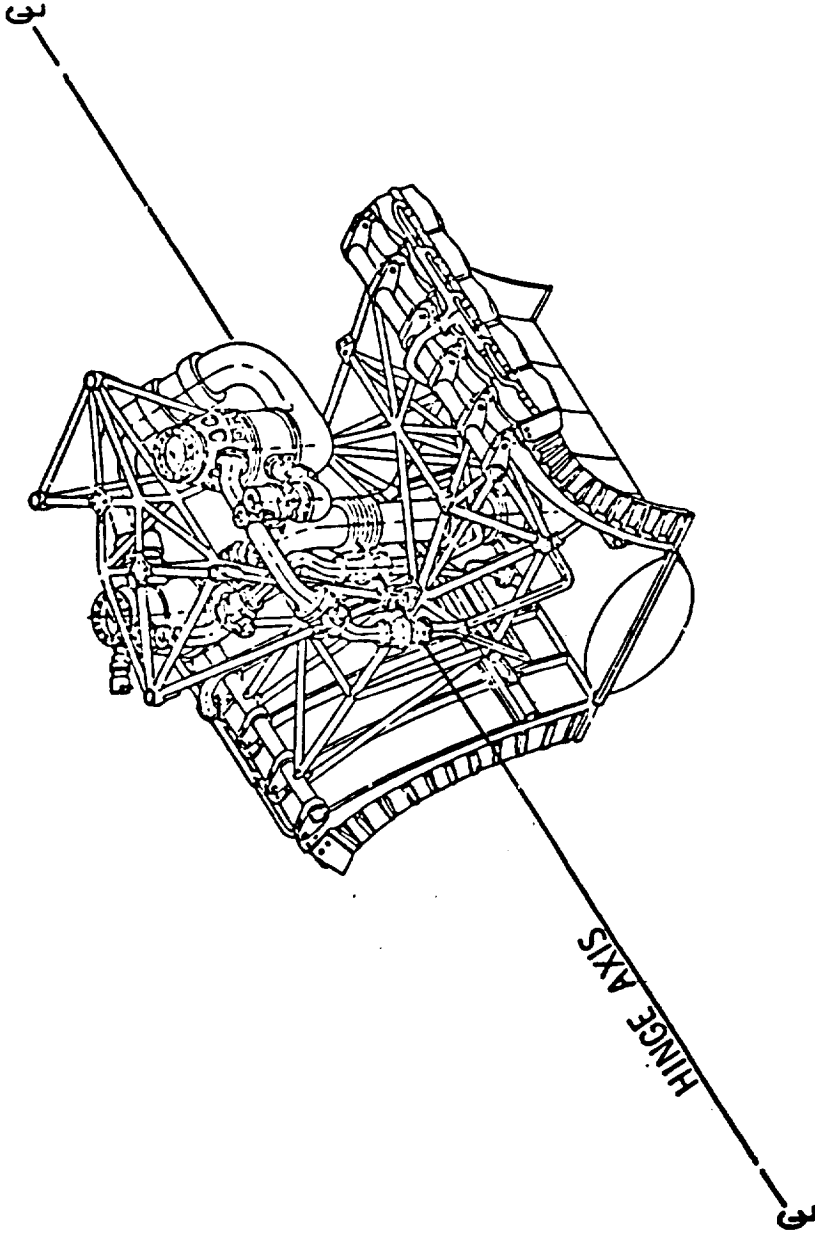


Figure 1. Advanced Breadboard Concepts Incorporating Thrust Vector Control (Test Bed No. 2)

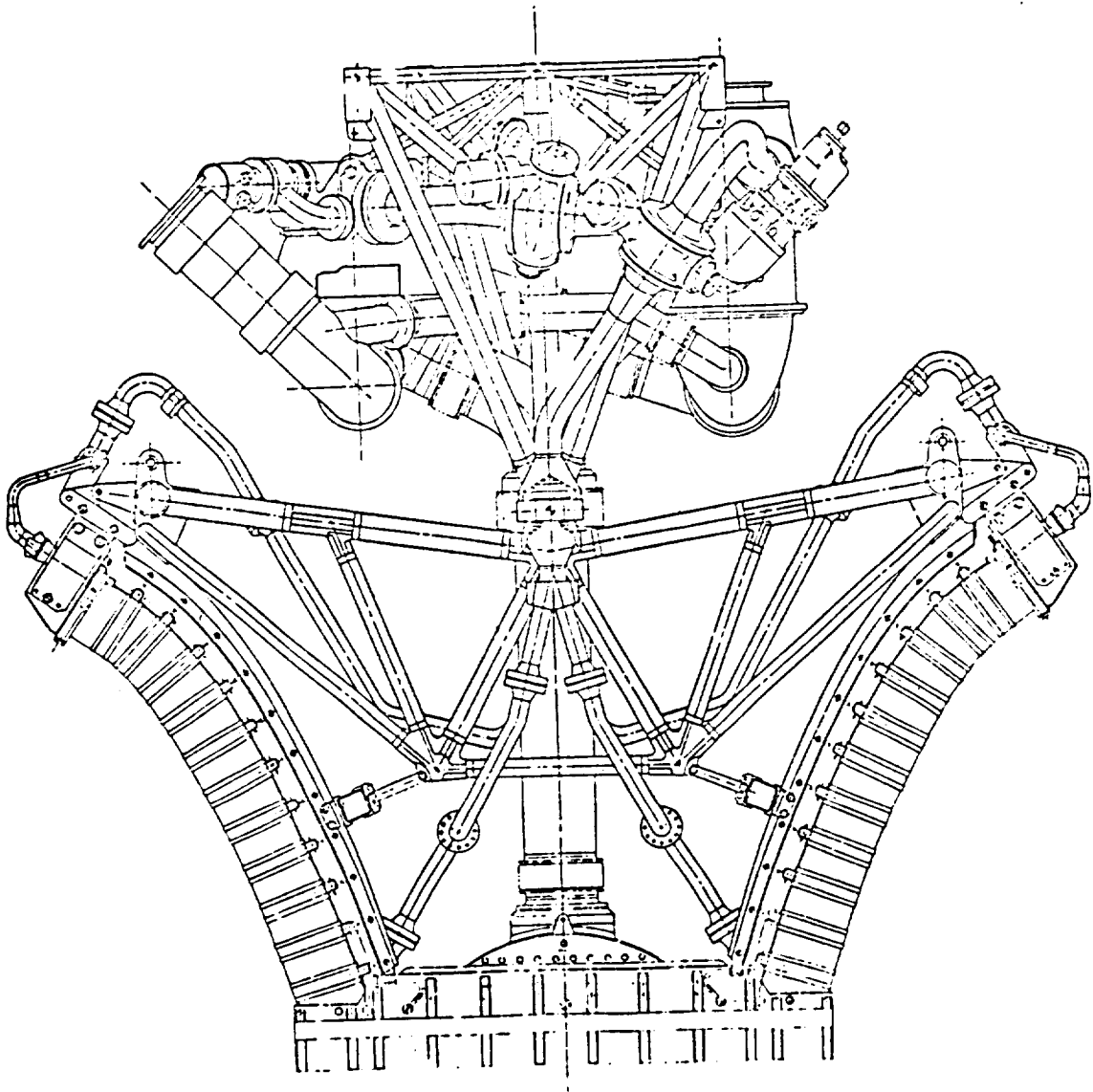


Figure 2. General Arrangement, End View

R-9049

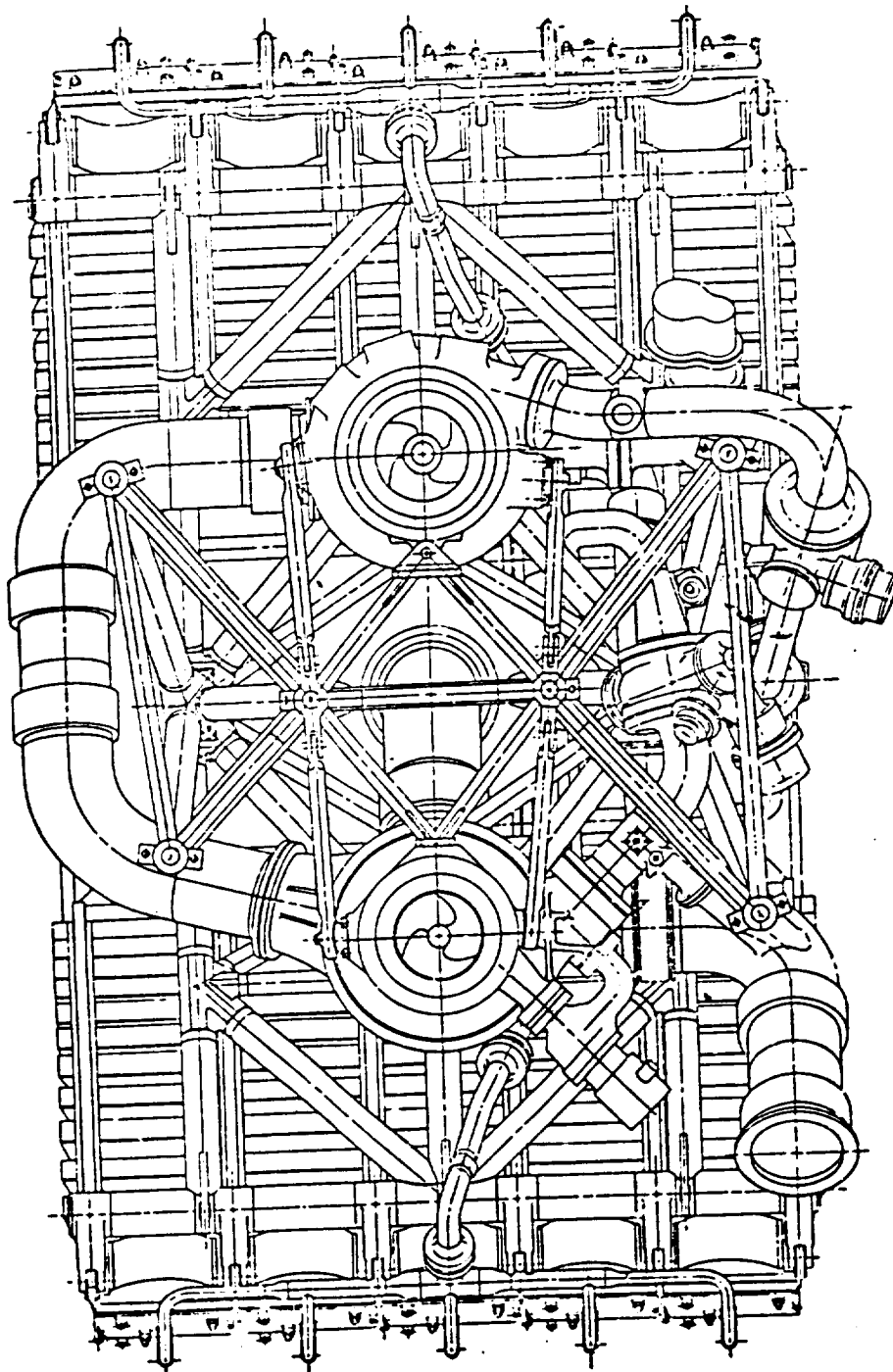


Figure 3. General Arrangement, Top View

R-9040

The objectives of the program on test bed No. 2 were as follows:

- Continue the development of the linear aerospike concept, develop better understanding of system operation, and develop the required operational sequences and control logic for a workable system.
- Develop alternate fabrication technology for the combustors, nozzles, base manifold, and thrust chamber assembly.
- Evaluate alternate materials in the combustors such as nickel coating of the combustor hot-gas inner wall.
- Evaluate thrust vector control techniques by dynamic hinging of the thrust chamber assembly through  $\pm 16$  degree excursions.
- Evaluate methods of independent control of the nozzle sides for advanced vehicle attitude control techniques.
- Evaluate methods of thrust optimization at sea level by independent hinging of the nozzle sides. By this technique, determine the nozzle angle required for optimum sea level thrust.
- Evaluate the effect on performance and base pressure by varying the percent base flow.
- Evaluate alternate ignition schemes. For test bed No. 2, the ignition system employed was the triaxial combustion wave ignition system.
- Evaluate high pressure flexible ducting designed for  $\pm 18$  degree gimbals angles.

All program objectives were achieved. Some of the significant accomplishments of the program are as follows:

- Start, mainstage operation, and shutdown of test bed No. 2 were satisfactory. The use of an oxidizer manifold controlled sequence purge, coupled

R-9049

with a post-cutoff turbopump spin, resulted in low thrust chamber mixture ratios throughout cutoff with a corresponding reduction in maximum temperatures and exposure to an oxidizing atmosphere.

- Several different techniques were employed in fabricating the combustors. These were successful and no combustor problems were encountered that resulted from fabrication experiments.
- The test bed was tested 29 times for 1199.5 seconds total accumulated duration. Tests were conducted over a chamber pressure range from 680 to 1200 psia and mixture ratios from 3.1 to 5.7. The program was highlighted by test 624-006 which was run for 300 seconds mainstage duration.
- Five cycles of dynamic hinging at  $\pm 12$  degrees and 20 cycles at  $\pm 16$  degrees were successfully demonstrated.
- Independent side hinging at static nozzle positions of  $(+7^\circ, +7^\circ)$  and  $(+17\frac{1}{2}^\circ, -5^\circ)$  were successfully demonstrated. The predicted sea level nozzle thrust vector, 14 degrees offset from the vertical, was experimentally verified.
- The secondary base flow was varied from 1 to 3 percent. The sea level base pressure was found to be independent of the percent secondary flow.
- The triaxial combustion wave ignition system operated satisfactorily and achieved 100-percent ignition reliability.
- The high-pressure flexible ducting functioned satisfactorily without failure.

## CONCEPT SELECTION

At the onset of the Linear Test Bed program, conceptual studies were conducted to determine the size, configuration, power cycle, ignition system, control system, and general arrangement of test bed No. 1. The ground rules were to use existing components where possible, to use the combustor design that evolved from the Cast Segment Evaluation (CSE) program, and to conduct a meaningful advanced experimental aerospike program within the imposed budget and time constraints.

J-2S Mark 29-F and Mark 29-0 turbopumps, main propellant valves, and pneumatic control packages were available and it was decided these would be used. Slave gas generators used for Mark 29-F component tests were also available. The combustors were designed for operation at 1200 psia chamber pressure and 6.0 mixture ratio.

Match-fit analysis between the turbomachinery, gas generator, and thrust chamber revealed that between 20 and 24 combustors best matched the turbomachinery H-Q and horsepower design capability. The thrust chamber fuel-side pressure demand was found to be near the upper limit of the Mark 29-F turbopump design capability when operating at 1200 psia  $P_c$  and 5.5 mixture ratio. Twenty combustors were found to best fit the fuel pump design capability while still providing adequate safety margin.

In selecting the thrust chamber configuration, several arrangements were considered including a round aerospike, linear one-sided, linear two-sided, and curved segments of a large diameter aerospike. High expansion ratio was considered desirable.

When considering cost, match-fitting, ease of fabrication, integration into existing test stands, and the return value of the experimental data to be acquired, the configuration of test bed No. 1 was chosen to be as follows:

- 20 combustors
- Two-sided linear configuration
- Tubular furnace brazed nozzle, with the combustors welded to the nozzle

- 110:1 expansion ratio
- Semi-monocoque design turbine exhaust base manifold
- Gas generator power cycle using series drive turbines
- Heavy-duty rigid thrust frame
- Fluorine ignition system, with studies to begin immediately to select a more suitable future ignition system.

In the above configuration, the test bed No. 1 envelope dimensions were 126 inches wide, by 120 inches long, by 96 inches high.

As the design and development work progressed on test bed No. 1, studies were conducted to determine future effort required to expand the working knowledge of aerospike technology, and to provide answers to the remaining questions regarding aerospike suitability for booster and upper-stage vehicle applications. The studies revealed areas where future effort beyond that planned for test bed No. 1 would be beneficial.

Vehicle thrust vector control, vehicle altitude control, and thrust optimization at sea level and intermediate altitudes were identified as areas requiring further exploration. Additional questions involved ignition system suitability over a wide range of operating conditions, flexible ducting design for high gimbal angles, base pressure variations with operating conditions, and design and fabrication technology required for a flightweight thrust frame.

These preliminary studies then led to detailed conceptual studies in the above areas. Contained in Appendix A is a report on the studies related to thrust vector control. The thrust vector control study was a comprehensive effort to define the mission requirements for an aerospike-type engine, to establish engine/vehicle integration requirements, and to define optimum engine configurations. In addition, it was necessary to determine the thrust vector requirements and capabilities of various concepts and to obtain answers to some of the technical problems inherent in application of these advanced concepts.

From the study, two concepts evolved showing promise of being suitable for use in a large booster-type vehicle or single stage-to-orbit vehicle. These were the peripheral and the checkerboard concepts.

The checkerboard concept is illustrated in Fig. A-1 (Appendix A) and consists of double-sided linear modules of a configuration similar to test bed No. 1 except that the thrust chamber assembly is hinged to provide thrust vector control in a single axis only. Vehicle attitude control is achieved by the alternate placement of the engine module hinge axis in both the pitch and yaw axes to attain control in both planes.

The peripheral concept is illustrated in Fig. A-2 (Appendix A) and consists of single-sided linear modules surrounding the vehicle boattail area, with each module consisting of a power package and a hinged thrust chamber assembly, with the turbine exhaust gas from each module venting into the common central base compartment. Vehicle thrust vector control is attained by hinging those modules whose axes are on the respective pitch and yaw axes.

The configuration of test bed No. 2 evolved as a hybrid concept to investigate problems related to both the peripheral and checkerboard concepts. The system was designed with a flightweight frame with the upper frame holding the power package stationary, and the lower frame and thrust chamber assembly being hinged through  $\pm 16$  degrees. This required flexible ducting between upper and lower frame designed to take the large angles. Special design concepts for flexible ducting thus evolved and were incorporated successfully in test bed No. 2.

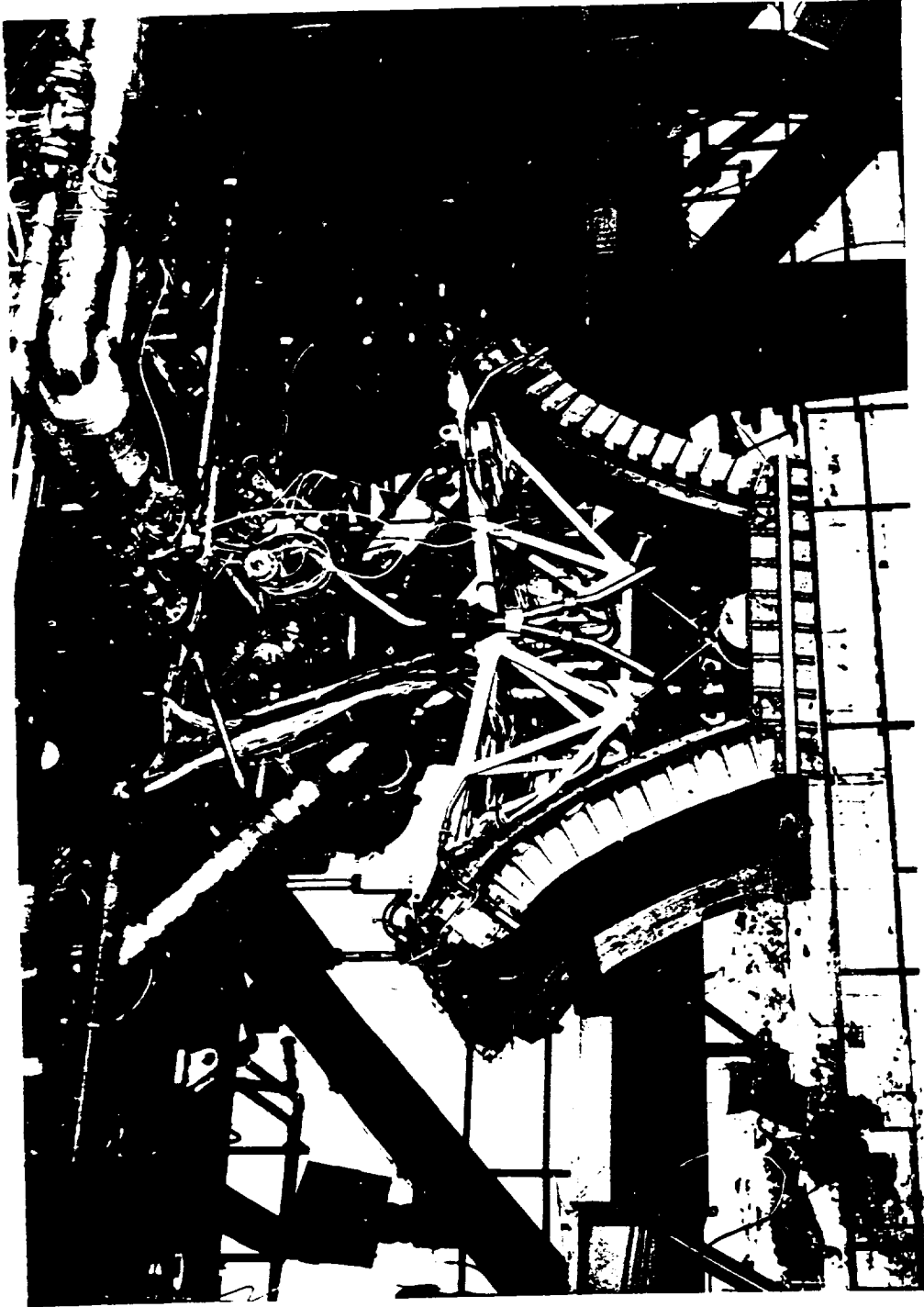
The nozzle sides were designed to be individually hinged on the thrust frame to evaluate the special problems unique to the peripheral concept such as base pressure effects from varying geometry, and to determine the optimum nozzle angle required for sea level operation.

Because of cost and time constraints, it was decided that test bed No. 2 would be built with less than 20 combustors. Studies revealed that with 16 or less combustors, it would be necessary to dump propellants overboard in order to meet the H-Q

demands of the turbopumps. With this established, it was decided that meaningful experiments could be conducted with 10 combustors (5 per side). The test bed was configured accordingly.

It was then decided that it would be desirable to evaluate the effects of varying the base exhaust gas flow. A hot-gas overboard dump system was therefore provided that would have the capability of varying base secondary flow from 1 to 3 percent of the thrust chamber flow.

Test facility installation of test bed No. 2 is shown in Fig. 4, and a flow schematic is shown in Fig. 5.



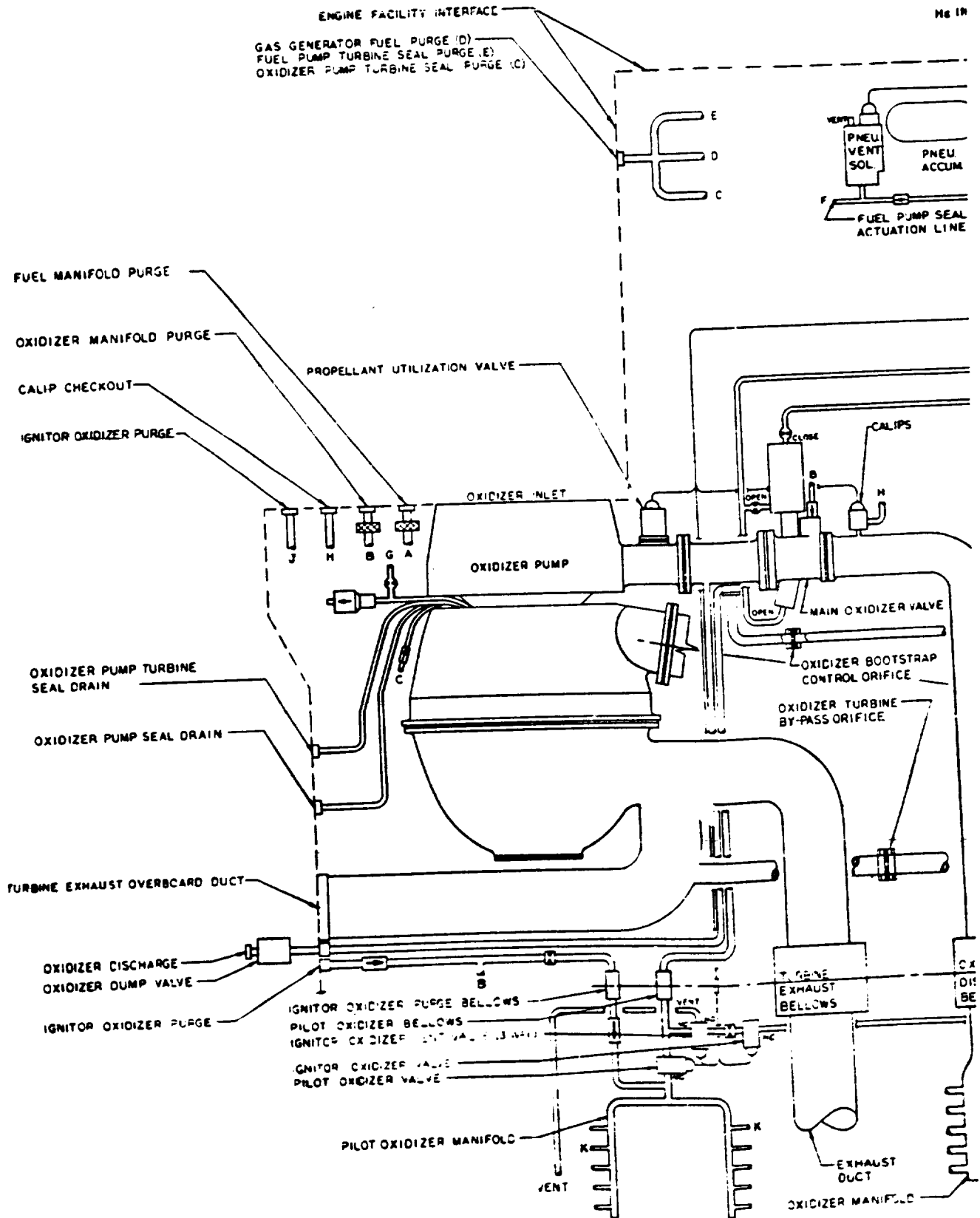
IXW23-10/31/72-SIB\*

Figure 4. Test Bed No. 2 Installed in the Delta-2B Test Facility

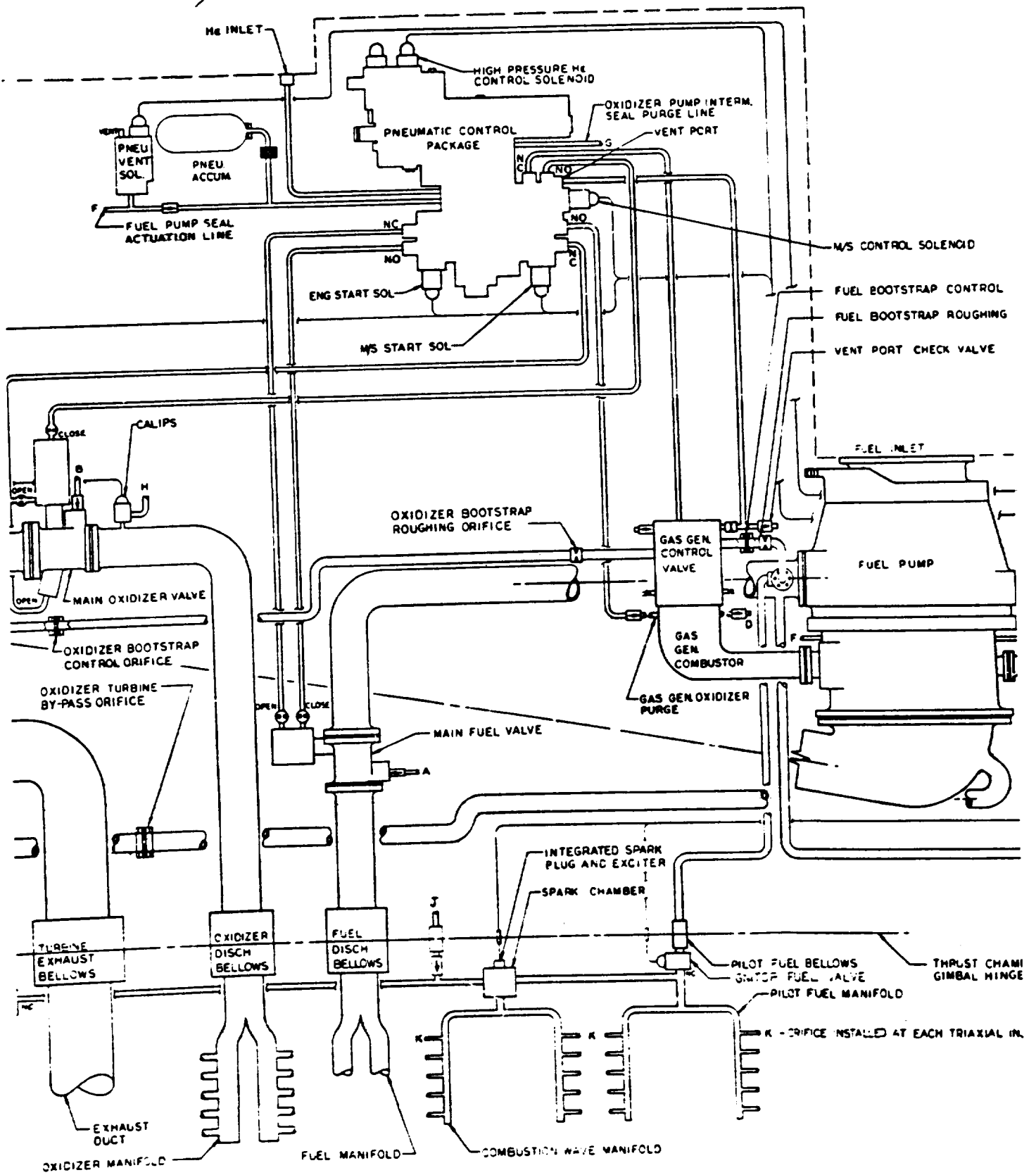
NOIT FRAMB

FOLDOUT

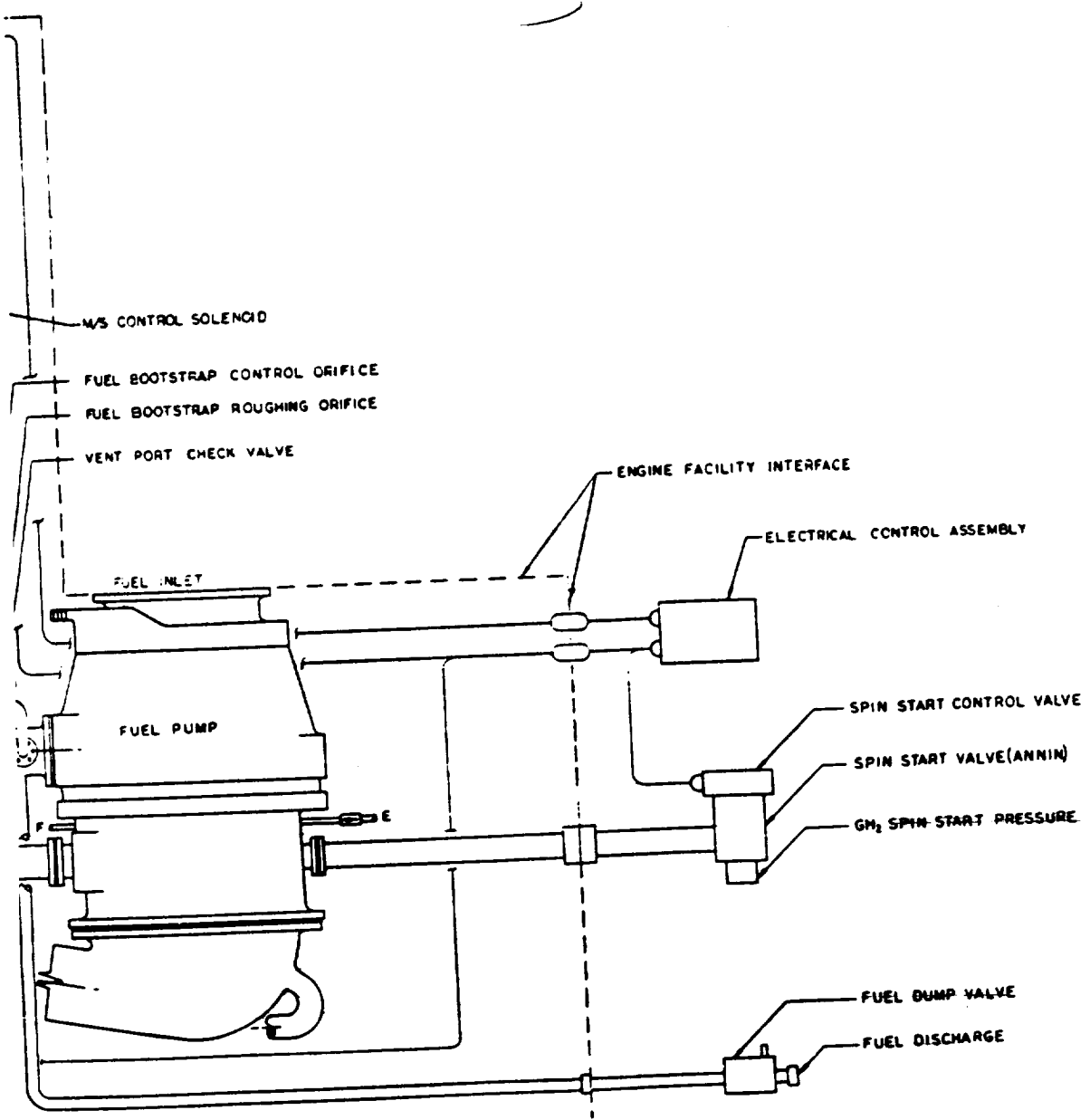
Hg IN



# FOLDOUT FRAME



ENGINE FRAME  
3



ORIFICE INSTALLED AT EACH TRIAXIAL INJECTOR PORT

Figure 5. Linear Engine Test Bed No. 2 Schematic

R-9049

## DESIGN AND FABRICATION

Presented in this section is the rationale that influenced the design and fabrication of test bed No. 2. The objectives of the test bed that dictated the design were as follows:

- Dynamic Hinging - Thrust vector control through large gimbal displacement angles was a principal objective. Dynamic hinging of  $\pm 16$ -degree maximum displacement angle was selected as the design point. Tradeoff studies were conducted to determine the best configuration to achieve this goal. The candidate configurations were to hinge the complete engine assembly with the flexible inlet ducting, or to hinge the thrust chamber assembly with flexible discharge ducting. The latter configuration was selected, principally because of the difficulty in designing 8-inch-diameter cryogenic inlet ducting capable of  $\pm 16$ -degree displacement angles.
- Independent Static Hinging of the Nozzle Sides - The nozzles were designed so that each nozzle bank could be independently hinged in the static position. The hinge angles selected were  $(+7^\circ, +7^\circ)$  and  $(+17\frac{1}{2}^\circ, -5^\circ)$ .
- Lightweight Thrust Frame and System Packaging - A lightweight thrust frame with a flight-type configuration was a principal objective. This resulted in a welded, thin-wall tubular design for the upper and lower thrust frame.
- Secondary Flow Variation - The ability to vary secondary flow to determine its effect on base pressure and site specific impulse was a program objective. This was achieved by an overboard turbine exhaust dump system. By the use of orifices in the base flow feed duct and in the overboard duct, the flow feeding the base manifold could be varied from 1 to 3 percent of the primary thrust chamber flow.
- Advanced Ignition System - The triaxial combustion wave ignition system was selected for use on test bed No. 2. This ignition system offered the promise of a flexible, reliable ignition system with the capability of a major advancement in the state of the art for multiple ignition applications.

- Fabrication Technology - Low-cost fabrication and alternate combustor fabrication techniques were explored on test bed No. 2. Combustors were fabricated employing annealing to preclude hydrogen embrittlement of the electroplated nickel. The annealing took the place of electroplated copper to protect the nickel in the areas of manifolds and feed passages. Two combustors (No. 1 and 4) were nickel plated (0.012-inch thick) in the combustion zone to evaluate the relative erosion resistance of nickel versus NARloy.

#### THRUST FRAME

The test bed No. 2 thrust frame consists of two tubular structures of a true geometric design. The geometric design concept was selected to provide a structure that would simulate, as close as possible, flight-type hardware. There were several redesigns favored for the upper structure that would have been even more similar to flight-type concept hardware; however, to minimize facility modification costs, the existing design was selected. Also, the tubular, geometric design, while meeting all stress requirements expected in three axes, provided the mounting provisions for all engine systems hardware.

The upper stationary structure (power head) was fabricated basically of steel tubing which varied in diameters ranging from 1- $\frac{1}{2}$  to 3 inches. Machined fittings were utilized at the points of tube intersections, not only increasing the structural integrity of the thrust mount, but providing the means of obtaining the formation of the geometric design. Attachment of the main structural tubes to the machined fittings, as well as the inner support tubes, was accomplished by weldments of the Class I type. The upper thrust mount incorporates tubular support frames with appropriate fittings to facilitate the mounting of the Mark-29 fuel and oxidizer turbomachinery. The mount also incorporates miscellaneous brackets to facilitate the routing and support of control system, ignition system, instrumentation, purge, and drain lines. There are also mounting provisions for various engine system components. Interfacing of the mounts to the facility was accomplished by the utilization of six machined ball fittings which were installed into fittings on the mount. Upon installation in the facility, the machined fittings engaged recesses in the facility thrust plate, and bolts were installed to

complete the installation. Interfacing the upper mount to the lower movable mount was accomplished by engagement of two clevis fittings located at the base of the upper mount major support tubes with two tongue fittings incorporating self-aligning bearings mounted on the lower mount. Machined pins were installed through the clevises and tongue fittings to complete the interfacing.

The lower movable structure was also fabricated of steel tubing which varied in diameters ranging from 2 to 4 inches. Machined fittings again were utilized at the points of tube intersections to increase structural integrity of the thrust mount and to obtain the formation of the geometric design. Attachment of main structural tubes to the machined fittings, and inner support tubes in this assembly was accomplished by weldments of the Class I and Class II types. The lower mount design was based on a need to support the two 5-segment thrust chamber nozzles in such a manner as to allow the thrust chamber nozzles to be placed in various positions in relation to the hinge point centerline. This was accomplished by the utilization of clevises incorporating self-aligning bearings on the two upper tubular support assemblies. Upon installation of the thrust chamber nozzles, the rib assemblies of the nozzle panels were engaged and bolted within the clevises. This permitted rotational movement of the panels. The various positions were obtained during hot-fire testing by using various length links which were attached from the base of the nozzle panels to the lower support tubes of the mount. The lower mount also incorporated miscellaneous brackets to facilitate the routing and support of ignition system, instrumentation, purge, drain, and water coolant lines. Tongue plate assemblies were welded to the upper support structure to facilitate the utilization of an F-1 gimbal actuator which was the means of hinging (gimbaling) the lower movable structure for the thrust vector control studies. The mount also incorporated brackets to facilitate installation of the hot-gas base manifold support links. The main ignition (combustion wave) panel was located and mounted on the lower mount.

## COMBUSTOR (RS002245X)

Combustor segment design for test bed No. 2 was identical to test bed No. 1 except for variations in fabrication techniques to evaluate the effectiveness of several methods of electrodeposited nickel (EDNi) hydrogen embrittlement and redesign of the igniter port to accept the combustion wave or resonance tube igniter configuration. Essentially, fabrication of combustors for test bed No. 2 was a continuation of the production line setup for test bed No. 1. Operating parameters, design parameters, thermal analyses, structural requirements, and fabrication sequence given in Ref. 1 are applicable to test bed No. 2 design.

Figure 6 shows the test bed No. 2 combustor igniter receptacle design used. The design was changed from a standard threaded fitting to a four-bolt flanged fitting to allow utilization of the larger igniter designs for resonance or combustion wave ignition techniques. The brazed-in port redesign was made to allow rework of the test bed No. 1 LOX injector manifold casting without rework of the actual casting molds. Manifold castings for use on future engines could have the port cast integral with the remainder of the casting.

Three concepts of EDNi protection from  $H_2$  embrittlement were utilized. Four combustors were fabricated with no electrodeposited copper (EDCu) layer on  $H_2$  exposed surfaces. These assemblies were annealed at  $650^\circ F$  for embrittlement protection. Four of the remaining six combustor assemblies utilized "primary" EDCu plating closeout over the NARloy-A flow channels prior to adding the EDNi structural backup. These four were also annealed to give double protection against embrittlement in the  $H_2$  channel closeout region. Two segment assemblies utilized "primary" and "secondary" EDCu plating to protect all nickel surfaces exposed to  $H_2$  from embrittlement. (Figure 7 shows the location of the "primary" and "secondary" copper plating.) These two segments were not annealed to give the additional nickel protection. Table 1 gives the mix and location of combustors with the various EDNi protection techniques.

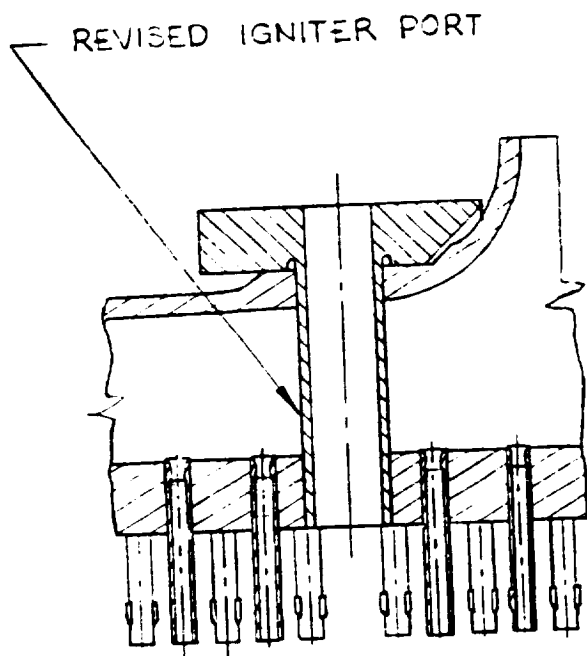


Figure 6. Test Bed No. 2 - Thrust Chamber Segment Igniter Port Design

R-9049

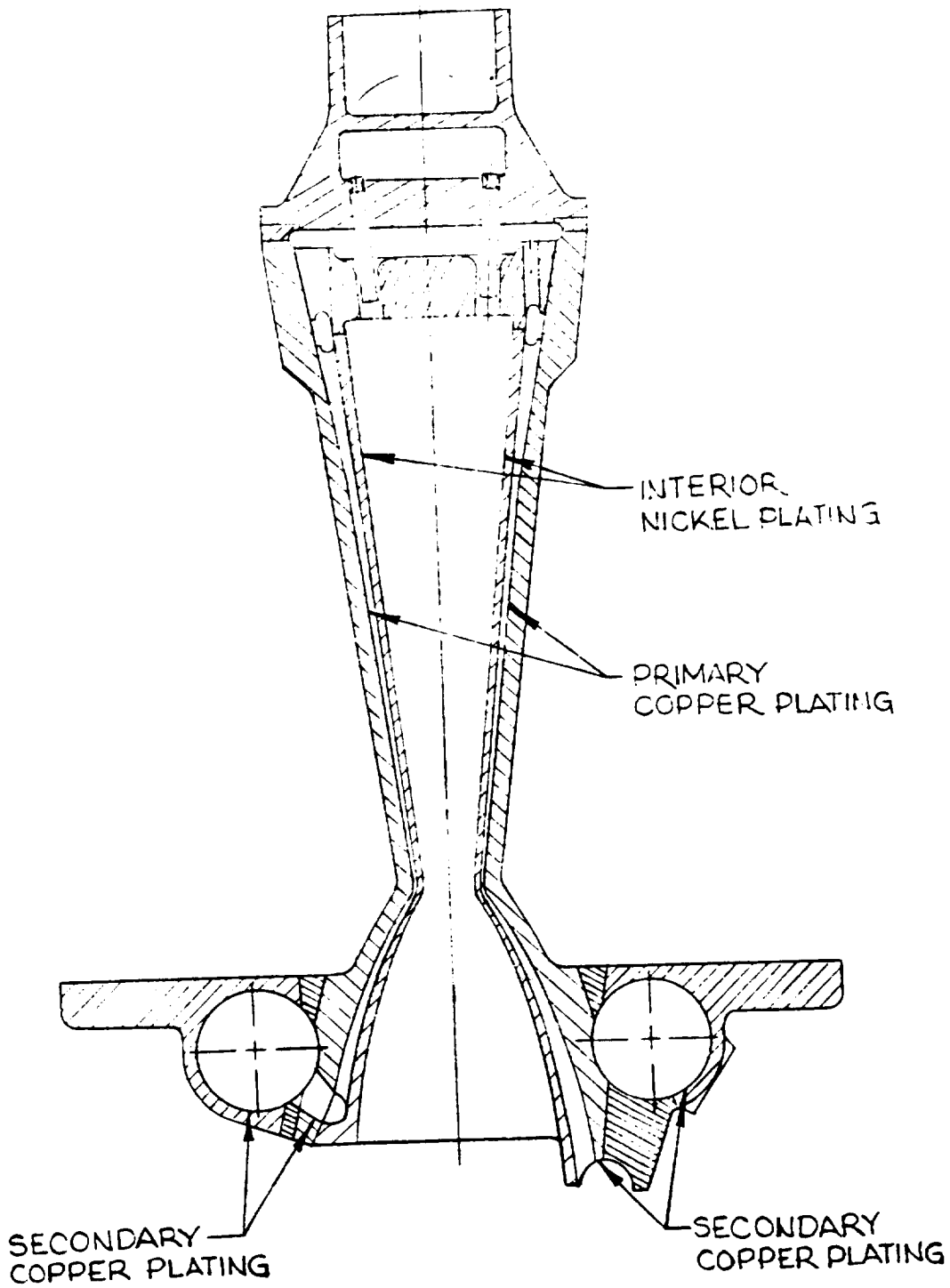
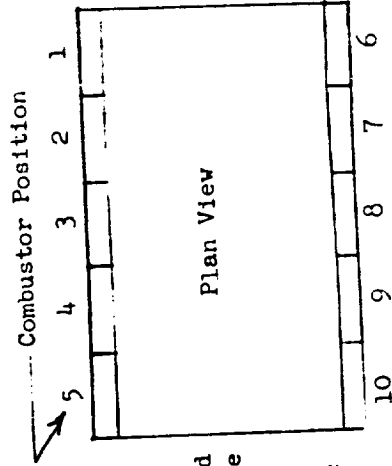


Figure 7. Test Bed No. 2 - Thrust Chamber Segment  
Primary and Secondary Copper Plating,  
Interior Nickel Plating

R-9049

TABLE 1. SUMMARY OF TEST BED NO. 2 COMBUSTOR II, EMBRITTLEMENT PROTECTION

Engine Position	Segment Identity	Primary EDCu (1)	Secondary EDCu (2)	No EDCu	650° F EDNi Anneal	Combustor Interior Nickel Plate	Machined Liner
1	C-42	X			X	X	
2	C-46	X			X		
3	C-45			X	X	X	
4	C-41	X			X		X
5	M-01			X	X		
6	C-43			X	X		
7	C-34	X	X				
8	C-29			X	X		
9	C-32	X	X				
10	C-40	X			X		



- (1) Channel closeout only
- (2) All EDNi surfaces exposed to H<sub>2</sub>

△ 2B Combustor Installation Schematic

After combustor fabrication completion, it was decided to nickel plate the primary combustor zone of two segments for evaluation of thermal and oxidation protection of the NARloy-A during operation. Table shows the position of these two segments on the engine. The plating was 0.002 to 0.003 inch thick, and extended from immediately between the injector face through the throat region. No other changes that affect thermal operation were made on these combustors to allow direct operational correlation with the unprotected combustion zone surfaces.

In the preliminary stages of the linear engine fabrication program, liner casting difficulties and delivery delays led to the design and start of fabrication of a backup, non-cast, hot-gas liner. The backup configuration liner was a multiple-pieced machined channel configuration that was EB-welded together. All sections were fabricated from wrought NARloy-A.

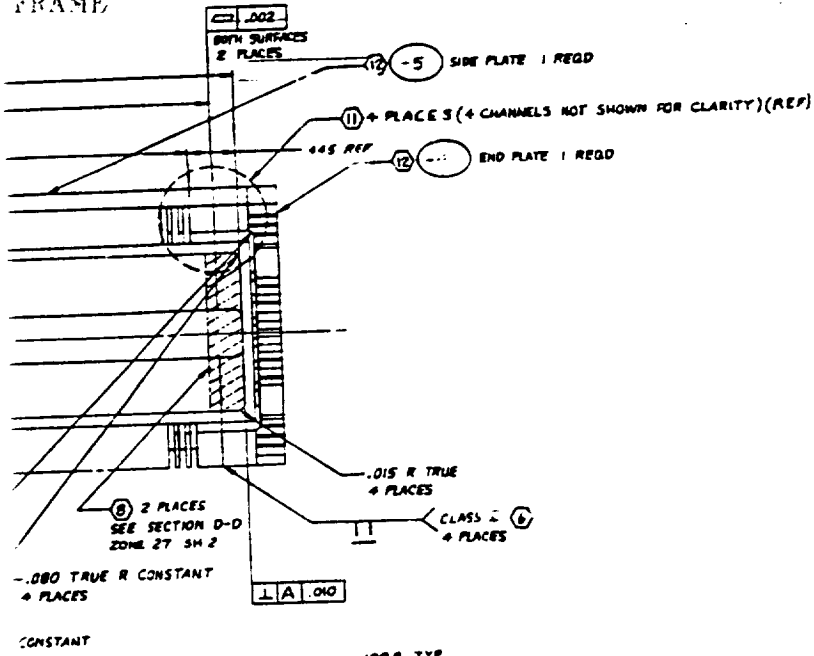
The design is shown in Fig. 8. The "machined" liner duplicated the cast liner design from combustor segment assembly fabrication, heat transfer, and operational standpoints, and was considered interchangeable in all aspects. Fabrication of "machined" liners was initiated during the test bed No. 1 fabrication stage, but delivery of castings was sufficient to support the fabrication schedule. Subsequently, it was decided to continue fabrication of one machined liner on a low-priority basis that was to be utilized in test bed No. 2. Fabrication completion was successful, and the unit was installed at position 5 on test bed No. 2 (see Table 1).

#### NOZZLE (RS003761X)

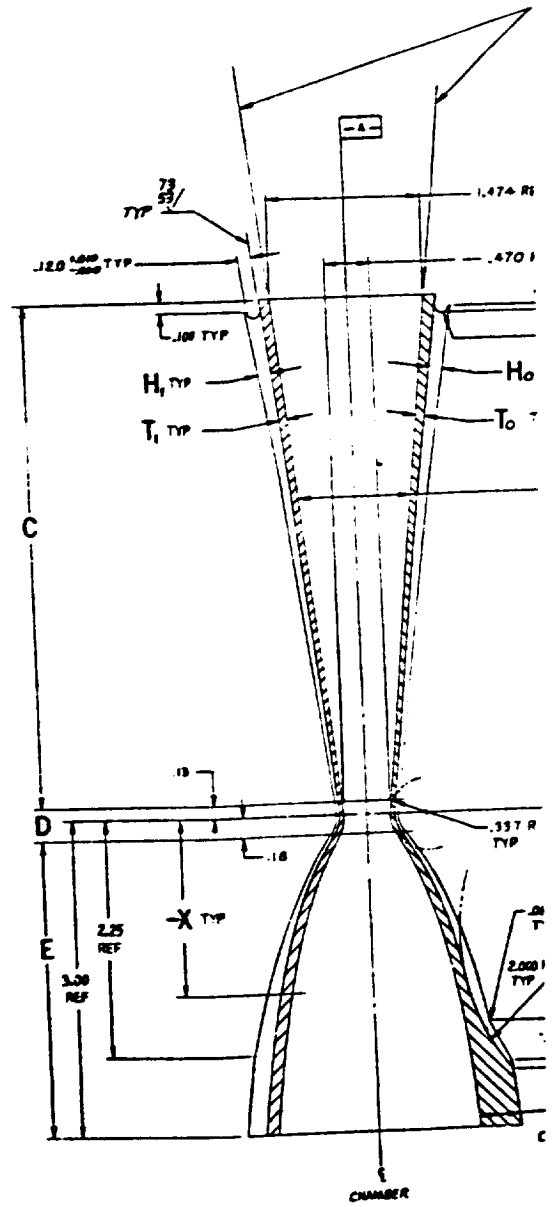
The nozzle design for test bed No. 2 is identical to the design defined in Ref. 2 except that it is one-half as long (5 versus 10 feet) and has reduced fuel manifold capacity to compensate for the lower fuel flowrates. The 347 CRES constant wall thickness, nontapered, 0.200-inch OD by 0.015-inch wall coolant tubes were furnace brazed to each other and to the structural support hat bands in a single furnace cycle. Adapter bars were concurrently furnace brazed to each end of the nozzle for the tube bundle attachment to the aft end fuel inlet manifold and the forward end combustors by welding and TIG brazing.



FRAME



FOLDOUT FRAME



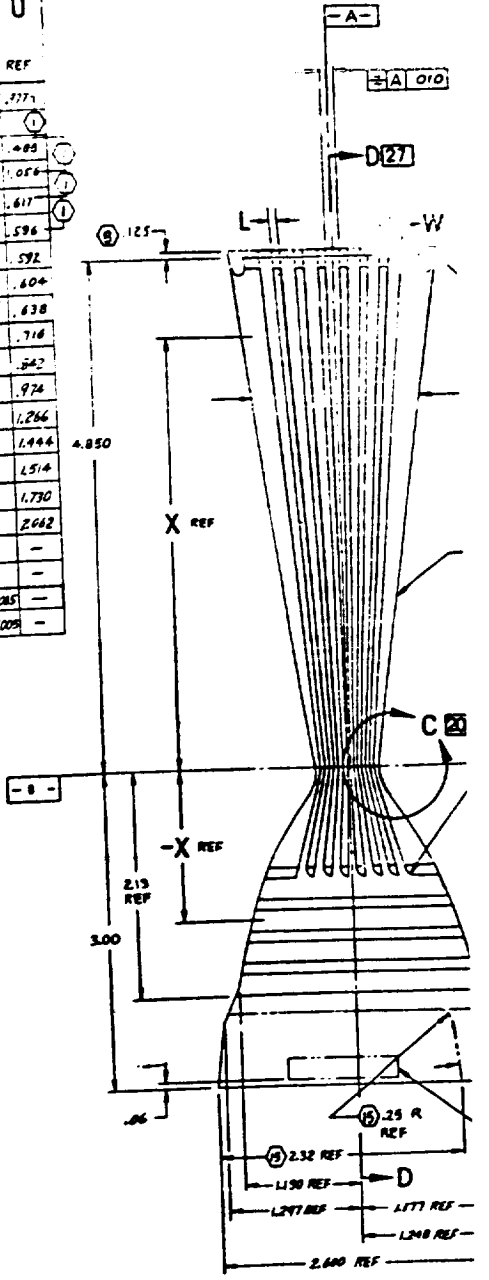
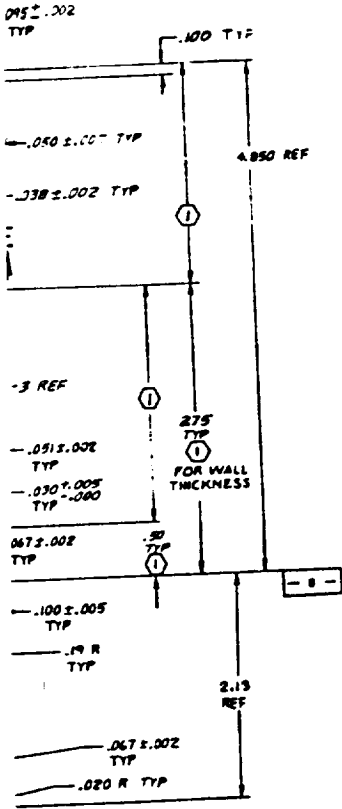
SECTION A-A 15





FOLDOUT

X	-X	Y	L	W	H	T	U	
BASIC	BASIC	BASIC			(19)	(18)	REF	
		3A.00	2.033	2.029	.002	.001		
4.850	-	1.474	-	-	.145	.05	2.13	.971
4.75	-		.074	.125				
3.50	-				.072			.408
2.00	-	(1)	(3)	(3)	(1)	.05	.005	1.058
.13	-				.031			.617
.035	-	.474						.596
.000	.000	.470	.036	.036				.592
-	.057	.478	-	-				.604
-	.114	.504	-	-	.031	.030	.005	.638
-	.178	.557	-	-				.718
-	.287	.666	-	-	(1)			.842
-	.392	.768	-	-		(7)		.974
-	.661	1.008	-	-				1.266
-	.844	1.146	-	-				1.444
-	.930	1.205	.077	.077				1.514
-	1.200	1.370	-	-				1.730
-	1.700	1.600	-	-				2.482
-	2.080	1.725	-	-				-
-	2.130	1.743	-	-				-
-	2.250	1.775	-	-	.180	.105	.005	-
-	3.000	1.920	-	-	.180	.105	.005	-



VIEW B-B 5x1

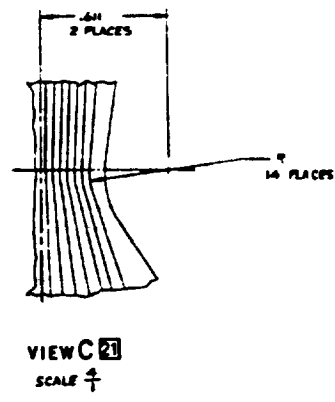
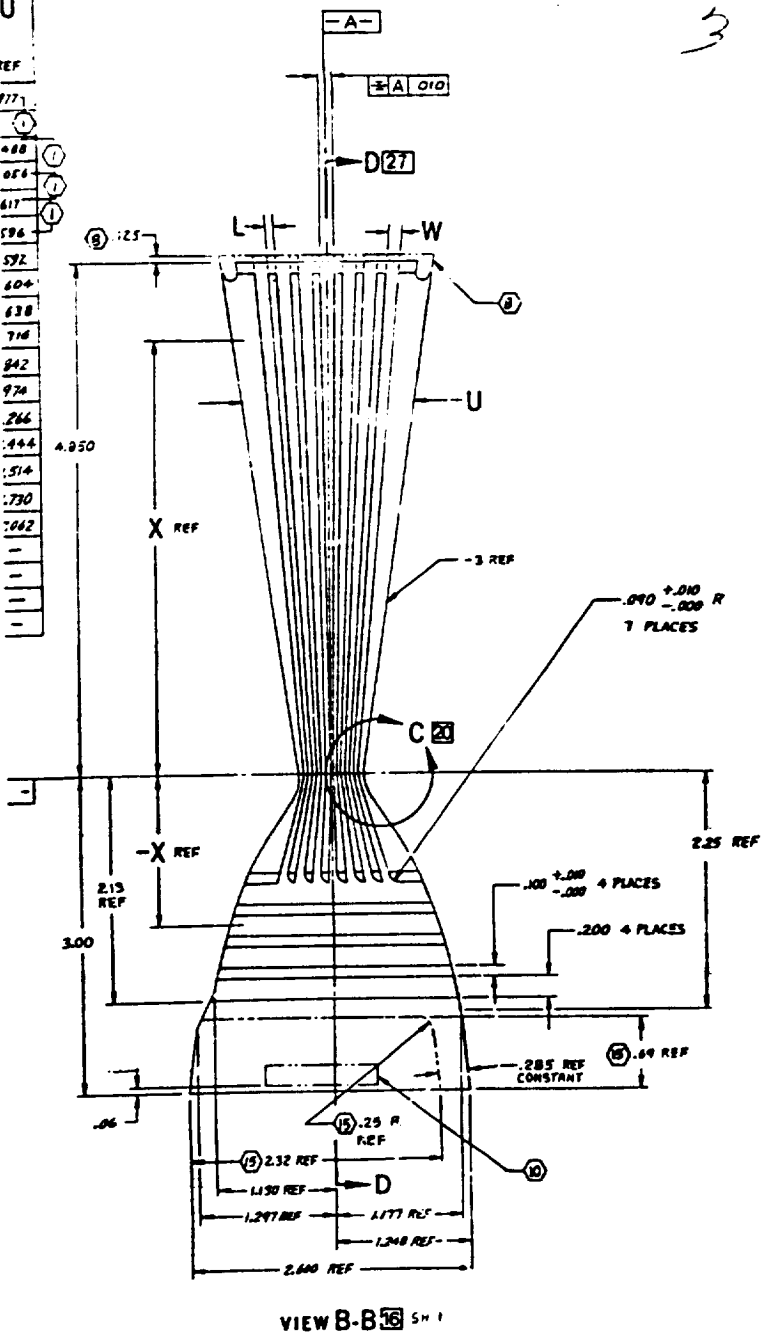
-3 SHOWN  
-4 OPPOSITE

23

-260

U
REF
177
088
054
617
596
592
604
638
716
842
970
266
444
514
730
1062
-
-
-
-

~~STANDARD FRAME~~  
3



VIEW B-B 26 SH 1  
-3 SHOWN  
-4 OPPOSITE

Figure 8. (Concluded)

Each 5-foot nozzle rail was attached to the backup structure of supporting ribs by rod end bearings to maintain nozzle contour, to provide nozzle support from operating loads, and to compensate for variations in thermal growth. Each rail was completed by attaching the five combustors to the support ribs and welding the aft end of the segments to the forward end of the nozzle tube bundle. The heat generated due to combustor-to-nozzle weld attachment on the rail containing combustor positions 1 through 5 caused opening up of tube-to-end bar furnace braze joints at the nozzle forward end. Attempts to repair these by hand braze caused coolant tube buckling. The nozzle had to be separated from the combustor bank to allow mechanical straightening of the tube buckles and further repair attempts of the leak paths. Most leaks were stopped, but a backup collection and dump manifold was attached to the backside of the forward end of the nozzle tube section to provide a harmless means of disposing of hot gas or H<sub>2</sub> leakage during testing. Figure 9 shows the installation of the added dump manifold.

Nozzle tubes were plasma coated with a layer of zirconium oxide for the 3 inches immediately aft of the forward end bar for thermal protection of this high-temperature operation area.

#### TURBINE EXHAUST MANIFOLD (RS003765X)

The turbine exhaust manifold was completely redesigned for the test bed No. 2 engine. The large, open manifold, "football-shaped" design with a single-piece perforated CRES plate gas injection technique was replaced with the manifolded tube bundle design shown in Fig. 10. A simpler, lighter, less expensive, and improved structural configuration was obtained. Each of 10 sheet metal rectangles was drilled in the center section for turbine exhaust gas injection, rolled and welded into 5.7-inch cylinders, and seam welded together to provide a rectangular base with a uniform gas injection pattern on the bottom. The cylinder ends were capped and an upper distribution manifold and inlet flange were attached to complete the assembly. This stacked tubular assembly design proved to be a successful configuration with minimum fabrication and operational problems.

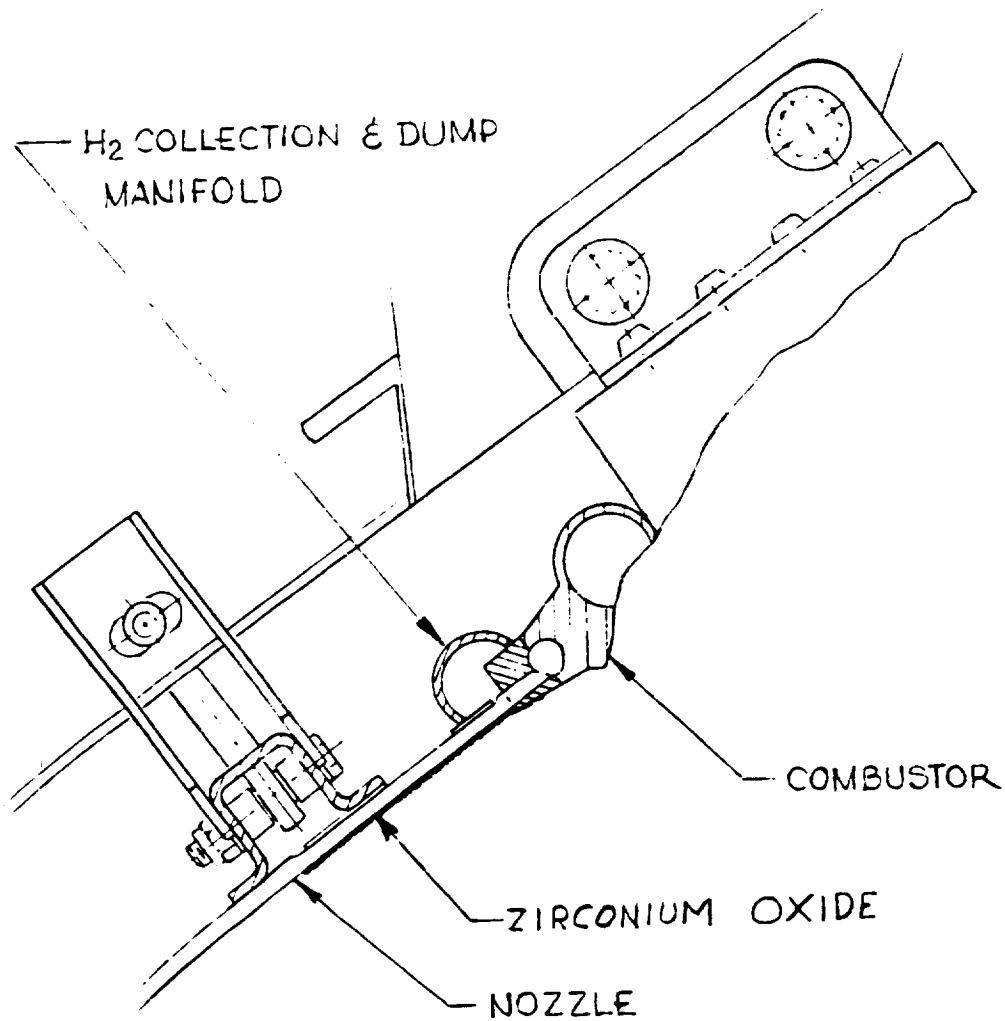
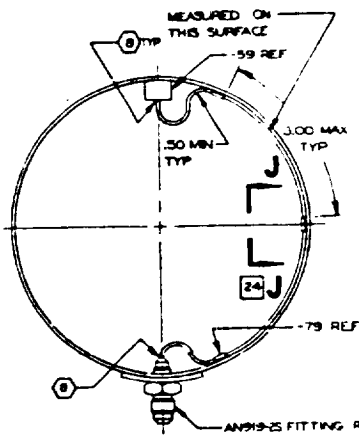
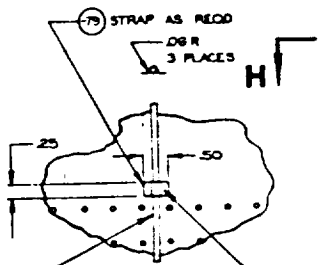


Figure 9. Test Bed No. 2 Thrust Chamber Added Nozzle,  
H<sub>2</sub> Collection, and Dump Manifold

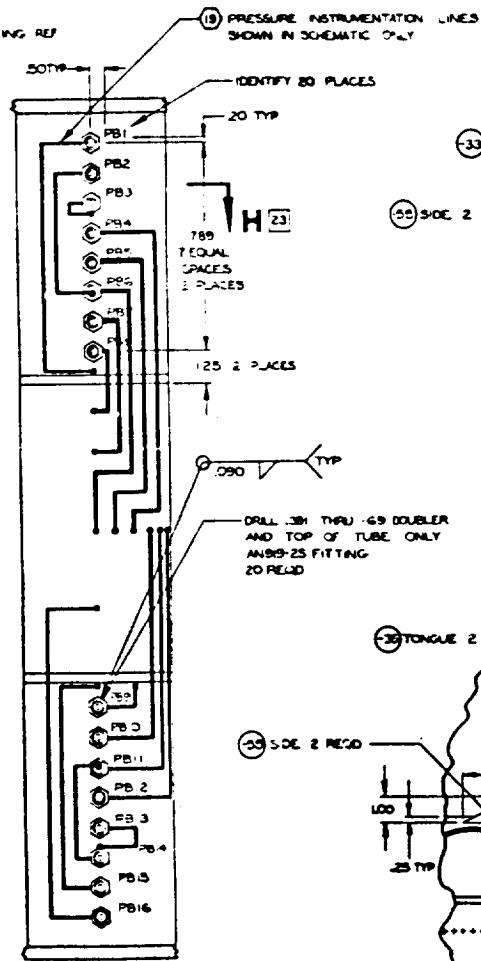
H  
G  
F  
E  
D  
C  
B  
A



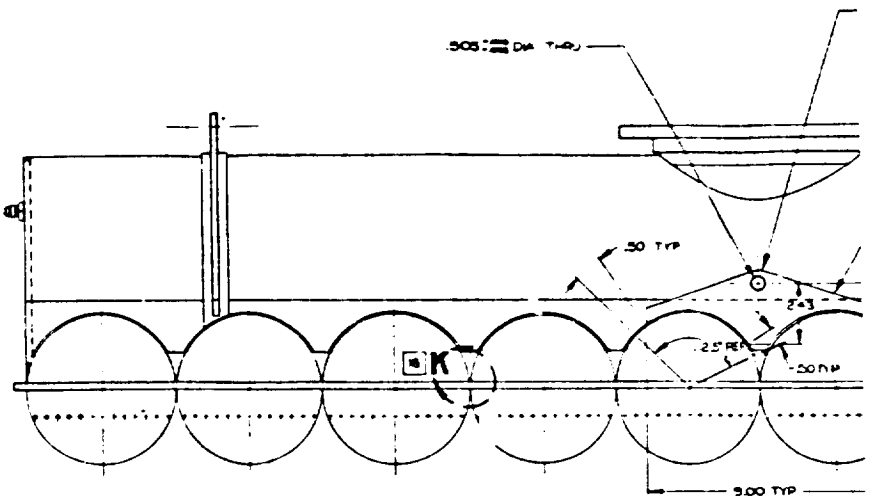
SECTION H-H 22  
SCALE: 1/2



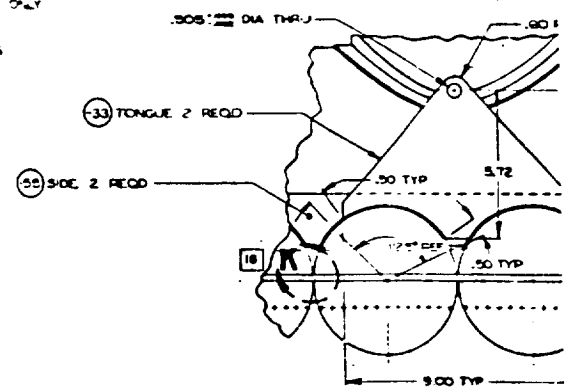
VIEW J-J 23  
SCALE: 1/2



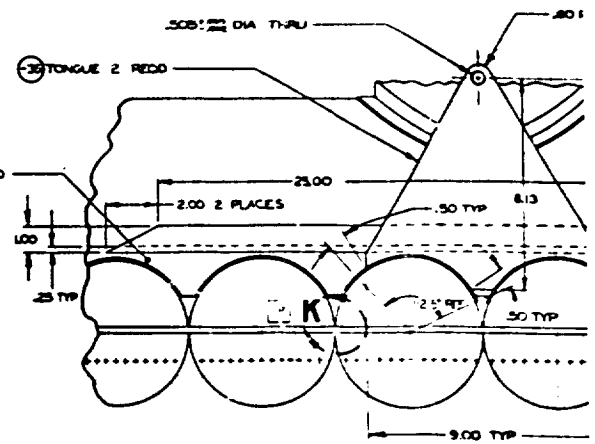
VIEW G 15



VIEW B-B 9  
FOR BASK ONLY



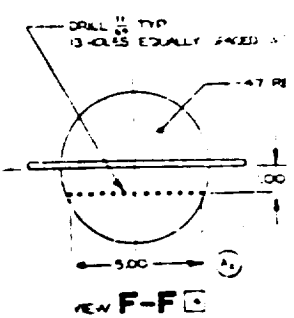
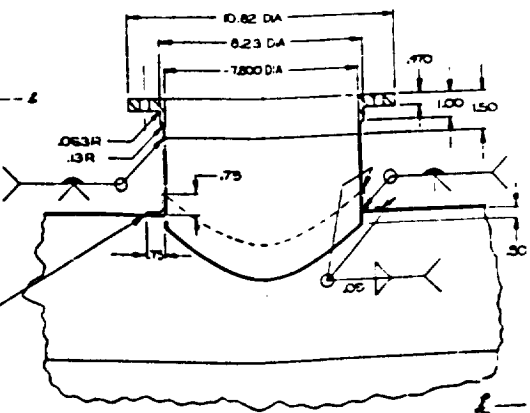
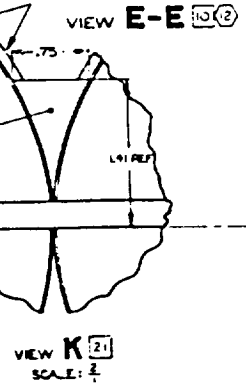
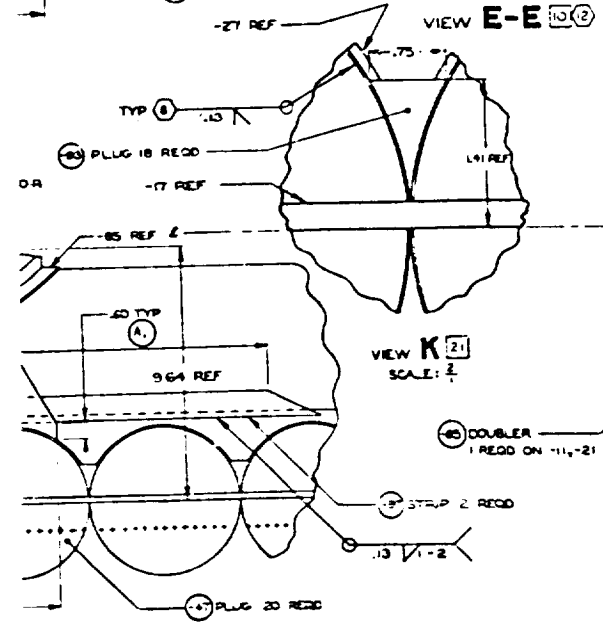
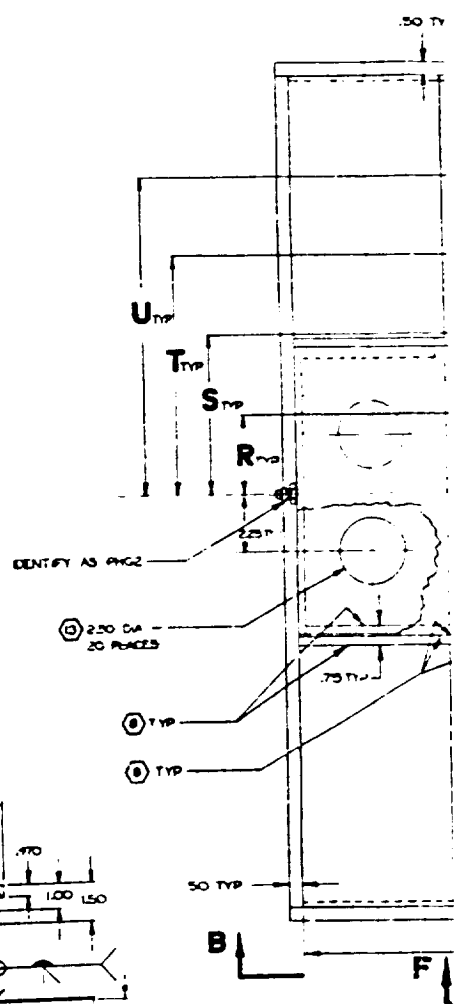
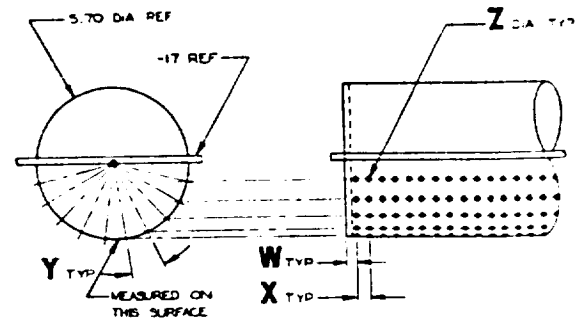
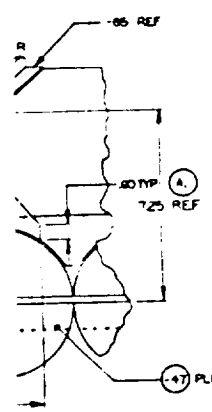
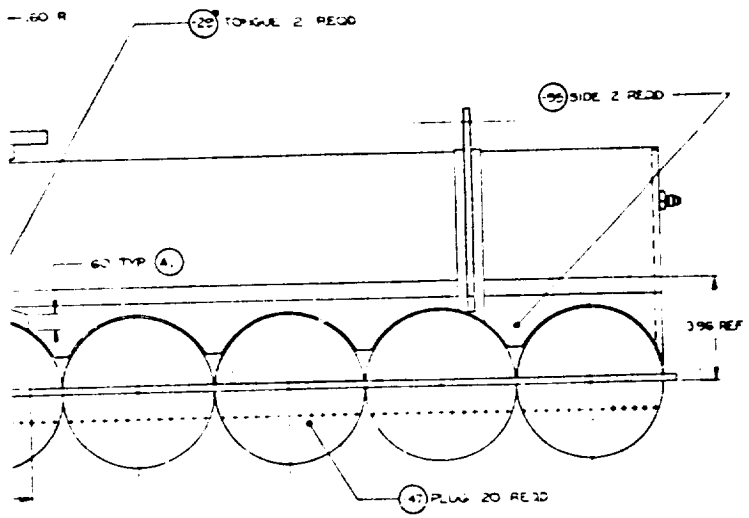
VIEW B-B 10  
FOR -11 ONLY



VIEW B-B 11  
FOR -21 ONLY

DO NOT WRITE

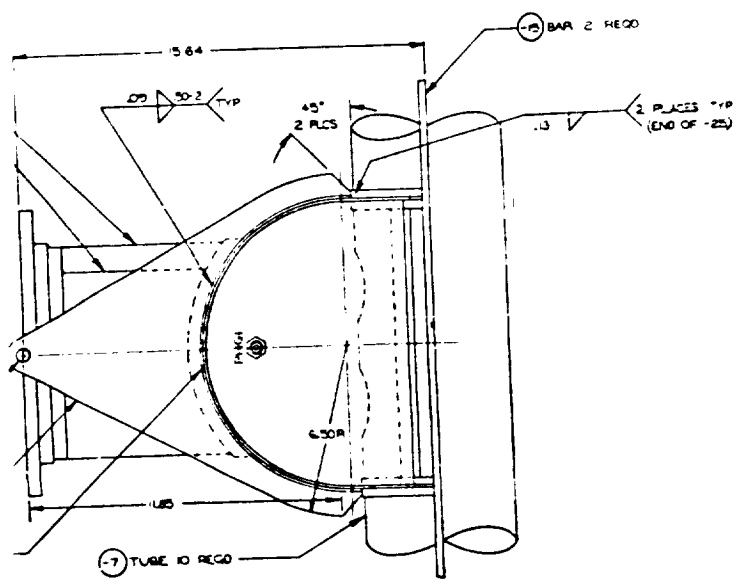
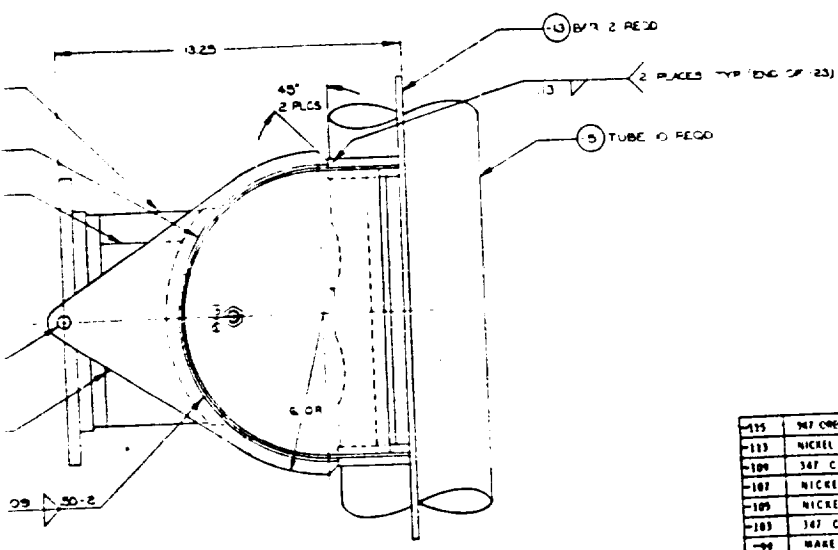
	BASIC	-11	-21
P	31.84	45.29	60.38
R	3.00	4.50	6.00
S	6.00	9.00	12.00
T	9.00	13.50	18.00
U	12.00	18.00	24.00
V	9.00	13.50	18.00
W	.42	.37	.49
X	.55	.55	.55
Y	.80	.80	.80
Z	.04	.08	.16
DR	.50	6.75	1.00







OUT FRAMES



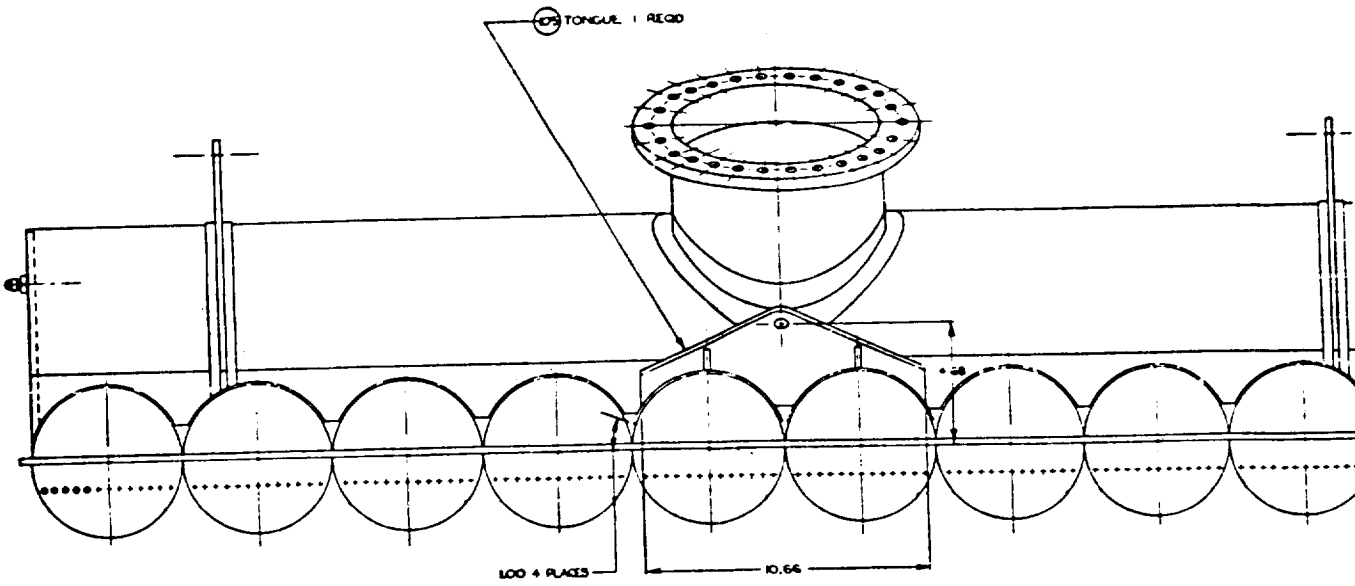
- 1) SCAM LOCATION ON -17, -19, -43, -109 DUCTS IS OPTIONAL FOR BASIC ONLY.
- 2) HOLES MAY BE MADE WHILE MATERIAL IS IN EITHER FLAT OR ROLLED CONDITION.
- 3) SAMPLE HOLE PATTERN TO BE TEST FLOWED BEFORE FINAL PARTS ARE MADE.
- 4) HEAT TREAT DETAILS PER RAD101-019 TO 175,000 - 700,000 PSI UTS 18, 30, 45, 1.
- 5) THIS SURFACE TO BE FREE OF NICKS, SCRATCHES OR OTHER IMPERFECTIONS WHICH IMPAIR ITS SEALING FUNCTION.
- 6) USE PROTECTIVE COVERS TO PROTECT INLET FLANGE.
- 7) BRAZE PER RAD107-009 USING NO. 3 ALLOY, SPEC. Q2-S-SHER, CLASS 3.
- 8) SEAM WELD PER S70107R-006.
- 9) PASSIVATE ASSEMBLY PER RAD110-010.
- 10) CLEAN DETAILS PER RAD110-010.
- 11) MACHINE PER RAD103-022.
- 12) IDENTIFY PER RAD104-008 (EXCEPT DO NOT IMPRESSION STAMP).
- 13) STANDARD DETAILS PER RAD107-007.
- 14) WELD PER RAD107-027, CLASS 11.

NO.	MATERIAL	SIZE	SPECIFICATION	ZONE
19	347 CRES SHEET	090 X 5.00 X 8.50	Q2-S-766 CL 347 COND A	1
15	NICKEL BASE ALLOY SHEET	250 X 1.00 X 7.00	R02170-030	12
5	347 CRES SHEET	300 X 1.20 X 7.50	Q2-S-766 CL 347 COND A	10
3	NICKEL BASE ALLOY SM	250 X 1.70 X 9.50	R02170-030	65
11	NICKEL BASE ALLOY SM	250 X 1.70 X 11.50	R02170-030	64
9	347 CRES SHEET	090 X 1.00 X 7.00	Q2-S-766 CL 347 COND A	41
8	347 CRES SHEET	090 X 1.00 X 7.00	Q2-S-766 CL 347 COND A	10
7	347 CRES SHEET	090 X 1.00 X 7.00	Q2-S-766 CL 347 COND A	10
6	347 CRES SHEET	090 X 1.00 X 7.00	Q2-S-766 CL 347 COND A	10
5	347 CRES SHEET	090 X 1.00 X 7.00	Q2-S-766 CL 347 COND A	10
4	347 CRES SHEET	090 X 1.00 X 7.00	Q2-S-766 CL 347 COND A	10
3	347 CRES SHEET	090 X 1.00 X 7.00	Q2-S-766 CL 347 COND A	10
2	347 CRES SHEET	090 X 1.00 X 7.00	Q2-S-766 CL 347 COND A	10
1	347 CRES SHEET	090 X 1.00 X 7.00	Q2-S-766 CL 347 COND A	10

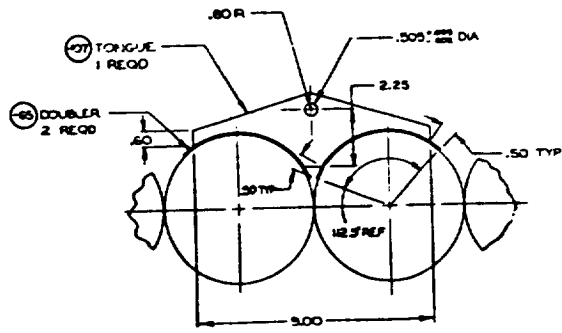
NO.	MATERIAL	SIZE	SPECIFICATION	ZONE
115	347 CRES SHEET	090 X 5.00 X 8.50	Q2-S-766 CL 347 COND A	1
113	NICKEL BASE ALLOY SHEET	250 X 1.00 X 7.00	R02170-030	12
109	347 CRES SHEET	300 X 1.20 X 7.50	Q2-S-766 CL 347 COND A	10
107	NICKEL BASE ALLOY SM	250 X 1.70 X 9.50	R02170-030	65
105	NICKEL BASE ALLOY SM	250 X 1.70 X 11.50	R02170-030	64
103	347 CRES SHEET	090 X 1.00 X 7.00	Q2-S-766 CL 347 COND A	41
100	WAKE FROM R5001705X 11			30
97	347 CRES SHEET	250 X 1.00 X 10.00	Q2-S-766 CL 347 COND A	10
95	347 CRES SHEET	090 X 1.75 X 8.00	Q2-S-766 CL 347 COND A	10
93	347 CRES BAR	875 X 875 X 1.50	Q2-S-763 CL 347 COND A	20
90	347 CRES SHEET	090 X 1.50 X 7.50	Q2-S-766 CL 347 COND A	10
87	347 CRES PLATE	50 X 1.50 X 7.5	Q2-S-766 CL 347 COND A	10
85	347 CRES SHEET	063 X 2.00 X 35.00	Q2-S-766 CL 347 COND A	10
83	347 CRES SHEET	090 X 1.50 X 1.50	Q2-S-766 CL 347 COND A	11
79	304 CRES FOR	0025 X .25 X .75	Q2-S-766 CL 347 COND A	24
77	347 CRES TUBE	125 DIA X 100.00	WIL-T-8008 COMP 347 TYPE I	24
75	347 CRES TUBE	125 DIA X 510	WIL-T-8008 COMP 347 TYPE I	24
73	347 CRES TUBE	125 DIA X 810	WIL-T-8008 COMP 347 TYPE I	24
70	347 CRES SHEET	090 X 1.50 X 10.00	Q2-S-766 CL 347 COND A	13
69	347 CRES BAR	250 X 1.00 X 1.75	Q2-S-763 CL 347 COND A	7
68	347 CRES SHEET	090 X .75 X 9.00	Q2-S-766 CL 347 COND A	12
67	347 CRES SHEET	090 X 1.00 X 20.00	Q2-S-766 CL 347 COND A	9
66	347 CRES SHEET	50 DIA X .45	Q2-S-763 CL 347 COND A	13
65	347 CRES SHEET	090 X 1.00 X 10.70	Q2-S-766 CL 347 COND A	6
63	347 CRES SHEET	090 X 3.50 X 50.00	Q2-S-766 CL 347 COND A	10, 22
62	347 CRES SHEET	090 X 1.00 X 10.00	Q2-S-766 CL 347 COND A	9
60	347 CRES PLATE	312 X 8.00 X 11.00	Q2-S-766 CL 347 COND A	8
57	347 CRES SHEET	180 X 8.00 X 6.50	Q2-S-766 CL 347 COND A	19
55	347 CRES PLATE	1.50 X 11.00 X 11.00	Q2-S-766 CL 347 COND A	9, 33
53	347 CRES SHEET	090 X 8.00 X 20.00	Q2-S-766 CL 347 COND A	6
50	347 CRES SHEET	090 X 8.00 X 20.00	Q2-S-766 CL 347 COND A	6
47	347 CRES SHEET	090 X 3.00 X 20.00	Q2-S-766 CL 347 COND A	9
45	NICKEL BASE ALLOY SM	250 X 9.00 X 9.50	R02170-030	21
43	NICKEL BASE ALLOY SM	250 X 7.00 X 9.50	R02170-030	22
41	NICKEL BASE ALLOY SM	250 X 1.00 X 9.50	R02170-030	10
39	NICKEL BASE ALLOY SM	090 X .75 X 9.00	Q2-S-766 CL 347 COND A	12
37	347 CRES SHEET	090 X .75 X 9.00	Q2-S-766 CL 347 COND A	12
35	NICKEL BASE ALLOY SM	250 X 16.50 X 11.50	R02170-030	6
33	NICKEL BASE ALLOY SM	250 X 11.50 X 12.50	R02170-030	6
31	NICKEL BASE ALLOY SM	250 X 7.50 X 12.50	R02170-030	9
29	347 CRES BAR	250 X .50 X 10.50	Q2-S-763 CL 347 COND A	3
27	347 CRES BAR	250 X .50 X 10.50	Q2-S-763 CL 347 COND A	3
25	347 CRES BAR	250 X .50 X 10.50	Q2-S-763 CL 347 COND A	3
23	347 CRES BAR	250 X .50 X 10.50	Q2-S-763 CL 347 COND A	3
21	347 CRES BAR	250 X .50 X 10.50	Q2-S-763 CL 347 COND A	3
19	347 CRES SHEET	032 X 18.00 X 61.50	Q2-S-766 CL 347 COND A	3
17	347 CRES SHEET	032 X 18.00 X 40.50	Q2-S-766 CL 347 COND A	3
15	347 CRES SHEET	032 X 18.00 X 37.00	Q2-S-766 CL 347 COND A	3

Figure 10. Turbine Exhaust Manifold, Test Bed No. 2

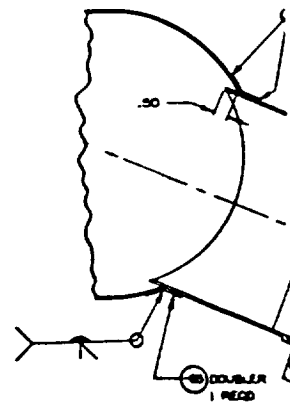
R-9049  
27/28



VIEW BB-BB 23



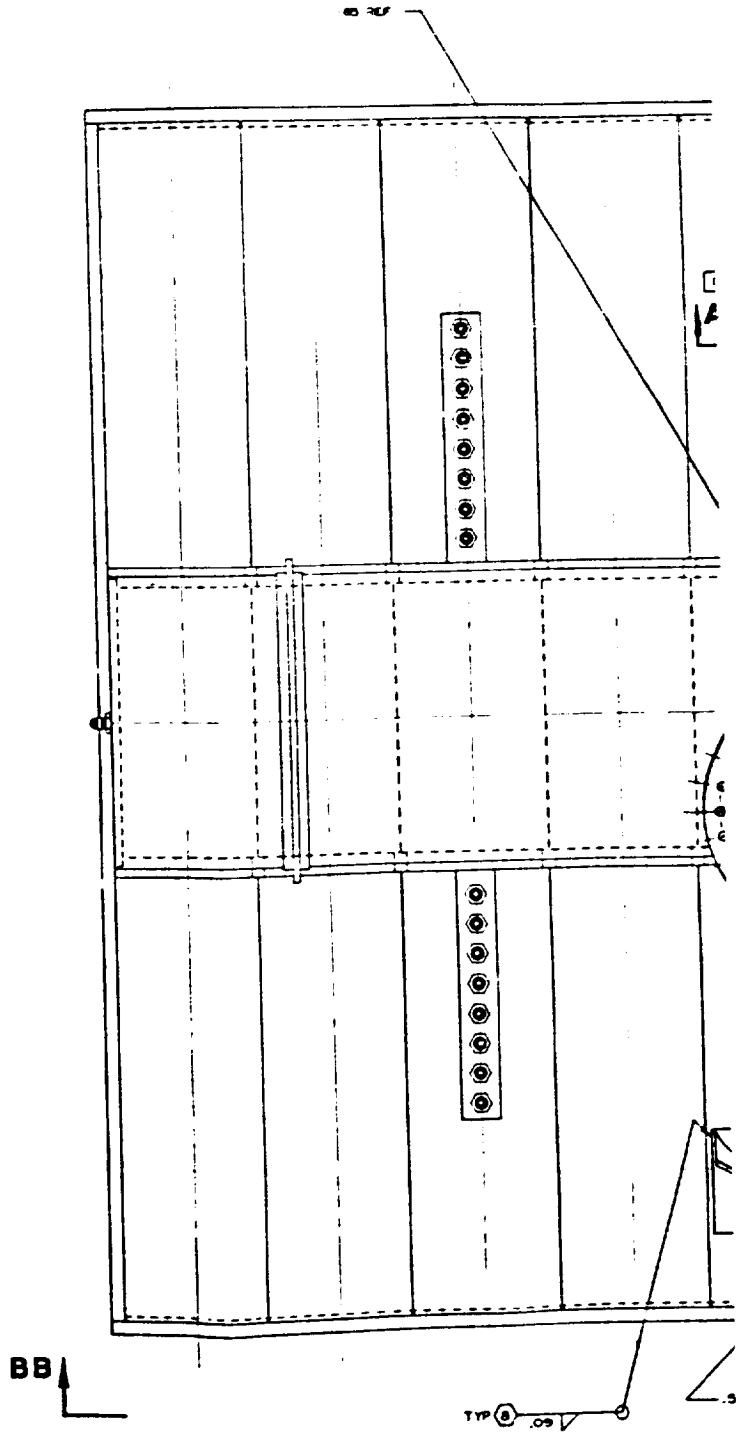
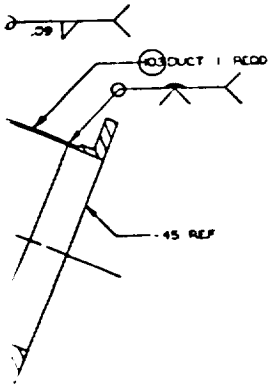
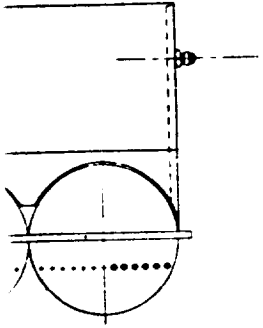
SECTION AA-AA 27



SECTION N-N 28

T FRAME

FOLDOUT





# SCOUT FRAME

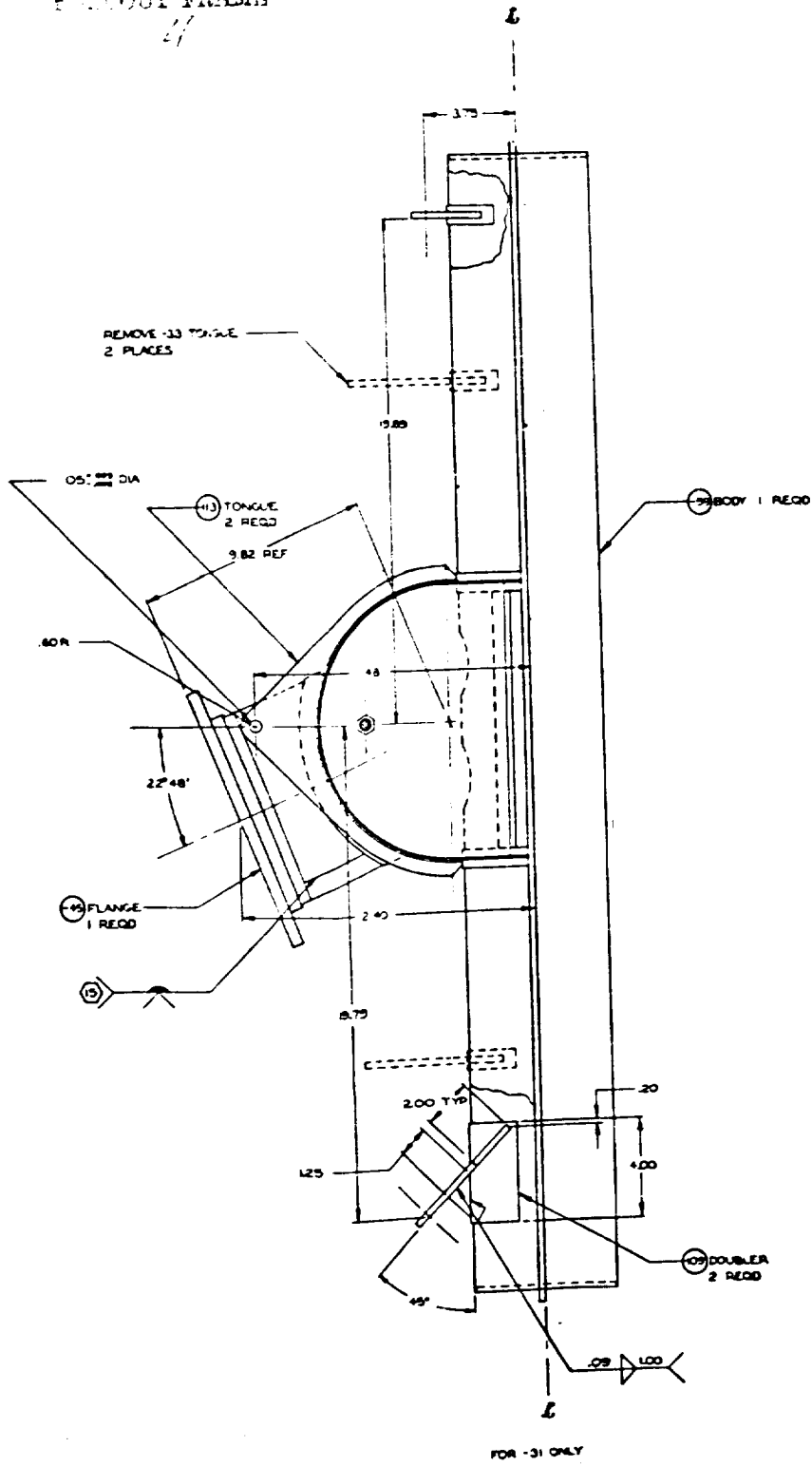


Figure 10. (Concluded)

R-9049

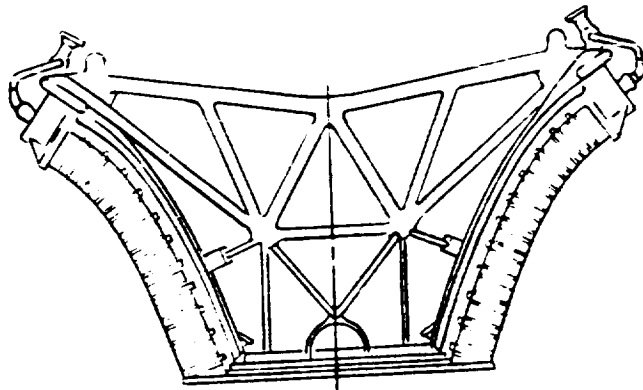
29/30

## THRUST CHAMBER ASSEMBLY (RS003770X)

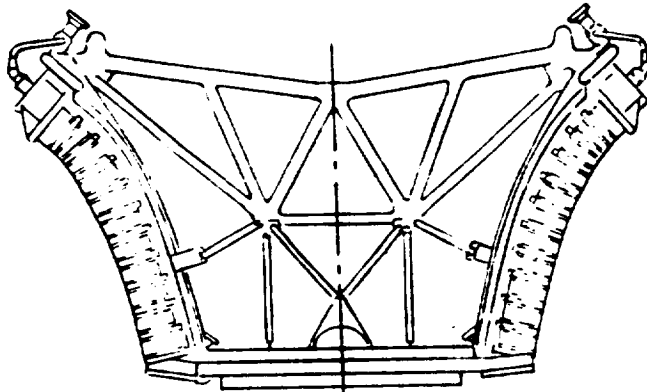
The two 5-foot nozzle assemblies, including combustors and manifolds, had the water-cooled end fences attached. The 5-foot rails were installed on the engine assembly. The tubular stacked turbine exhaust manifold was installed and the closeout seal between the hot-gas manifold and the rails was the formed CRES waffle configuration used on test bed No. 1. No assembly problems were experienced, with all subassemblies meeting design expectations. The nozzle wall contour and position were designed for an expansion ratio of 113.

The test bed No. 2 rails were mounted to allow changing the nozzle angles by swinging them about the upper pin mounting and replacing the lower support struts with various lengths. This repositioning could be done only by engine modification between tests, and required installing wider or narrower turbine exhaust manifolds to compensate for the varying positions. The capability for variation in nozzle angle was to allow comparison of sea level thrust chamber performance at positions other than the optimized altitude configuration.

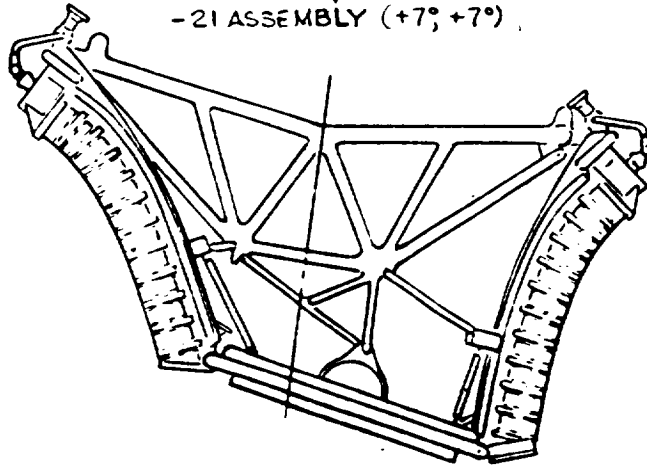
Two nozzle angle positions were tested on the No. 2 linear engine in addition to the altitude ideal or nominal configuration. All engine modifications necessary for the various hinged positions were made with the engine remaining in the test stand. The first modification swung each rail 7 degrees outboard (+7°, +7° position) and required installation of a new, wider turbine exhaust manifold. After testing at this position, a third configuration was made utilizing the same turbine exhaust manifold (+7°, +7°) and creating a (+17½°, -5°) position as compared to the original. However, to allow testing of this position in the test facility required swinging the entire thrust chamber assembly -10 degrees to have flame direction approximately vertical. The three configurations are shown schematically in Fig. 11.



BASIC ASSEMBLY



-21 ASSEMBLY (+7°, +7°)



-41 ASSEMBLY (-5°, +17°21', OVERALL-10°)

Figure 11. Test Bed No. 2 Thrust Chamber Tested Positions of Nozzle Banks

## FLEXIBLE DUCTING

### Hot-Gas Bypass Bellows Assembly

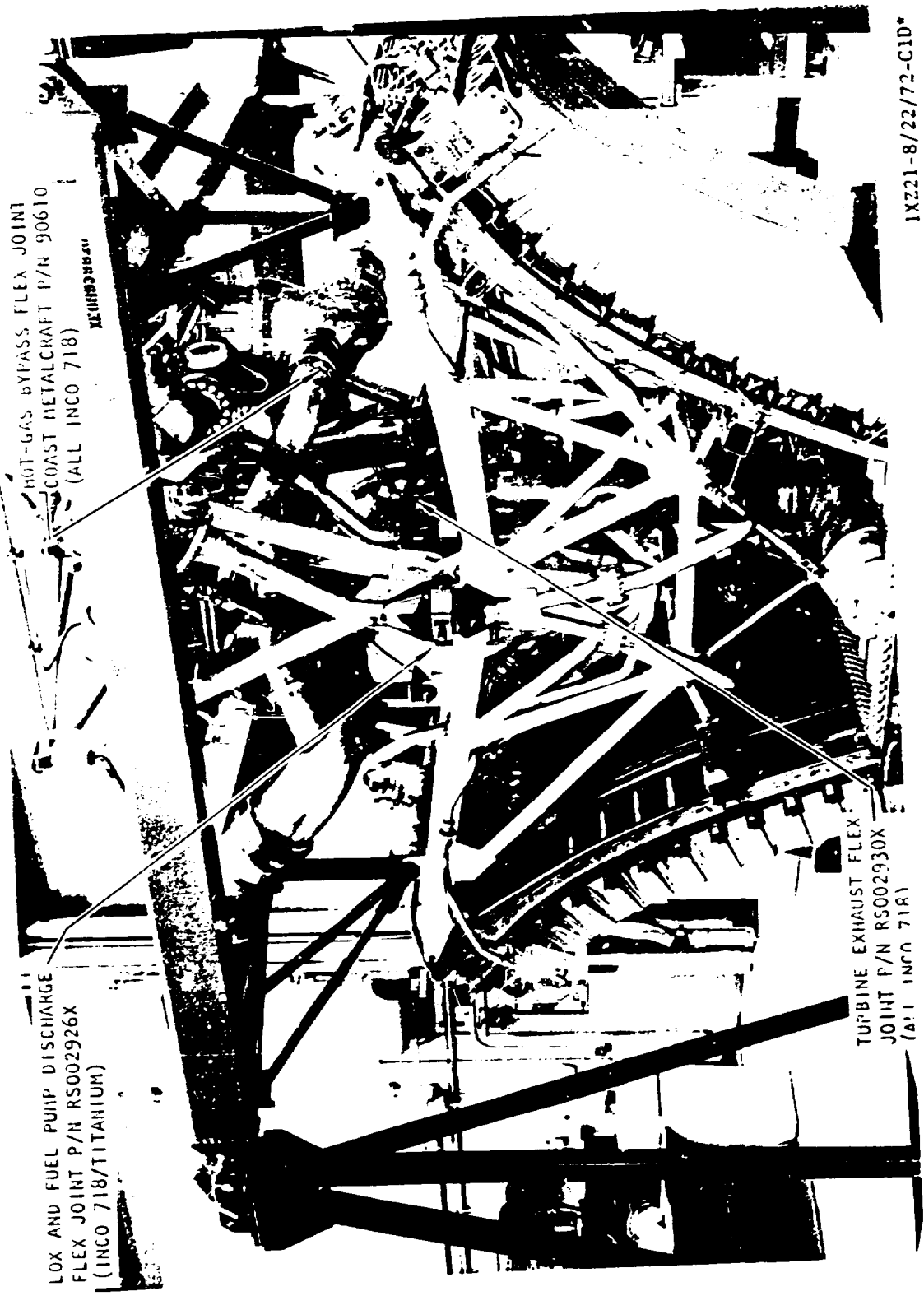
Engine test evaluation of the redesigned bellows in the bypass duct revealed that the internally tied flex joint configuration satisfied all functional and operational requirements. Flex joint redesign, due to duct rerouting and changes in operating conditions, incorporated internal flow sleeves to eliminate the possibility of flow-induced vibration of the bellows and internal strut and end rings machined from one piece to eliminate strut-to-flow sleeve fillet welds. Location of the flex joint in the engine system is shown in Fig. 12. Internal configuration of this flex joint is shown in Fig. 13.

### LOX and Fuel Pump Discharge Flex Joint

High-pressure propellant joints made of INCO 718 with a titanium gimbal ring were developed and engine tested during this program. These joints, designed for 18-degree angulation, incorporated two bellows separated by a spool piece which allowed each bellows to uniformly angulate 9 degrees. All engine hinging requirements were met without incident, and posttest inspection revealed no anomalies. Location of this joint on the engine is shown in Fig. 12 and the external configuration of the bellows assembly is shown in Fig. 14.

### Turbine Exhaust Flex Joint

To accommodate the 18-degree hinging motion requirement of the turbine exhaust duct, at operating conditions, a ball and socket joint assembly made of INCC 718 was developed. This design incorporates a close-tolerance ball and socket joint that is welded to a tripod strut assembly which provides uniform loading to mating components when gimbaled in any plane. The ball and socket mating surfaces are coated with dry film lubricant to reduce friction during bellows angulations, and the bellows convolutions are protected from high-velocity flow by internal liners. Electron-beam welding was used extensively during fabrication to produce a flex joint assembly with minimum distortion. Visual examination of the flex joint



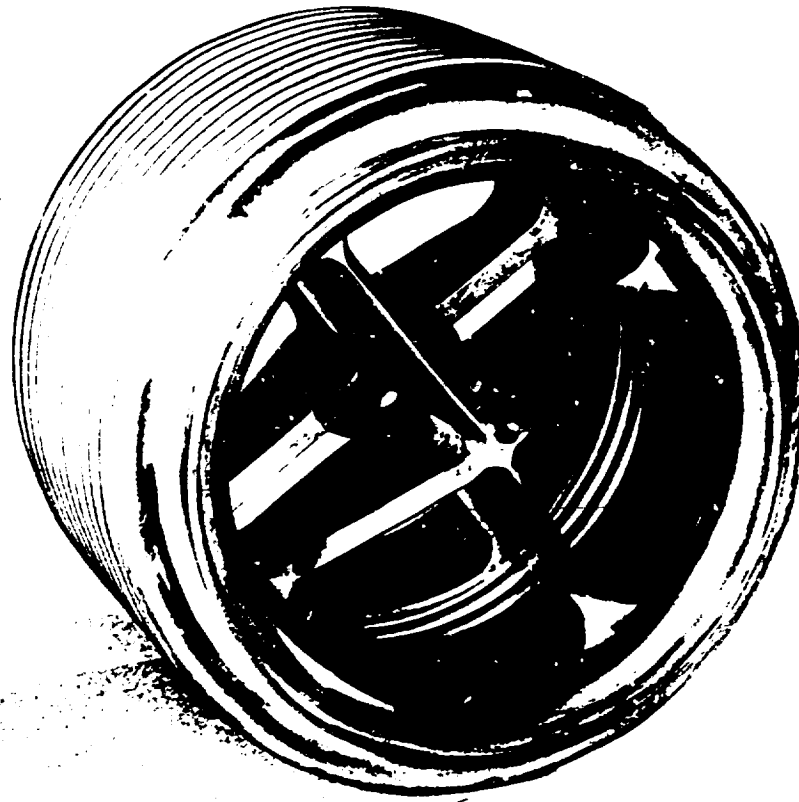
LOX AND FUEL PUMP DISCHARGE  
FLEX JOINT P/N RS002926X  
(INCO 718/TITANIUM)

HOT-GAS BYPASS FLEX JOINT  
COAST METALCRAFT P/N 90610  
(ALL INCO 718)

TURBINE EXHAUST FLEX  
JOINT P/N RS002930X  
(ALL INCO 718)

1XZ21-8/22/72-C10\*

Figure 12. Flexible Ducting Configuration

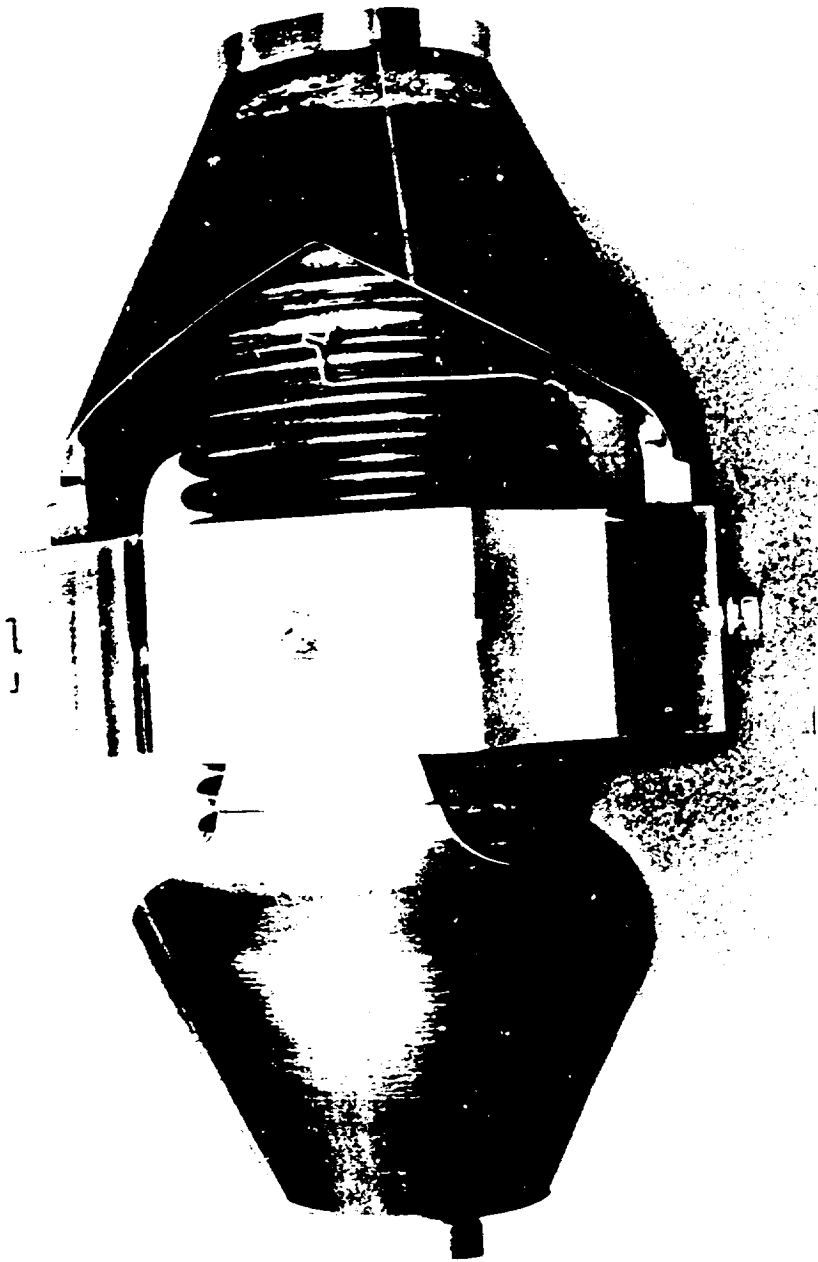


1CT62-4/21/72-C1

Figure 13. Internal Configuration of the Hot-Gas Bypass Bellows Assembly

R-9049

35



1XZ61-6/13/12-C1B

Figure 14. LOX/Fuel Pump Discharge Flex Joint

R-9049

following completion of engine testing revealed that the assembly was in satisfactory condition. Location of this joint on the engine is shown in Fig. 12 and the flex joint configuration is shown in Fig. 15.

#### COMBUSTION WAVE IGNITION SYSTEM

The combustion wave ignition system selected for test bed No. 2 is shown schematically in Fig. 16. The 10 triaxial igniter elements (Fig. 17) are similar in internal dimensions to the elements successfully tested during the initial concept demonstration tests (Ref. 2). The internal tube serves as the combustion wave passage during ignition and flows hydrogen only after combustion wave generation. The internal tube is surrounded by concentric tubes that flow pilot propellants during ignition and mainstage. The pilot element is ignited by the passage of the combustion wave prior to main propellant valve actuation, and the ignition is therefore independent of the main engine start sequence.

Propellants for the ignition system are supplied from the bootstrap takeoff flanges on the high-pressure propellant ducting. The propellant feed lines (Fig. 18) are provided with flexible sections to accommodate thrust chamber hinging and incorporate normally closed solenoid valves which serve as the igniter oxygen valve (IOV) and igniter fuel valve (IFV). A normally closed three-way solenoid valve with overboard vent capability is installed upstream of the IOV. A normally closed solenoid valve serving as the pilot oxidizer valve (POV) is also provided in the pilot oxidizer feed line. The premixer (Fig. 19) employs a single concentric-tube mixing element and an integrated spark plug and exciter unit (ISE), Fig. 20.

#### ELECTRICAL CONTROL SYSTEM

The experience and success encountered with the external, relay logic-type control assembly (K-box) used on test bed No. 1 led to the use of an almost identical system for test bed No. 2.

The engine logic, being basically the same for both engines, required only a 25-percent modification in the K-box. The primary difference centered around the



Figure 15. Turbine Exhaust Flex Joint

ICT31-11/21/72-C1B

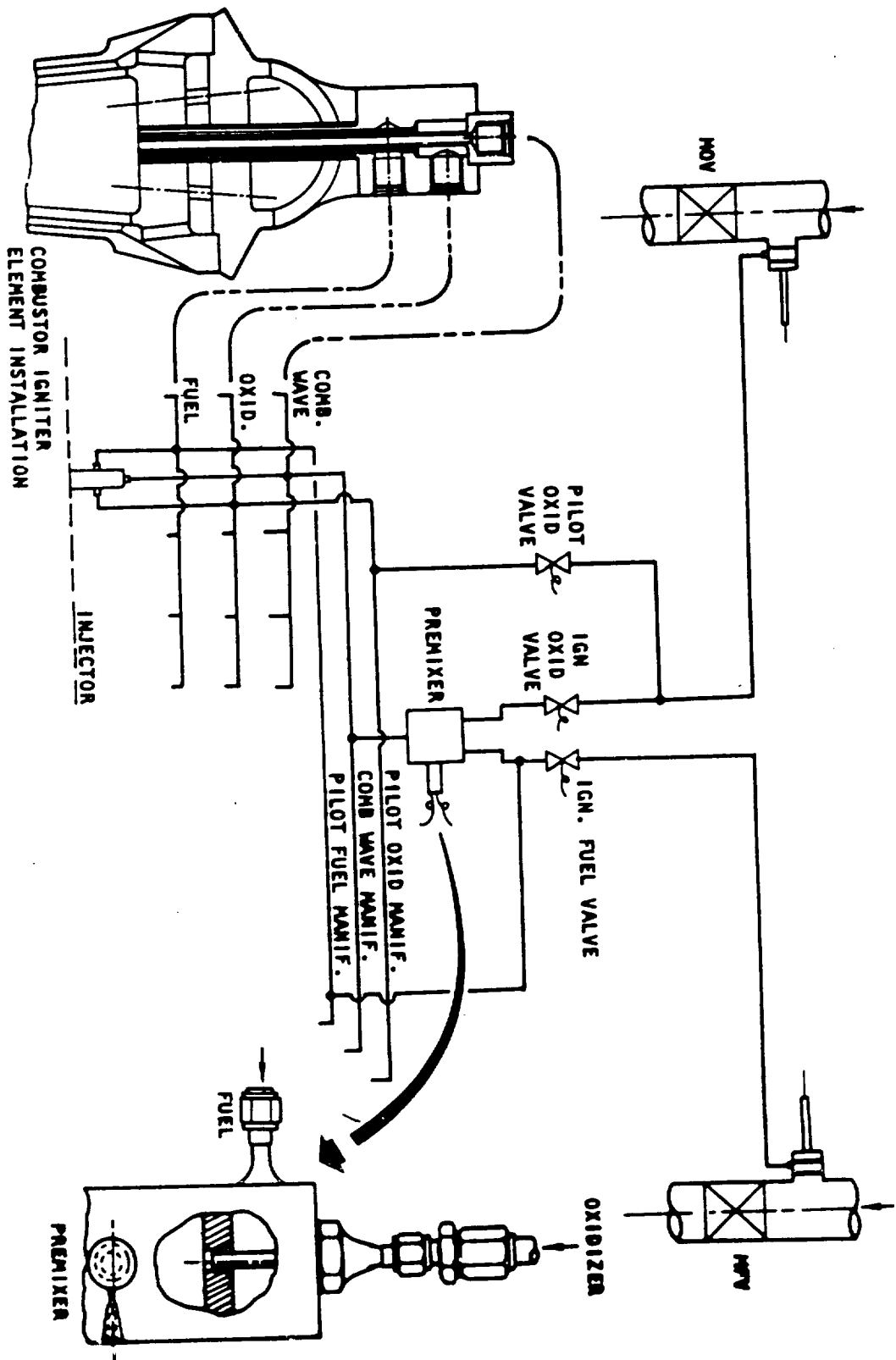


Figure 16. Test Bed No. 2 Triaxial Combustion Wave Ignition System

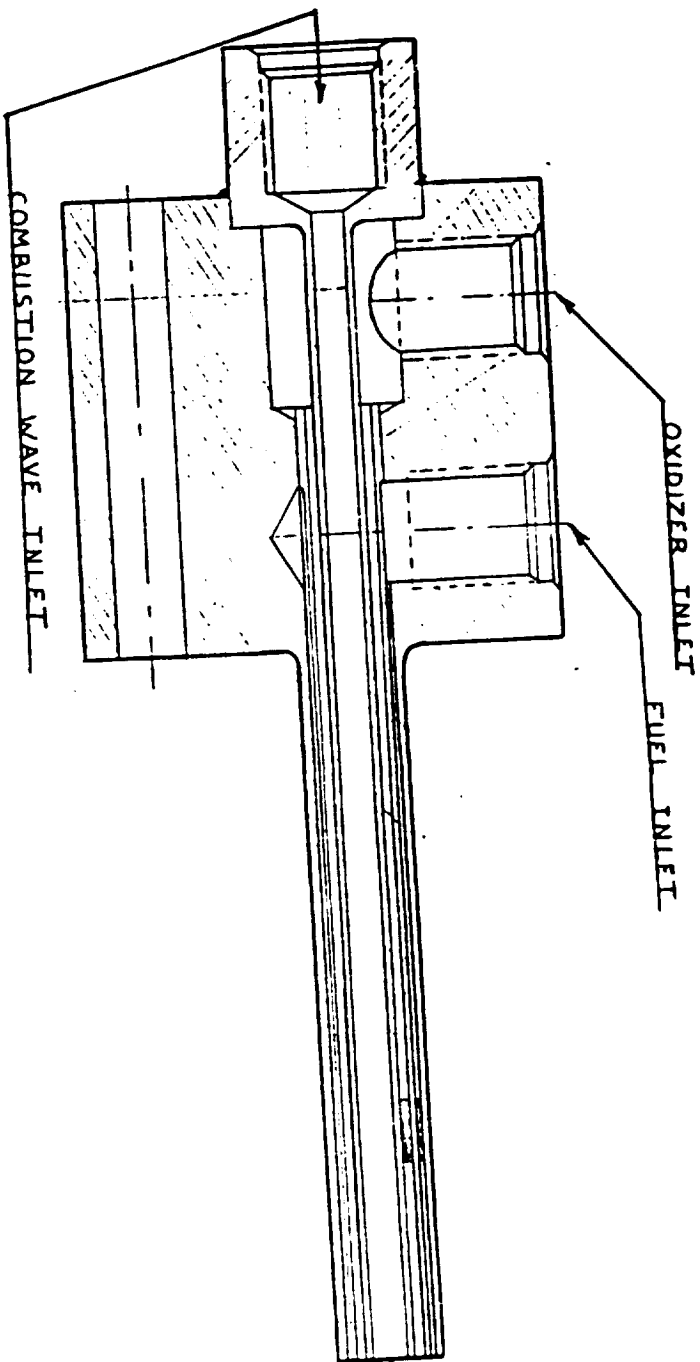


Figure 17. Triaxial Combustion Wave Element

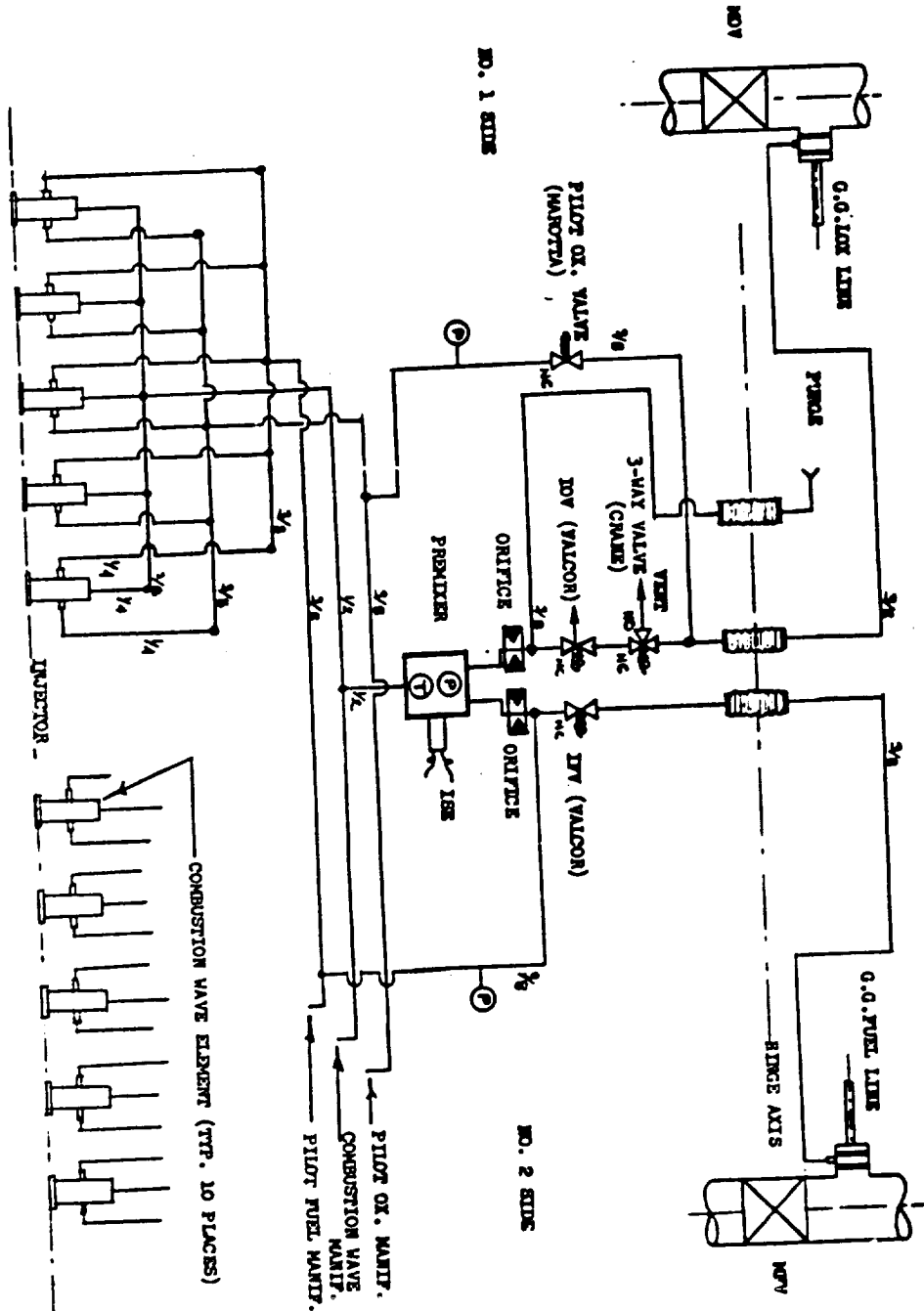


Figure 18. Test Bed No. 2 Combustion Wave Manifolding and Valve Arrangement

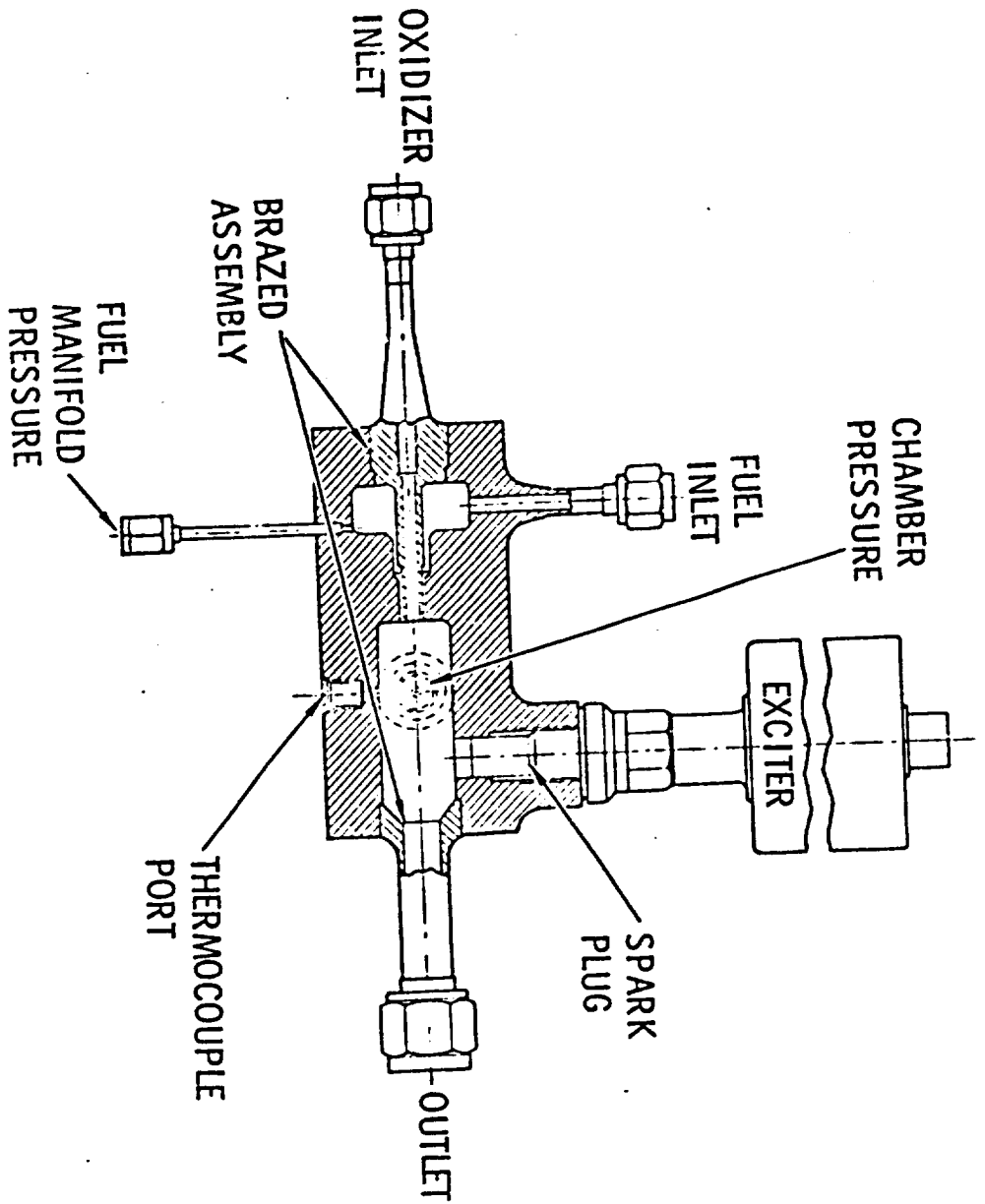


Figure 19. Test Bed No. 2 Premixed With Miniaturized Spark System



Figure 20. Combustion Wave Ignition System Spark Igniter Unit

ICT61-8/24/71-C1

post-cutoff spin and associated interlocks. Also, the introduction at the ASI-type combustion wave ignition system required the addition of several solenoid valves into the system.

The start sequence was initiated by signaling helium control "on" and activating the combustion wave system. After a short delay allowing propellants to flow through the ignition system, sparks are turned on to initiate the combustion wave and the engine start and mainstage start solenoids are activated (main valves begin to open). The sequence is again delayed to allow main chamber ignition (a cutoff is generated if an ignition detect signal is not received), after which turbine spinup is initiated. Gas generator igniters are fired during the spin phase. At the conclusion of a 2.5-second spin, the facility spin system is signaled to shut down and mainstage control solenoid is energized, opening the gas generator and ramping the main oxidizer valve to full open. After several seconds, the mainstage OK pressure switch verifies a mainstage operating mode or generates a cutoff signal if the engine has not reached its mainstage level (see Fig. 21).

The cutoff spin was required to eliminate the "trapped" volumes of oxidizer--a result of the mechanical design of the engine. In its final form, the logic consisted of cutoff re-energizing the facility spin system and initiating an oxidizer manifold purge. The main fuel valve was kept open during this time to keep mixture ratio at a minimum. The expiration of the helium de-energize timer then shut down the spin system and concluded the cutoff phase of engine operation (Fig. 22 ).

General system design was, as stated earlier, basically identical to that of test bed No. 1. Relay logic again proved adequate; redundant and/or two-out-of-three voting solid-state timers provided sequencing. Several diode and resistor failures were encountered, due primarily to interfacing with previous wiring or incorrect wiring installation. Significant problems were encountered interfacing with the facility electronics, due to system wiring saturation from previous programs. With the elimination of these problems, the electrical controls proved 100 percent reliable.

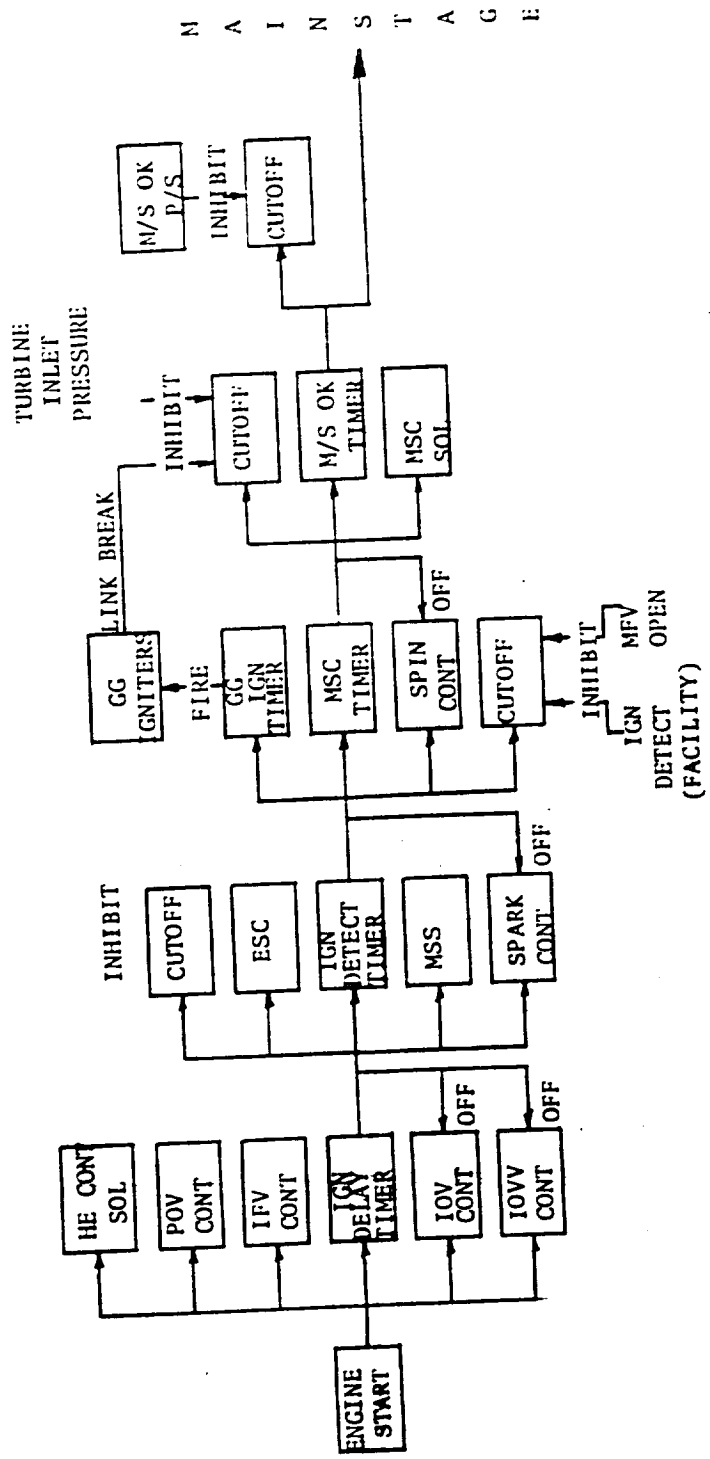


Figure 21. Test Bed No. 2 Start Sequence

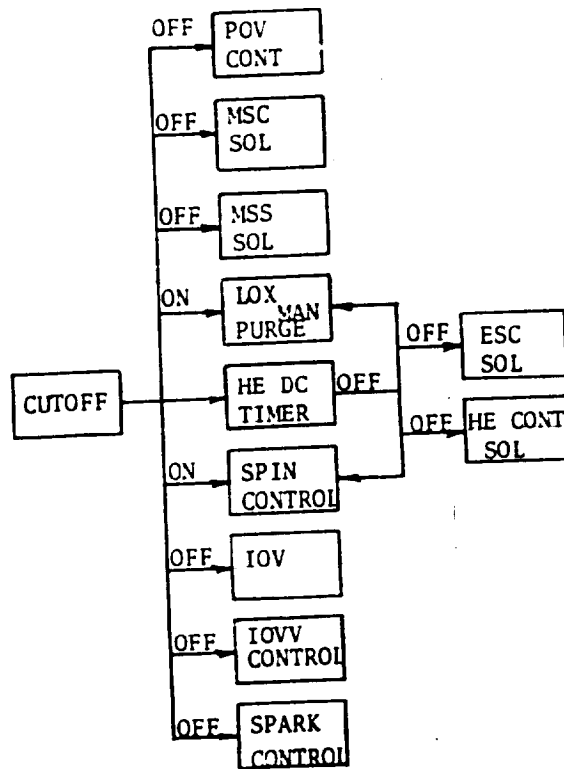


Figure 22. Test Bed No. 2 Cutoff Sequence

## PURGE AND DRAIN SYSTEM

Experience gained during the No. 1 test program was the basis for No. 2 purging, the two systems being almost identical. Where the same purges were required, temperatures and flowrates were not changed though, in some cases, minor sequencing changes were made. Three major differences were introduced: (1) elimination of the fuel manifold cutoff purges, (2) introduction of the post-cutoff oxidizer manifold purge and (3) cutoff use of the ignition system pilot oxidizer manifold purge.

Purging of the main propellant ducts after cutoff was again dictated by the "trapped" volume of oxidizer. However, in the case of the No. 2 engine, i.e., the mechanical design necessitated by gimbal capability, the volume of residual oxidizer was much greater than that on the No. 1 engine cutoff modeling and calculations showed that purging of the fuel manifold, as done on No. 1, would probably result in excessively high mixture ratios and subsequent thrust chamber erosion. Purging of the oxidizer manifold after closing the main oxidizer valve, combined with spinup of the fuel turbopump, provided the only promise of a safe shutdown. This proved to be the case as, in all but one test, this sequence was successful. In one instance, the purge did not activate at cutoff, and extensive nozzle damage resulted.

Ignition system purging was changed only by the addition of the pilot oxidizer manifold purge. This was sequenced with the oxidizer manifold purge and acted primarily to dry the manifold and eliminate any oxidizer at cutoff.

Table 2 shows the final purge sequencing.

Figure 5 shows the pneumatic control system and engine system as a whole. Pneumatic system design was unchanged from test bed No. 1. The J-2S instrumentation package, used in its accumulator capacity only, was replaced by the 200 cu in. bottle used in the J-2X program.

The system operated satisfactorily with no malfunctions.

TABLE 2. PURGE SYSTEMS SEQUENCE OF OPERATION

Purge Parameters		Sequence of Operations			
System	Fluid	Propellant Drop	Engine Start	Spin Start	Cutoff
Turbopumps and Gas Generator Fuel	Helium: 150 ± 25 psig 50 - 150°F	30 min	45 min **		15 min
Fuel Manifold	Helium: 2 Minutes 600 ± 25 psig 100 - 150°F 28 Minutes 150 ± 25 psig 100 - 150°F	2 min	1 min		
Premixer Purge ***	Nitrogen: -78 F Dew Pt. 100 ± 25 psig 25 ± 5 SCFM		Beckman Start		He De-eng
LOX Manifold and Pilot Oxidizer Manifold ***	Nitrogen: 150 ± 25 psig 100 - 150°F Helium: 650 ± 25 psig 100 - 150°F				MFV Closed

\* This two minute pre-purge is only a surge pressure used to blow out any water bridging of the fuel annuli.

\*\* Existing facility plumbing shall dictate maximum pre-purge pressure.

\*\*\* The turbopumps and gas generator purge will be turned on 1 minute prior to engine start as part of Facility Ready, and will be turned off at Spin Start.

\*\*\*\* Purge shall not activate at CUTOFF unless sequence has progressed past GC igniter timer.

## FACILITY MODIFICATIONS - DELTA-2B, SSFL

Facility modifications delineated herein are divided into two main groups: those new to test bed No. 2 and those used on test bed No. 1 and modified to conform to the requirements of the former.

Test bed No. 2, due to the constraints of the turbomachinery, required that a large quantity of propellant and expended hot gas be bypassed so that they would not flow into the main engine combustion systems. To facilitate this, three overboard "dump" systems were installed.

A system was installed to handle the excess oxidizer at a maximum flowrate of 148 lb/sec. This system used the Delta-2A LOX run tank as a "catch tank." This was necessary because of the hazardous condition that would exist if both GOX and large quantities of  $\text{GH}_2$  were expelled within the confines of the Delta area. The oxidizer recovery system was outfitted with a turbine-type flowmeter, orifice, and instrumentation provisions.

Another system, capable of a 41 lb/sec flowrate of  $\text{LH}_2$  was installed to handle the excess fuel. This system was routed under the facility flame deflector and outfitted with a  $\text{GH}_2$  burner system. The exit location and burner were considered safety requirements. This system was also equipped with a turbine-type flowmeter, orifice, and instrumentation provisions.

The third overboard system was installed to handle the excess turbine exhaust gases. Orifice and instrumentation capabilities were provided. A  $\text{GH}_2$  burner system was also installed as a safety precaution against excess accumulation of unburned propellants.

The thrust system was modified to meet the requirements of the facility interface criteria for vertical, pitch, and roll thrust loads. The system was designed for a nominal vertical thrust of 110,000 pounds and a maximum horizontal thrust component of  $\pm 30,000$  pounds. The pitch thrust system consisted of two vertical restraining load cells and flexures attached to the facility thrust plate. The roll thrust

system consisted of two parallel horizontal restraining load cells attached to the facility thrust plate perpendicular to the test bed hinge centerline and one load cell attached to the facility thrust plate parallel to the hinge centerline.

A dynamic thrust vector control system was installed to rotate the thrust chamber as a complete unit about the test bed hinge axis through  $\pm 16$  degrees. An F-1 production hydraulic actuator was used in this system. The existing facility hydraulic system and electronic control systems were modified to support this requirement.

Several existing systems required minor modification to be compatible with test bed No. 2. These included the relocation of the fence coolant water line and  $\text{CH}_2$  spin line interfaces. Also, the hole pattern in the flame deflector was changed, as was the flame deflector blow back shield opening. The electrical control assembly (K-box) was modified to meet the start and cutoff sequence requirements of the test bed. This effort was accomplished at Canoga Park. Instrumentation requirements for the test bed were similar to test bed No. 1 with the exception of the additional overboard dump systems.

## TEST BED INSTALLATION AND CHECKOUT

Test bed No. 2 was received in the Delta area on 23 August 1972. No major problems were encountered during this period of installation and checkout. The minor problems encountered are delineated below.

Relocation of the  $\text{GH}_2$  spin and fence coolant water interface connections were required. Mocking up and final fabrication of the engine LOX and  $\text{LH}_2$  overboard lines were accomplished after the test bed was installed in the test stand.

J-2S inlet ducts were used to interconnect the turbomachinery to the facility. This required a 1-inch spacer to be fabricated and installed on the oxidizer side of the test bed to allow mating with the facility.

Minor clearance problems were encountered with the attaching and the extension/retraction of the gimbal actuator and yoke assemblies. These interferences were relieved by use of shims and some minor cutting away of excess metal on the thrust mount.

Electrical problems encountered during checkouts were limited to the electrical control assembly (K-box). Minor wiring errors were discovered and rectified during electrical system checkouts with no damage to the hardware and little loss of time.

The proper sequencing of the facility overboard dump valves required the changing of the control heads on several of the valves.

Instrumentation requirements were met with no difficulty and no other mechanical or control problems were encountered.

## SYSTEM OPERATION AND PERFORMANCE

### TEST SUMMARY

Thirty-six tests were conducted on test bed No. 2 at the Delta-2B test facility. Thirteen tests were ignition/transition tests, and 23 tests were mainstage tests. The total time of mainstage duration for the test series reached 1199.5 seconds. Major test objectives, conditions, and results are shown in Table 3.

### ENGINE START

The start techniques for the linear test bed No. 2 were defined with the aid of a digital engine transient model. Inputs to the model such as turbine spin time, first-stage main oxidizer valve angle, main propellant valve ramp rates, and hydrogen spin pressure response were varied until acceptable fuel turbopump surge margin and gas generator bootstrap conditions were obtained. Examples of the CRT output from the start model case selected to characterize the test bed No. 2 start sequence are presented in Fig. 23 through 27.

The engine start sequence derived from the start model is presented in Fig. 28. At engine start signal, the helium control solenoid is opened to charge the engine accumulator, and the combustion wave ignition system propellant valves are opened. A 0.6-second ignition delay timer is started to allow sufficient time for the combustion wave and pilot oxidizer manifolds to prime with ignition propellants. Upon expiration of the ignition delay timer, the engine start solenoid and mainstage start solenoids are opened to supply helium pressure to the opening actuators of the main propellant valves, and the combustion wave precombustor is sparked to provide thrust chamber ignition. The combustion wave precombustor oxidizer valve is closed within 50 milliseconds of the spark signal to prevent further combustion in the combustion wave manifold, and an ignition detection timer is initiated. During the 0.8-second detection timer period, the main oxidizer valve opens to the 12 degree position and the main fuel valve ramps fully open. When the ignition stage timer expires and ignition has been detected in all 10 segments, the ignition stage is completed, the precombustor sparks are de-energized, and the spinup stage is enabled.

TABLE 3. LINEAR TEST BED PROGRAM, TEST BED NO. 2 TEST SUMMARY, IGNITION AND START

TEST	DATE	OBJECTIVE	1ST POSITION MOV ANGLE	FUEL PUMP		LOX PUMP IN. PR.	CUTOFF PURGES		COMMENTS
				IN. PR.	IN. PR.		LOX	FUEL	
624-032	10-20-72	LOX BLOWDOWN	10.5°	-	-	39.9 PSIG	YES	NO	LOX INJ. PRESS. TOO HIGH FOR IGNITION M/R OF < 2
624-033	10-23-72	LOX BLOWDOWN	10.5°	-	-	24.8 PSIG	YES	NO	LOX INJ. PRESS. TOO HIGH FOR IGNITION M/R < 2. LOX PURGE FORCES LOX SLUG THROUGH INJECTOR AT CUTOFF
624-034	10-24-72	IGNITION SYSTEM BLOWDOWN	-	-	29.8 PSIG	39.4 PSIG	-	-	PREMIXER LOX INLET PRESSURE TOO HIGH FOR RELIABLE COMBUSTION WAVE GENERATION
624-035	10-25-72	LOX BLOWDOWN	8.5°	-	-	25.7 PSIG	YES	NO	LOX INJECTION PRESS. OK FOR IGNITION M/R OF 1-2. LOX PURGE STILL FORCES LOX SLUG THROUGH INJECTOR AT C/O
624-036	10-26-72	LOX BLOWDOWN	8.5°	-	-	24.7 PSIG	NO	NO	DELETION OF PURGE RESULTED IN GASEOUS OXYGEN THROUGH INJECTOR AFTER C/O
624-037	10-31-72	IGNITION ONLY	8.5°	29.6 PSIG	25.7 PSIG	NO	NO	NO	SUCCESSFUL COMBUSTION WAVE IGN. DETECTED ON ALL 10 SEGMENTS. AVERAGE IGNITION M/R = 1.3
624-038	11-8-72	IGNITION AND FUEL AND OVER- BOARD PROPELL- ANT SPIN	8.5°	29.9 PSIG	25.7 PSIG	YES	YES	NO	SUCCESSFUL IGNITION, SPINUP AND OVERBOARD DUMP. SLIGHT NOZZLE BUCKLING FROM THERMAL STRESSES
624-039	11-10-72	IGNITION, SPINUP AND LOX FEED SYSTEM PRIME	8.5°	29.9 PSIG	25.6 PSIG	YES	YES	NO	SUCCESSFUL IGNITION. PREMATURE CUTOFF CAUSED BY EXCESSIVE SPIN PRESSURE. LOX FEED SYSTEM PRIME NOT ACCOMPLISHED

TABLE 3. (Continued)

TEST	DATE	OBJECTIVE	1ST POSITION MOV ANGLE	FUEL PUMP IN. PR.	LOX PUMP IN. PR.	COMMENTS
624-040	11-16-72	IGNITION AND SPINUP TO LOX DOME PRIME	8.5°	29.9	25.4	2.5 SECOND SPINUP DID NOT RESULT IN LOX DOME PRIME. FTIP = 320
624-041	11-20-72	IGNITION AND SPINUP TO LOX DOME PRIME	9.0°	29.6	26.1	INCREASED MOV ANGLE DID NOT RESULT IN LOX DOME PRIME
624-042	11-20-72	IGNITION AND SPINUP TO LOX DOME PRIME	9.0°	29.8	26.1	SPIN TIME INCREASED TO 2.8 SEC FTIP INCREASED TO 360 LOX DOME PRIME ACCOMPLISHED
624-043*	11-28-72	PARTIAL TRANSITION	9.0°	29.6	26.0	G.G. BOOTSTRAP ACCOMPLISHED G.G. UNDERPRESSURE CUTOFF AT 225 PSIG. REDLINE RESET TO 150 PSIG FOR NEXT TEST

\*TEST 624-043 COMPLETED THE IGNITION AND START SERIES OF THE TEST PLAN

TABLE 3. (Continued)

MAINSTAGE TEST SUMMARY

TEST	DATE	OBJECTIVE	INTENDED DURATION, SEC	ACTUAL DURATION, SEC	AVERAGE PC/M.R. CUTOFF	TYPE OF CUTOFF	COMMENTS
624-044	11-29-72	MAINSTAGE NULL, PU	5.0	5.0	760/3.0	PROGRAMMED	ALL OBJECTIVES OBTAINED
624-045A	11-30-72	MAINSTAGE 5 SEC NULL 10 SEC MAX	15.0	0	-	NO IGN. DETECT #1 COMBUSTOR	FAULTY FIT THERMOCOUPLE
624-045B	11-30-72	MAINSTAGE 5 SEC NULL 10 SEC MAX	15.0	0	-	PREMIXER TEMP EXCEEDED 1000F REDLINE PRIOR TO SPARK SIGNAL	COMBUSTION WAVE MANIFOLD IGNITED FROM EXTERNAL T/C EXIT IGNITERS
624-046	12-8-72	MAINSTAGE 5 SEC NULL 10 SEC MAX	15.0	15.0	690/- 984/-	PROGRAMMED	IMPROVED SPIN SYSTEM RESPONSE, EXIT IGNITERS ON AT MS START. NO PREMATURE IGNITION. O/B FLOWMETER DIFFUSERS INSTALLED, BUT O/B FLOWMETERS READ INCORRECTLY. ALL OTHER OBJECTIVES OBTAINED.

TABLE 3. (Continued)

MAINSTAGE TEST SUMMARY

TEST	DATE	OBJECTIVE	INTENDED DURATION, SEC	ACTUAL DURATION, SEC	AVERAGE PC/M.R. CUTOFF	TYPE OF CUTOFF	COMMENTS
624-047	12-12-72	MAINSTAGE 10 SEC NULL 40 SEC MAX	50.0	50.0	779/3.1 1031/3.6	PROGRAMMED	O/B FLOWMETERS STILL NOT READING CORRECTLY. ALL OTHER OBJECTIVES OBTAINED.
624-001	1-3-73	MAINSTAGE 5 SEC NULL 95 SEC MAX	100.0	100.0	744/- 1026/-	PROGRAMMED	SLIGHT EROSIONS IN COMBUSTORS 2 AND 5. FUEL INJECTION TEMPS DID NOT RISE DURING 95 SEC MAX PU.
624-002	1-8-73	SPIN BLOW-DOWN	-	-	-	-	TURBOMACHINERY SPUN UP WITH MAIN PROP. VALVES CLOSED AND OVERBOARD VALVES OPEN. OVERBOARD FLOWMETERS CALIBRATED AGAINST FACILITY FLOWMETERS.
624-003	1-29-73	MAINSTAGE DYNAMIC HINGING ( $\pm 12^\circ$ ) MULTISTEP PU	300	0	-	RLCD	NO IGNITION DETECT COMBUSTOR #3 - FAULTY SENSING ELEMENT
624-004	1-29-73	MAINSTAGE DYNAMIC HINGING ( $\pm 12^\circ$ ) MULTISTEP PU	300	11	790/3.5	OBSERVER	FIRE IN ENGINE AREA

TABLE 3. (Continued)

MAINSTAGE TEST SUMMARY

TEST	DATE	OBJECTIVE	INTENDED DURATION, SEC	ACTUAL DURATION, SEC	AVERAGE PC/M.R. CUTOFF	TYPE OF CUTOFF	COMMENTS
624-005	1-31-73	MAINSTAGE DYNAMIC HINGING ( $\pm 12^\circ$ ) MULTISTEP PU	300	0	-	RLCD	SPIN OVERPRESSURE CUTOFF. REDLINE SET INCORRECTLY
624-006	1-31-73	MAINSTAGE DYNAMIC HINGING ( $\pm 12^\circ$ ) MULTISTEP PU	300	300	700-1030/ PROGRAMMED 3.5-3.9	RLCD	ALL OBJECTIVES ATTAINED - 5 CYCLES DYNAMIC HINGING AT $\pm 12^\circ$
624-007	4-6-73	MAINSTAGE DYNAMIC HINGING ( $\pm 16^\circ$ ) MULTISTEP PU 1 $\frac{1}{2}$ SECONDARY FLOW	500	0	-	RLCD	OPEN THERMOCOUPLE ON FACILITY EXIT IGNITER
624-008	4-16-73	MAINSTAGE DYNAMIC HINGING ( $\pm 16^\circ$ ) MULTISTEP PU 1 $\frac{1}{2}$ SECONDARY FLOW	500	124	700-906/ RLCD 3.1-3.7	RLCD	LOST INSTRUMENTATION ON BUCKET WATER PRESSURE (10 CYCLES $\pm 16^\circ$ HINGING DEMONSTRATED)
624-009	4-25-73	MAINSTAGE DYNAMIC HINGING ( $\pm 16^\circ$ ) MULTISTEP PU 1 $\frac{1}{2}$ SECONDARY FLOW	500	1.8	-	RLCD	OPEN THERMOCOUPLE ON FACILITY EXIT IGNITER
624-010	4-25-73	MAINSTAGE DYNAMIC HINGING ( $\pm 16^\circ$ ) MULTISTEP PU 1 $\frac{1}{2}$ SECONDARY FLOW	500	177	972/4.0 OBSERVER	RLCD	FIRE IN ENGINE AREA AND LOSS OF ENGINE INSTRUMENTATION. 10 CYCLES HINGING $\pm 16^\circ$ ACCOMPLISHED.

R-9049

TABLE 3. (Continued)

MAINSTAGE TEST SUMMARY

TEST	DATE	OBJECTIVE	INTENDED DURATION, SEC	ACTUAL DURATION, SEC	AVERAGE PC/M.R. CUTOFF	TYPE OF CUTOFF	COMMENTS
624-011	6-5-73	MAINSTAGE +70,+70 NOZZLE 3% SECONDARY FLOW	100	100	1013/ 3.92	PROGRAMMED	ALL OBJECTIVES ACHIEVED
624-012	7-12-73	MAINSTAGE +70,+70 NOZZLE 3% SECONDARY FLOW	80	80	925/4.4	PROGRAMMED	ALL OBJECTIVES ACHIEVED
624-013	7-20-73	MAINSTAGE +70,+70 NOZZLE 3% SECONDARY FLOW	60	60	1197/ 5.7	PROGRAMMED	ALL OBJECTIVES ACHIEVED. FULL PU PROGRAM RUN. SEVERE EROSIONS OCCURRED AT MAX PU @ 1200 P.c.
624-014	9-20-73	MAINSTAGE +170,-50 NOZZLE 3% SECONDARY FLOW	100	57.9	998/4.0	OBSERVER	OBSERVER C/O FROM FIRE BELOW NO. 6 COMBUSTOR. NOZZLE FUEL LEAK CAUSED FIRE.
624-015	9-24-73	MAINSTAGE +170,-50 NOZZLE 3% SECONDARY FLOW	100	0	-	NO IGNITION DETECTED	IGNITION OCCURRED BUT SIGNAL NOT RECEIVED

TABLE 3. (Concluded)

MAINSTAGE TEST SUMMARY

TEST	DATE	OBJECTIVE	INTENDED DURATION, SEC	ACTUAL DURATION, SEC	AVERAGE PC/M.R.	TYPE OF CUTOFF	COMMENTS
624-016	9-24-73	REPEAT OF -015	100	0	-	RLCD	ERRONEOUS F/P OVERSPEED 100 NSEC AFTER MS CONTROL
624-017	9-25-73	REPEAT OF -015	100	16	982/3.94	OBSERVER	CUT BECAUSE OF FIRE BELOW NO. 6 COMBUSTOR. NOZZLE FUEL LEAK CAUSED FINE
624-018	10-4-73	MAINSTAGE +17 $\frac{1}{2}$ °, -50 NOZZLE 1 $\frac{1}{2}$ SECONDARY FLOW	100	1.8	-	RLCD	ECA CUT FROM ELECTRICAL PROBLEM IN K-BOX
624-019	10-4-73	MAINSTAGE +17 $\frac{1}{2}$ °, -50 NOZZLE 1 $\frac{1}{2}$ SECONDARY FLOW	100	100	975/4.0	PROGRAMMED	ALL OBJECTIVES ACHIEVED NO HARDWARE DAMAGE

TOTAL TESTS - 36

TOTAL MAINSTAGE TESTS - 23

TOTAL MAINSTAGE DURATION - 1199.5

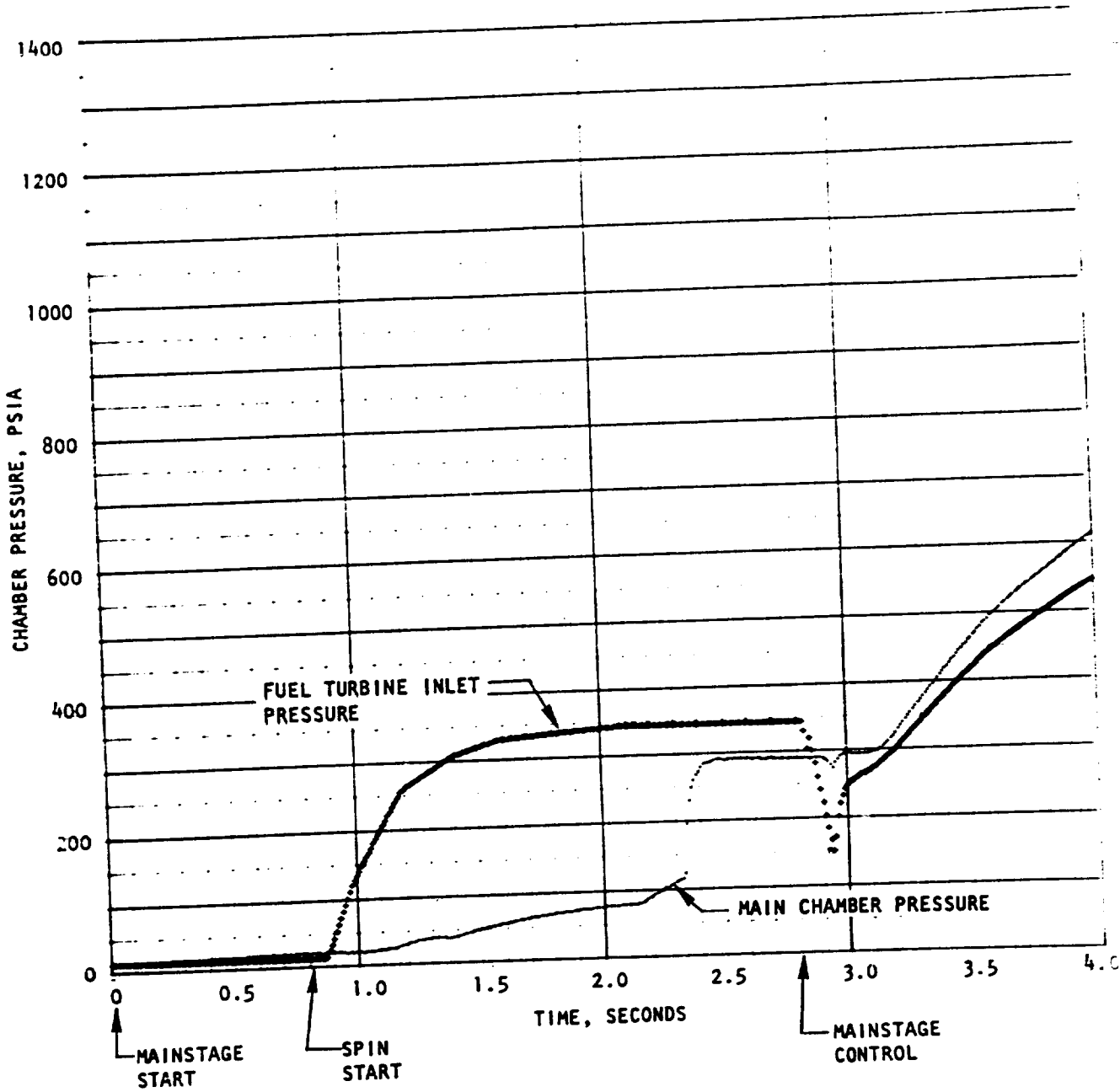


Figure 23. Start Model Chamber Pressure

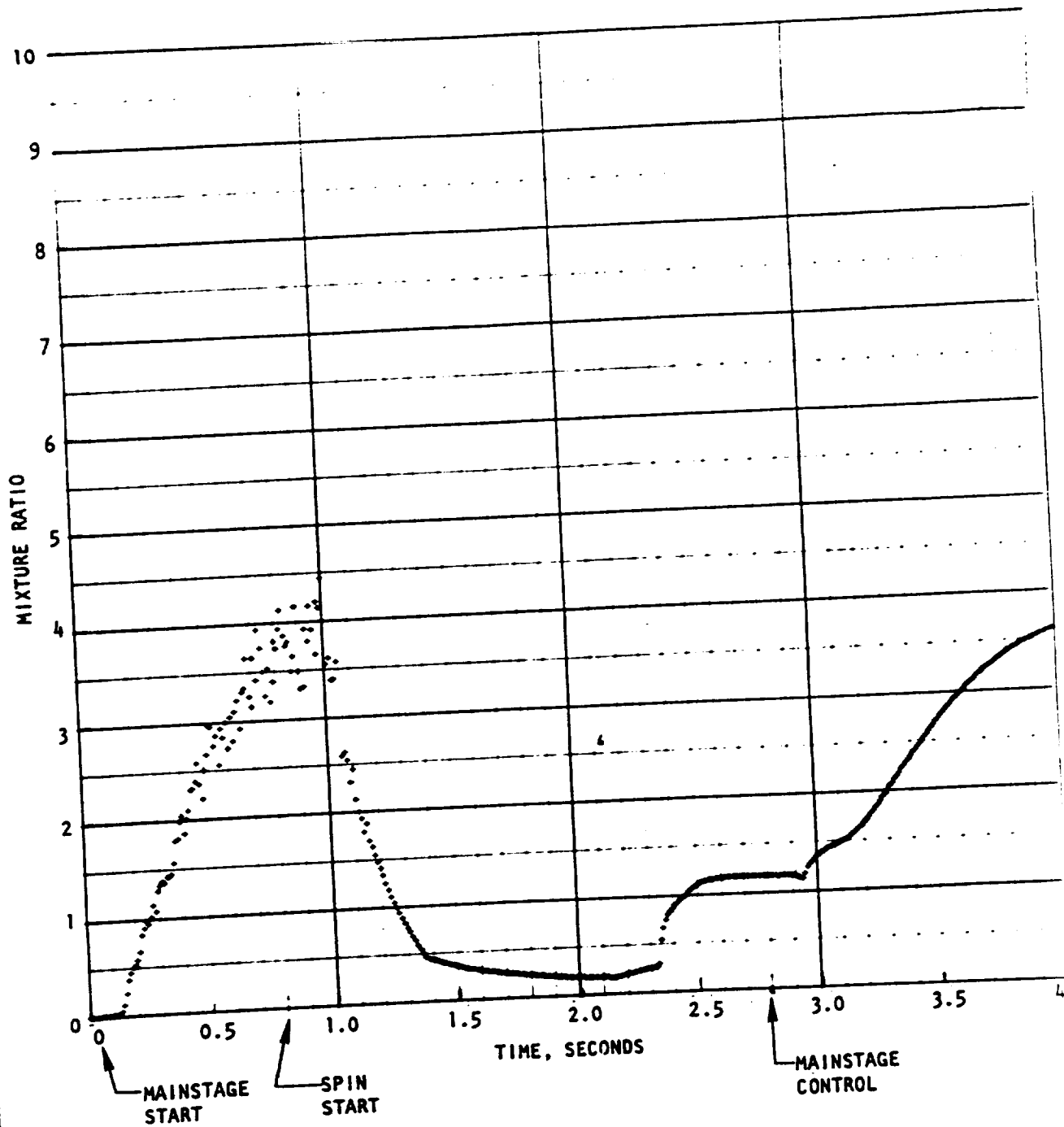


Figure 24. Start Model Thrust Chamber Mixture Ratio

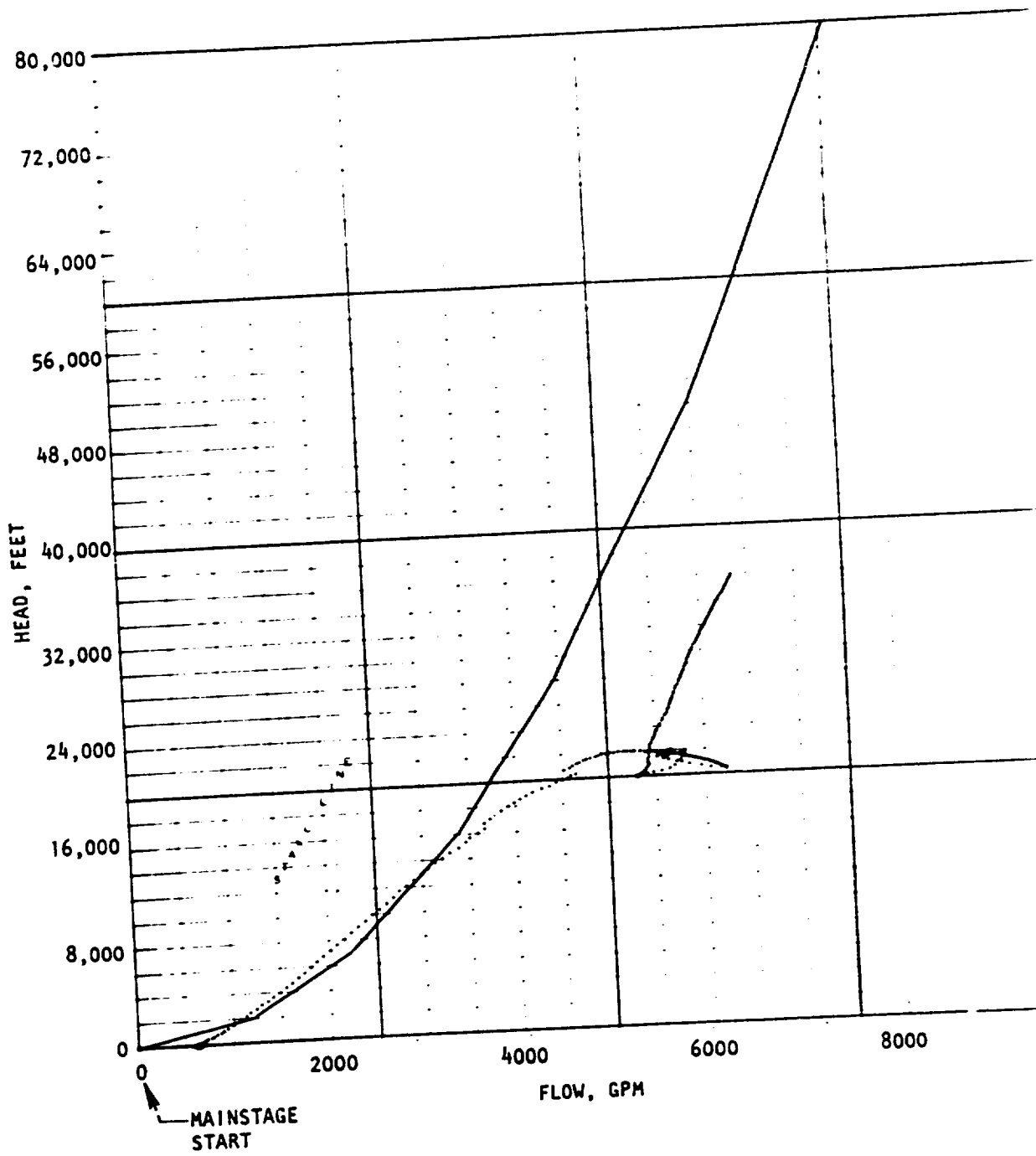


Figure 25. Start Model Fuel Turbopump H vs Q

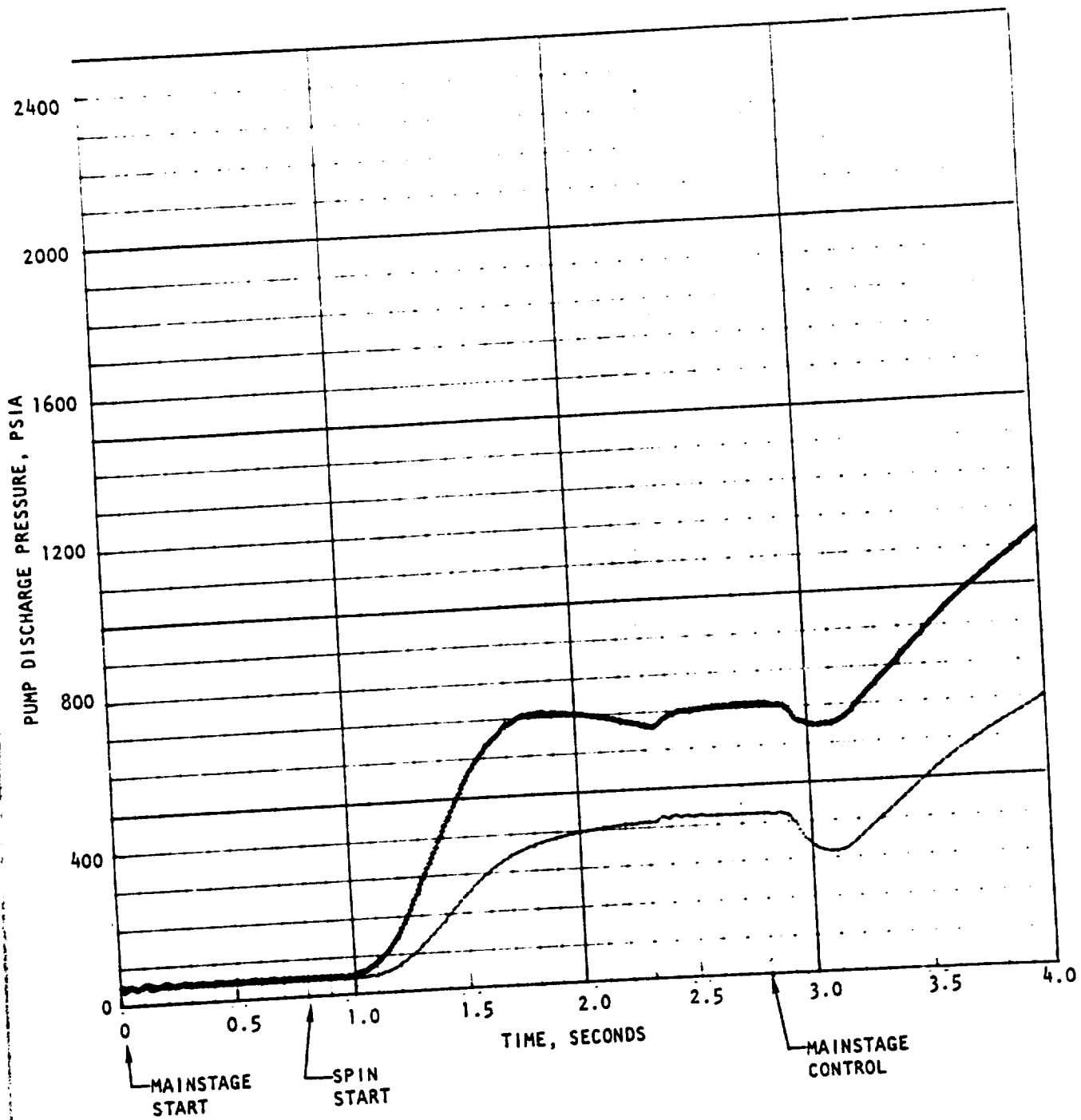


Figure 26. Start Model Pump Discharge Pressures

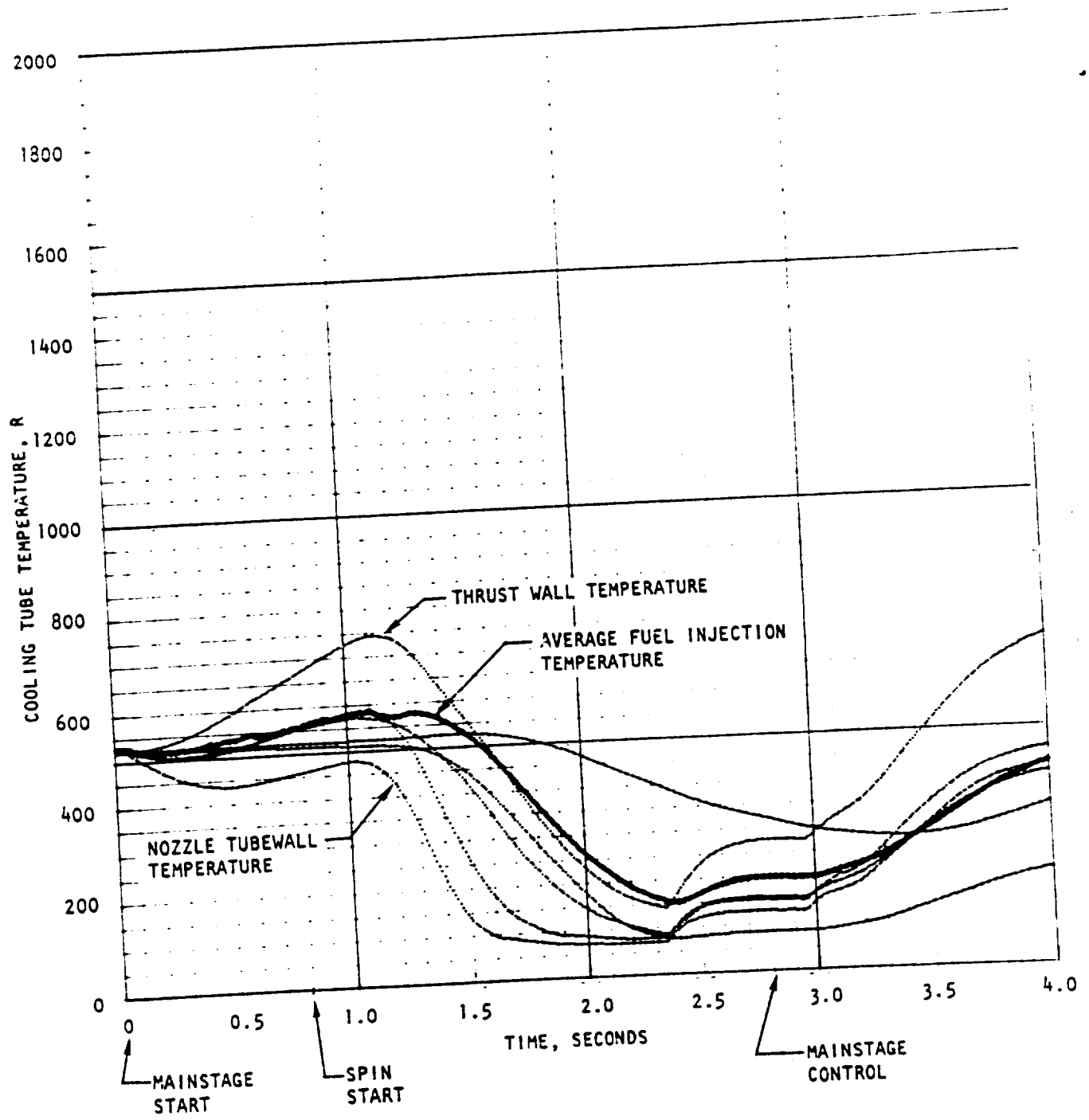


Figure 27. Start Model Fuel Injection and Chamber Gas-Side Wall Temperatures

R-9049

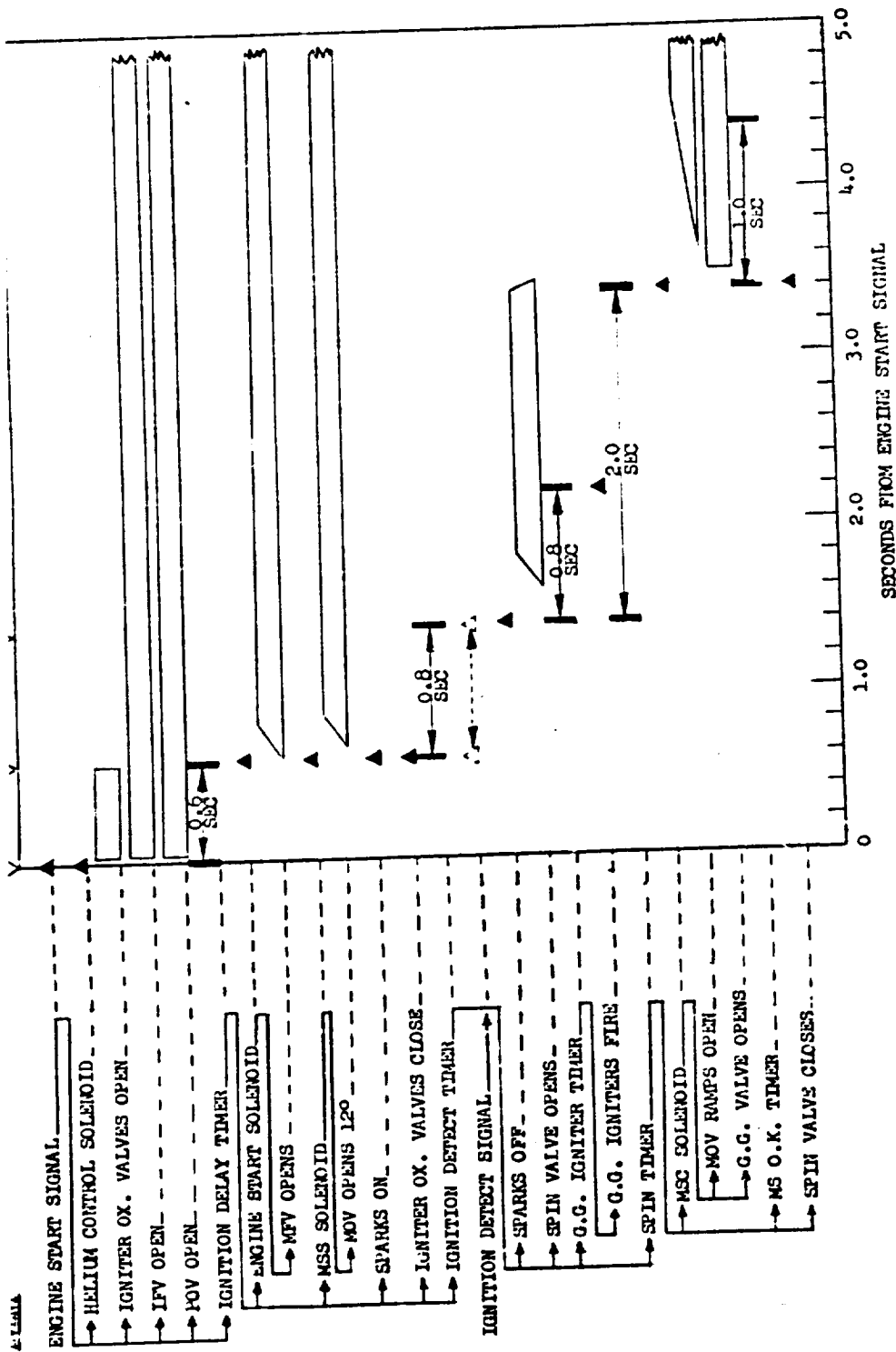


Figure 28. Linear Test Bed No. 2 Start Sequence, Combustion Wave Ignition System

During the spinup stage, the hydrogen spin system valve is opened to supply spin gas to the turbopump turbines, and the spinup stage timer and gas generator igniter timer are started. When the gas generator igniter timer expires, both pyrotechnic igniters in the gas generator combustor are fired. When the spinup stage timer expires, and a link break signal has been received from the gas generator igniters, the secondary buildup stage is enabled.

Secondary buildup is initiated when the mainstage control solenoid opens to supply opening pressure to the second-stage actuator of the main oxidizer valve. The main oxidizer valve ramps to the full-open position, the gas generator propellant control valve opens to bootstrap turbine power, and the hydrogen spin valve is signaled closed. A 1.0-second mainstage OK timer is started and, on actuation of the calibrated pressure switch in the oxidizer pump discharge duct, the engine is allowed to bootstrap into mainstage.

The analytically determined engine start sequence proved successful with a minor modification to spin timer duration. Two-phase flow through the main oxidizer valve during the spinup stage increased the effective resistance of the main oxidizer propellant feed system and necessitated a 0.5-second increase in spin time from the 2.0 seconds anticipated. CRT records of a typical start on test bed No. 2 are presented in Fig. 29 through 32. Engine chamber pressures responded as expected during the start transient (Fig. 30) and diverged in mainstage according to the individual injector and feed line resistances. Fuel turbine inlet pressure dropout on spin valve closure (Fig. 31) was less severe than predicted by the model, and an excellent bootstrap-to-gas generator operation was obtained. The fuel turbine inlet temperature spike at bootstrap was no problem, as predicted.

#### ENGINE CUTOFF

The amount of stored oxidizer in the oxidizer feed system at cutoff for test bed No. 2 is approximately 50 pounds. The stored oxidizer weight per combustor is, therefore, greater on this engine than on test bed No. 1. After a careful

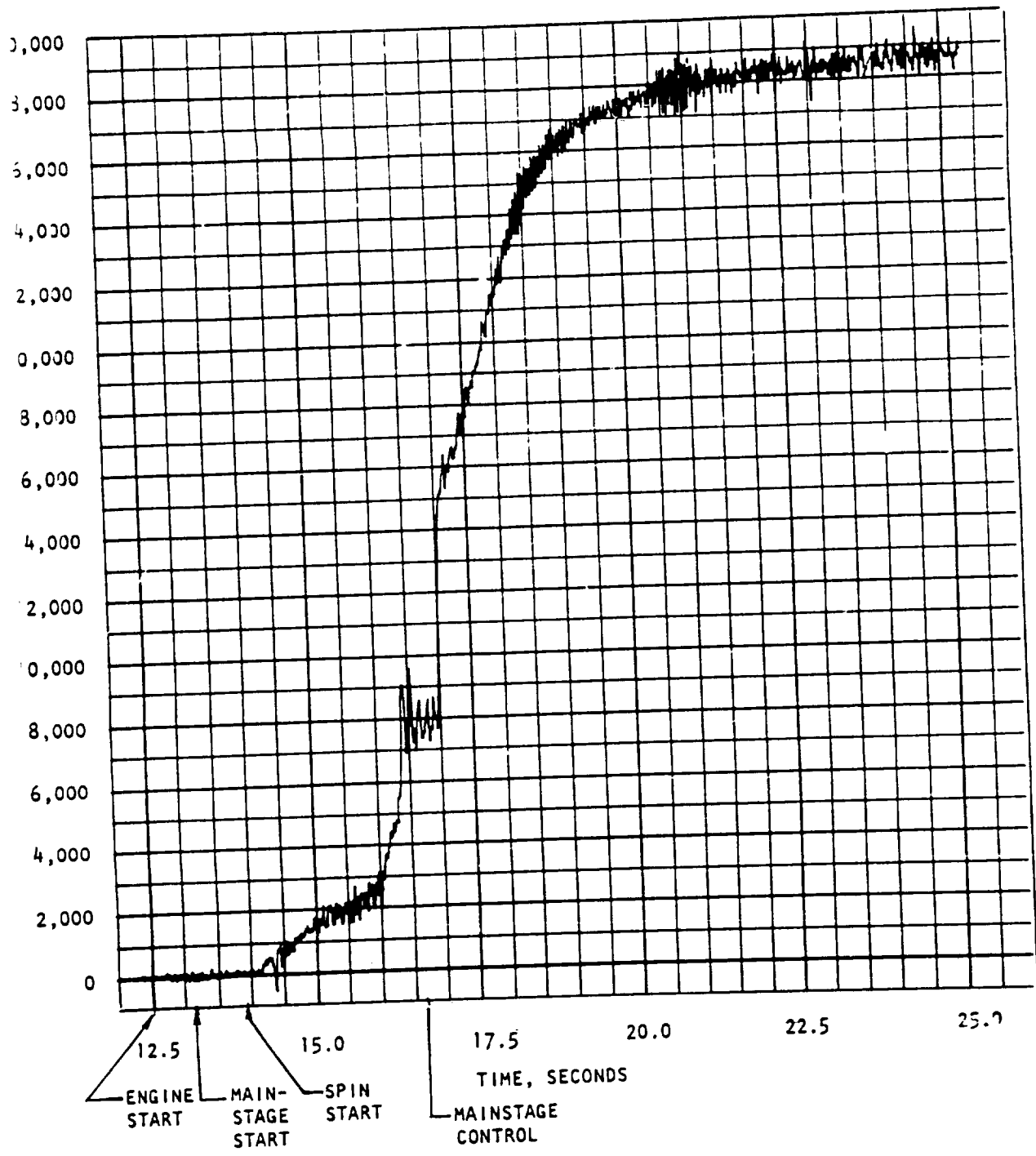


Figure 29. Main Thrust vs Time

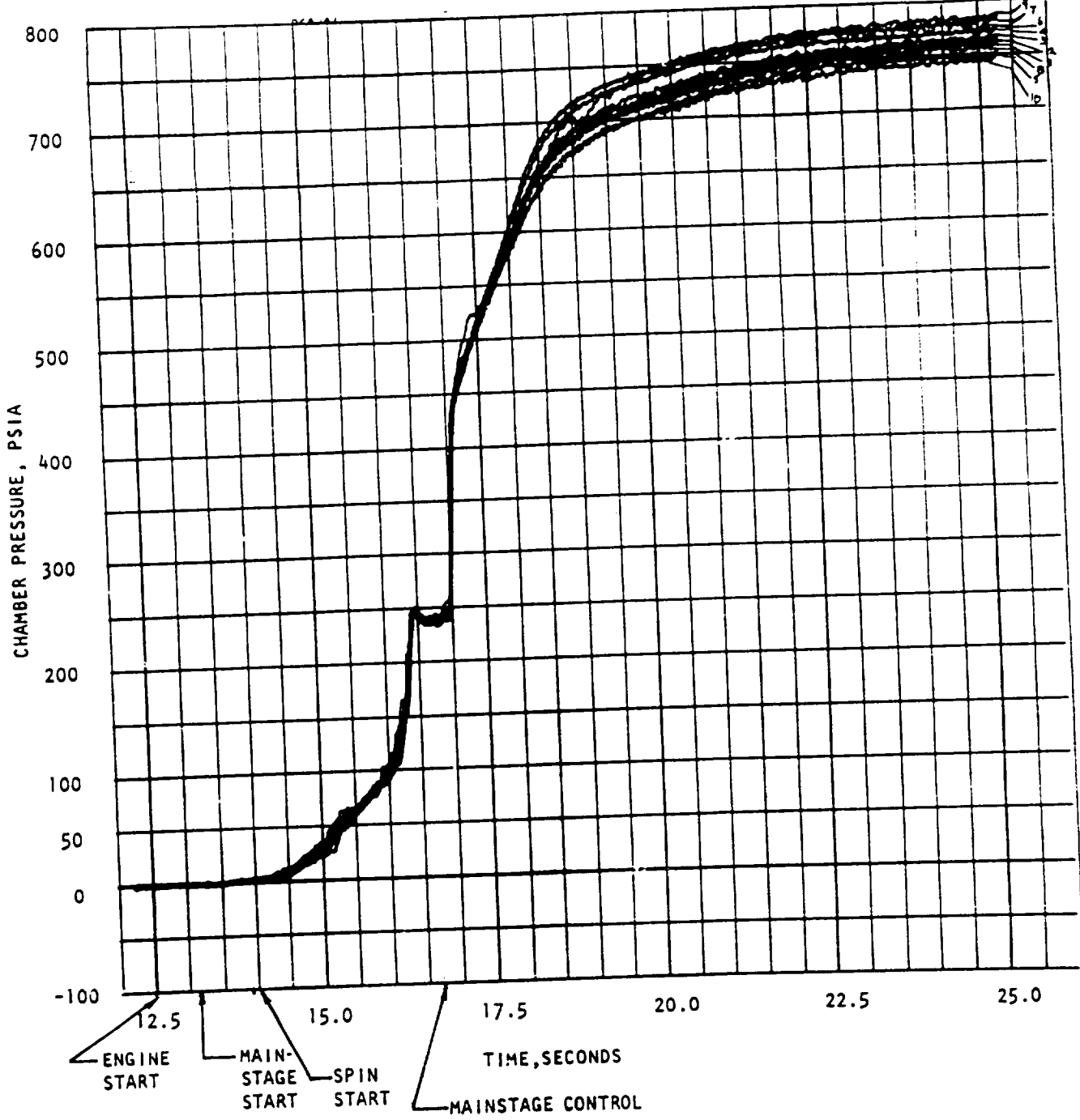


Figure 30. Chamber Pressure vs Time

R-9049

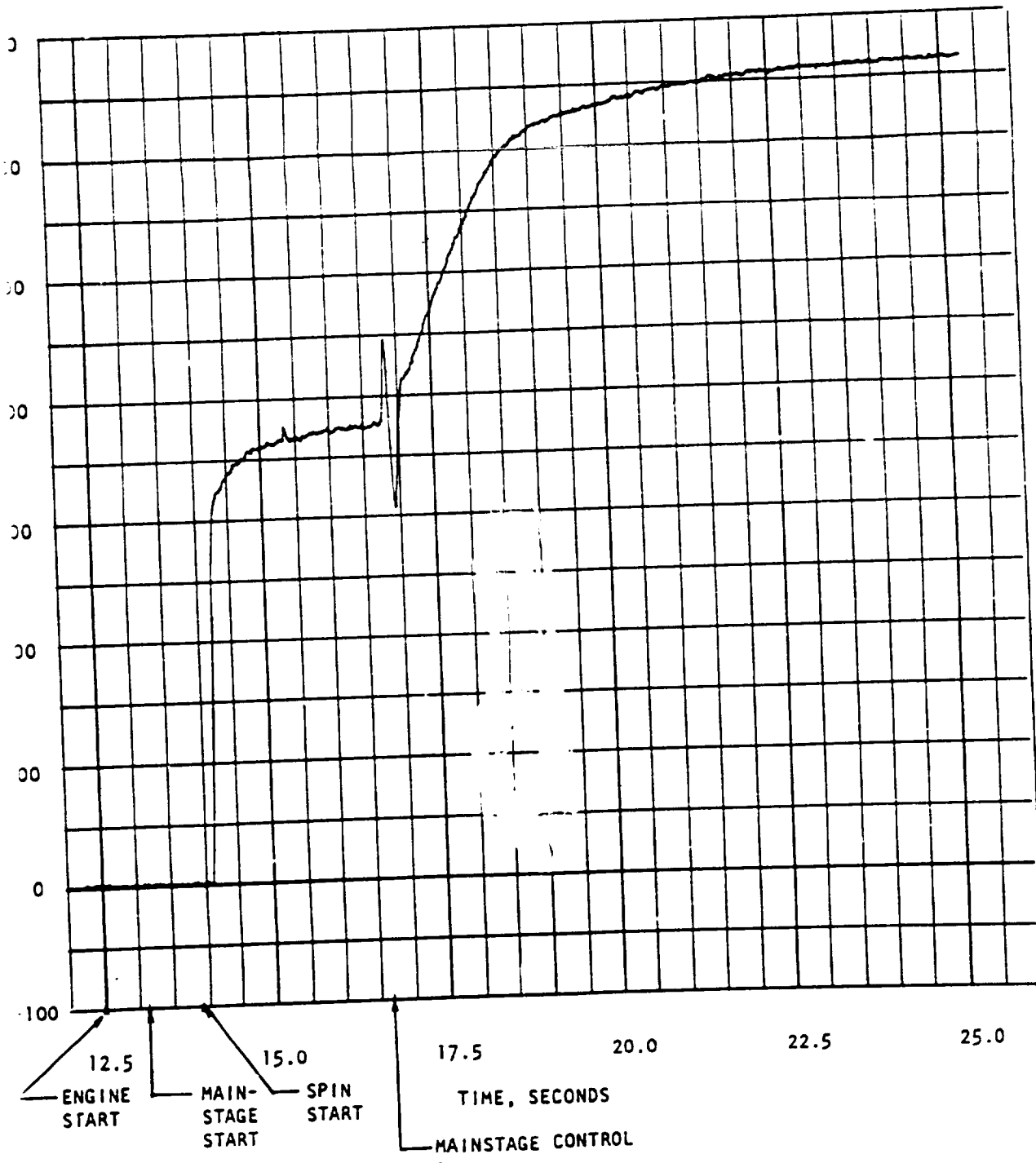


Figure 31. Fuel Turbine Inlet Pressure vs Time

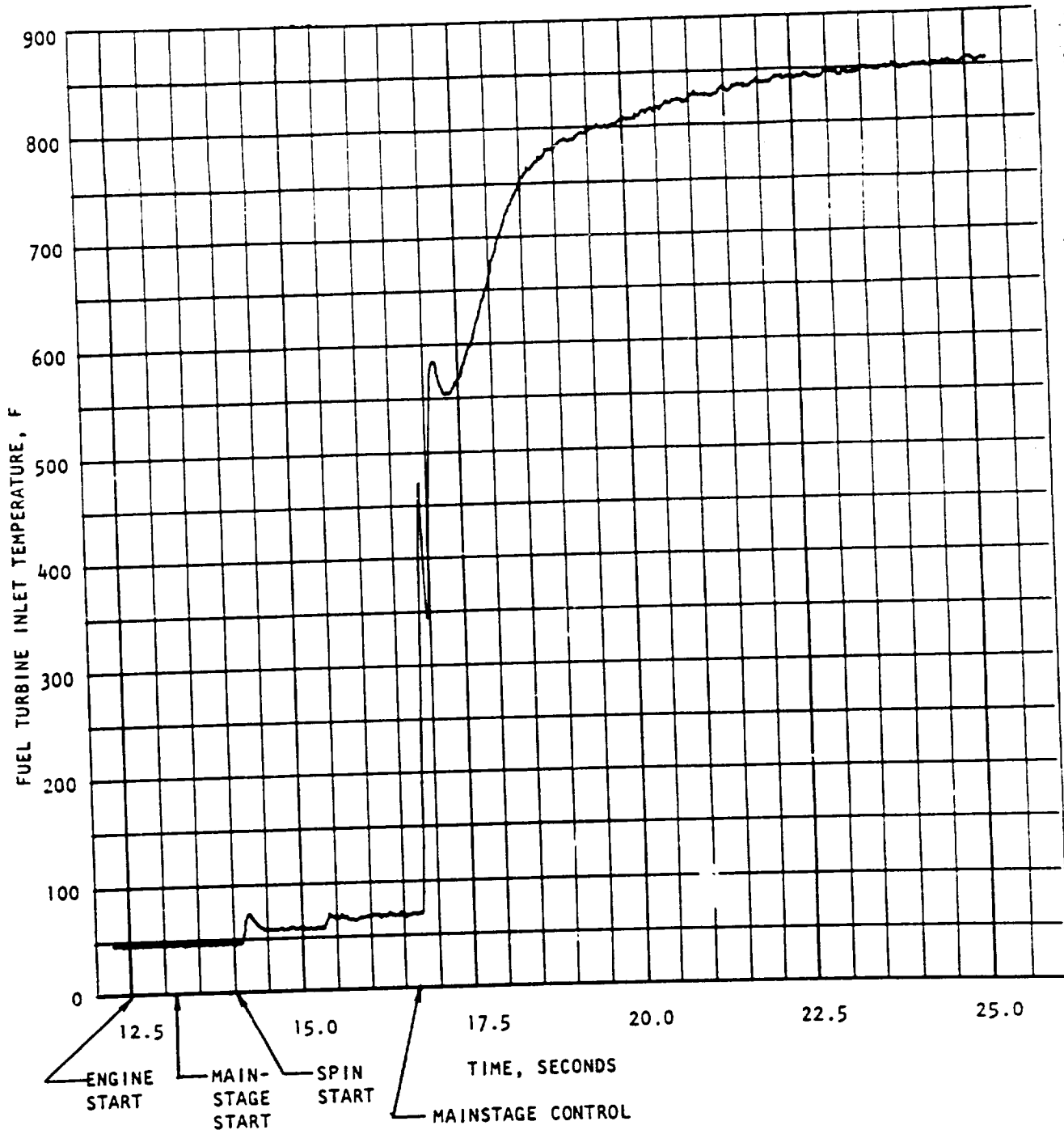


Figure 32. Fuel Turbine Inlet Temperature vs Time

review of fuel injection temperature response at cutoff, high-speed photography, and test-to-test hardware condition on test bed No. 1, it became evident that the massive fuel-side cutoff purge method gradually deteriorated the surface condition of the NARloy combustors. A detailed analysis of various cutoff methods that were less severe and more applicable to flight engines was undertaken using a digital engine cutoff model. The method selected for test bed No. 2 cutoff is a turbopump re-spin with a closed main oxidizer valve and an open main fuel valve. Stored oxidizer downstream of the main oxidizer valve is purged at a controlled rate and burned at low mixture ratio in the combustors. Selected CRT traces from this cutoff model are presented in Fig. 33 through 35. For a fuel turbine inlet spin pressure of 350 psia, and an oxidizer purge flowrate of 5 lb/sec, the resulting main chamber pressure was predicted to be approximately 350 psia (Fig. 33). The thrust chamber mixture ratio (Fig. 34) was predicted to be less than 3.1 during cutoff, and the fuel turbopump (Fig. 35) showed satisfactory flow coefficient recovery following chamber pressure buildup at the initiation of oxidizer purge flow.

The engine cutoff sequence derived from the cutoff model analysis is presented in Fig. 36. At engine cutoff signal, the mainstage start and mainstage control solenoids are de-energized to depressurize both opening control stages of the main oxidizer valve. The main oxidizer valve and gas generator control valve are both closed by solenoid dropout. The cutoff signal also signals the pilot oxidizer valve of the combustion wave ignition system to close, and the hydrogen spin system valve to reopen. Upon main oxidizer valve closure, the oxidizer purge valve opens and stored oxidizer is purged from the engine manifolds. A 2.0-second helium control de-energized timer is started at engine cutoff and, on expiration, the engine start solenoid is de-energized to close the main fuel valve, the igniter fuel valve is signaled closed, and an igniter purge valve is opened. The spin valve is signaled closed at timer expiration, and the oxidizer manifold purge valve is closed after the main fuel valve closes.

Test data from a typical engine cutoff, using the sequence of Fig. 36, is presented in Fig. 37 through 40. Chamber pressure (Fig. 38) was slightly higher than predicted as a result of a higher fuel turbine inlet pressure than modeled (Fig. 39).

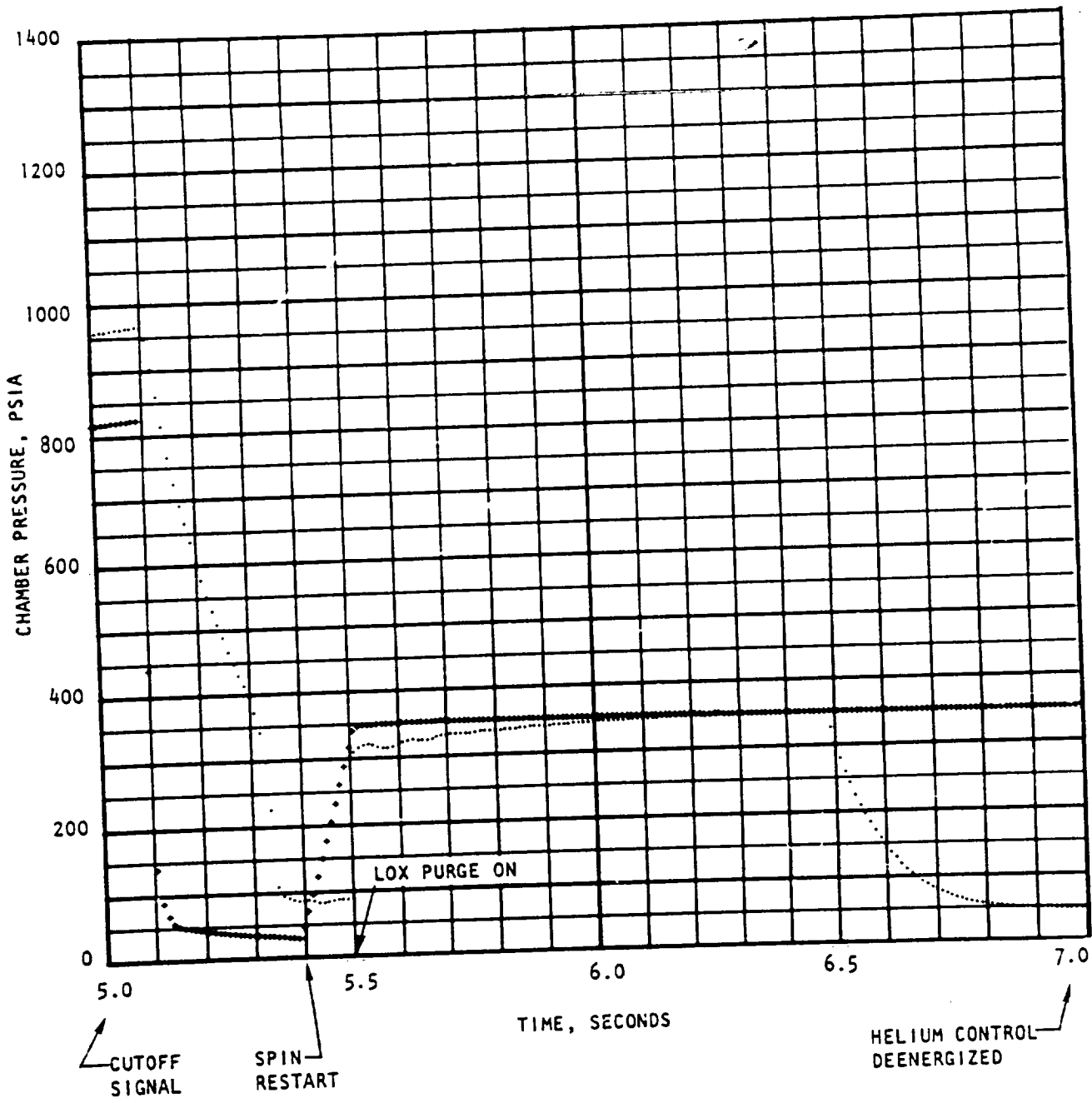


Figure 33. Cutoff Model Chamber Pressure and Fuel Turbine Inlet Pressure vs Time

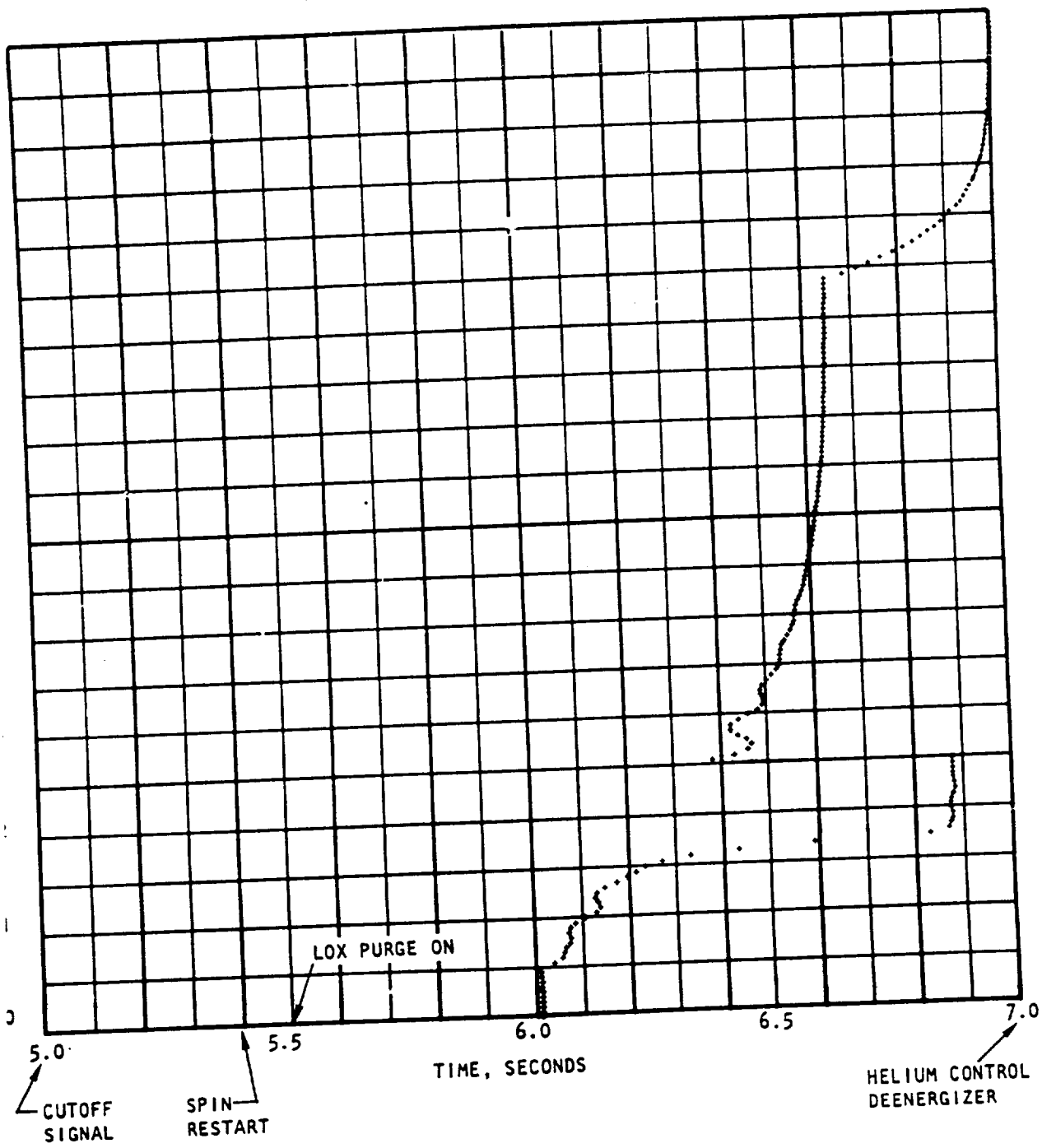


Figure 34. Cutoff Model Mixture Ratio vs Time

R-9049

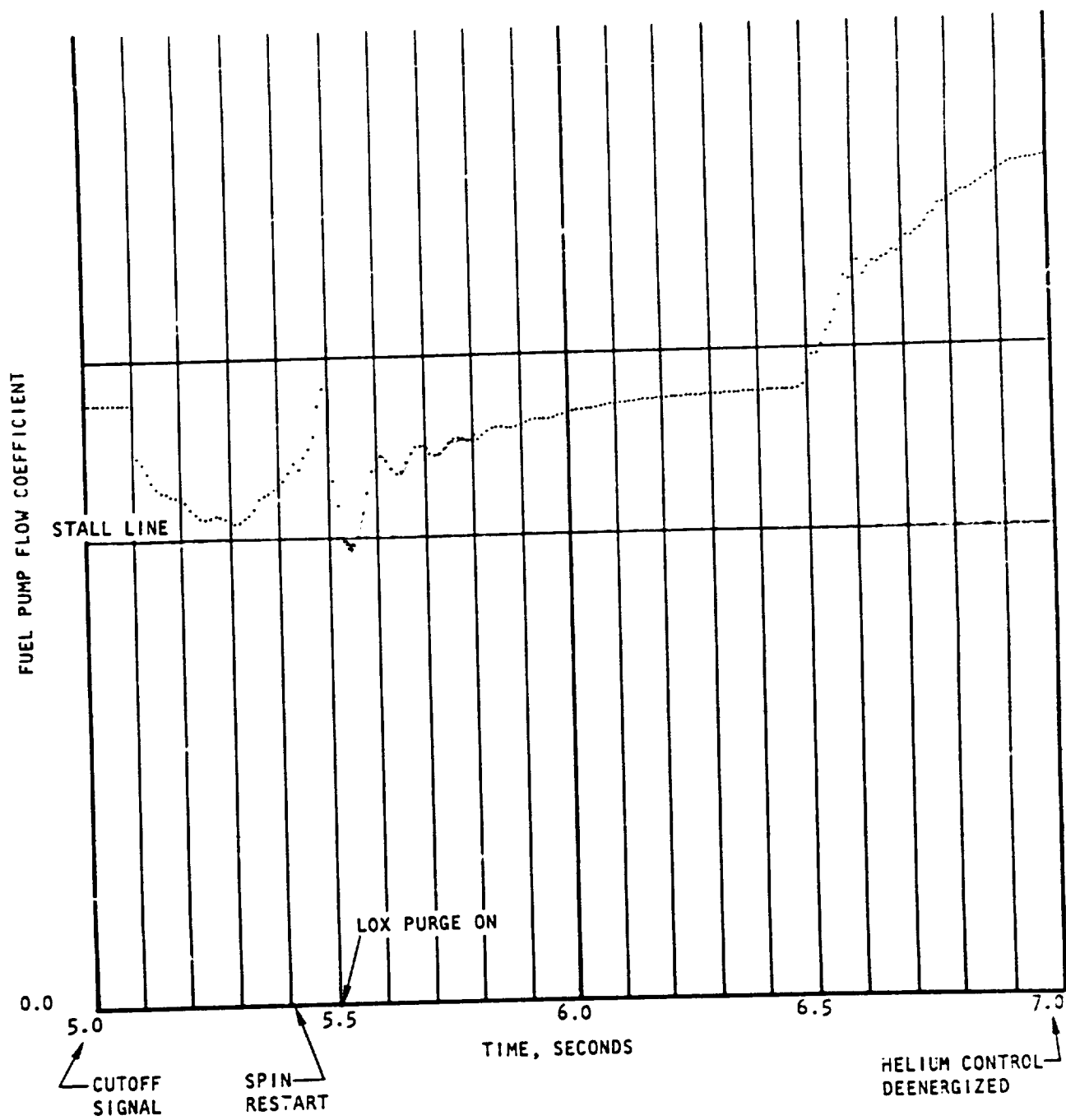


Figure 35. Cutoff Model Fuel Pump Flow Coefficient vs Time

**EVENT**

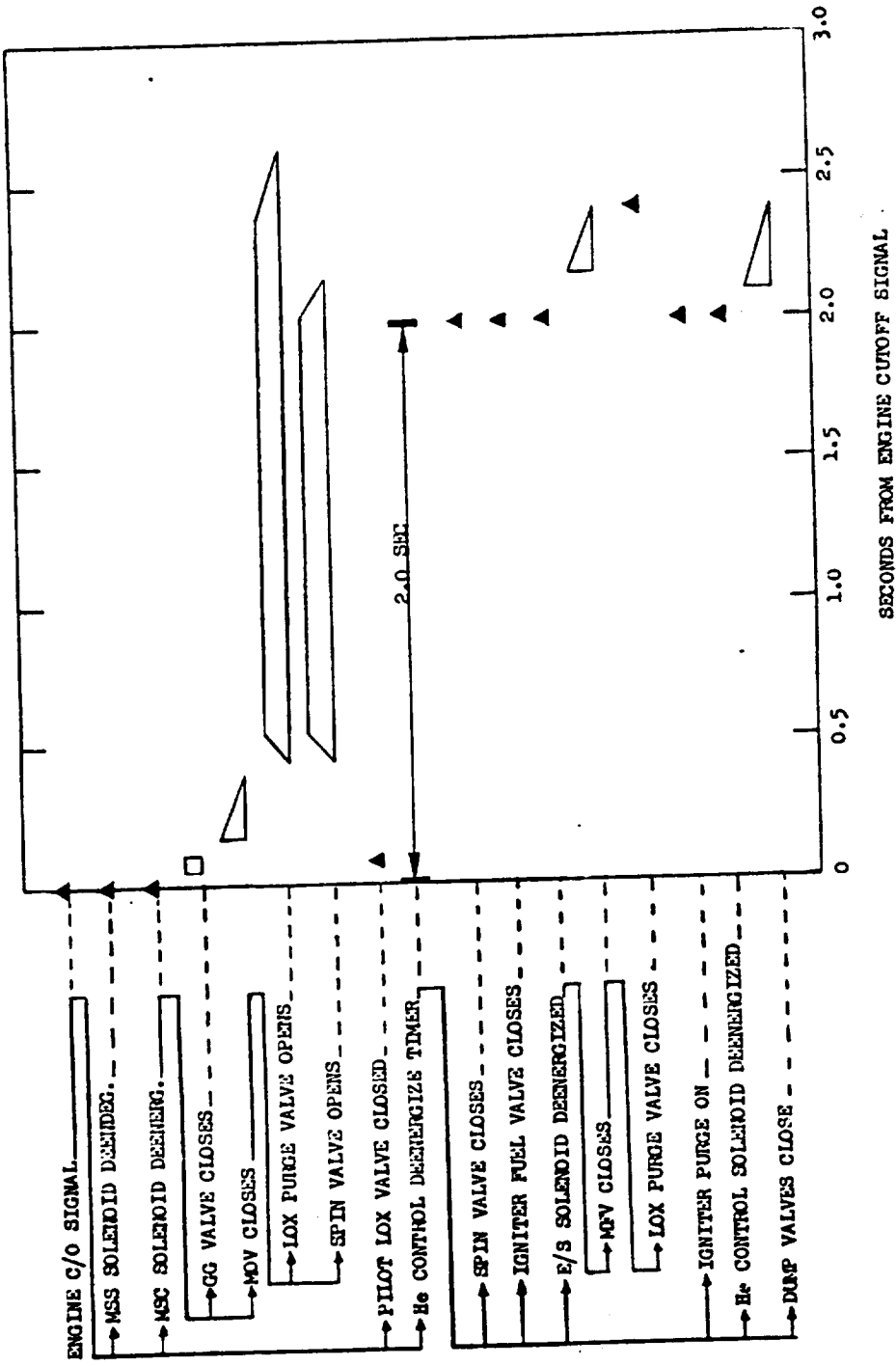


Figure 36. Linear Test Bed Program, No. 2 Test Bed Cutoff Sequence

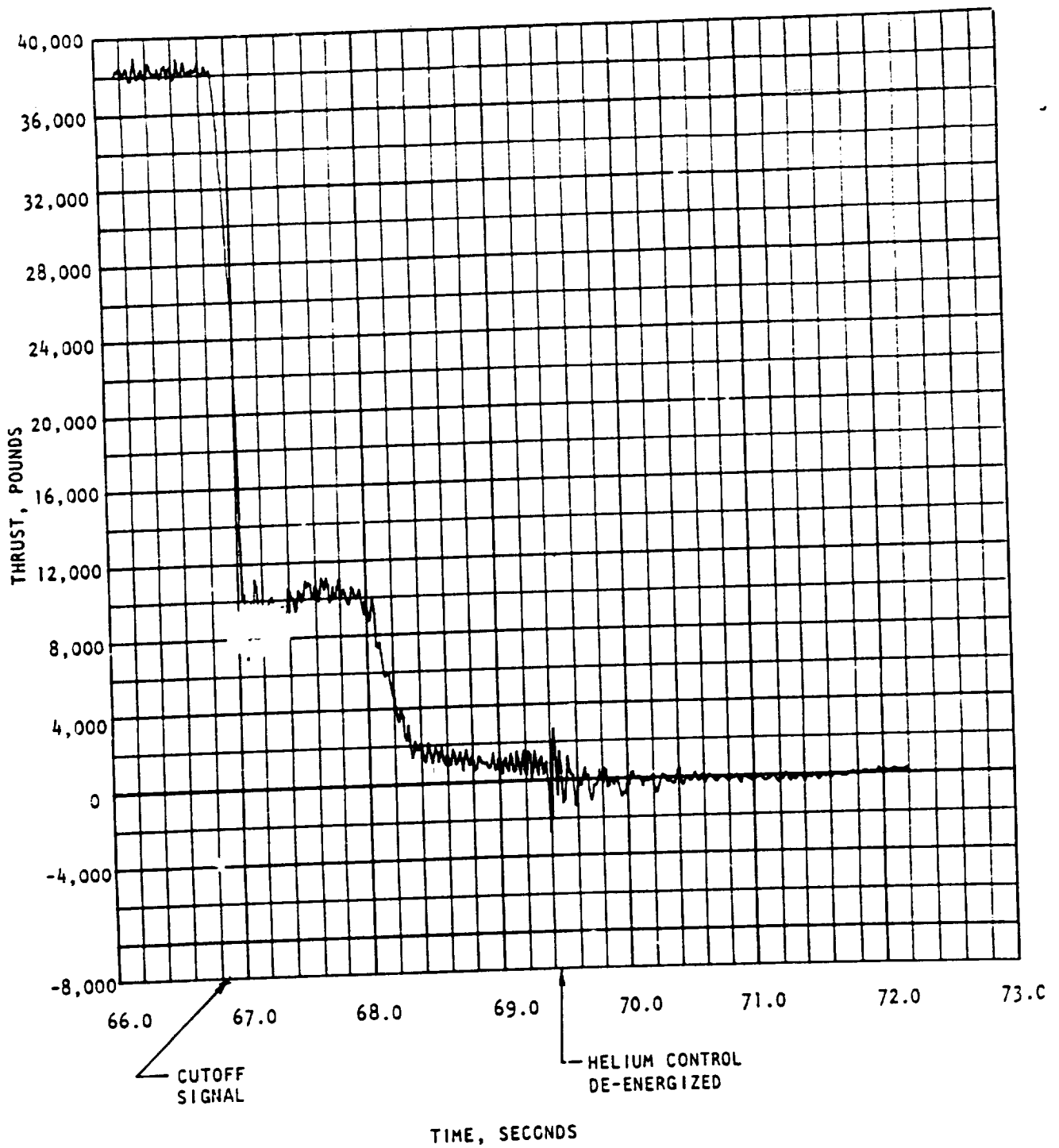


Figure 37. No. 2 Test Bed Cutoff, Main Thrust vs Time

R-9049

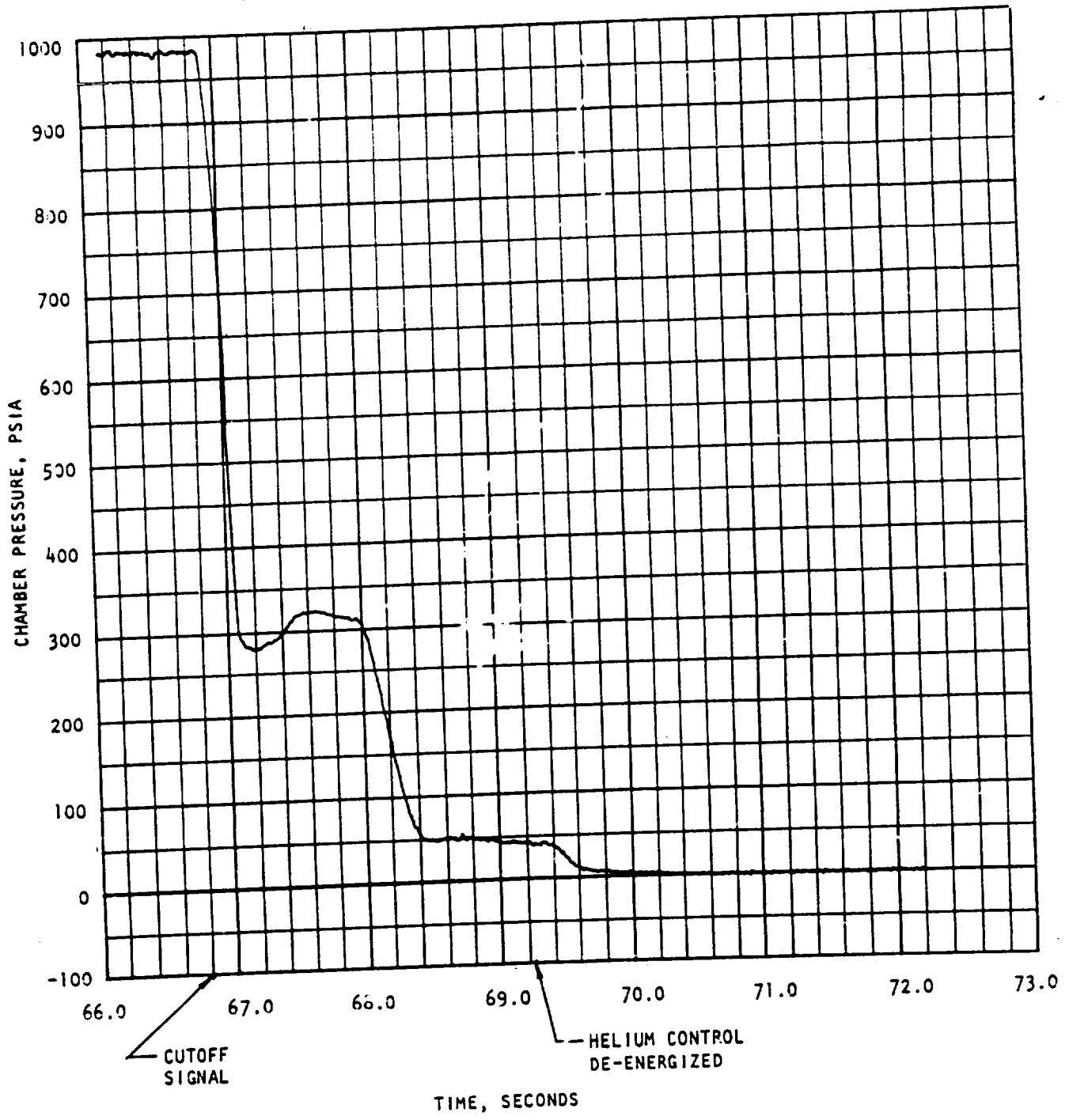


Figure 38. No. 2 Test Bed Cutoff, Typical Chamber Pressure vs Time

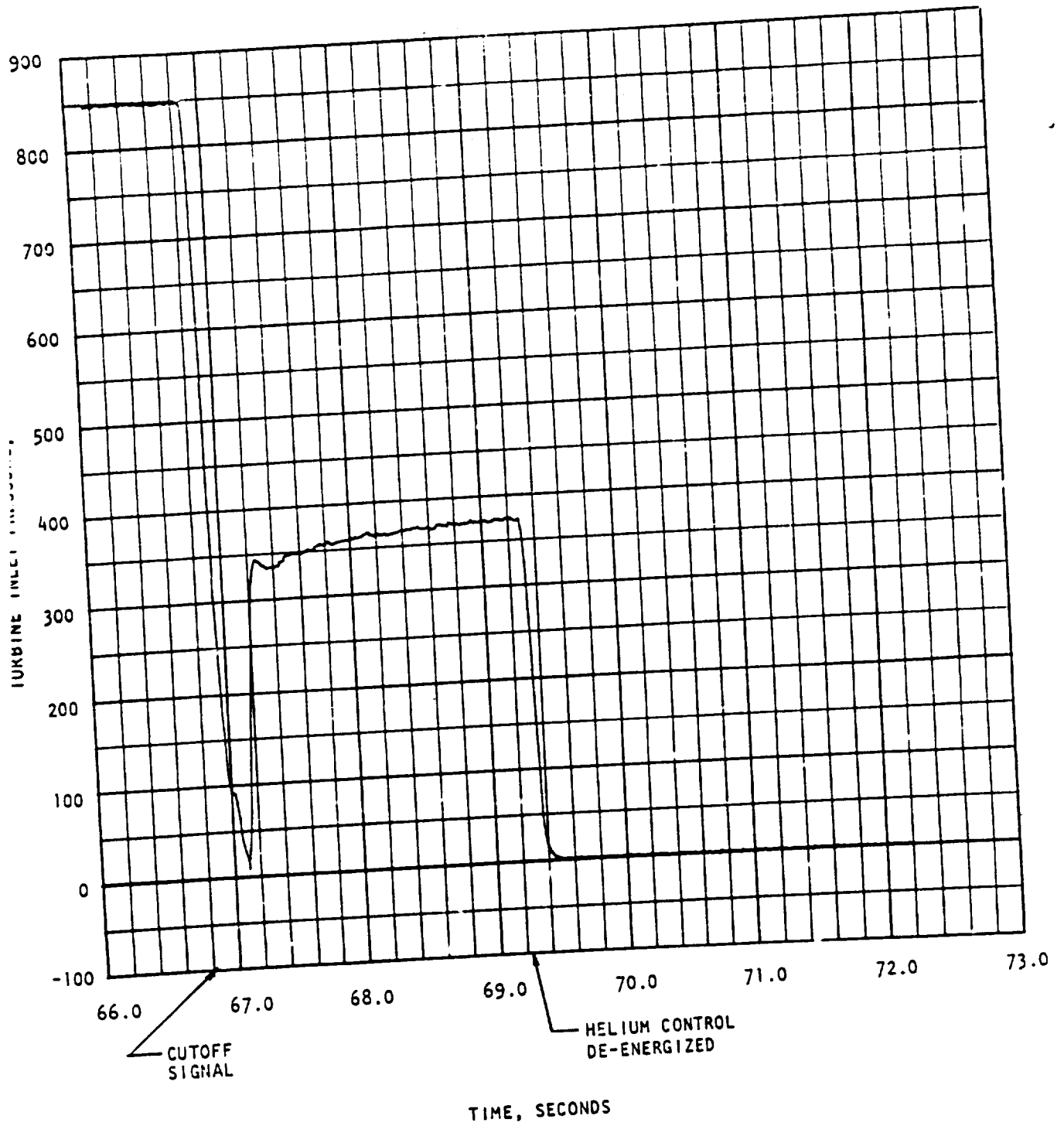


Figure 39. No. 2 Test Bed Cutoff, Turbine Inlet Pressure vs Time

R-9049

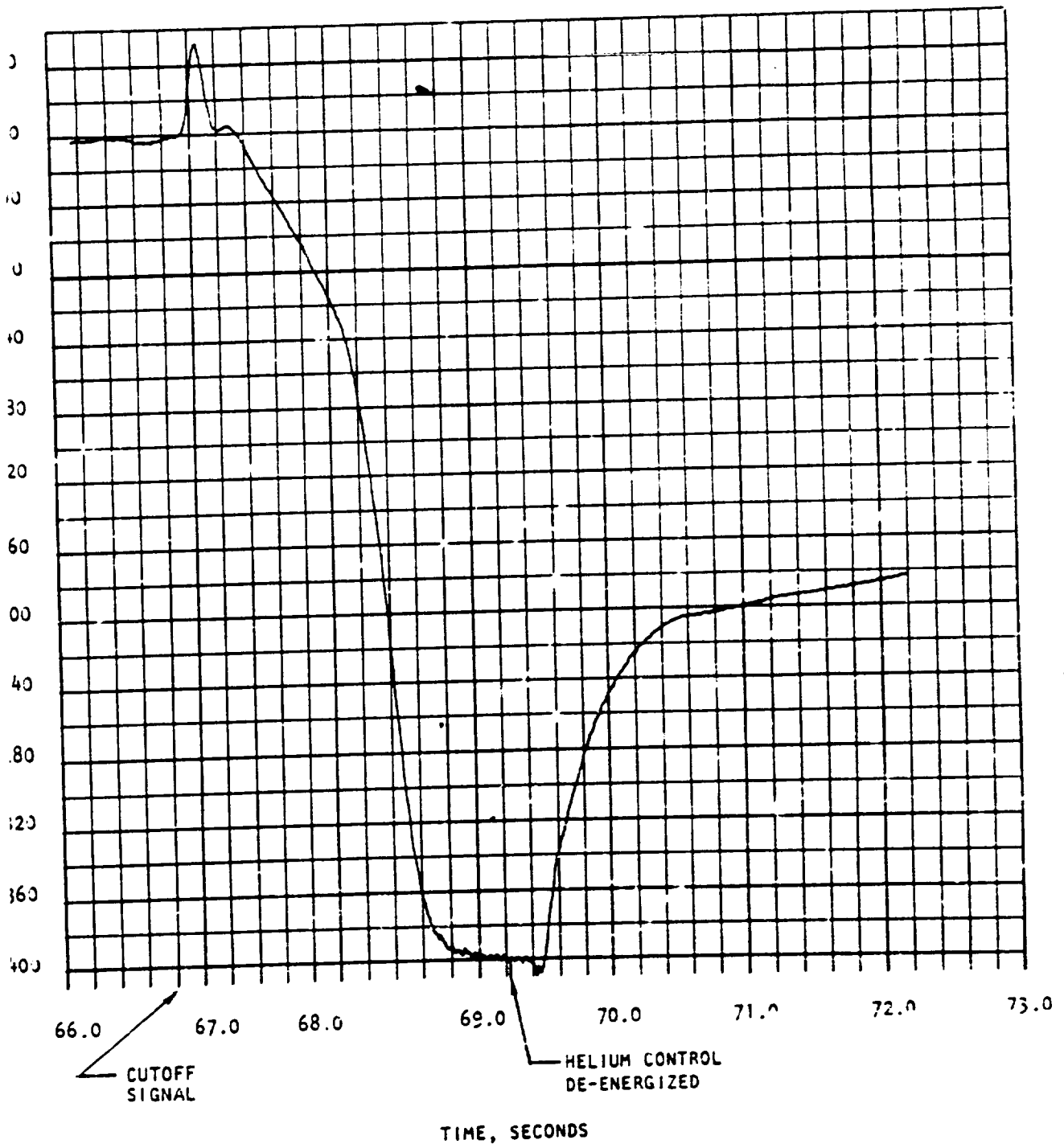


Figure 40. No. 2 Test Bed Cutoff, Typical Fuel Injection Temperature

Thrust chamber heat flux during cutoff was not excessive, as evidenced by a representative fuel injection temperature (Fig. 40). No evidence of thrust chamber overheating with this cutoff sequence was noted from analysis of the photographic coverage or from posttest hardware examination.

#### IGNITION SYSTEM OPERATION

Ignition system operation is presented in Fig. 41 and described as follows. At engine start, the igniter oxidizer valve (IOV), three-way valve, igniter fuel valve (IFV), and pilot oxidizer valve (POV) are opened allowing tankhead fuel and oxidizer to prime the premixer, the combustion wave manifolds, and the pilot propellant manifolds. After a predetermined time sufficient for priming, the ignition system is energized and a combustion wave is generated through the combustion wave manifold and results in ignition of the pilot propellants at the thrust chamber injector face. The IOV is closed shortly after the spark signal to prevent sustained combustion in the premixer, and the three-way valve is closed to vent the propellant line upstream of the IOV. The three-way valve prevents fuel from the premixer from entering the GG oxidizer line in the event of IOV leakage or malfunction.

During turbine spinup, transition, and mainstage, fuel is allowed to flow through the premixer, combustion wave manifold, and pilot fuel manifold. Pilot oxidizer flow is also maintained during these periods to result in an igniter element mixture ratio of about 1.3 to 2.2 in mainstage depending on the PU position and power level. At engine cutoff signal, the POV is closed. Upon expiration of the helium de-energize timer, the IFV is closed and the igniter premixer purge is activated.

The triaxial element combustion-wave ignition system was successfully tested 30 times (tests 624-037 to -047 in 1972 and 624-001 to -019 in 1973) in conjunction with test bed No. 2. Starting propellant supply pressures to the ignition system were approximately the same for each test. The predicted mixture ratios and propellant flows at start and for several mainstage cases are presented in Table 4.

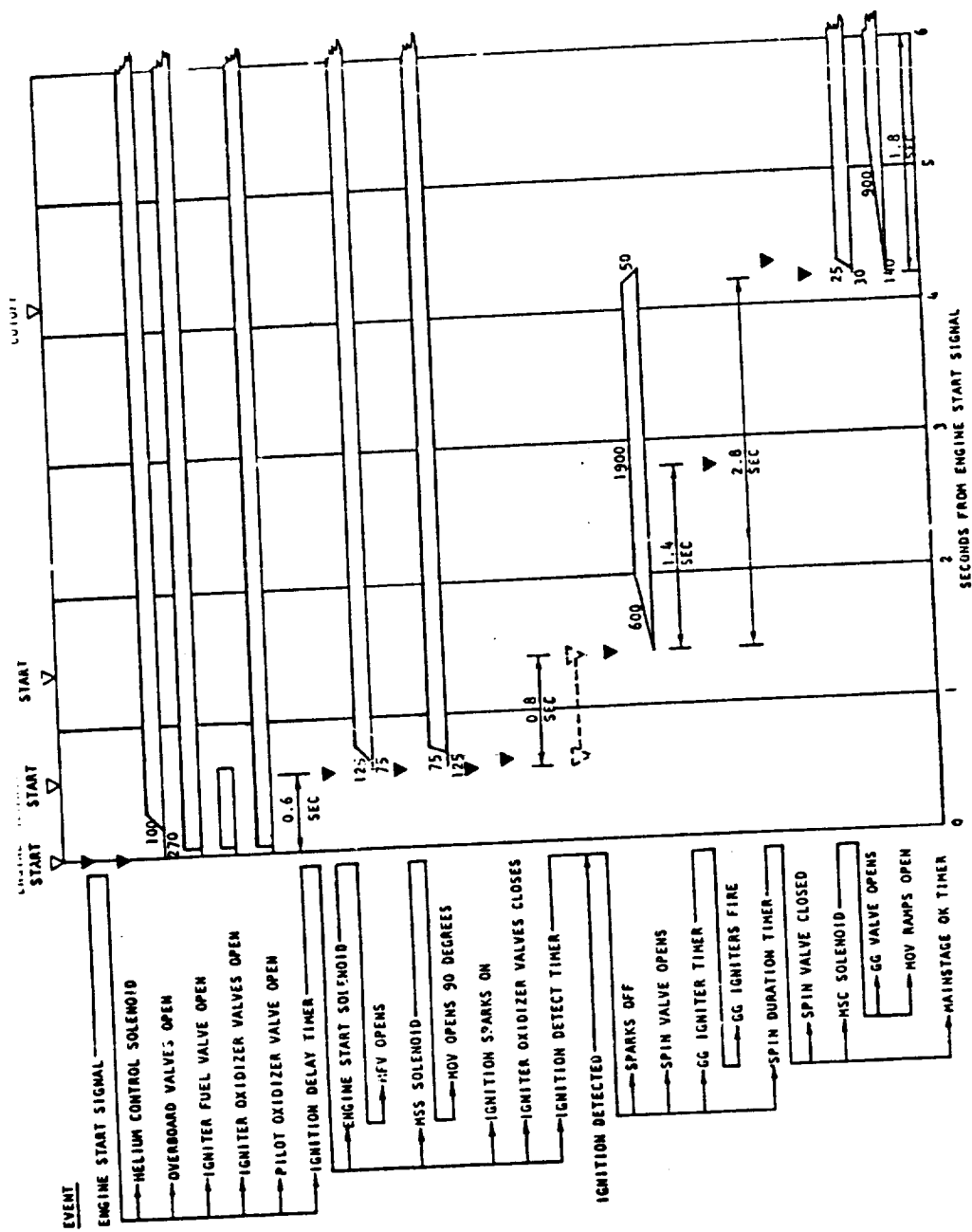


Figure 41. Test Bed No. 2 Low-Power Level Start Sequence

TABLE 4. COMBUSTION WAVE IGNITER MIXTURE RATIOS AND FLOWS

	At Pilot Ignition	At Thrust Chamber Ignition	Maximum PU (1200 P <sub>c</sub> )	Null PU (1068 P <sub>c</sub> )	Maximum PU (900 P <sub>c</sub> )	Null PU (745 P <sub>c</sub> )
<u>Premixer</u>						
Mixture Ratio	12.2	0	0	0	0	0
Total Flow	0.00086	0.0021	0.16	0.18	0.19	0.19
<u>Pilot</u>						
Mixture Ratio	2.6*	2.5	2.2	1.8	1.5	1.3
Total Flow (10 elements)	0.019*	0.022	1.64	1.49	1.40	1.31

\*Does not include pre-mixer flows

These mixture ratio and flow conditions proved to be very satisfactory; however, they could be easily changed if necessary, within a wide operating range by orifice changes and/or by propellant supply pressure changes.

One attempted mainstage test (test 624-045B) was prematurely terminated shortly after the mainstage start signal because an overtemperature redline was exceeded in the combustion wave pre-mixer. This overtemperature condition was caused by premature ignition and burning in the pre-mixer beginning approximately 250 milliseconds before normal spark ignition. The most probable cause for the premature ignition was a "backfire" from the external thrust chamber exit igniters (after-burners). It is postulated that the exit igniters ignited the pilot propellants in at least one segment. The flame then propagated as a deflagration and detonation wave back through the mixed gas combustion wave manifold to the other segments, and to the pre-mixer where premature pilot and pre-mixer ignitions were experienced. On subsequent tests, the exit igniters were not sequenced on until after ignition and no premature ignitions occurred.

## IGNITION DETECTION SYSTEM

The ignition detection system for test bed No. 2 utilized the same system as test bed No. 1, i.e., a slope detection monitor of the main fuel injection temperature of each segment, requiring a "go" signal from all segments. Several tests were prematurely terminated by the failure to receive an ignition OK signal from one or more of the segments. Review of the test data indicated that, in all cases, ignition had actually occurred. The problem with detection seemed to be the sensitivity of the equipment being used and the subtlety of the slope changes in the parameter being monitored.

With this acquired expertise, it was decided to allow any one "go" signal from each of the two sides be enough for continuation of the start sequence.

This modified system performed satisfactorily for all subsequent tests.

## MAINSTAGE PERFORMANCE

Mainstage operation was achieved during 23 tests on test bed No. 2. Most of the tests were conducted at a chamber pressure of approximately 1000 psi and a mixture ratio of 4.0. With mixture ratio excursions, data were obtained at 680-psi chamber pressure and at a 3.1 mixture ratio. Limited testing was conducted at higher levels up to 1200-psi chamber pressure and a 5.7 mixture ratio. Typical performance data at three operating levels which span the test range are presented in Table 5.

## THRUST CHAMBER PERFORMANCE

The thrust chamber characteristic velocity efficiency and specific impulse of test bed No. 2 correlated very closely with that of test bed No. 1, when the scatter in the data was reduced by properly accounting for the variables contributing to the scatter. The thrust chamber performance of test bed No. 1 was published in Volume 1 of R-9049 (Ref. 2). Since then, further analysis of test bed No. 1 data was performed to: (1) reduce data scatter, (2) calculate statistical  $2-\sigma$  deviations,

TABLE 5. LINEAR TEST BED NO. 2 MAINSTAGE PERFORMANCE

Test Number	624-011	624-006	624-013
Slice Time, seconds	90	58	60
<b>ENGINE PERFORMANCE</b>			
THRUST, pounds	53,728	76,070	95,929
MIXTURE RATIO	3.26	3.93	5.62
$I_s$ , seconds	334.45	340.95	339.72
$\dot{\omega}_\phi$ , lb/sec	122.92	177.90	239.75
$\dot{\omega}_F$ , lb/sec	37.72	45.22	42.63
$\dot{\omega}_{TOTAL}$ , lb/sec	160.64	223.12	282.38
<b>THRUST CHAMBER PERFORMANCE (avg)</b>			
MIXTURE RATIO	3.62	4.33	6.34
PRESSURE (INJ), STATIC, psia	721.2	1002.8	1196.6
$C^*$ (INJ)	8264.1	8304.0	7830.3
$\eta_{C^*}$ (NOZZLE)	1.017	1.029	1.023
$\dot{\omega}_\phi$ (TOTAL), lb/sec	119.60	173.28	234.70
$\dot{\omega}_F$ (TOTAL), lb/sec	33.00	40.02	37.04
$\dot{\omega}_{TOTAL}$ , lb/sec	152.60	213.29	271.74
$A_t$ CORRECTED (TOTAL), in. <sup>2</sup>	54.35	54.89	55.27
EXPANSION RATIO (est.)	115.82	115.82	115.82
<b>FUEL PUMP PERFORMANCE</b>			
$P_{INLET}$ (total), psia	43.3	42.7	43.3
$P_{OUTLET}$ (total), psia	1460	1837	1980
$\rho_{INLET}$ , lb/ft <sup>3</sup>	4.416	4.425	4.416
$\rho_{OUTLET}$ , lb/ft <sup>3</sup>	4.555	4.582	4.584
PUMP SPEED, rpm	25,722	29,164	29,966
HEAD, feet	44,171	55,343	59,620
VOLUME FLOW, gpm	7807	8820	8668
WEIGHT FLOW, lb/sec	76.81	86.95	85.28
$\eta$ , percent	0.732	0.715	0.710
REQUIRED HORSEPOWER	8433	12,232	13,013

TABLE 5. (Continued)

Test Number	624-011	624-006	624-013
Slice Time, seconds	90	58	60
<b>OXIDIZER PUMP PERFORMANCE</b>			
$P_{INLET}$ , (TOTAL), psia	45.7	44.9	43.4
$P_{OUTLET}$ , (TOTAL), psia	890	1277	1651
$\rho_{INLET}$ , lb/ft <sup>3</sup>	70.867	70.793	70.993
$\rho_{OUTLET}$ , lb/ft <sup>3</sup>	70.346	70.657	70.976
PUMP SPEED, rpm	7467	9024	10,499
HEAD, feet	1729	2512	3261
VOLUME FLOW, gpm	1410	1886	2371
WEIGHT FLOW, lb/sec	222.63	297.43	375.04
$\eta$ , percent	0.704	0.650	0.669
REQUIRED HORSEPOWER	1422	2167	3434
<b>GAS GENERATOR PERFORMANCE</b>			
$\dot{\omega}_{\phi}$ , lb/sec	3.32	4.62	5.05
$\rho_{\phi}$ , lb/ft <sup>2</sup>	70.867	70.793	70.993
$\dot{\omega}_F$ , lb/sec	4.72	5.20	5.59
$\rho_F$ , lb/ft <sup>2</sup>	4.366	4.364	4.354
$\dot{\omega}_{TOTAL}$ , lb/sec	8.04	9.82	10.64
MIXTURE RATIO	0.703	0.888	0.904
PRESSURE (INJ) (CALC), psia	683.3	890.6	968.7
<b>FUEL TURBINE PERFORMANCE</b>			
$\dot{\omega}_{TOTAL}$ , lb/sec	8.04	9.82	10.63
$P_{INLET}$ , (TOTAL), psia	650	848	922
$P_{EXIT}$ , STATIC, psia	65.6	85.0	105.7
PRESSURE RATIO	9.916	9.976	8.729
$P_{INLET}$ , STATIC, psia	641	836	910
$T_{INLET}$ , F	793.6	1113.2	1139.4
$T_{EXIT}$ , F	487.6	700.8	717.0
DEVELOPED HORSEPOWER	8433	12,232	13,013
$\eta$ , percent	0.600	0.626	0.636

TABLE 5. (Concluded)

Test Number	624-011	624-006	624-013
Slice Time, seconds	90	58	60
OXIDIZER TURBINE PERFORMANCE			
$\dot{W}$ TOTAL, lb/sec	5.28	6.39	9.04
P INLET, (TOTAL), psia	63.1	81.9	102.5
P EXIT, STATIC, psia	33.1	41.4	43.9
PRESSURE RATIO	1.906	1.980	2.333
P INLET, STATIC, psia	61.9	80.4	100.1
T INLET, F	487.6	700.8	717.0
T EXIT, F	436.4	514.8	526.8
DEVELOPED HORSEPOWER	1422	2167	3434
$\eta$ , percent	0.584	0.632	0.581

and (3) correlate data to test bed No. 2. Before discussing results of the data correlations, the results of test bed No. 1 data analysis conducted during this report period to achieve the objectives outlined above are discussed.

#### Characteristic Velocity Efficiency

The characteristic velocity efficiency data of test bed No. 1 had approximately  $\pm 2.25$  percent scatter. The characteristic velocity efficiency is calculated using the equation:

$$c^* = \frac{P_c A_t g}{W c^*_i}$$

where

- $P_c$  = chamber stagnation pressure, corrected for Rayleigh losses and injection momentum
- $A_t$  = measured throat area
- $\dot{W}$  = measured total primary flowrate
- $c^*_i$  = calculated ideal characteristic velocity for propellants at measured inlet conditions of pressure, temperature, and mixture ratio

By far the major source of uncertainty in the above equation is the throat area. The throat area was measured accurately before the start of the hot-firing program. As the hot-firing program progressed, changes occurred in the throat area caused by erosion of the throat and by subsequent polishing of throat surfaces. The largest of these changes occurred after approximately 300 seconds of operating time when a change of approximately 2 percent in throat area due to erosion was estimated. A plot of the parameter  $(\dot{W}/P_c)$  versus accumulated run time in Fig. 42 gives an indication of the change in throat area with time. This parameter is directly proportional to  $A_t/c^*_i$ . If the parameter is limited to a narrow range in  $P_c$ , which automatically limits mixture ratio to a narrow range, the characteristic velocity will be fixed and the parameter  $(\dot{W}/P_c)$  will be a function of throat area only, since no changes occurred in the injector performance with time. As shown in Fig. 42, for the range of chamber pressure of 880-913, the throat area remained practically constant for the first 350 seconds, with a step increase of 1.83 percent before 400 seconds of run time had been accumulated. This agrees closely with estimates made from visual throat observations. After 400 seconds, the parameter  $\dot{W}/P_c$  indicates a gradual 1.91-percent increase in throat area up to the 3000 seconds of total accumulated running time. Flowrate and chamber pressure data random scatter are present in the data in Fig. 42. Data for chamber pressures above 913 psia and below 880 psia also are shown.

The variation of  $(\dot{W}/P_c)$  from its initial value was curve fitted as a function of accumulated running time. This variation was taken as equivalent to the throat area change for each test. Using the pretest measured value, a throat area was

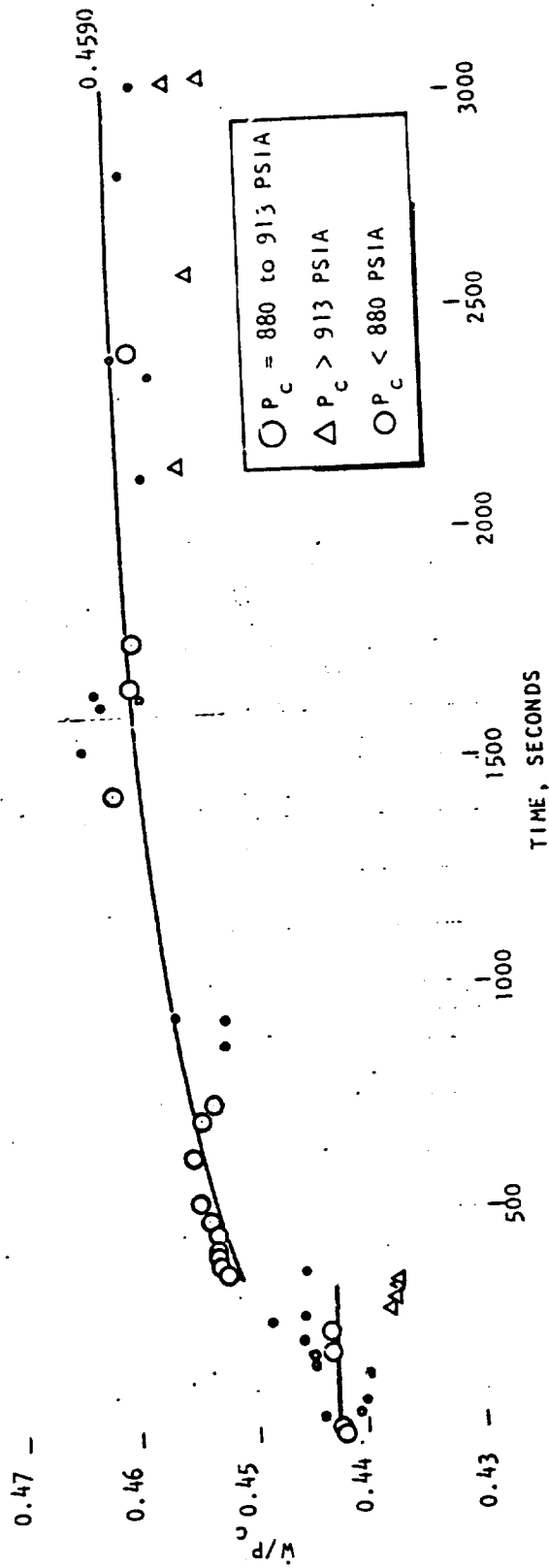


Figure 42. Linear Engine Test Bed No. 1,  $w/P_c$  vs Accumulated Run Time

then calculated for each test. With the new throat area, the characteristic velocity efficiencies ( $\eta_{c^*}$ ) were recalculated and are shown in Fig. 43. The scatter was reduced considerably. A curve fit of the data indicated a variation with mixture ratio as shown by the solid line in Fig. 43, at a constant chamber pressure of 1200 psia. The variation with chamber pressure was less significant than the mixture ratio variation. The equation relating  $\eta_{c^*}$  to chamber pressure ( $P_c$ ) and primary mixture ratio ( $MR_p$ ) is shown in Fig. 43. The calculated 2- $\sigma$  variation for the data in Fig. 42 was  $\pm 0.69$  percent.

It should be mentioned that fuel leaks in the thrust chamber tubes experienced toward the end of the program, tend to increase the value of the ( $W/P_c$ ) parameter and yield a virtual increase in throat area. This is rectified, however, in the calculated  $c^*$  because the uncorrected flowrate is used.

Correlation of test bed No. 1 and 2  $c^*$  data is shown in Fig. 44. As can be seen, the correlation is good because injector and combustor geometry were identical for both units. The larger scatter present in test bed No. 2 data is believed to have been caused by the increased scatter in the flowrate measurement. No attempt was made to reduce data scatter as was done with test bed No. 1 data.

### Specific Impulse

The tests in the beginning of test bed No. 1 test series that showed the least amount of change in throat area with time were selected for determination of engine projected performance. These tests were conducted at chamber pressures ranging from 806 to 1155 psia at primary mixture ratios of 3.83 to 5.98, and at expansion area ratios from 113.5 to 116.7 (since chamber pressure affects the throat area). Each data point was corrected to one set of conditions, i.e.,  $P_c = 1120$  psia,  $MR_p = 5.5$ ,  $\epsilon = 115$ , and  $P_a = 13.77$ . The mean site ( $P_a = 13.77$ ) specific impulse calculated in this manner was 345.5 seconds with a 2- $\sigma$  variation of  $\pm 1.62$  percent.

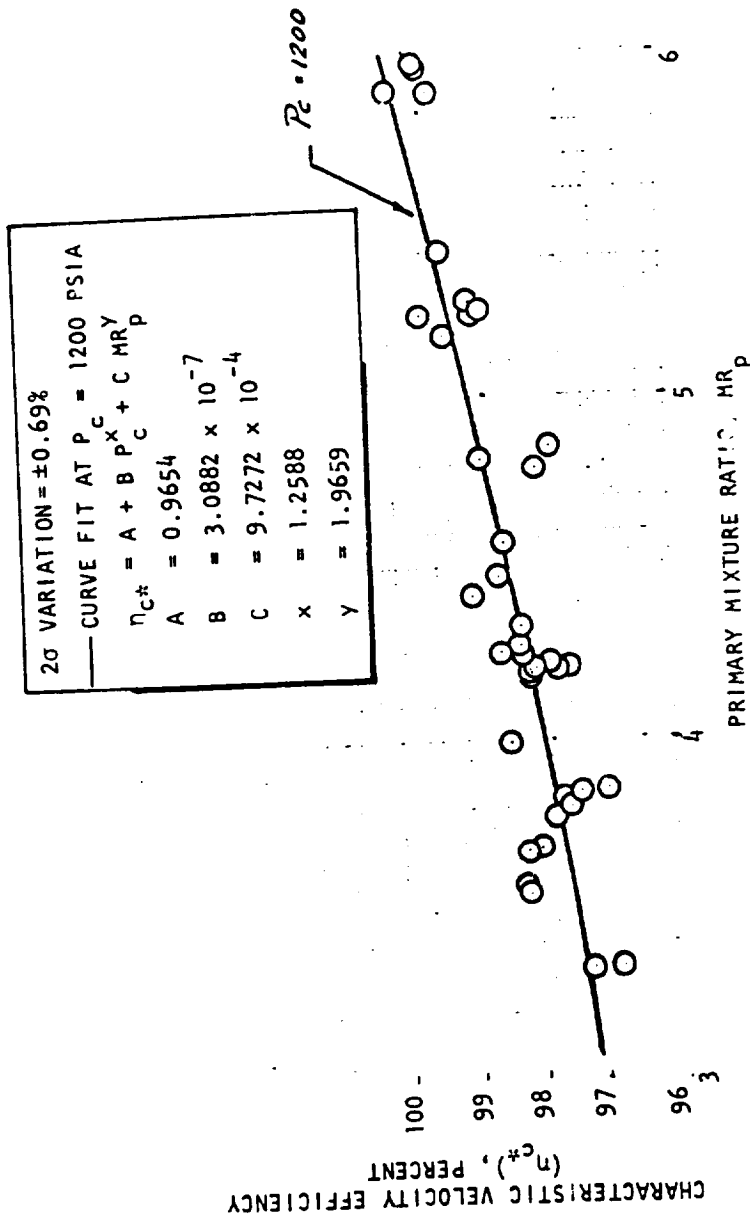


Figure 43. Linear Engine Test Bed No. 1, Characteristic Velocity Efficiency vs Mixture Ratio

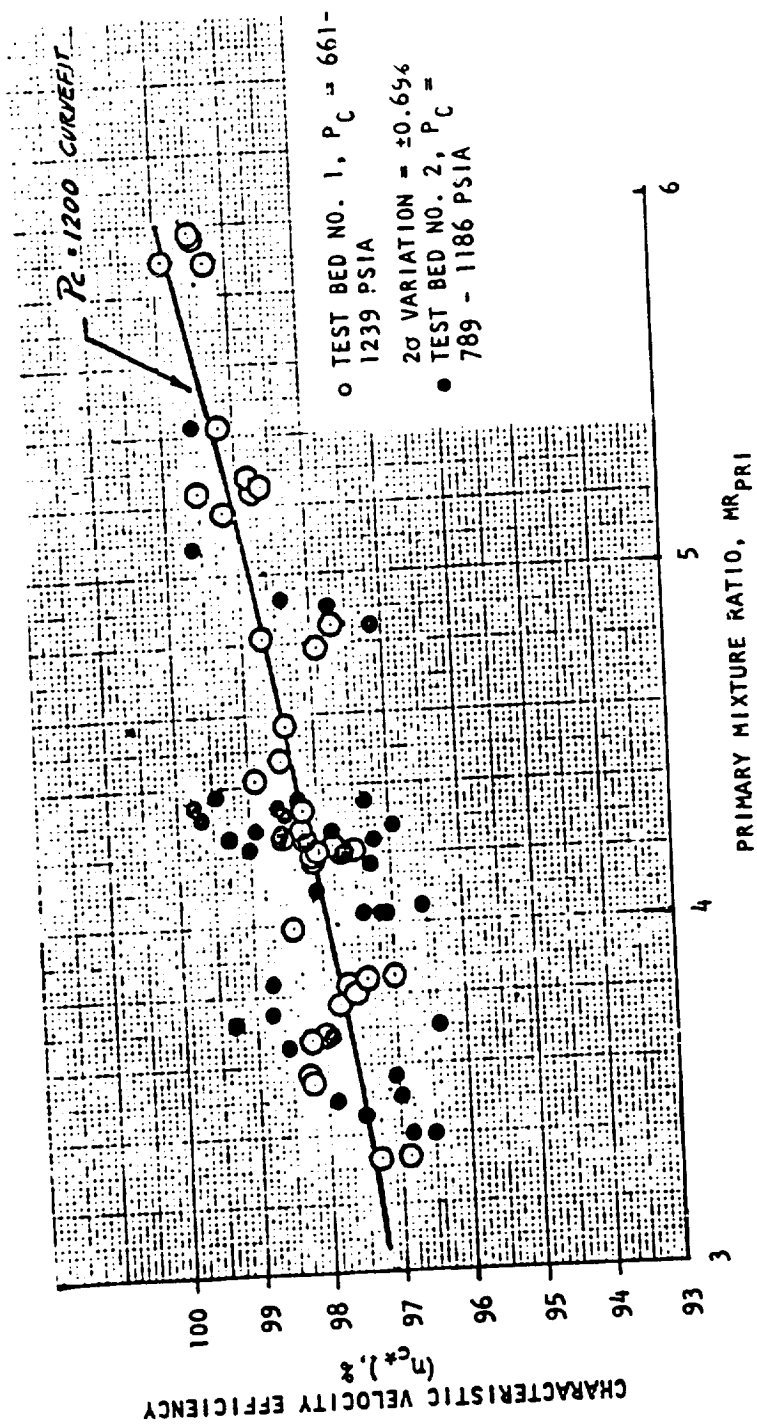


Figure 44. Linear Engine Test Bed No. 1 and 2,  $\eta_{c^*}$  vs MR

Vacuum specific impulse was also determined from site data with procedures presented in Ref. 1. For the conditions of  $P_c$ ,  $MR_p$ , and  $\epsilon$  indicated above, the projected mean vacuum specific impulse was 455.7 seconds. The 2- $\sigma$  deviation for this mean value was  $\pm 1.26$  percent. The  $c^*$  efficiency for these conditions is 99.3 percent (Fig. 43).

The correlation of test bed No. 1 and 2 specific impulse data is shown in Fig. 45 as a function of pressure ratio. Characteristic velocity efficiency and mixture ratio data are also shown. Very good correlation was obtained in the specific impulse data. The typical altitude compensation of the aerospike nozzle performance is indicated by the data. At a chamber-to-ambient pressure ratio ( $P_c/P_a$ ) of 81.6 ( $P_c = 1200$  psia,  $P_a = 14.70$ ), a sea level specific impulse of 346 is obtained, at a primary mixture ratio of 5.5.

#### SECONDARY FLOW EFFECTS

Test experience with the aerospike has shown that nozzle performance varies with secondary flow and that an optimum secondary flow exists which, for a given geometry, depends on pressure ratio (altitude). Also, larger gains in performance are obtained at the lower altitudes than in vacuum but require larger secondary flows than in vacuum. For the linear engine, predictions had indicated that at vacuum (Ref. 1), an increase in specific impulse of approximately 1 percent would be obtained by decreasing the secondary flow by 1 percent from the reference secondary flow (2 percent of the primary flow). Also, a decrease of 1 percent in specific impulse would be obtained from an increase in secondary flow of 1 percent from the reference secondary flow.

Test results obtained with test bed No. 1 (secondary flow of 2 percent) and test bed No. 2 (secondary flows of 1 and 3 percent) are shown in Fig. 46.

At the higher pressure ratios tested, the measured specific impulse appears to follow the predicted vacuum trends with secondary flow. For most pressure ratios,

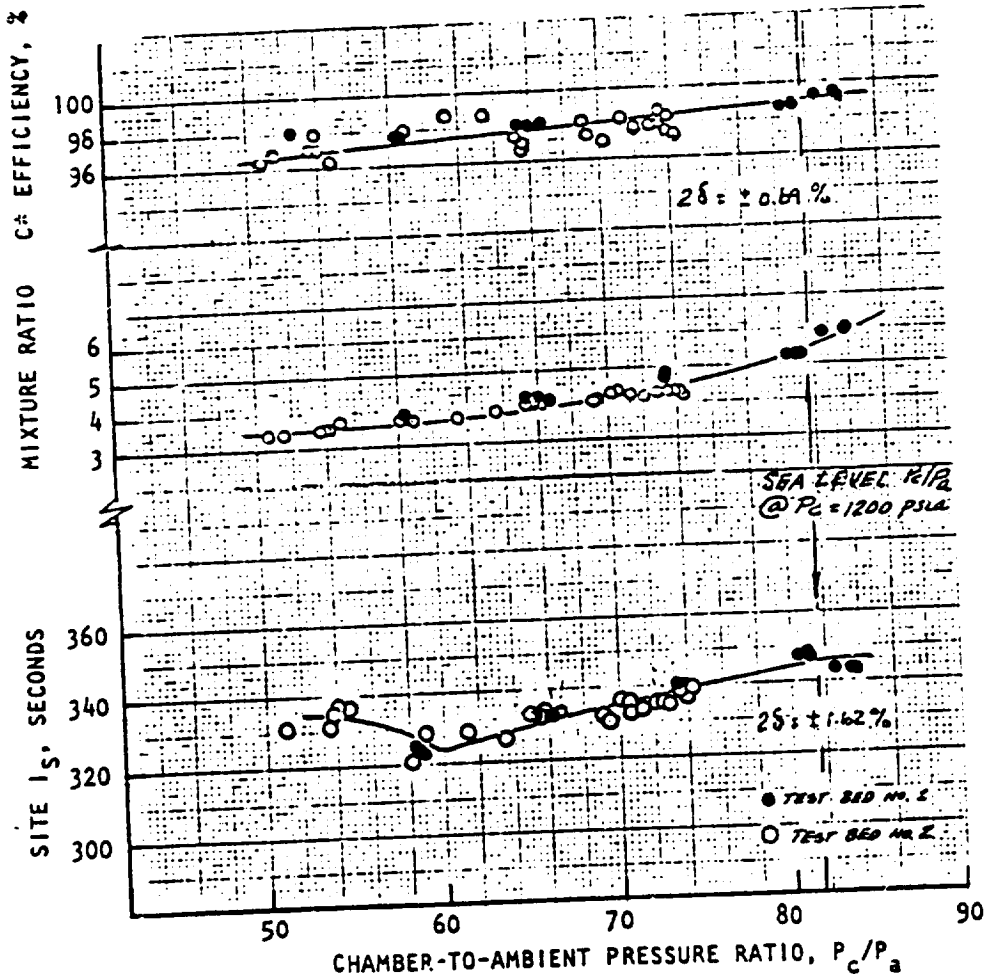


Figure 45. Linear Engine Site Performance Parameters

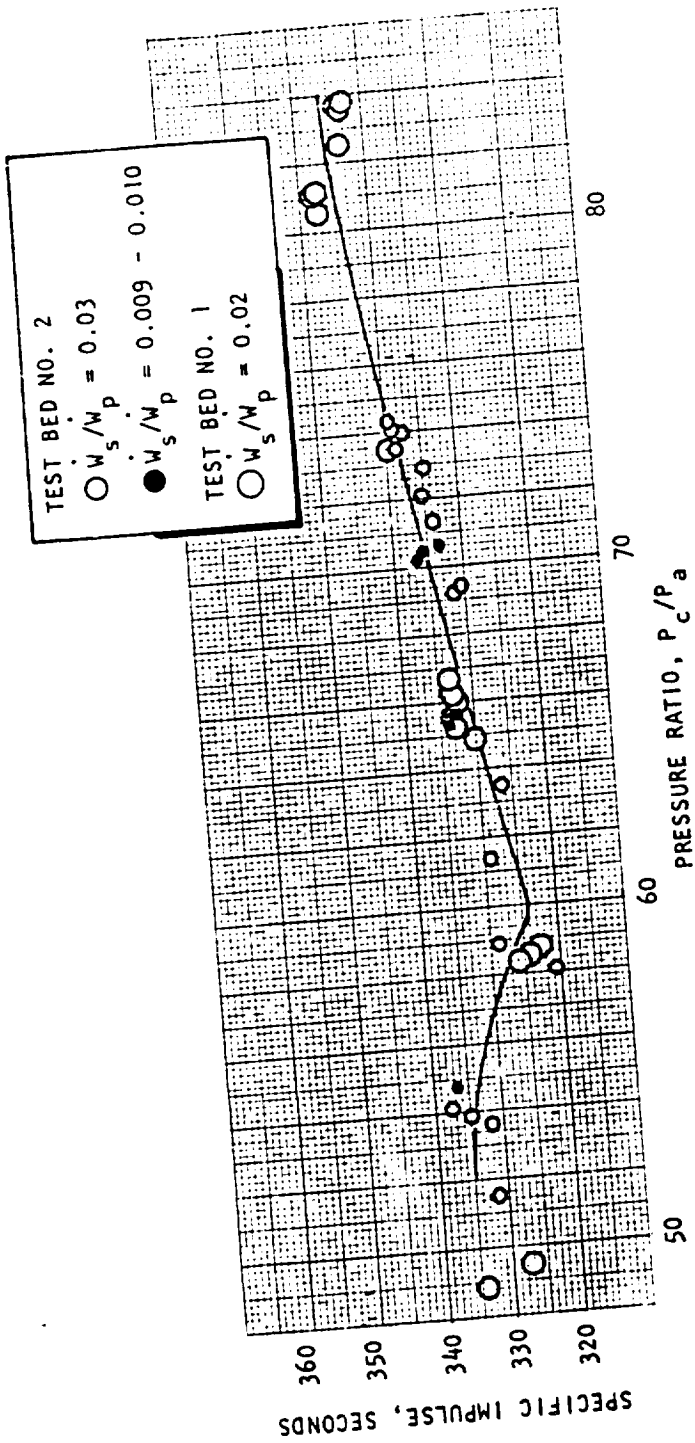


Figure 46. Linear Engine Test Beds, Secondary Flow Effect

the 1-percent secondary flow data are higher than the average curve through the 2-percent secondary flow data. For the higher pressure ratios, the 3-percent secondary flow data are lower than the average curve for the 2-percent secondary flow data. Not enough data were obtained to more completely define trends with secondary flow and pressure ratio and to remove inherent data scatter. However, it appears that the trends at pressure ratios greater than 65 are similar to those predicted for the vacuum case.

#### BASE PRESSURE TRENDS

Average base pressures were obtained from measurement of the base pressures at 20 locations in the base of test bed No. 2. Similar measurements made with the test bed No. 1 engine indicated the base pressure was a maximum in the center of the rectangular base and decreased near the sides of the rectangle.

Arithmetic averaging was used. The variation of the arithmetic average base pressure with engine operating pressure ratio is shown in Fig. 47 for both test beds. For test bed No. 1, the upper and lower limits of the base pressure measurements at each pressure ratio are indicated by vertical bars. In all tests conducted, the average base pressures were between 96 to 100 percent of ambient pressure. As expected, the lowest base pressures were obtained in the 1-percent secondary flow tests. The 3-percent secondary flow tests showed base pressures higher than the 2 percent, also as expected. At pressure ratios above 52, the (+7°, +7°) hinged configuration with 3-percent secondary flow indicated higher base pressures than the reference not-hinged configuration. The thrust coefficient (+7°, +7°) hinged configuration also followed similar trends. The higher base pressure contributed to the higher performance of the hinged configuration.

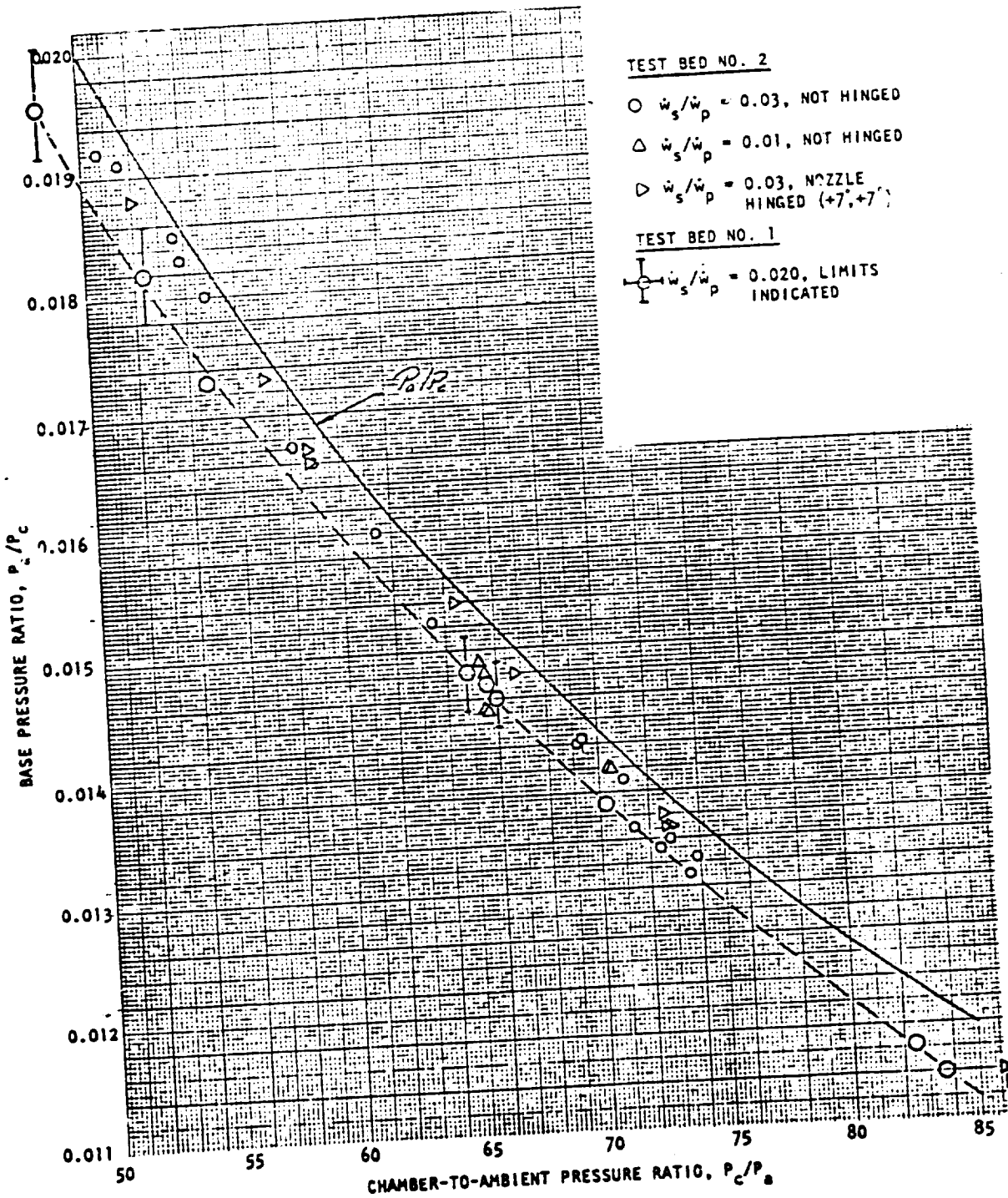


Figure 47. Linear Engine Average Base Pressures

R-9049

97/98

## THRUST VECTOR CONTROL STUDIES

### DYNAMIC HINGING

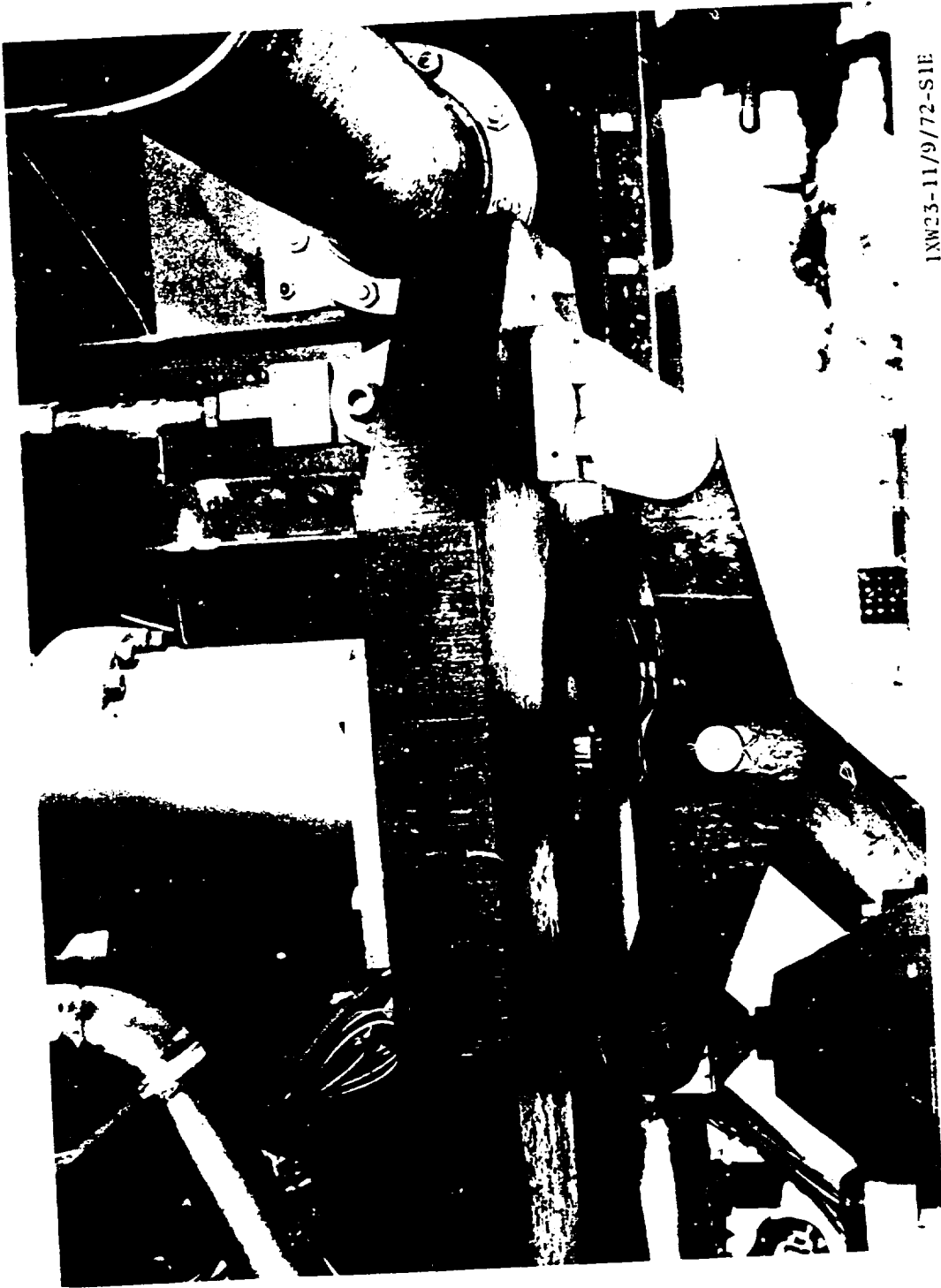
Dynamic hinging of test bed No. 2 was accomplished through the use of an F-1 engine gimbal actuator. The actuator was mounted to the Delta-2B test stand and attached through a bell crank to the lower thrust frame, as shown in Fig. 48. The total travel of the actuator was approximately 6 inches and the bell crank leverage was designed so that  $\pm 5.5$  inches actuator motion would result in  $\pm 16$  degrees rotation of the thrust chamber assembly about the hinge axis. The actuator was driven by hydraulic fluid supplied from a test facility hydraulic system. The actuator was much larger than necessary to provide the forces required for hinging but was used because of availability. The actuator piston area was 57 sq in. and hydraulic supply pressure up to 1500 psi was available.

Dynamic hinging was accomplished on three tests. On test 624-006, five complete hinge cycles at  $\pm 12$  degrees were accomplished. On tests 624-008 and -010, 10 cycles at  $\pm 16$  degrees were accomplished on each test. The hinging rate at  $\pm 16$  degrees was approximately 5 seconds per cycle. This was the highest hinging rate possible because of flow limitations in the ground hydraulic system and the large flow demand of the large diameter actuator. Hinging operation on all tests was smooth and trouble free. Operation was stable throughout with no undue vibrations or anomalies encountered.

Posttest inspection of the flexible ducting and other engine hardware did not reveal any damage resulting from the hinging. Figure 49 shows the engine at the  $\pm 16$ -degree hinge angle during one of the hot-fire hinge cycles.

### STATIC HINGING

Two configurations were tested to determine the thrust vector and performance potential of hinging combustor-nozzle banks of the linear engine. One of these configurations consisted of repositioning each of the two combustor-nozzle banks outward



1XW23-11/9/72-S1E

Figure 48. Test Bed No. 2 Dynamic Hinging Gimbal Actuator



IX224-4/25/73-S1\*

Figure 49. Test Bed No. 2 Dynamic llinging at  $\pm 16$  Degrees

+7 degrees (Fig. 11) from their normal orientation. The other consisted of pre-positioning one bank inward 5 degrees and the other outward 17 degrees. The first configuration improves axial thrust, while the second provides a side force with little change in axial thrust.

#### Symmetric Staric Hinging Configuration (+7°, +7°)

It had been estimated that the (+7°, +7°) configuration would increase the thrust chamber performance a maximum of approximately 3 percent by discharging the primary combustion gases more axially. The increase in thrust would vary with pressure ratio (altitude) since the effective gas discharge angle changes with altitude. At design pressure ratio where the gas discharges axially in the reference (not-hinged) configuration, the performance of the hinged configuration would be below that of the reference configuration.

Testing confirmed this initial estimate. The ratio of thrust-to-chamber pressure is shown in Fig. 50, plotted as a function of chamber-to-ambient pressure ratio, for the reference (not-hinged) configuration, and for the (+7°, +7°) hinged configuration.

The parameter  $F/P_c$  is proportional to the product of the nozzle thrust coefficient ( $C_F$ ) and throat area ( $A_t$ ). The nozzle thrust coefficient is a function of pressure ratio and orientation of the combustor-nozzle banks, while the throat area is not. Therefore, the parameter  $F/P_c$  follows the same trends with pressure ratio and nozzle orientation as  $C_F$ . Average curves have been drawn through each set of data in Fig. 50. By comparing these two curves, it can be seen that the thrust coefficient was increased by approximately 3 percent at a pressure ratio of 62.5, and by 1.8 percent at a pressure ratio of 75. Above that pressure ratio, the increase in thrust will diminish, although no data were obtained above that range. Below a pressure ratio of 62.5, the increase in thrust again diminishes. This is caused by the effect of recompression on the nozzle flow discharge angle.

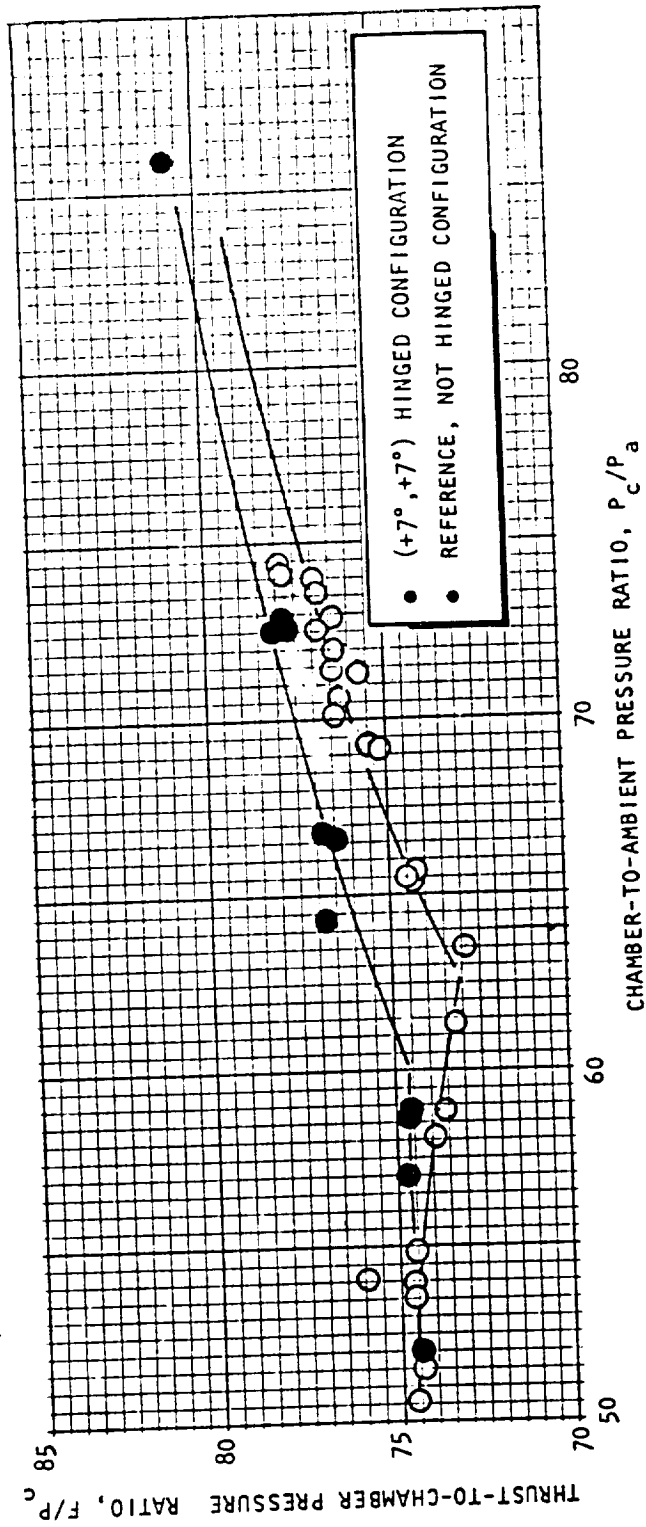


Figure 50. Linear Engine Test Bed No. 2 Static Hinging Tests,  $F/P_c$  vs  $P_c/P_a$

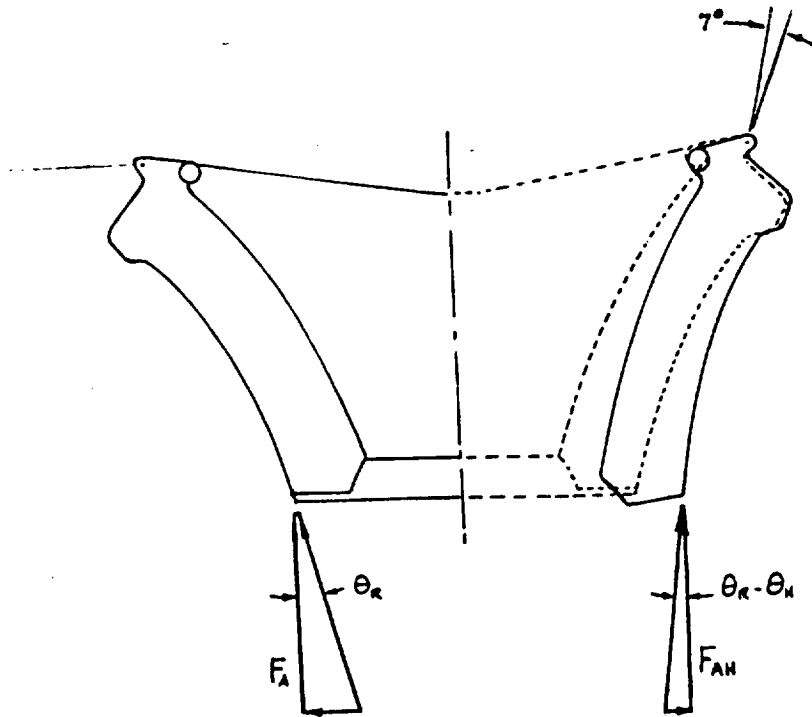
It is possible to calculate the initial angle (for the reference configuration) of the resultant force acting on each nozzle bank as a function of pressure ratio from the measured axial forces (Fig. 50) of the (+7°, +7°) hinged configuration and the reference configuration. The equations necessary for calculating the resultant angle before hinging are shown in Fig. 51. In this simplified analysis, it is necessary to know only the axial thrusts before and after hinging as a function of pressure ratio, and the hinge angle. The calculated resultant angle,  $\theta_R$ , varied from 14 degrees at a pressure ratio of 62.5 to 12.5 degrees at a pressure ratio of 72. The variation of  $\theta_R$  with pressure ratio is utilized in the analysis of the unsymmetric static hinged configuration, made to determine effective gimbaling angles.

#### Unsymmetric Static Hinging Configuration (+17½°, -5°)

Figure 52 displays the skewed configuration relative to load cell locations and engine coordinates. Rotating one combustor-nozzle bank outward +17½° positions the resultant force more axially, simultaneously reducing the side force on that side (Fig. 53). Positioning the opposite combustor nozzle bank inward 5 degrees increases the side force on that side and reduces the axial thrust. The net effect is the generation of a side force which, as initially estimated, would provide a maximum of 11 degrees of equivalent gimbaling angle with no appreciable change in thrust.

The engine could not be tested with the basic (+17½°, -5°) configuration since the exhaust would have missed the facility flame deflecting duct. Instead the pre-hinged engine was rotated 10 degrees to bring its exhaust gas axis in coincidence with the flame bucket axis.

Axial thrust-to-chamber pressure ratio data ( $F/P_c$ ) obtained with this configuration are shown in Fig. 54 compared to the (+7°, +7°) configuration and the basic "not-hinged" configuration. These data are also shown in Table 6 together with the side force data (divided by chamber pressure) measured during the same test series. It is necessary to convert this axial thrust and side force data to what would have been measured had the engine been tested in its basic (+17½°, -5°) orientation.



EQUATIONS:

$$F_A = R \cos \theta_R$$

$$F_{AH} = R \cos(\theta_R - \theta_H)$$

$$\theta'_R = \theta_R - \theta_H$$

$$\theta_H = 7^\circ$$

AXIAL THRUST BEFORE HINGING

AXIAL THRUST AFTER HINGING

RESULTANT ANGLE AFTER HINGING

HINGE ANGLE

SOLUTION:

$$\theta_R = \theta_H + (\cos^2 \theta_H - 1) / (.2 \phi \cos \theta_H - 1 - \phi^2)$$

$$\phi = F_A / F_{AH}$$

Figure 51. Equations for Calculation of Linear Thrust Chamber Resultant Force Angle

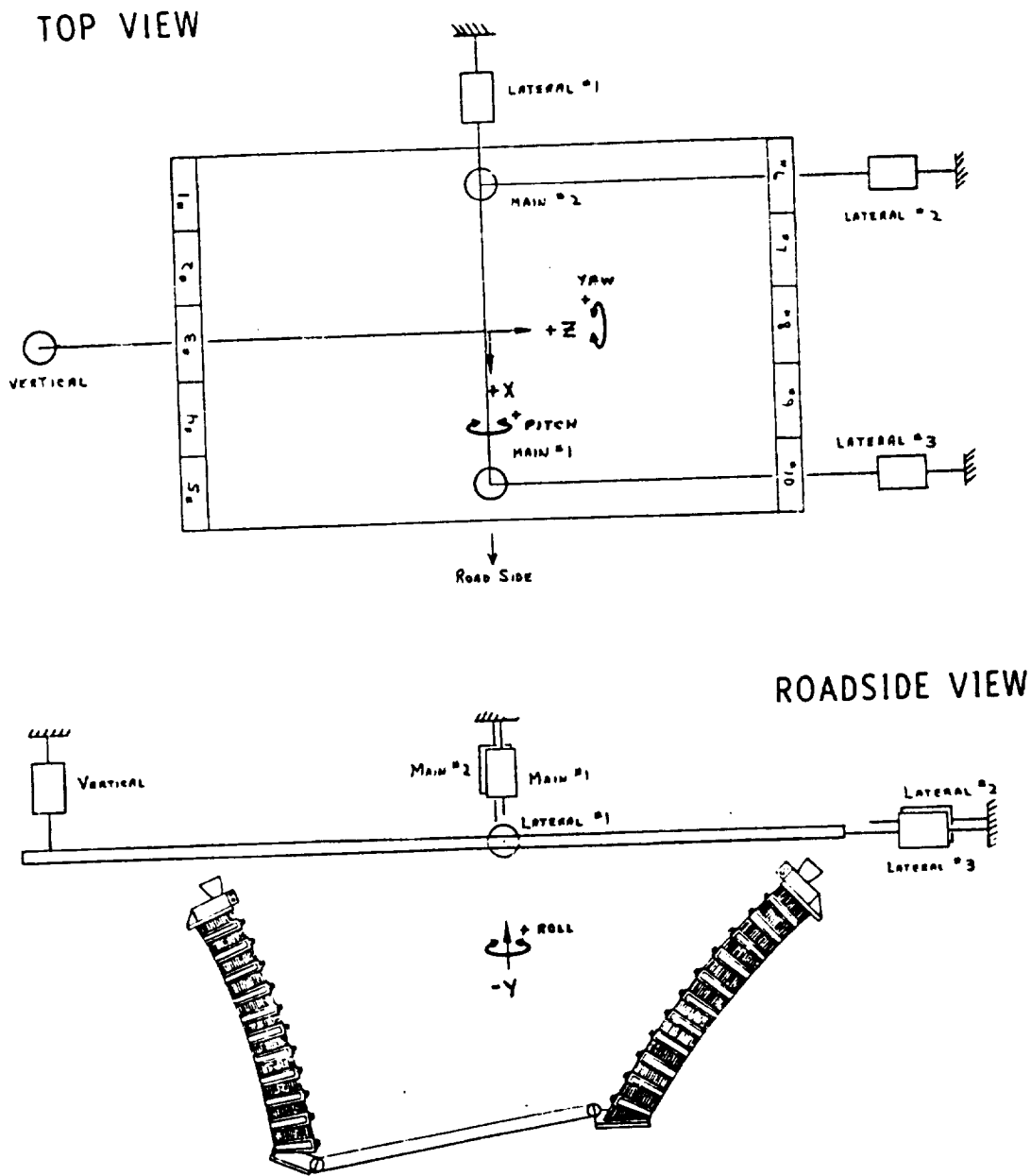
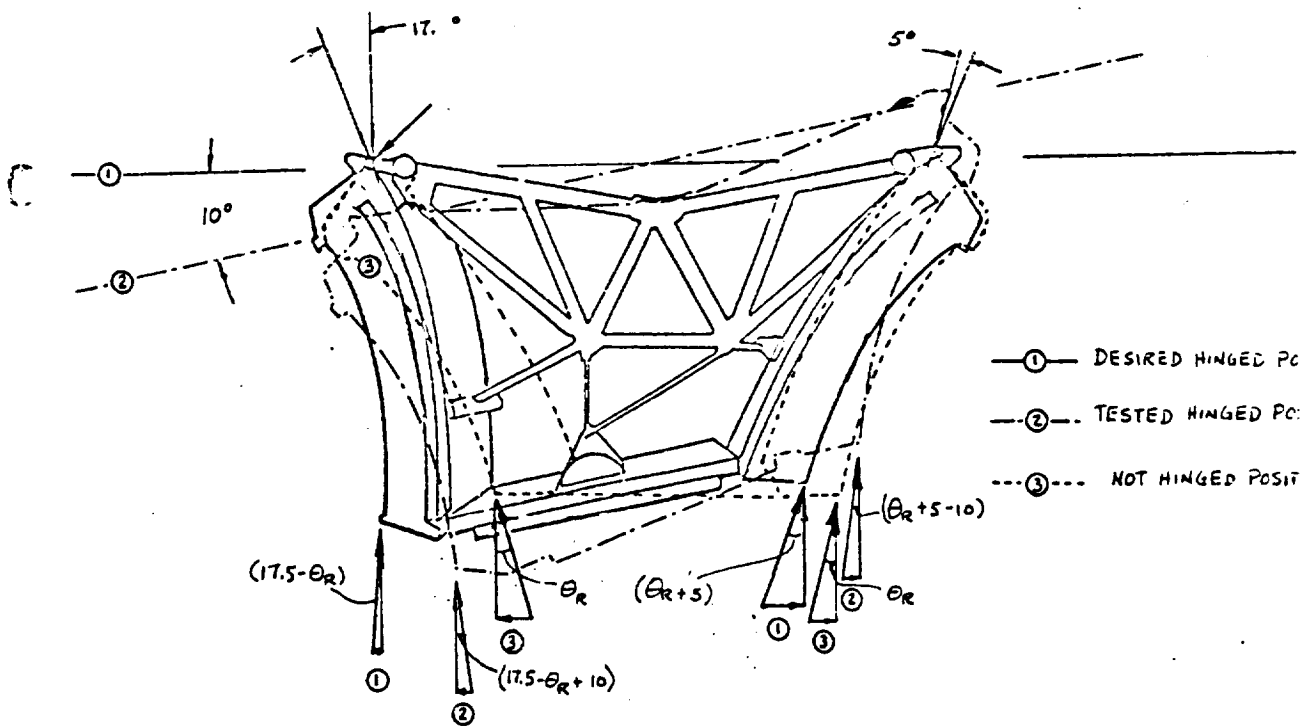


Figure 52.  $+17\frac{1}{2}^\circ$ ,  $-5^\circ$  Static Hinging Configuration,  
Test Bed No. 2



Equations:

$$\begin{aligned}
 F_{AT} &= R [\cos (17.5-\theta_R +10) + \cos (\theta_R +5 -10)] && \text{As tested axial thrust} \\
 F_{ST} &= R [-\sin (17.5-\theta_R +10) + \sin (\theta_R +5 -10)] && \text{As tested side force} \\
 F_A &= R [\cos (17.5-\theta_R) + \cos (\theta_R +5)] && \text{Desired hinged axial force} \\
 F_S &= R [\sin (17.5-\theta_R) + \cos (\theta_R +5)] && \text{Desired hinged side force} \\
 \theta_G &= \tan^{-1} F_A/F_S && \text{Equivalent gimbal angle}
 \end{aligned}$$

Solution:

$$\begin{aligned}
 F_A &= P_c \frac{F_{AT}}{P_c} \frac{\cos (17.5-\theta_R) + \cos (\theta_R +5)}{\cos (17.5-\theta_R +10) + \cos (\theta_R +5 -10)} \\
 F_S &= P_c \frac{F_{ST}}{P_c} \frac{\sin (17.5-\theta_R) + \cos (\theta_R +5)}{-\sin (17.5-\theta_R +10) + \sin (\theta_R +5 -10)} \\
 \theta_G &= \tan^{-1} F_A/F_S
 \end{aligned}$$

Figure 53. Equation for Calculation of Linear Engine Equivalent Gimbal Angle

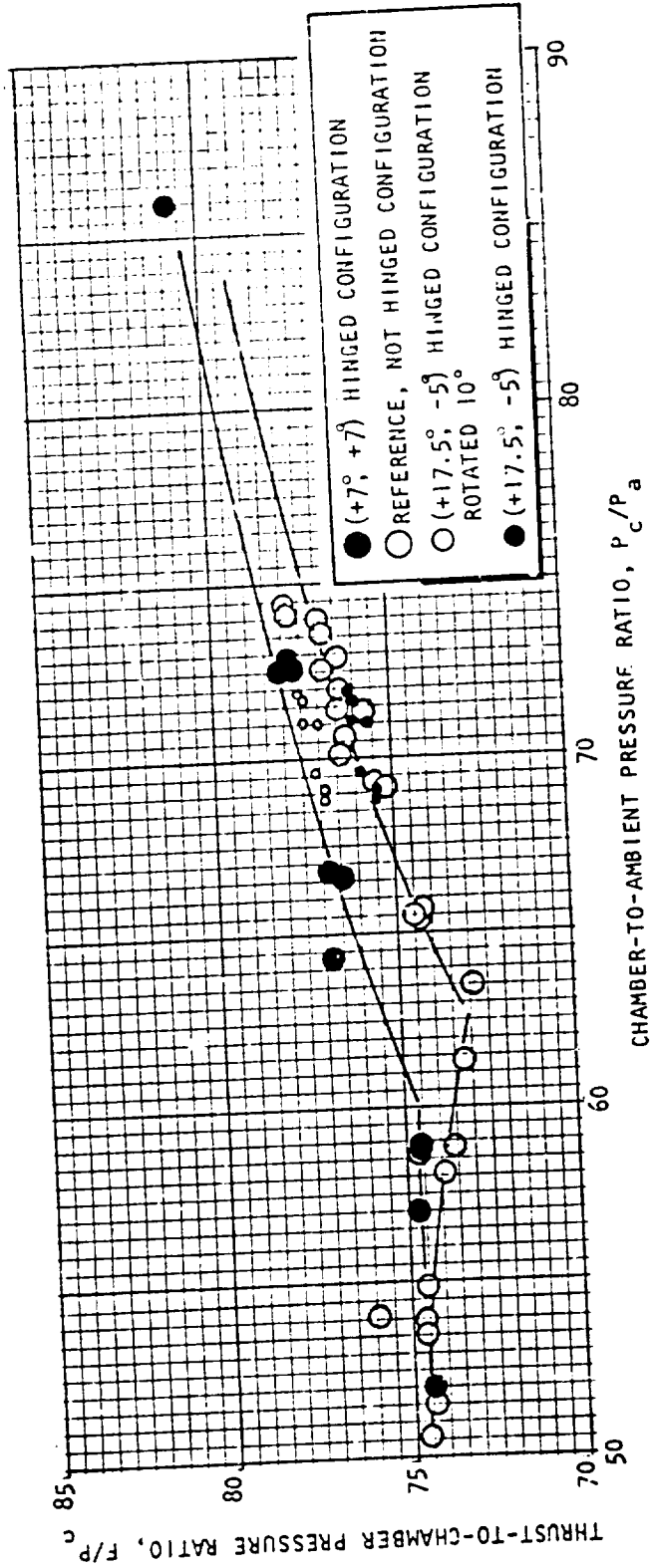


Figure 54. Linear Engine Test Bed No. 2 Static Hinging Tests  
 ( $F/P_c$  vs  $P_c/P_a$ )

It was possible to do this conversion since the angle of the thrust chamber resultant force is known as a function of pressure ratio from the previously tested (+7°, +7°) configuration. The equations required for the subject conversion are shown in Fig. 53.

TABLE 6. TEST AND CALCULATED DATA FOR LINEAR ENGINE  
(+17½°, -5°) HINGED CONFIGURATION\*

Test No.	Slice Time, seconds	$P_c/P_a$	$F_{AT}/P_c$	$F_{ST}/P_c$	$F_A/P_c$	$F_S/P_c$	$\theta_R$ , degrees	$\theta_G$ , degrees
624-014	15.5	71.10	774.47	1.002	76.02	9.64	13.09	7.30
	35.5	71.68	77.41	1.006	75.97	9.64	12.78	7.33
	57.8	71.91	77.50	1.068	76.06	9.63	12.46	7.78
624-016	15.9	71.09	77.01	0.953	75.58	9.18	13.09	6.98
624-019	15.1	68.80	76.9	1.1174	75.47	11.32	13.45	8.62
	30.1	69.20	76.9	1.0979	75.43	10.58	13.15	8.06
	60.0	69.70	77.2	1.054	75.70	10.16	13.42	7.71

\*Symbols defined in Fig. 53.

In Table 6, one can see that a maximum equivalent gimbal angle of 8.62 degrees was obtained at a pressure ratio of 68.8. The calculated resultant force angles are shown in the table for each pressure ratio tested. The corrected axial thrust data for the (+17½°, -5°) hinged configuration are plotted in Fig. 54. It can be seen that the data correlate well with the reference, not-hinged configuration, indicating no loss in axial thrust as a result of hinging (+17½°, -5°).

Table 7 presents data samples of nine time slices from the three tests (624-014, -017, and -019) of this configuration which reached mainstage operation. These data slices cover two thrust levels at which the engine operated and are compared to data from tests at other nozzle positions at both equivalent and varying thrust levels. Table 8 is a sample of the TVC program printout which provided the data for compilation of Table 7. Included on the printout are corrections that were applied to the resultant thrust vector data to account for any propellant inlet duct forces. The values shown on the table are indicative of the typical correction magnitudes observed for all other time slices.

TABLE 7. LINEAR TEST BED NO. 2 THRUST VECTOR DATA

TEST NUMBER	624-046 (0°, 0°)	621-047 (0°, 0°)	624-001 (0°, 0°)	624-006 (0°, 0°)	624-008 (0°, 0°)
SLICE TIME, SECONDS	4.9	9.4	3.9	58.0	269.5
ENGINE THRUST, LBS	55,463	58,009	56,359	75,945	52,345
ENGINE MIXTURE RATIO, MRU	3.279	3.432	3.306	3.971	3.328
THRUST CHAMBER MIXTURE RATIO, MRU	3.524	3.685	3.552	4.217	3.410
CHAMBER PRESSURE (AVERAGE), PSIA	750.4	786.2	747.2	1000.4	697.5
"X" AXIS THRUST, LBS	-49	-72	-82	162	44
"Y" AXIS THRUST, LBS	55,453	57,997	56,350	75,945	52,345
"Z" AXIS THRUST, LBS	1028	1188	1020	5	-131
"X-Z" PLANE PIERCE POINT DISPLACEMENT, INCHES	1.187	1.361	1.072	1.194	0.816
d <sub>X</sub> DISPLACEMENT, INCHES	-0.565	-0.578	-0.405	-1.105	-0.801
d <sub>Z</sub> DISPLACEMENT, INCHES	-1.044	-1.232	-0.993	-0.454	0.153
PITCH, INCH-LBS	57,888	71,424	55,944	34,488	-7992
YAW, INCH-LBS	31,320	33,552	22,848	83,904	41,952
ROLL, INCH-LBS	7392	10,464	7200	-120	1656
THRUST VECTOR ANGLE FROM THE VERTICAL, DEG	1.063	1.176	1.040	0.122	0.151

TABLE 7. (Continued)

TEST NUMBER	624-008 (COUNT) (0°, 0°)	624-010 (0°, 0°)	624-011 (+7°, +7°)	624-012 (+7°, +7°)	624-013 (+7°, +7°)					
SLICE TIME, SECONDS	58.5	10.4	10.2	30.2	80.2	90.2	4.6	60.0	43.7	51.4
ENGINE THRUST, LBS	66,979	56,427	73,323	59,212	78,072	60,768	53,720	68,106	70,431	78,306
ENGINE MIXTURE RATIO, MRU	3.936	3.638	4.200	3.399	3.999	3.360	3.210	4.465	4.534	5.004
THRUST CHAMBER MIXTURE RATIO, MRU	4.024	3.721	4.287	3.667	4.295	3.619	3.470	4.897	4.968	5.499
CHAMBER PRESSURE (AVERAGE), PSIA	902.4	754.3	969.4	792.0	1010.7	815.2	721.2	891.6	925.0	1009.4
"X" AXIS THRUST, LBS	207	-43	134	310	441	262	252	326	398	405
"-Y" AXIS THRUST, LBS	66,976	56,427	73,321	59,211	78,068	60,767	53,719	68,105	70,428	78,299
"Z" AXIS THRUST, LBS	614	128	528	180	-678	-248	-239	-371	-394	-996
"X-Z" PLANE PIERCE POINT DISPLACEMENT, INCHES	1.675	0.685	1.471	1.113	1.142	0.878	0.843	1.015	0.816	1.114
d <sub>x</sub> DISPLACEMENT, INCHES	-1.269	-0.643	-1.146	-0.911	-1.012	-0.872	-0.822	-1.010	-0.815	-1.047
d <sub>z</sub> DISPLACEMENT, INCHES	-1.093	-0.237	-0.922	-0.640	0.529	-0.107	-0.188	0.097	0.035	0.382
PITCH, INCH-LBS	75,224	13,392	67,608	37,872	-41,328	6480	10,080	-6624	-2448	-26,928
YAW, INCH-LBS	84,984	36,264	84,000	53,952	79,008	52,968	44,160	68,808	57,504	73,728
ROLL, INCH-LBS	2592	-768	-4608	-720	-4128	4128	312	2952	13,296	6576
THRUST VECTOR ANGLE FROM THE VERTICAL, DEG	0.554	0.137	0.426	0.347	0.594	0.340	0.370	0.415	0.378	0.787



TABLE 8. THRUST VECTOR CONTROL DATA

TEST NUMBER	TEST DATE	TEST STAND	SLICE TIME
624.014	92073	DELTA 2B	57.8 SECS

	ENGINE	THRUST CHAMBER
THRUST (LBS).....	76870.	76870.
MIXTURE RATIO (MRU).....	4.093	4.412 (AVG)
SPECIFIC IMPULSE (LB-SEC)....	344.987	356.937
CHAMBER PRESSURE (PSIA).....		998 (AVG)

ENGINE TOTAL THRUST COMPONENTS ARE:

X (ROADSIDE).....	308 LBS
Z (DELTA 1).....	1059 LBS
-Y (VERTICAL).....	76862.1 LBS

PIERCE POINT DISPLACEMENT (IN X-Z PLANE) IS..... 2.17954 INCHES

DISPLACEMENT COMPONENTS ARE: X=-.982331 INCHES  
Z= 1.94561 INCHES

ANGLE FROM GIMBAL CENTER IS: 16.2166 DEGREES

ENGINE TORQUES (IN INCH-LBS) ARE: PITCH...-149544  
YAW..... 75504  
ROLL.....-24

THE THRUST VECTOR IS ANGLED .822071 DEGREES FROM THE VERTICAL

CORRECTIONS:

L0X DUCT.....	239.829
FUEL DUCT.....	-114.748

Figure 55 presents a curve of engine system thrust versus chamber pressure. The curve established is over a thrust range of 43,000 pounds and a chamber pressure range of 500 psi.

The thrust vector pierce point displacements from the gimbal center in the X-Z plane are shown in Fig. 56. There is a noticeable trend exhibited in that a definite majority of the nominal configuration data points are concentrated in the (-X, -Z) quadrant of the graphical display while the (+7°, +7°) configuration data tend to straddle the X-axis. The skewed configuration displacement values at the higher thrust level are clustered about the X = -0.01, Z = +2.2) coordinates at the extreme left side. The lower thrust level displacements come along with the (+7°, +7°) configuration data.

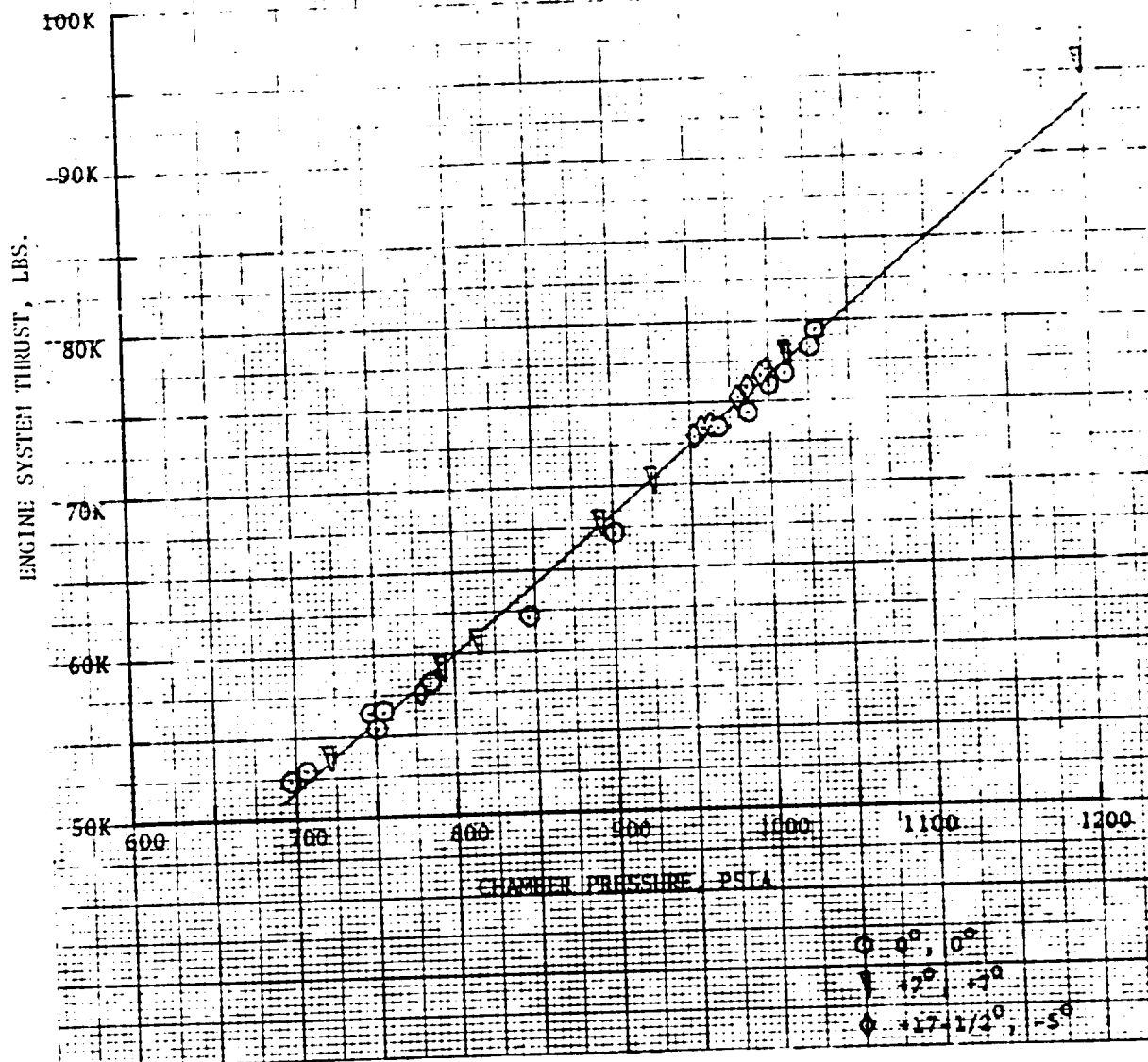


Figure 55. Test Bed No. 2 Engine Thrust vs Chamber Pressure

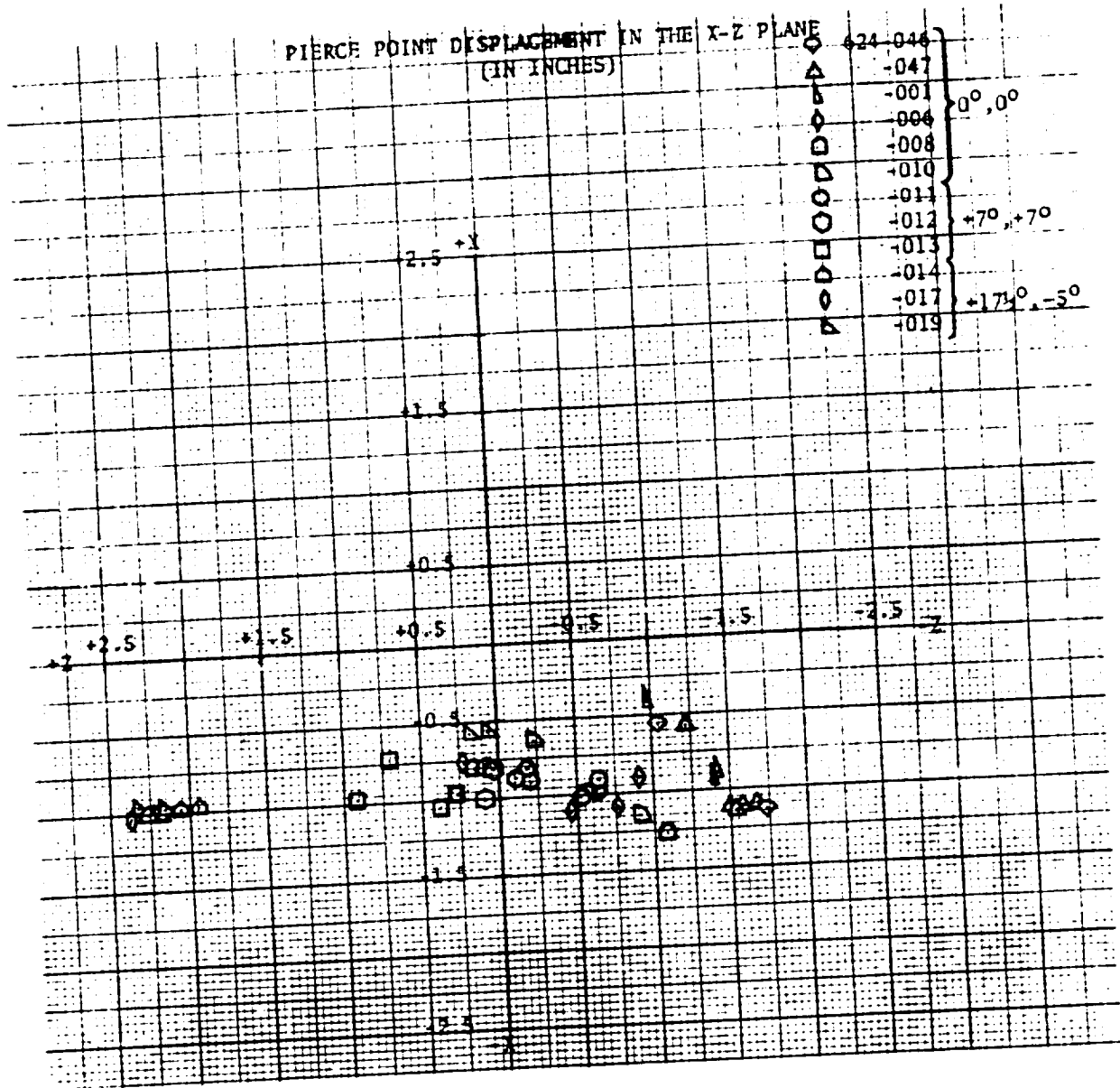


Figure 56. Test Bed No. 2 Thrust Vector Analysis

## THRUST CHAMBER HARDWARE DURABILITY

### NOZZLE DURABILITY

Nozzle durability was very good. The only tube erosions that were experienced occurred on test 010 as the result of an operating error that caused a high mixture ratio shutdown. Damage incurred on test 010 included erosion through the zirconium oxide protective coating and through the hot-gas side of 40 tube crowns on the No. 6-No. 10 nozzle bank of the engine. Also, tube-to-tube braze alloy melted away, leaving visual tube-to-tube gaps in the forward 18 inches of the nozzle. Erosion from the hot shutdown typically started within 1/8 inch of the forward copper end bar transition piece and extended 1/2 to 1 inch aft. Repairs were successfully made by torch brazing insert patches into the tube erosions and covering the patches with the zirconium oxide plasma spray coating. Tube-to-tube gaps were closed by torch brazing to fill the recesses between tubes. The repairs were successful and the nozzle bank damage area required only repairs associated with the original erosion region throughout the remainder of the test program.

The other nozzle region requiring repairs intermittently throughout the test program was the coolant tubes adjacent to the nozzle bank corners. Tube splits on the hot-gas side and tube cracks adjacent to or under the support hat bands on the nozzle back side, causing engine compartment fires, occurred regularly in all four corners. These were the result of structural discontinuities at the square corners between the nozzle and the end fences, and tube material thermal growth differences causing high material strain levels between the H<sub>2</sub> cooled nozzle tubes and the adjacent water-cooled end fence tubes.

The nozzle contour remained essentially intact throughout the test program. All hot-gas side tube surfaces remained within 0.060 inch of the original contour except for thermal distortion areas caused during braze repair of the tube-to-tube leakage after the hot shutdown on test 010. Chipping and flaking of the zirconium oxide protected area was progressive throughout the test program. Approximately 75 percent of the originally protected area was still covered at the conclusion of the test program. No tube erosions, except for those specified previously, occurred where the coating came off.

R 9049

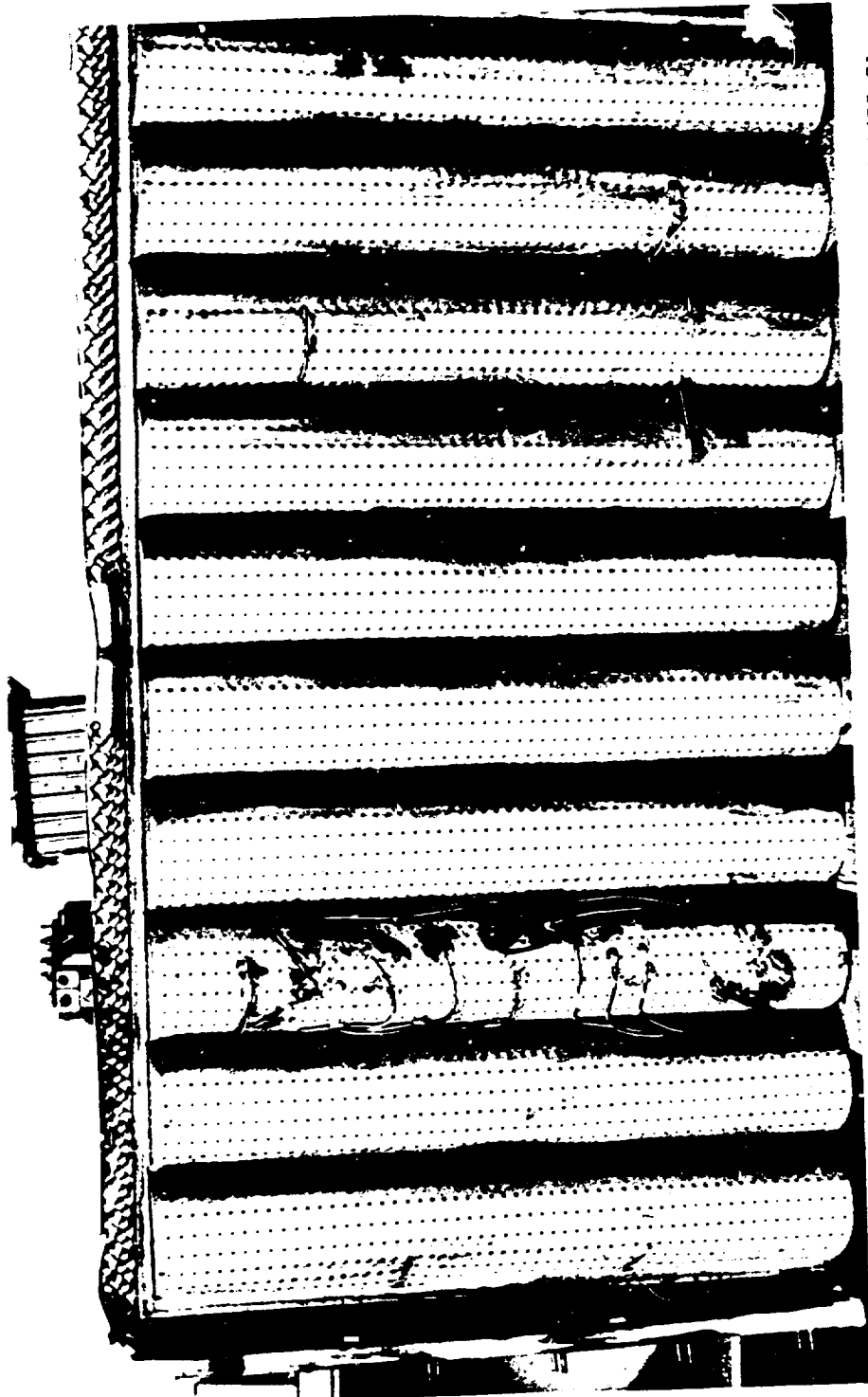
## END FENCE DURABILITY

The water-cooled end fences are considered as facility items and do not represent finalized designs. They operated satisfactorily, with failures due to operation confined to thermal buckling of the tube bundles and thermal cracking of tubes adjacent to the corners where attached to the nozzle. Both discrepancies are considered caused by the thermal difference during operation of the water-cooled fences and liquid H<sub>2</sub>-cooled nozzle. No attempt was made to remedy the situation. Operation of the engine was not compromised by the between test repair of the thermal tube cracks.

## TURBINE EXHAUST MANIFOLD AND HOT-GAS SEAL DURABILITY

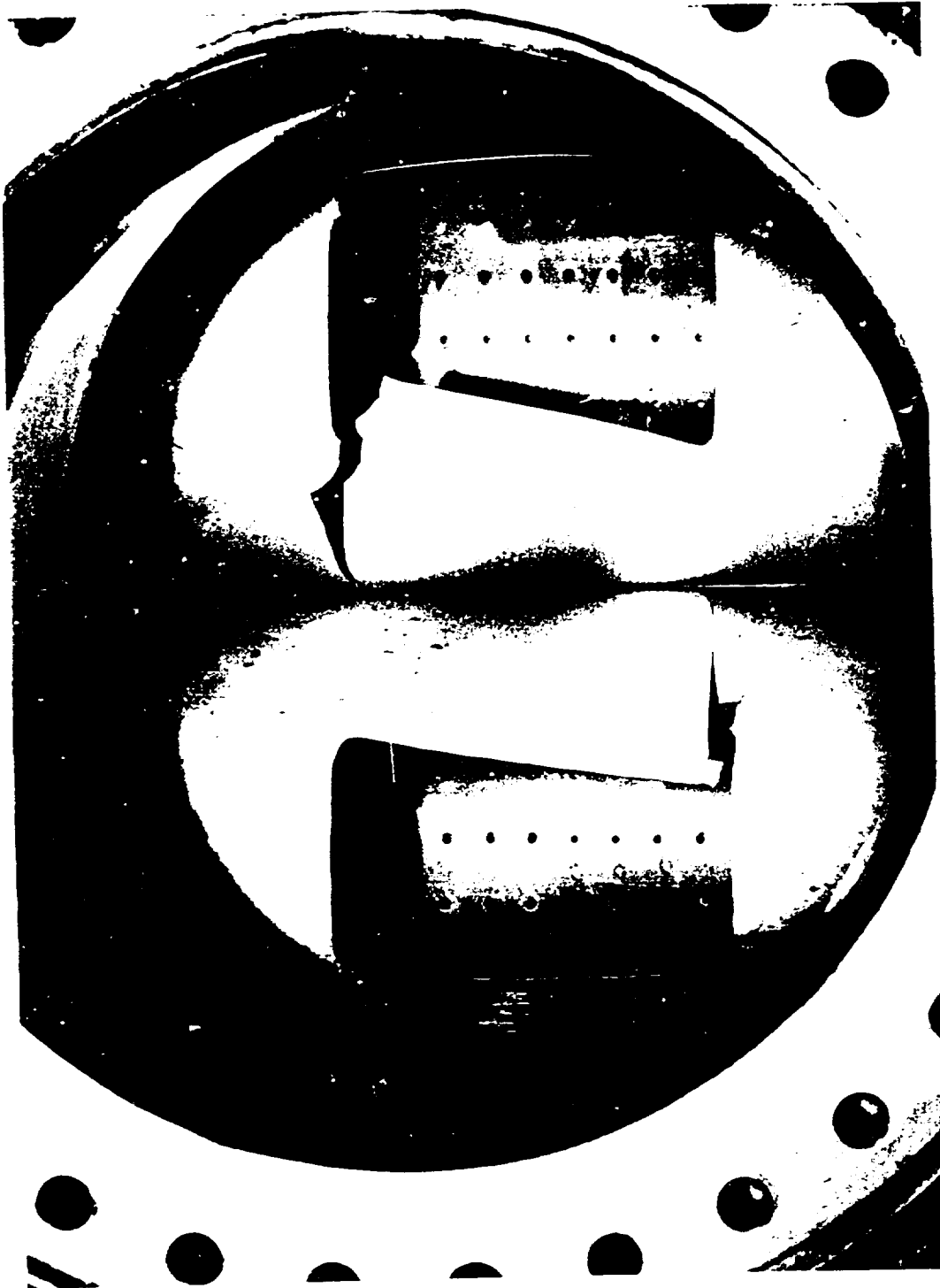
Testing of the initial turbine exhaust manifold for eight mainstage tests and 786 seconds of accumulated duration showed the redesign configuration (from test bed No. 1) to have excellent durability capabilities. At this point of the test program, a new, wider base was installed for the (+7°+7°) nozzle positions. Figures 57 and 58 show the posttest condition of this manifold. Figure 57, a view of the perforated base, shows the hardware to have sustained essentially no thermal distortion or degradation. The external lines shown are base pressure instrumentation lines added after the hardware was completed. The fatigue cracks at the corners of the gas distribution inlet ports (Fig. 58) resulted from incorrect fabrication. The ports should have been dual circular inlets instead of the single rectangular inlet to provide a design stiffer and more resistant to corner strains and concentrations.

A hot-gas closeout seal design of the formed waffle-type configuration developed for test bed No. 1 showed parent metal cracking during testing at the corners of the individual metal formed sections throughout the test program. A section of the seal used throughout the initial 876 seconds of the engine test program (prior to repositioning the nozzle sides) was removed for metallurgical analysis. The analysis showed that the 321 CRES material fractures were too brittle to be the result of low cycle fatigue. The crack branching, crack appearance, and the presence of a corrosive environment on the test stand led to an investigation for stress cracking. The residual stress necessary for stress cracking was demonstrated by



ICT65-9/14/73-C1

Figure 57. Posttest Condition of Turbine Exhaust Manifold Base, Test Bed No. 2



ICT35-6/26/73-CIB

Figure 58. Posttest Condition of Turbine Exhaust Manifold Inlet,  
Test Bed No. 2

subjecting the sample to boiling  $Mg Cl_2$  solution and producing additional seal cracks in previously uncracked areas. It was concluded that changing the seal material from 321 CRES to an alloy less susceptible to stress cracking such as Inconel 600 would be a solution for future hardware fabricated.

Testing the engine at reduced secondary gas flowrates by bypassing a greater portion of the turbine exhaust gas showed increased seal operating temperatures due to less coolant for the base region. Testing with only 20 percent of the turbine exhaust gas flow through the base region caused minor erosion of the hot-gas seal parent metal. Testing at the 50-percent gas flow level (which would be typical of full gas generator flow on a nondumped engine configuration) and more adequately cooling the seal cavity should prevent seal erosion problems.

#### COMBUSTOR DURABILITY

No external failures occurred on any of the segments throughout the test program. Leak checks and visual inspection showed no discernible external degradation of castings, welds, electroformed nickel, or braze joints. No electroformed nickel failures as the result of hydrogen embrittlement occurred with the previously described techniques of exposed surface protection.

Combustor interior condition of the injector face plate injection elements and igniter elements remained good throughout the test program. Interior surfaces of the NARloy-A segment walls showed gradual deterioration with accumulated test time, resulting in some severe erosions at the program completion.

Since no design changes were made on the test bed No. 2 combustors pertinent to thermal operation or protection (compared to test bed No. 1), except for nickel plating the interior surfaces of two combustors, there was no reason to expect any improvement in segment hot-gas wall resistance to erosion. Therefore, segment line surface roughening and erosions progressed essentially identically to those described in Ref. 2 for test bed No. 1. At chamber pressures up to about 1000 psi, the interior surfaces typically roughened and progressed to minor erosions in line with some injector elements in the throat region over an operating period of several hundred seconds. Interim hand polishing to remove the rough sections and smooth

the minor erosions delayed progression of the surface deterioration. Even with regular interior surface maintenance, erosions still occurred. Purposely not polishing the roughened areas on one segment showed that the condition continued to worsen and that surface erosion progressed more rapidly. Operation for short time periods at the design point of 1200-psi  $P_c$  caused major hot-gas wall erosions that exposed some coolant channels to the combustion zone. The locations, types, and general geometry of the erosions were thoroughly covered in Ref. 2. Figure 59 shows the composite progression of hot-gas wall surface deterioration with test time and chamber pressures. In this figure, surface roughening is defined as a sandpaper-type finish with no measurable parent metal removal. Surface erosions are defined as being the grooves where metal was removed in alignment with oxidizer posts, but which had only progressed to about 0.060-inch width and did not allow channel coolant leakage. Exposed channels are those through the hot-gas wall which allow dumping  $H_2$  coolant directly to the combustor, bypassing the injector. The effects of operating at 1200  $P_c$  are seen to show rapid increases in erosion rates.

Figure 60 (derivations in Ref. 1) shows a correlation of estimated average calculated wall temperature that a typical segment liner would experience for the various test levels. This parameter can be considered a convenient comparison of test severity experienced during testing of the engine, and not an accurate representation of actual wall temperature. It represents a linearization of the effect of various operating parameters on predicted wall temperature at an average chamber pressure. The increase of wall temperature shown at 985 to 1025 seconds accumulated duration was caused by reorificing the engine for increased mixture ratio operation. This caused higher combustion temperature, and higher  $H_2$  coolant temperature from the tubular nozzle exit, resulting in higher combustion hot-gas wall operating temperatures.

A comparison of a normalized average combustor heat load parameter (shown in Ref. 1) for comparison at varying operating conditions is given in Fig. 61. These levels are comparable to test bed No. 1. The parameter did not show the variation to be as much as test bed No. 1, probably because of a more determined attempt to keep the combustor interior surfaces polished.

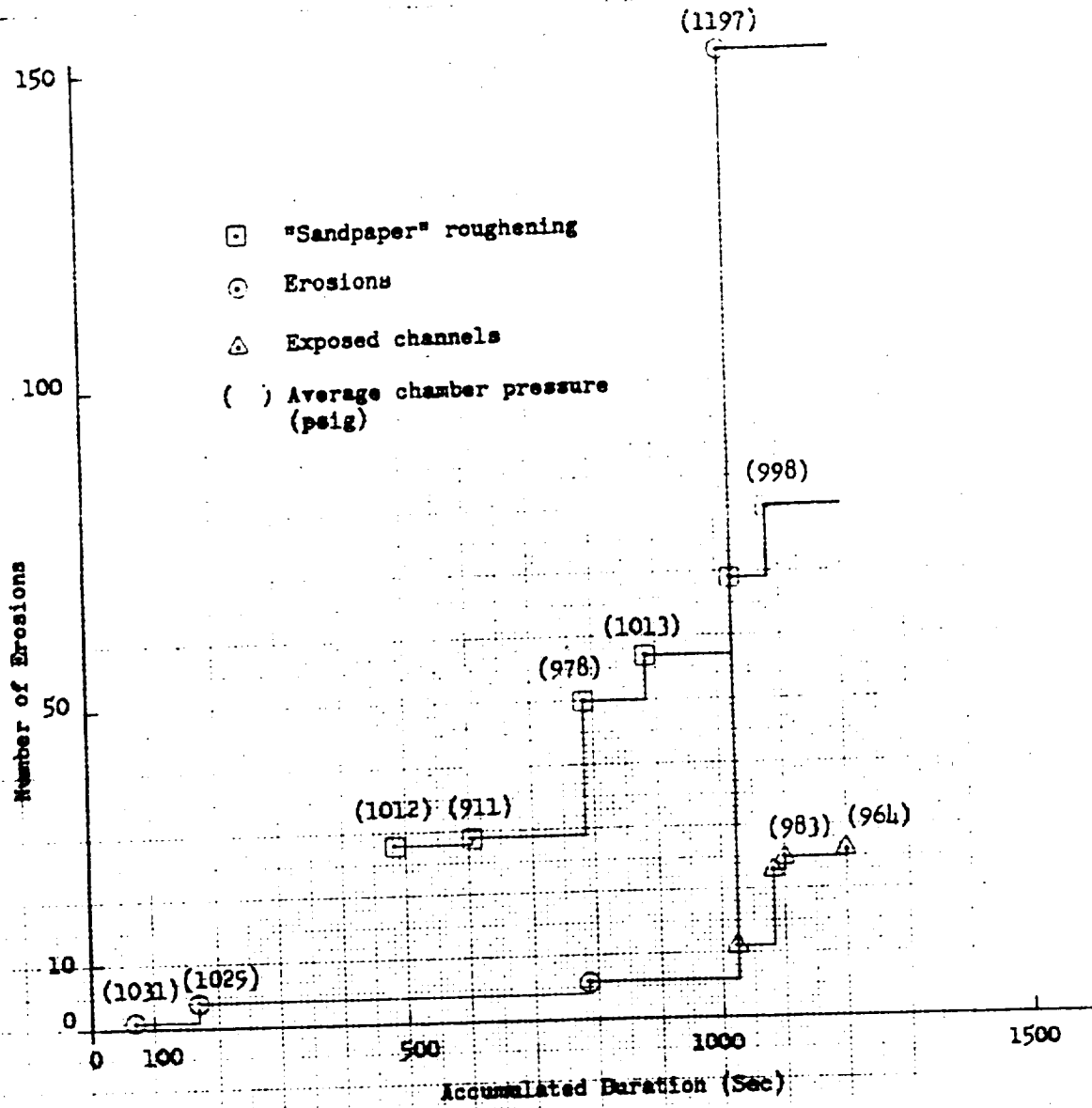


Figure 59. Test Bed No. 2 Chamber Conditions vs Accumulated Duration

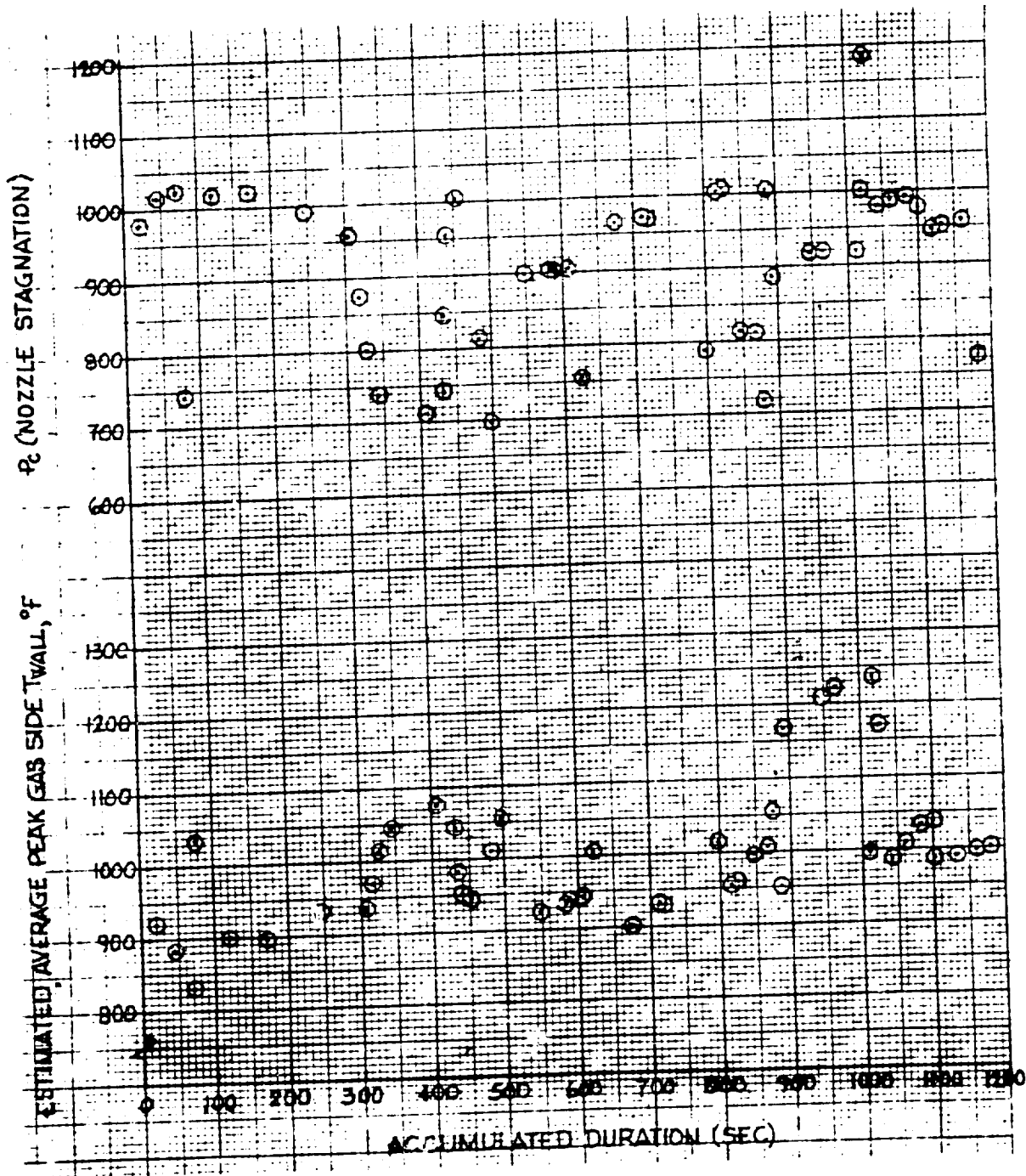


Figure 60. Test Bed No. 2 Thrust Chamber Estimated Average Peak Wall Temperature vs Accumulated Duration

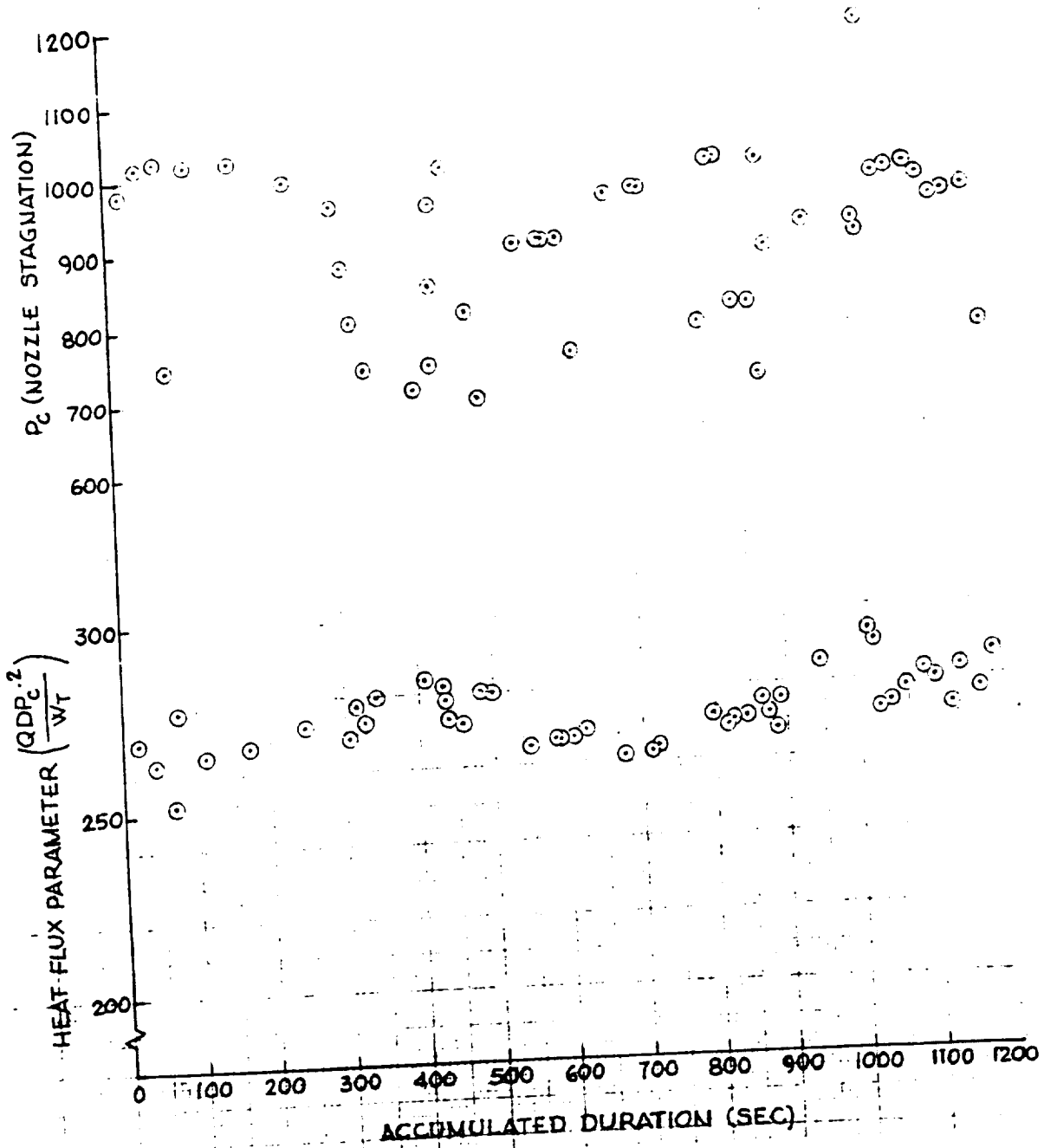


Figure 61. Test Bed No. 2 Thrust Chamber Heat Flux Parameter vs Accumulated Duration

Eight of the 10 segments had no specific surface preparation (nickel plating) prior to testing and should have shown repeatable erosion tendencies. A variation of frequency and severity of erosion did occur on the individual combustors, but all eight combustors incurred erosions. The variation among segments probably occurred due to variations in hardware fabrication tolerances and ranges of propellant mixture ratio. Calculated mixture ratio variation among the eight segments was 5.09 to 6.54 at the design 1200-psi  $P_c$ . Erosion severity ranking of the individual segments showed a relationship to the increasing calculated individual segment mixture ratio. This trend is shown in Fig. 62, but estimates of individual segment mixture ratio and erosion severity are less than accurate. Inner wall erosions were somewhat more predominant than the outer wall, but both hot-gas walls experienced severe erosion on some segments. This indication was also seen on test bed No. 1, and is probably attributed to uneven  $H_2$  coolant distribution.

The two combustors with 0.002- to 0.003-inch electrodeposited nickel on the combustion zone hot-gas walls showed less erosion than those without. One segment did not have NARloy erosions. However, this one had a hydraulic balance that placed it at the low end (number 9 of 10) of segment individual operating mixture ratios. It is likely that this segment would have experienced only minor erosion anyway. However, the other nickel-plated segment operated at the highest mixture ratio unit (number 1 of the 10 segments at 1200-psi  $P_c$ ), but sustained only one erosion region throughout the entire program. The condition of the nickel plating gradually deteriorated on both segments by cracking and pitting locally throughout the 1199.5 seconds of accumulated operation. The end condition of the plating, other than the one erosion area, was that a small portion had separated from the high heat load region of the combustion zone. In general, it is considered that the nickel plating showed the capability to provide erosion protection during operation, but that the repeated thermal cycling caused portions of the covering to crack and subsequently leave the base material in the high heat load areas.

The "machined liner" fabricated from wrought NARloy-A showed no structural problems, but had erosion tendencies at least as severe as the cast liners. Erosion experienced was as severe as any of the 10 segments, but the calculated operating mixture ratio was also among the highest (number 3 of 10 at 1200-psi  $P_c$ ). Based on the one sample,

\* COMBUSTOR POSITION ON ENGINE -  
REF. TABLE 1 SKETCH

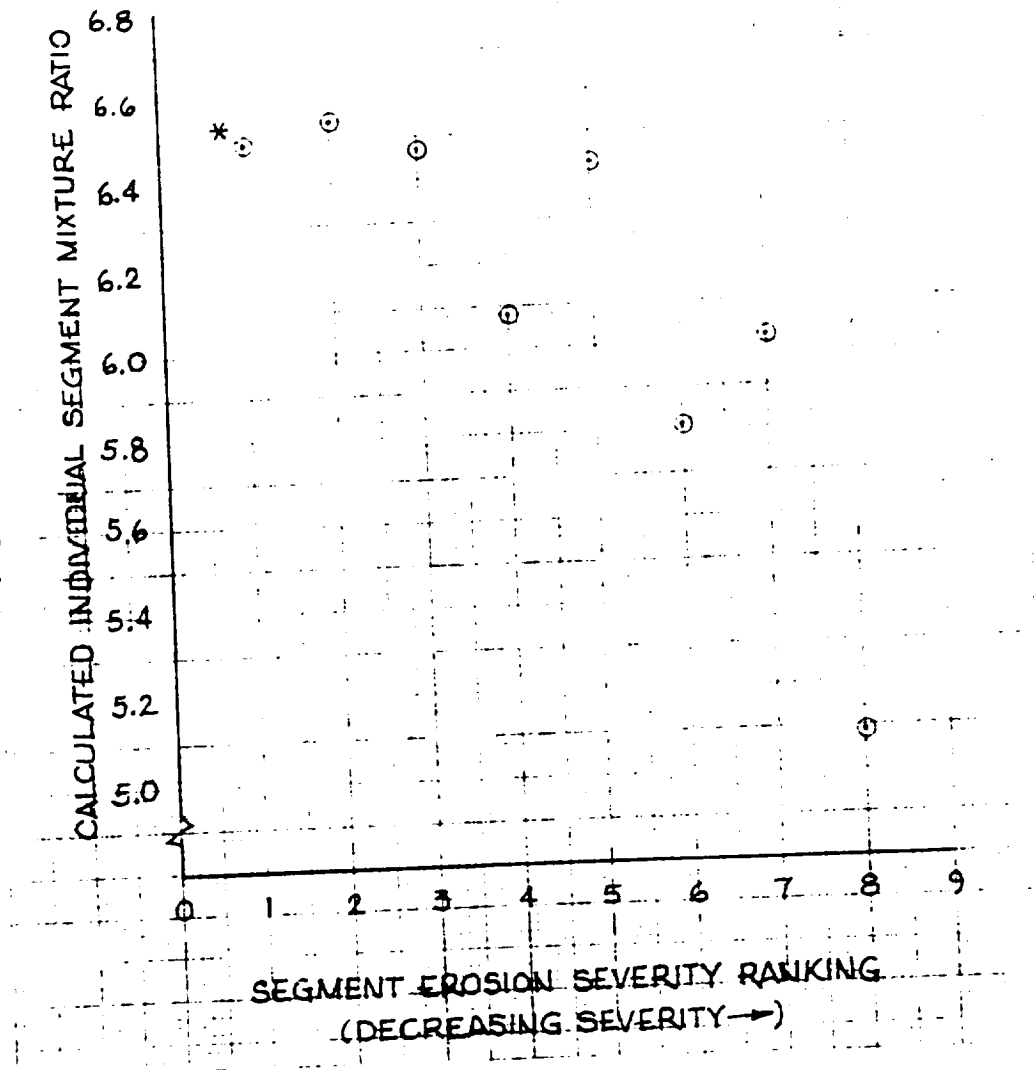


Figure 62. Test Bed No. 2 Thrust Chamber Calculated Segment Mixture Ratio vs Accumulated Erosion Severity (Nickel-Plated Hot-Gas Wall Combustors not Included)

it is considered that liner erosion resistance is approximately the same as for castings, and that the fabricated concept could be utilized as a backup concept for castings. However, costs for a machined liner are significantly above those for a cast liner.

An interim check on possible combustor throat gap change during the test program showed the area to be within 0.5 percent of the original measured gap. However, local changes due to local erosion were not measured. This is considered to be within measurement accuracy and no changes to data reduction input quantities were made, but it was estimated that throat area increased about 2 percent due to erosion occurring in the NARloy.

The combustor liner erosions experienced on test beds No. 1 and 2 are caused by an injector design that has "hot streaks" below the injector elements. The current 68-element design gives marginal hardware compatibility for operation to 1000-psi  $P_c$ , but causes rapid erosions at the 1200-psi  $P_c$  design operating level. An injector-segment combination that allows satisfactory operation will require a component test program to develop the configuration for reliable hardware operation at design  $P_c$  conditions. Such variables as cup design, injection velocities, injector pattern, element position, number of elements, element angle with respect to confining surfaces, and liner heat load capabilities would be reviewed.

REFERENCES

1. ASR 70-295, Linear Engine Design and Parametric Performance Analysis, 31 July 1970.
2. R-9049, Linear Test Bed Final Report, Vol. I: Test Bed No. 1, Rocketdyne Division, Rockwell International, 30 August 1972.

R-9049

129/130

## APPENDIX A

### BREADBOARD THRUST CHAMBER TEST BED THRUST VECTOR CONTROL STUDY

Rocketdyne is currently developing a breadboard thrust chamber test bed which employs segmented combustors under the Saturn Engines O&FS Program, contract NAS8-25156. A part of this program was devoted to evaluation and selection of a segmented combustor thrust vector control concept for use on follow-on test bed programs.

Determining an optimum segmented combustor TVC system requires a tradeoff study of TVC concepts. The study objectives were to conduct a generalized analysis of TVC concepts applicable to future vehicles and to determine optimum configurations which warrant further evaluation on the No. 2 breadboard test bed. This report presents the detailed analyses, design considerations, and study results used to define optimized TVC systems for a segmented combustor engine application.

#### SUMMARY

Nine TVC concepts were evaluated. From these, two were selected as being optimum for the segmented combustor engine concept and were studied in depth. The two concepts were the peripheral system and the checkerboard system. These systems were subjected to detailed analysis in the areas of: (1) performance, (2) structural complexity, (3) propellant feed and exhaust system design, and (4) engine-to-vehicle interface design. The Space Shuttle booster TVC requirements were used as a baseline in establishing overall design requirement. The peripheral system showed superiority in performance and propellant feed and exhaust system design. The checkerboard system appeared less complicated structurally because it follows more contemporary design practices. No advantage was determined for either system with the engine-to-vehicle interface design.

## CONCLUSIONS

The following conclusions were made from this study:

1. The two most feasible thrust vector control concepts for a Space Shuttle booster-type application are the checkerboard system and the peripheral system.
2. The optimum thrust vector control concept for a segmented combustor system appears to be the peripheral system because of its higher performance potential.
3. The structural complexity of the peripheral system is greater; however, the required peripheral system structural design is within the state of the art.

## DESIGN REQUIREMENTS

To conduct a meaningful study related to thrust vector control for a vehicle which employs engines with segmented combustors, it was necessary to establish a set of guidelines for this study. The intent was to study TVC concepts with broad application to future booster and upper stage vehicles. At the same time, the study must be specific enough that direct comparisons with existing type systems can be made. This direct comparison permits evaluation of the proposed new concepts, in light of existing technology, and provides meaningful decision-making information relative to the candidate systems.

The Space Shuttle booster vehicle was selected to provide specific requirements for the study, with the further ground rule that the study must encompass more broad applications and be suitable for use on advanced vehicles as well. The Space Shuttle booster engine gimbal requirement is  $\pm 10$  degrees in either pitch or yaw. The pitch maneuver is required for continuous tracking of the vehicle center of gravity, for the planned vehicle pitch programs, and for short-term emergency corrections for cross winds, etc. The effective 10-degree pitch gimbal angle is required to meet these needs. The yaw maneuvers are required for planned vehicle yaw programs and for short-term emergency correction for cross winds, etc. Typically, yaw maneuvers are less severe than pitch maneuvers; therefore, the maximum effective yaw gimbal requirement was established to be  $\pm 8$  degrees.

The resultant effective TVC requirements for the subject study are as follows:

1. Effective Gimbal Angle
  - a. Pitch  $\pm 10$  degrees
  - b. Yaw  $\pm 8$  degrees
2. Gimbaling rate: 10 degrees/second
3. Gimbal acceleration rate: 3 to 10 rad/sec<sup>2</sup>
4. Thrust density: 5500 lbf/ft<sup>2</sup> of boattail area
5. Boattail size: 30 x 40 feet (approximately)

R-9049

A-3

The effective gibal angle is defined as the net angular change in resultant thrust vector from all engines. The thrust density is defined as total sea level thrust from all engines divided by cross-sectional boattail area normal to the vehicle axis.

R-9049

A-4

## CANDIDATE THRUST VECTOR CONTROL SYSTEMS

Included in the study was an evaluation of all potential candidate designs for thrust vector control. In each system evaluated, the requirements of the TVC system were as described earlier, i.e., each system must meet the requirements for effective gimbal angle, gimbal rate, thrust density, and boattail size.

It was found that some of the systems studied were suitable for most any engine/boattail arrangement and provided broad application to different missions and/or vehicle designs. Other systems were more limited in scope and were only suitable for particular types of application.

The systems studied are listed in Table A-1.

Table A-1. Thrust Vector Control Evaluation

### Types of TVC

- Side-gas injection TVC
- Gas deflector
- Differential throttling
- Conventional gimbal bearing - linear engine
- Conventional gimbal bearing - round engine
- Double parallel hinge axis
- Double hinge axis
  - Parallelogram
  - Independent sides
- Single-hinge axis
- Peripheral engines

## THRUST VECTOR CONTROL SYSTEM EVALUATION

A tradeoff evaluation was conducted for each system, listing system features, unique characteristics, advantages and disadvantages of each, and potential application for each. The variables considered were performance, performance loss as a function of gimbal angle, unique design features, engine design complexity, boattail design complexity, cost, weight, and appearance.

Table A-2 presents a listing of the features, with advantages and disadvantages of each system. Three systems, the single-hinge axis, the double-hinge axis, and the peripheral were selected for further study because they exhibited the greatest potential for meeting the established requirements and because they lend themselves to broad application to future vehicles. The other systems were discarded for reasons such as low performance, inability to meet the basic requirements, structural complexity of either engine or boattail, or operational problems.

The three TVC systems which showed the greatest potential were further reduced to two by deleting the double-hinge system. There were two reasons for this reduction: (1) the performance features of the double-hinge system can be correlated to either the single-hinge or peripheral design, and (2) the double-hinge system contained problems in the base seal design which could not be clearly defined or eliminated without extensive detailed design effort which was outside the scope of this study.

Continuing the evaluation study on the selected TVC concepts requires additional engine-to-vehicle integration details. Again for convenience, the TVC concepts were tailored for a Space Shuttle booster application and 6.6 million pounds of booster sea level thrust. For clustered single-hinge engine and peripheral engine modules, the major consideration in engine arrangement was performance. The Space Shuttle requires continuous pitch variation to track the vehicle center of gravity. If not all engines are used to track the center of gravity, the engine thrust vectors do not all aim the same direction and the effective thrust is reduced. Thus, for maximum performance, the number of engines used for GG tracking must be maximized. At the same time, the number of engines required for yaw and roll

Table A-2. TVC System Feature Comparison

S OF TVC	TVC DESIGN	FEATURES	CONCLUSION
Side Gas Injection	<ul style="list-style-type: none"> <li>o Combustors Mounted To Aft End Of Engine</li> <li>o 40% Additional Combustors</li> <li>o 12% Of Main Flow For ±10 Degrees TVC Capability</li> <li>o No Vehicle Net Thrust Contribution From Combustors</li> </ul>	<ul style="list-style-type: none"> <li>o Requires Complex Control System - Multiple Valves, Seals, Manifolds, Etc.</li> <li>o Additional Structure And Significant Cost &amp; Weight Penalty</li> <li>o Higher Turbopump Horsepower Required To Meet Flow Demands</li> <li>o Significant Performance Penalty</li> </ul>	<ul style="list-style-type: none"> <li>o Not Practical From Weight, Performance, Complexity And Cost Standpoints</li> </ul>
Gas Deflector Vanes	<ul style="list-style-type: none"> <li>o Large Regeneratively Cooled Vanes Mounted At Nozzle Exit, Or At Combustor</li> </ul>	<ul style="list-style-type: none"> <li>o Significant Cost &amp; Weight Penalty</li> <li>o Large Actuators</li> <li>o Unacceptable Drag Losses</li> <li>o Questionable TVC Capability</li> </ul>	<ul style="list-style-type: none"> <li>o Not Practical From Weight, Performance And Cost Standpoints</li> </ul>
Differential Throttling	<ul style="list-style-type: none"> <li>o Assumes 50% Throttling Of Selective Engines</li> <li>o 25% Over Thrust On Remaining Engines</li> <li>o Net Available Thrust Is Significantly Reduced</li> <li>o Conventional, Checkerboard, Or Peripheral Engine Arrangement</li> </ul>	<ul style="list-style-type: none"> <li>o Lightest Weight System</li> <li>o No Plume Impingement Problems</li> <li>o Engines Rigidly Mounted</li> <li>o Only Provides 1 To 3 Degrees TVC</li> </ul>	<ul style="list-style-type: none"> <li>o Unacceptable As System Cannot Meet Basic Requirements</li> </ul>

P.F.S. OF TVC	TVC DESIGN	FEATURES	CONCLUSION
<p>Conventional Gimbal Bearing With Linear Engine</p>	<ul style="list-style-type: none"> <li>o Engine Thrust Transmitted Through Single Point Gimbal Bearing</li> </ul>	<ul style="list-style-type: none"> <li>o Technology Well Understood</li> <li>o No Performance Penalty Due To CG Tracking</li> <li>o System Directly Interchangeable With Bell Engine</li> <li>o Power Package Mounted To Thrust Frame</li> <li>o Flexible Inlet Ducting <math>\pm 10^\circ</math> Each Axis</li> <li>o Complex And Heavy Thrust Structure As Distributed Engine Loads Must Be Transferred To The Bearing Then Redistributed On The Vehicle</li> <li>o Severe Plume Impingement When Clustered: One Edge Moves Up And Adjacent Edge Moves Down               <ul style="list-style-type: none"> <li>o Plume Impingement Requires Nozzle And Base Fences</li> <li>o Base Fences Must Be Lengthened Reducing Effective Envelope And Expansion Ratio (Approximately 2 Sec Isp Loss)</li> </ul> </li> </ul>	<ul style="list-style-type: none"> <li>o Contains Weight And Performance Penalties But Concept Feasible As Backup</li> </ul>

Table A-2(Continued)

PES OF TVC	TVC DESIGN	FEATURES	CONCLUSION
<p>Conventional Gimbal Bearing And Round Aerospike Engine</p>	<p>o Engine Thrust Transmitted Through Single Point Gimbal Bearing</p>	<ul style="list-style-type: none"> <li>o Technology Well Understood</li> <li>o All Engines Used For CG Tracking. No Performance Penalty</li> <li>o System Directly Interchangeable With Bell Engine</li> <li>o No Nozzle Or Base Fences</li> <li>o Simpler Engine Out TVC Capability In Cluster Arrangements</li> <li>o Nozzle Backup Structure Is Lightweight, Simple And Inexpensive</li> <li>o Short Engine Length And Lower Gimbal Mass</li> <li>o Power Package Mounted To Thrust Frame</li> <li>o Flexible Inlet Ducting <math>\pm 10^\circ</math> Each Axis</li> <li>o Lower Available Envelope</li> <li>o 29 Combustors Required Per Engine               <ul style="list-style-type: none"> <li>o 0.5+ Throat Gap</li> <li>o 1800 Pc</li> <li>o Higher Fuel Pump Discharge Pressure Because Of Smaller Throat</li> </ul> </li> </ul>	<p>o There Are Performance And Cost Penalties But Concept Feasible As Backup</p>

Table A-2. (Continued)

PES OF TVC	TVC DESIGN	FEATURES	CONCLUSION
Continued		<ul style="list-style-type: none"> <li>o Approximately 1/3 More Combustor Segments Are Required Over The Equivalent Thrust Linear Checkerboard Engine</li> <li>o Cluster Arrangements Utilize Approximately 3/4 Of The Expansion Ratio Available To Rectangular Configurations. Results in Is Loss</li> <li>o Central Gimbal Bearing Increases Structure And Weight</li> <li>o Severe Plume Impingement</li> <li>o No Thrust Vector Altitude Compensation</li> </ul>	

Table A-2. (Continued)

TES OF TVC	TVC DESIGN	FEATURES	CONCLUSION
<p>Double Parallel Hinge System</p>	<ul style="list-style-type: none"> <li>o Nozzles Hinged As A Parallelogram With <math>\pm 16^\circ</math> Hinge Angle</li> </ul>	<ul style="list-style-type: none"> <li>o Light Weight Structure</li> <li>o Power Package Rigidly Mounted</li> <li>o Flexible Joints In High Pressure Ducting And Exhaust System</li> <li>o Plume Impingement Less Severe Than Single Axis Hinge</li> <li>o Pitch Nozzles Mechanically Linked                             <ul style="list-style-type: none"> <li>o Fences Not Required On All Engines</li> </ul> </li> <li>o Flexible Base Seal Required</li> <li>o Will Not Permit Varying Nozzle Angle For Altitude Compensation</li> </ul>	<ul style="list-style-type: none"> <li>o System Is Practical However Similar But Improved Concepts Are Available</li> </ul>
	<ul style="list-style-type: none"> <li>o Nozzles Hinged Near Combustors Independent Gimbaling Of Sides</li> </ul>	<ul style="list-style-type: none"> <li>o Lightweight Structure - Less Weight Than Single Axis Hinge</li> <li>o Thrust Vector Altitude Compensation</li> <li>o Power Package Rigidly Mounted</li> <li>o Flexible Joints In High Pressure Ducting And Exhaust System</li> <li>o Flexible Base Seal Required</li> <li>o Plume Impingement Less Severe Than Single Axis Hinge</li> </ul>	<ul style="list-style-type: none"> <li>o System Is Practical If Flexible And Variable Area Base Can Be Developed</li> </ul>

Table A-2. (Continued)

TYPES OF TVC	TVC DESIGN	FEATURES	CONCLUSION
<p>7. Double Transverse Hinge Axis</p>	<ul style="list-style-type: none"> <li>o Hinge Lines Provided In Both Pitch And Yaw Axis</li> </ul>	<ul style="list-style-type: none"> <li>o Power Package Mounted To Gimbaleed Mass</li> <li>o Flexible Inlet Ducting</li> <li>o Complex Structure</li> <li>o Weight Is Approximately 300 Pounds Greater Than Conventional Gimbal Bearing</li> </ul>	<ul style="list-style-type: none"> <li>o No Advantage Over Conventional Single Point Gimbal Bearing</li> </ul>
<p>8. Single Hinge Axis</p>	<ul style="list-style-type: none"> <li>o Nozzle Hinged As Rigid Mass</li> </ul>	<ul style="list-style-type: none"> <li>o Power Package Can Be Rigidly Mounted Or Part Of Hinged Assembly</li> <li>o Some Plume Impingement Problems</li> <li>o Pitch Nozzles Mechanically Linked</li> <li>o Fences Not Required On All Engines</li> </ul>	<ul style="list-style-type: none"> <li>o System Is Practical For Further Study</li> </ul>

R-9049

A-12

Table A-2. (Concluded)

PES OF TVC	TVC DESIGN	FEATURES	CONCLUSION
<p>Peripheral Engine</p>	<ul style="list-style-type: none"> <li>o Nozzles Hinged For TVC And Altitude Compensation</li> </ul>	<ul style="list-style-type: none"> <li>o Simplified Propellant Ducting (Feeds One Manifold Only)</li> <li>o Approximately One Half Fewer Combustors Required (56K Combustors Versus 26K Combustors For Double Sided Engine)</li> <li>o Concept Maximizes Available Expansion Ratio As Base Area Is Totally Utilized</li> <li>o Shielding Not Required</li> <li>o No Base Fences Curtains And Shields Are Required To Constrain Base Flow</li> <li>o Each Nozzle Individually Hinged</li> <li>o Incorporates Thrust Vector Altitude Compensation</li> </ul>	<ul style="list-style-type: none"> <li>o System Is Practical For Further Study</li> </ul>

maneuvers must also be some reasonable value; otherwise, with yaw or roll maneuvering, the angular excursions for equivalent turning moments becomes excessive, a serious loss in vehicle performance results, and the engine design required to provide the high hinge angles is unduly complicated.

With the single-hinge and peripheral engine concept, many engine/boattail arrangements are possible and most of the practical arrangements were evaluated. A sampling of some of the single-hinge engine/boattail designs is shown in Fig. A-1. Each concept has its own unique problems and advantages, which will not be discussed here as they are beyond the scope of this report. However, the previously mentioned design consideration, low performance loss during TVC maneuvers, together with standard vehicle design considerations such as minimum complexity, simplicity of design and ease of maintenance, led to the following engine/boattail arrangements as being best for the selected concepts.

**Peripheral Design:** The peripheral design was incorporated into a 30 by 40-foot rectangular boattail with 14 engine modules 10 in pitch and 4 in yaw, as shown in Fig. A-2. Each engine module is 8 feet wide. Figure A-3 presents an end and back view of a single module.

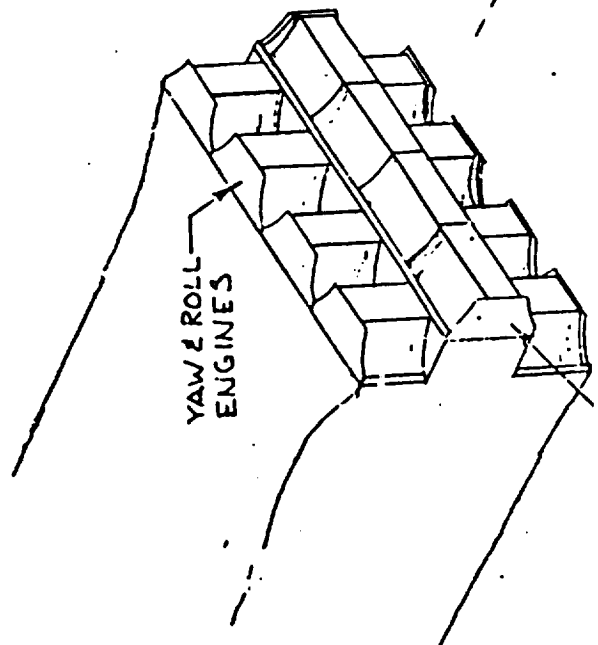
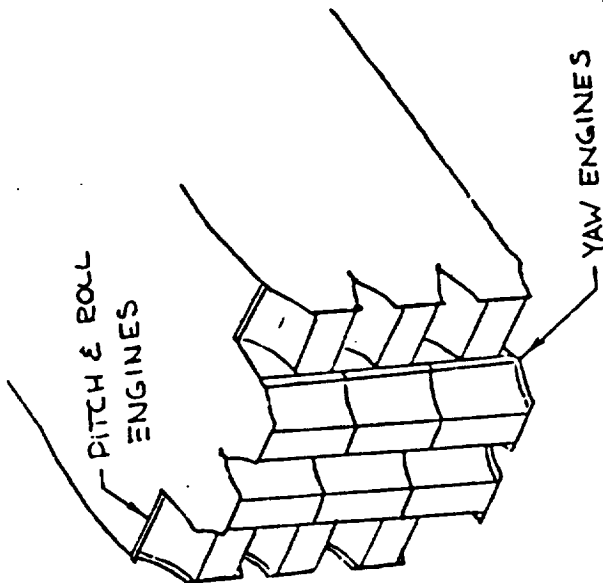
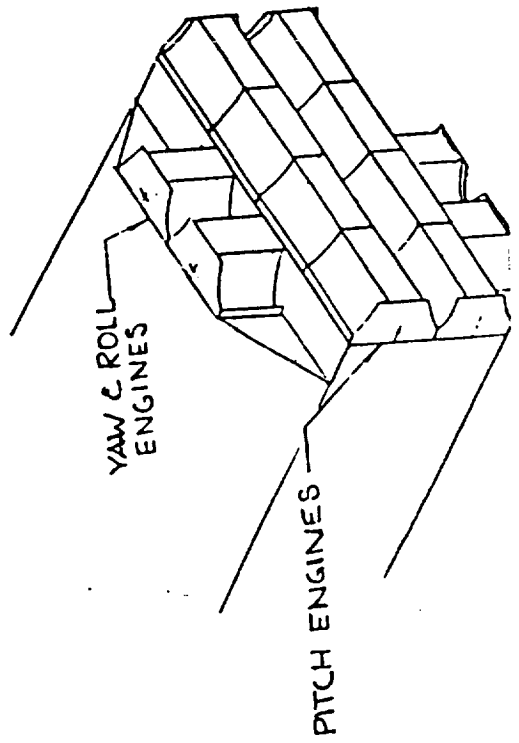
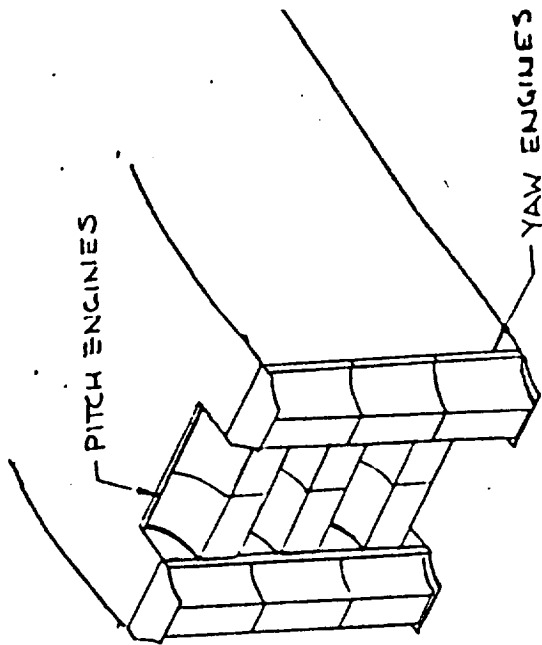
**Checkerboard Design:** The single-hinge design was incorporated into a 40-foot-diameter boattail with 12 engines arranged 2-4-4-2, 8 in pitch and 4 in yaw, as shown in Fig. A-4. Each engine module is 10 ft<sup>2</sup>. Figure A-5 shows the component arrangement of a single-engine module.

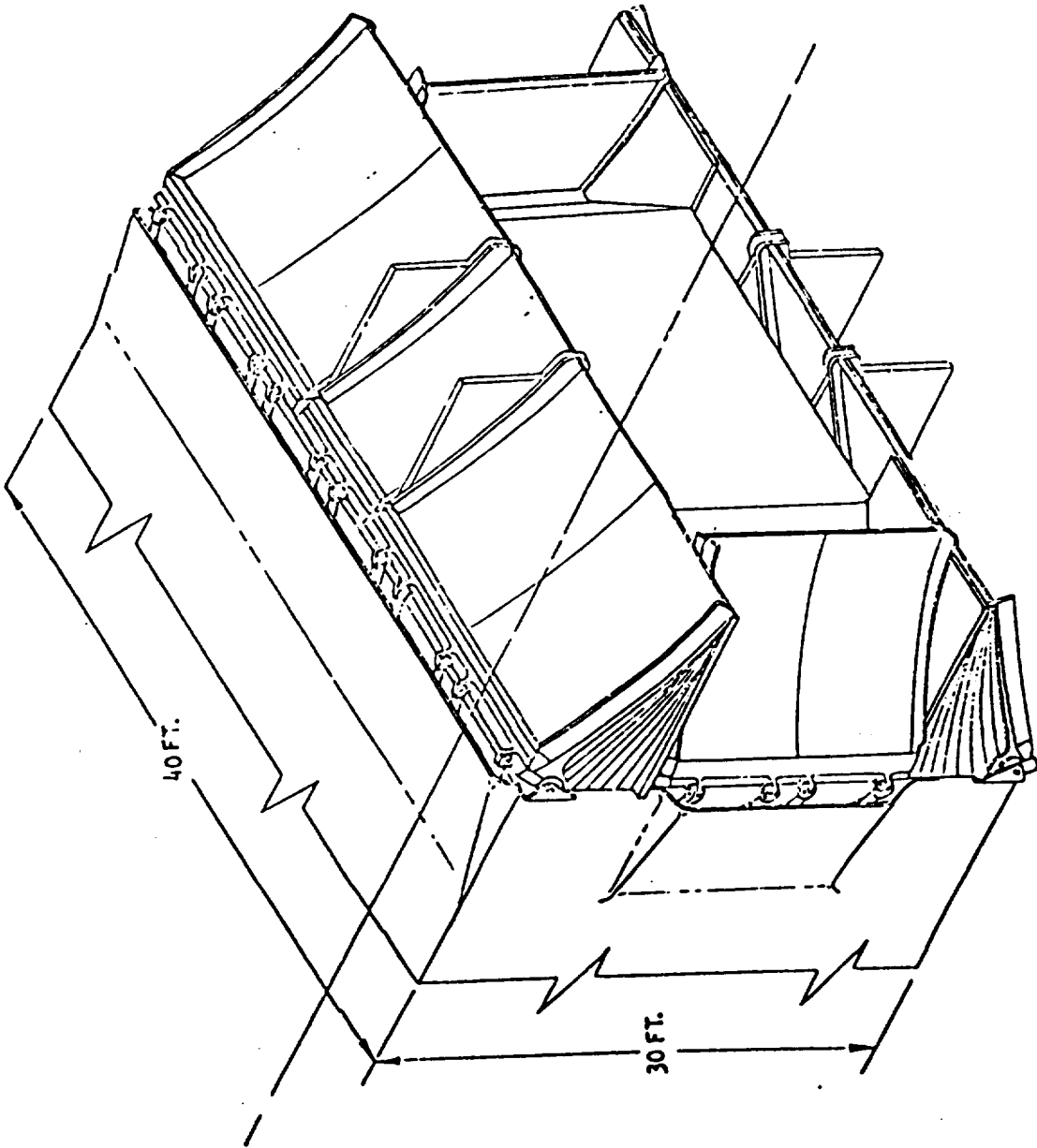
The determination of the optimum TVC concept requires detailed analysis in the following areas: (1) performance, (2) structural complexity, (3) propellant feed and exhaust system design, and (4) engine-to-vehicle interface design requirements. Each of these areas is discussed below as a separate item.

## PERFORMANCE

Table A-3 presents a comparison of checkerboard and peripheral engine system performance. The predicted performance of the peripheral concept is higher than that

R-9049



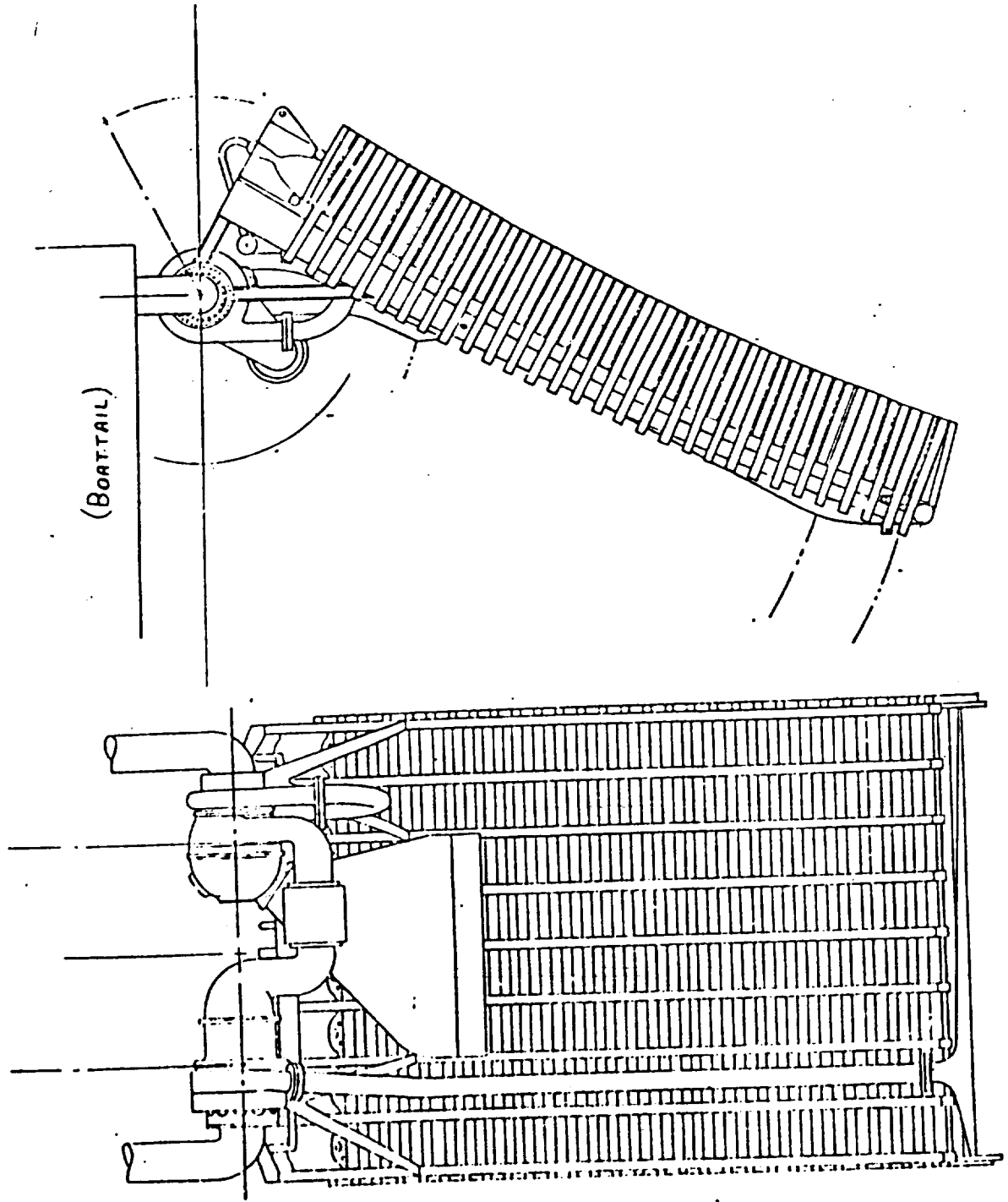


SCALE  $\frac{1}{120}$

Figure A-2. Peripheral Engine Arrangement

R-9049

A-16



R-9049

A-17

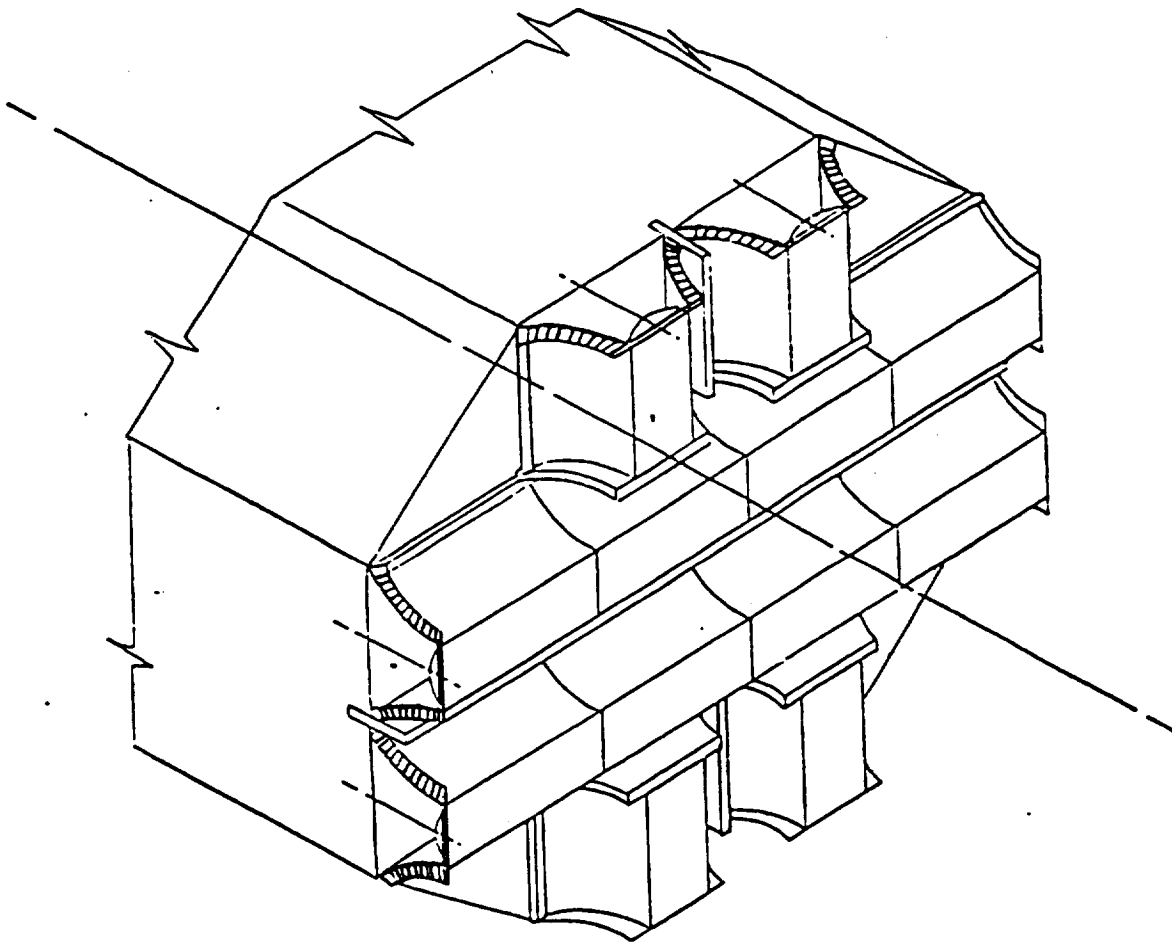


Figure A-4. Single Hinge Engine/Boattail Checkerboard Arrangement

R-9049

A-18

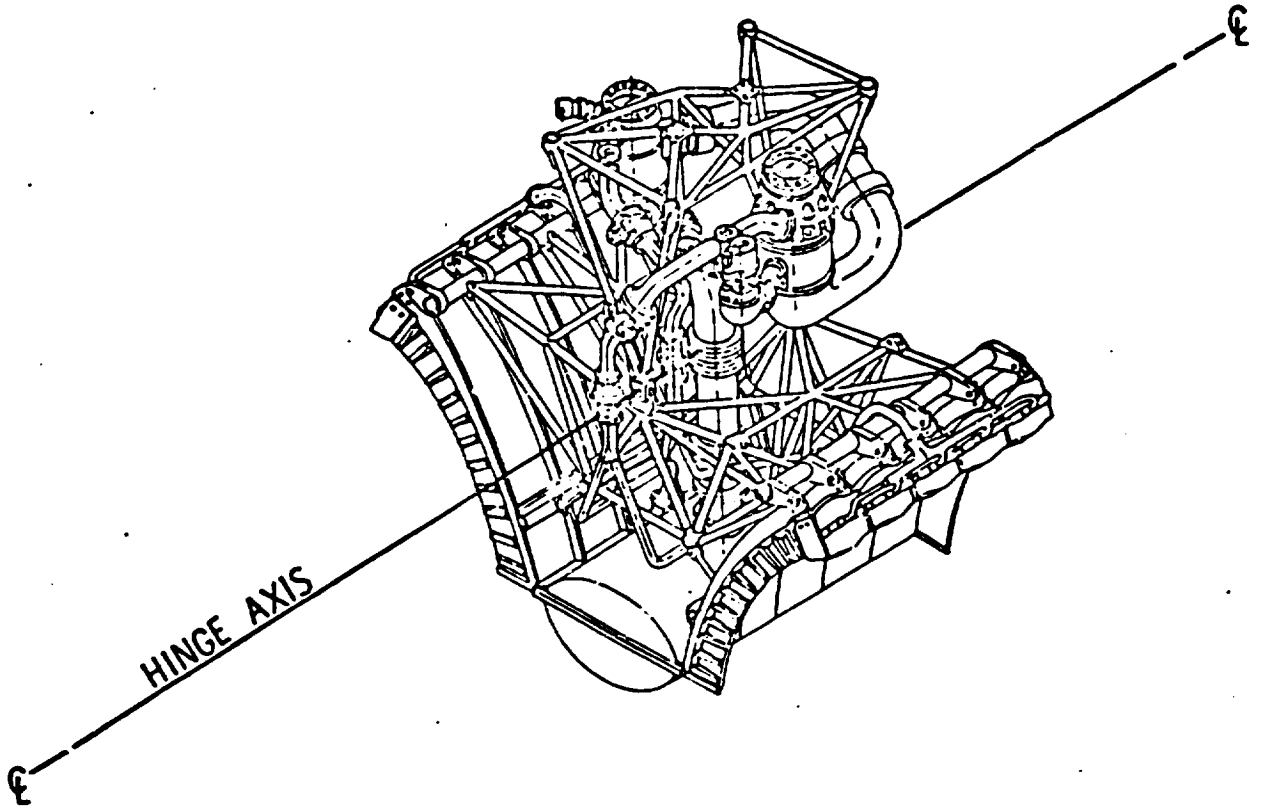


Figure A-5. Advanced Breadboard Concepts Incorporating Thrust Vector Control  
(Test Bed No. 2)

R-9049

A-19

Table A-3. Candidate Systems Performance Comparison

Feature	Checkerboard	Peripheral
Specific Impulse, seconds	442 @ Altitude	448 @ Altitude
P <sub>c</sub> (optimum), psia	1800	2000
Hinge Requirements, degrees from null	±24	+48 -10
Percentage Engines in Pitch	66.6	71 Sea Level 36 Altitude
Percentage Engines in Yaw	33.3	29 Sea Level 15 Altitude
Fuel Pump Discharge Pressure, psia	3500	3200
Number Of Combustors	240	112
Throat Gap, inches	.78	1.5
Thrust/Combustors	26K	47K
Weight (Approximate), pounds	6000	lower

expected in the checkerboard concept. The major reason for the higher performance is the greater base area of the peripheral design. Further details on predicted performance are presented in the Engine System Performance section at the end of this report. For this study, TVC effects on engine performance are considered.

Providing TVC with hinged engines rather than gimballed engines has some drawbacks because hinged engines can be rotated only in yaw or pitch, not in both axes. Thus, only a portion of the engines can effect either a yaw or pitch thrust vector maneuver, with the result that more hinge-angle capability must be provided for hinged-engine systems than for gimballed engine systems. The hinge-angle requirements shown in Table 3 are different for each concept. The checkerboard TVC angle requirements,  $\pm 24$  degrees, is based on the yaw engines TVC angle required to effect an 8-degree equivalent system TVC angle. The peripheral concept hinge angle is  $+48$  to  $-10$  degrees\* and combines TVC capability with altitude compensation (see Fig. A-6). Figures A-7 and A-8 show the engine hinge angle versus effective net thrust vector angle for the checkerboard and peripheral concepts in pitch and yaw, respectively. These curves show the hinge angle penalty resulting from not having all engines capable of yaw or pitch maneuvers. A range is shown for the peripheral concept from sea level to altitude because, at altitude, inboard engine rotation reaches a maximum (i.e., no further inboard rotation is possible), thereby doubling the hinge angle required of the outboard engines to effect a given TVC maneuver.

For a given TVC maneuver, a performance (thrust) loss is sustained when bank actuation occurs because the jet streams from the hinged engines leave the vehicle in different directions from the engines which remain stationary. Figures A-9 and A-10 present percent loss in thrust versus equivalent vector angle for the checkerboard and the peripheral concepts in pitch and yaw, respectively. A range is

\*For the peripheral concept, the vacuum or altitude position was selected as the reference point, with negative hinge angles implying inboard rotation and positive gimbal angles implying outboard rotation from the reference point. Also, only the yaw engines can rotate negatively because with the arrangement selected, pitch engine negative rotation would interact with the yaw engines.

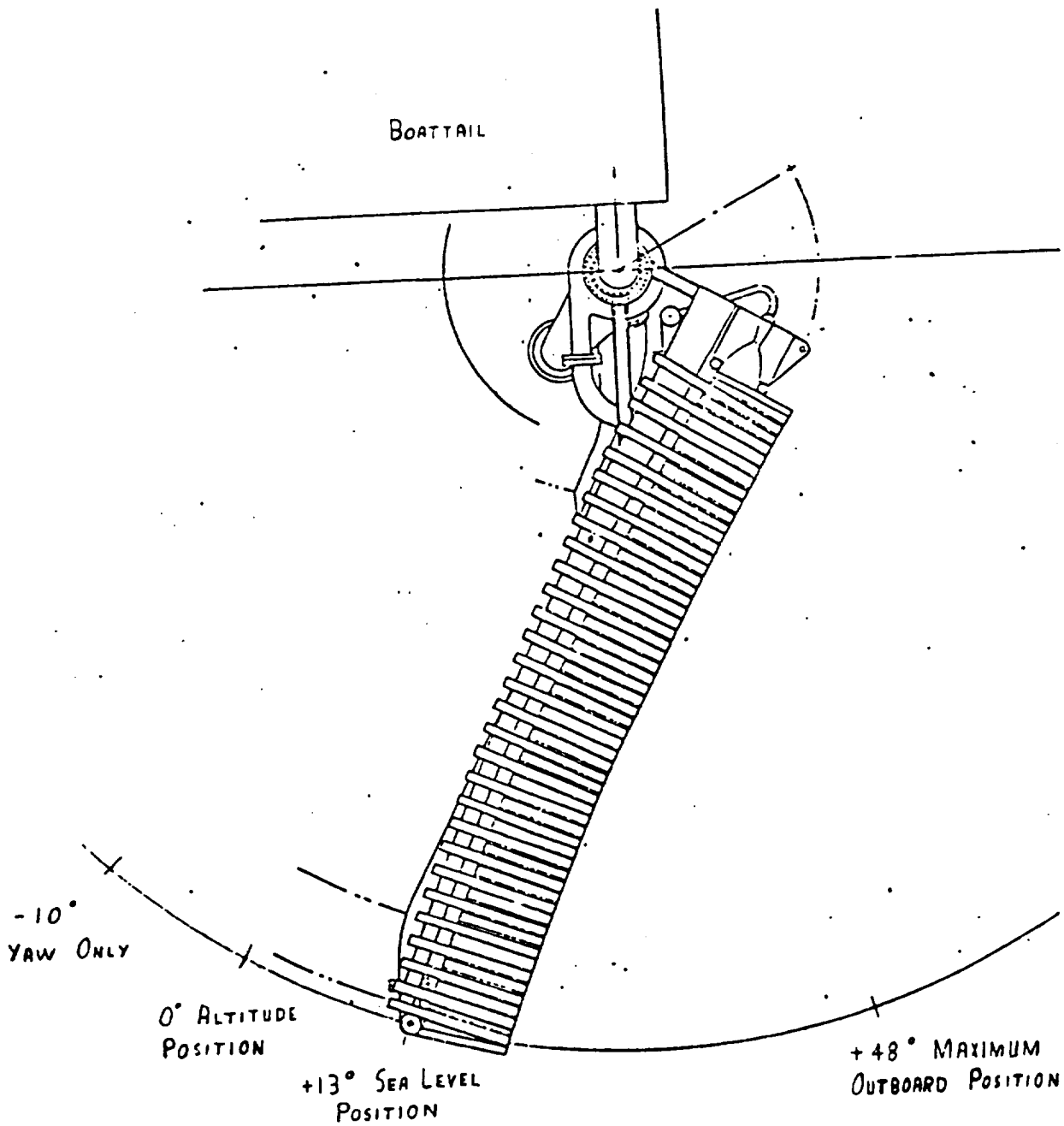


Figure A-6. Peripheral Engine Nozzle Hinge Angle Positions

R-9049

A-22

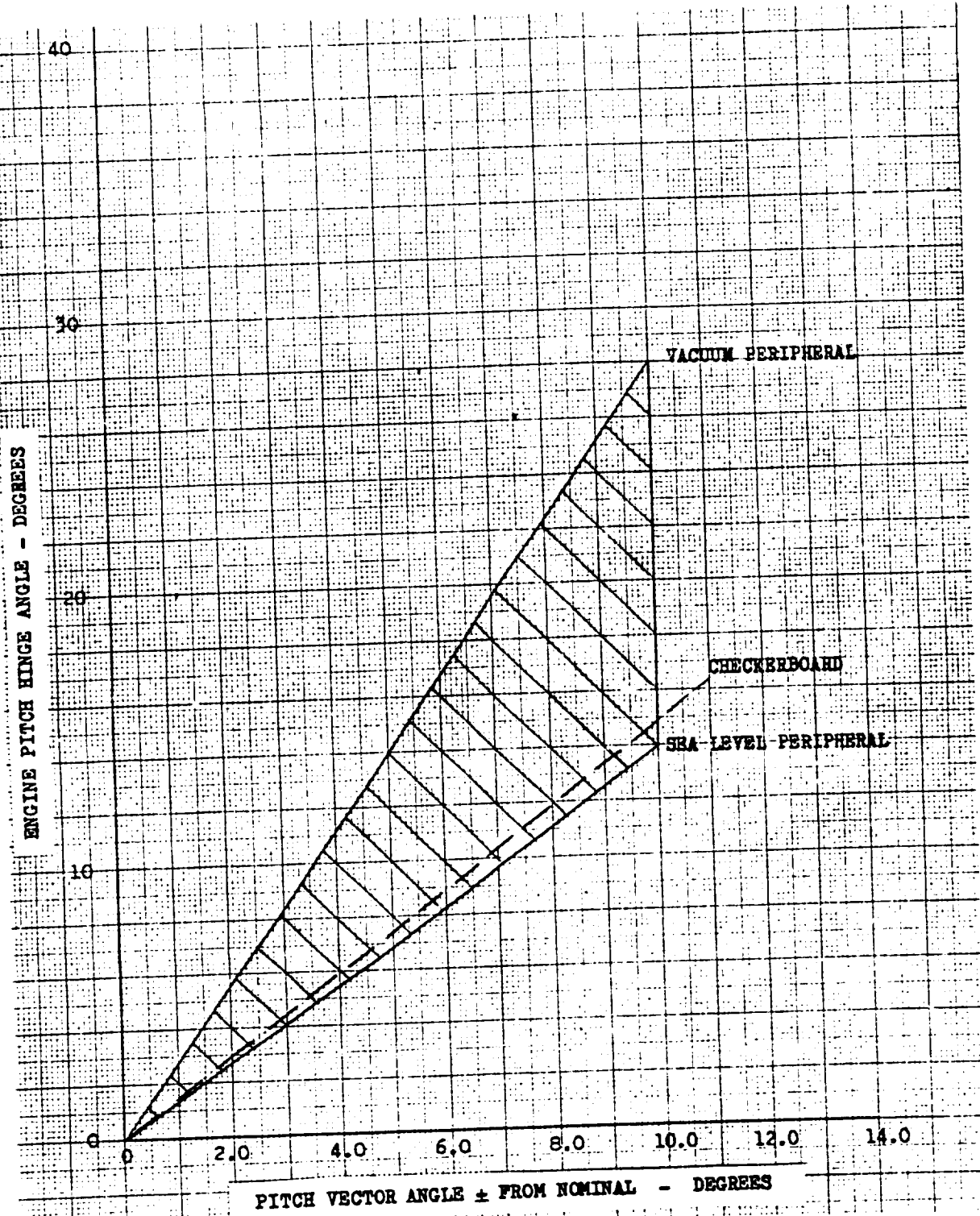


Figure A-7. Pitch Hinge Angle as a Function of Engine Net Vector Angle for Peripheral and Checkerboard Systems

R-9049

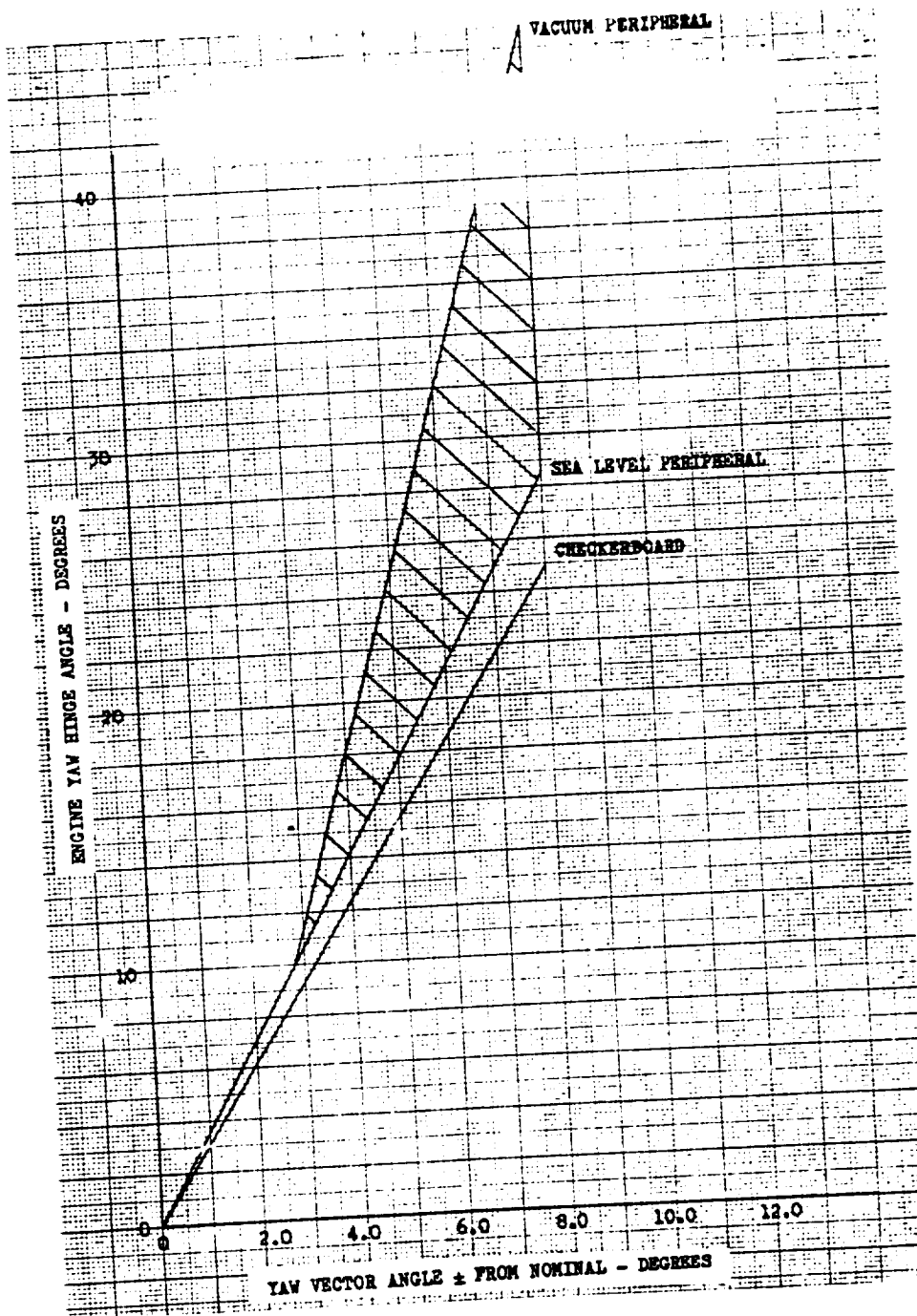


Figure A-8. Yaw Hinge Angle as a Function of Engine Net Vector Angle for Peripheral and Checkerboard Systems

R-9049

A-24

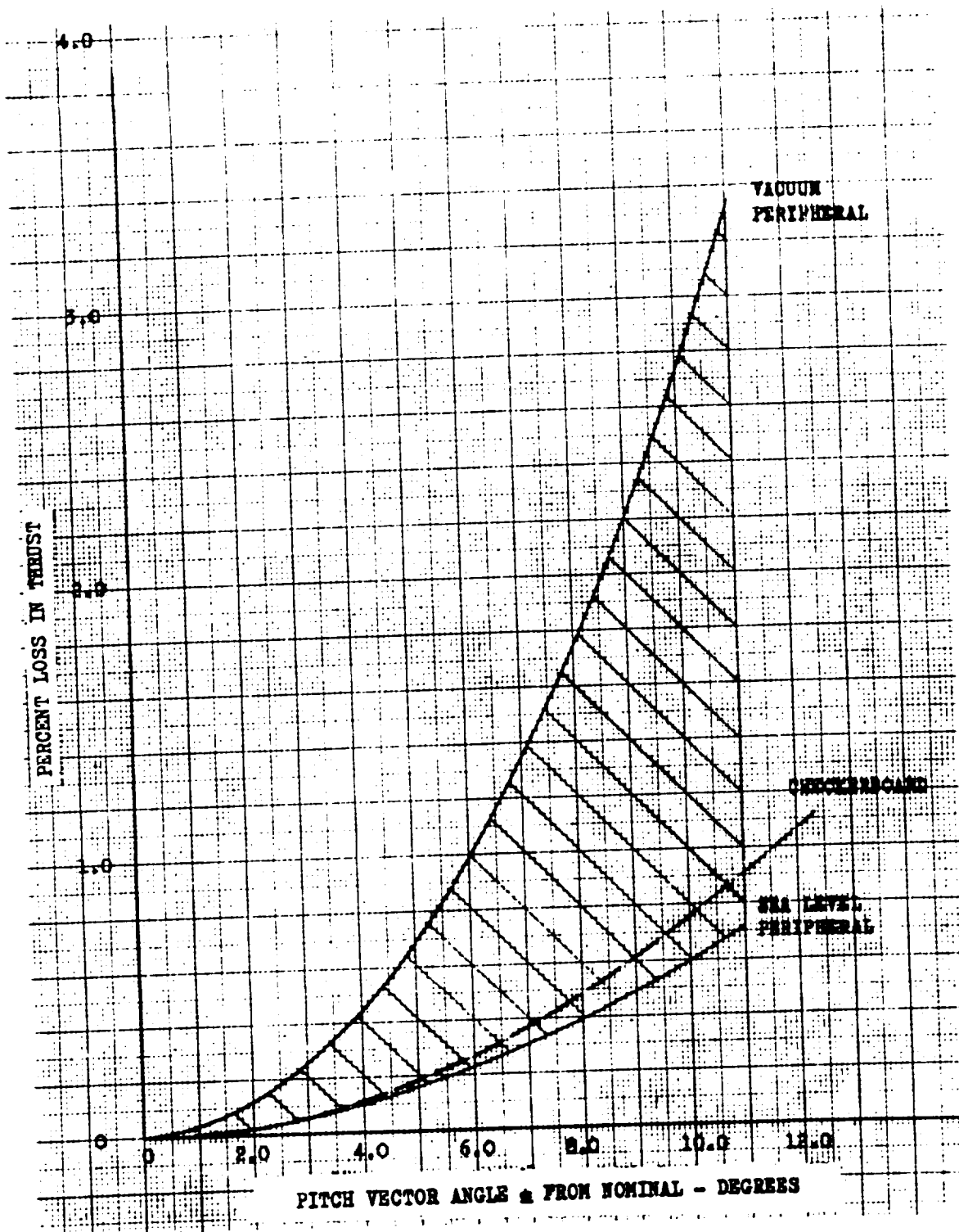


Figure A-9. Percent Loss in Thrust Versus Equivalent Pitch Vector Angle for the Checkerboard and Peripheral Engine Systems

R-9049

A-25

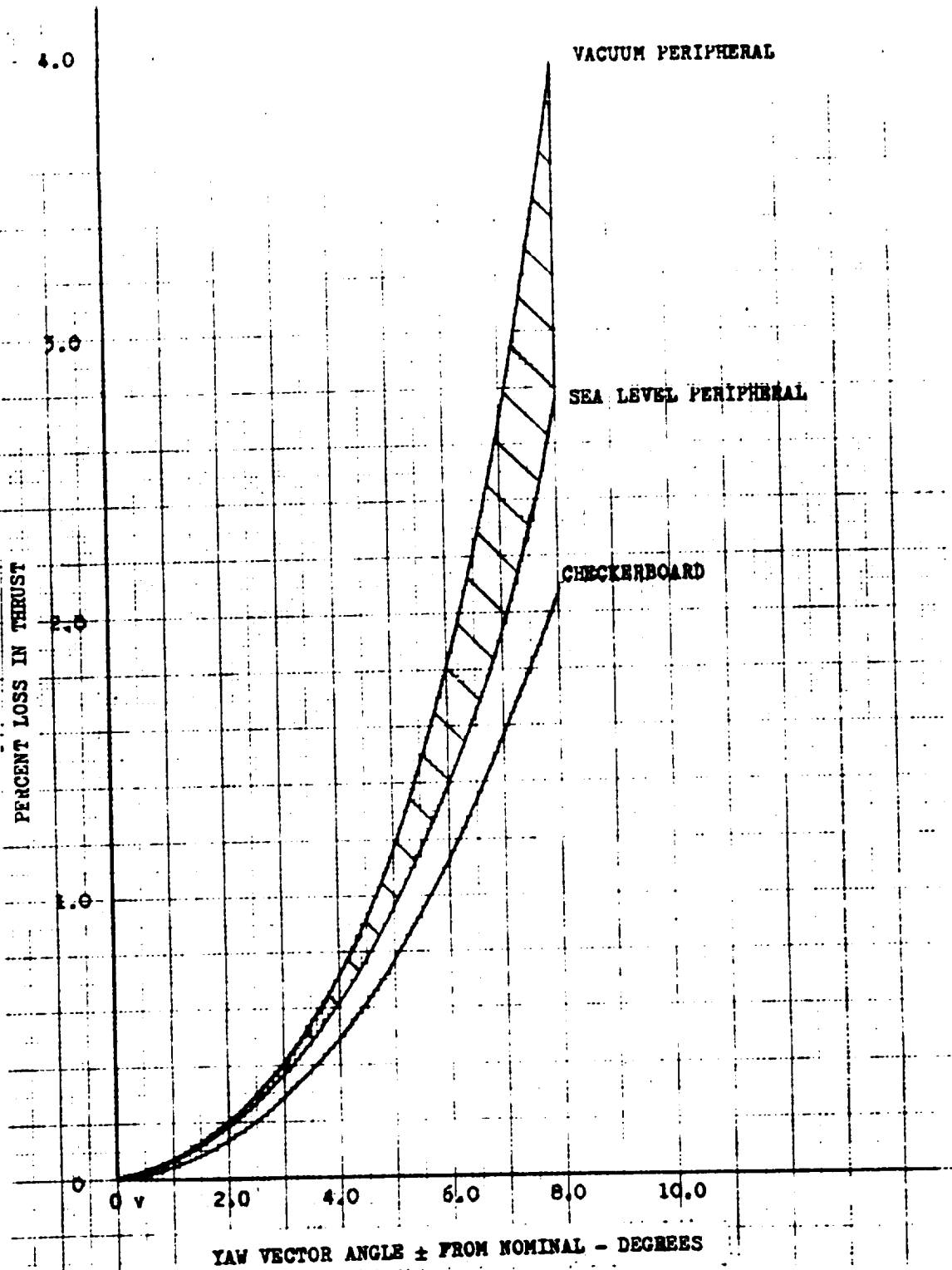


Figure A-10. Percent Loss in Thrust Versus Equivalent Yaw Vector Angle for the Checkerboard and Peripheral Engine Systems

R-9049

A-26

shown for the peripheral system because, at altitude, inboard gimbaling is limited in yaw and nonexistent in pitch, thus requiring the opposite engine bank, which can rotate outboard, to compensate by rotating through twice the required angle. These curves show that performance (thrust) losses during TVC maneuvers are greater with the peripheral system except for sea level pitch maneuvers.

Comparing candidate TVC system performance requires calculating performance losses over an entire flight profile. Again, it was germane to utilize the Space Shuttle flight profile pitch program for this comparison. The Space Shuttle proposed pitch programs shown in Fig.A-11 account for vehicle CG tracking and headwind, tailwind, or no wind conditions. The vehicle CG tracking maneuver, which is the major pitch maneuver contributor, is constant: changing during a flight because of propellant consumption. From examination of Fig.A-11 it can be seen that gimbal angle excursions could be significantly reduced by having the pitch engines biased 2.7 degrees initially. This action effectively shifts the engine null from 0 to +2.7 degrees at launch. Figure A-12 presents the same Shuttle Vehicle pitch profile with the bias incorporated. The pitch program shown in Fig.A-12 results in a small pitch angle bias at start which passes through zero (null pitch) approximately midway through the flight and finally ends up with an opposite pitch angle bias at burnout.

Using the no wind TVC flight profile (shown in Fig.A-12), a performance (thrust) loss was calculated for both the checkerboard and peripheral system arrangements. The flight profile was divided into nineteen 10-second time segments, and an average pitch gimbal angle was estimated for each time segment. These data are tabulated in Table A-4. Knowing the pitch angle, a percent thrust loss value can be derived from Fig. A-9 corresponding to each time segment. The average total flight performance loss is then calculated by summing the thrust losses and dividing this number by the number of time segments. An average total flight performance (thrust) loss of 0.04 and 0.06 percent was calculated for the checkerboard and peripheral systems, respectively. Table A-4 includes the percent thrust loss data and the average total flight performance loss calculations for the peripheral and checkerboard systems.

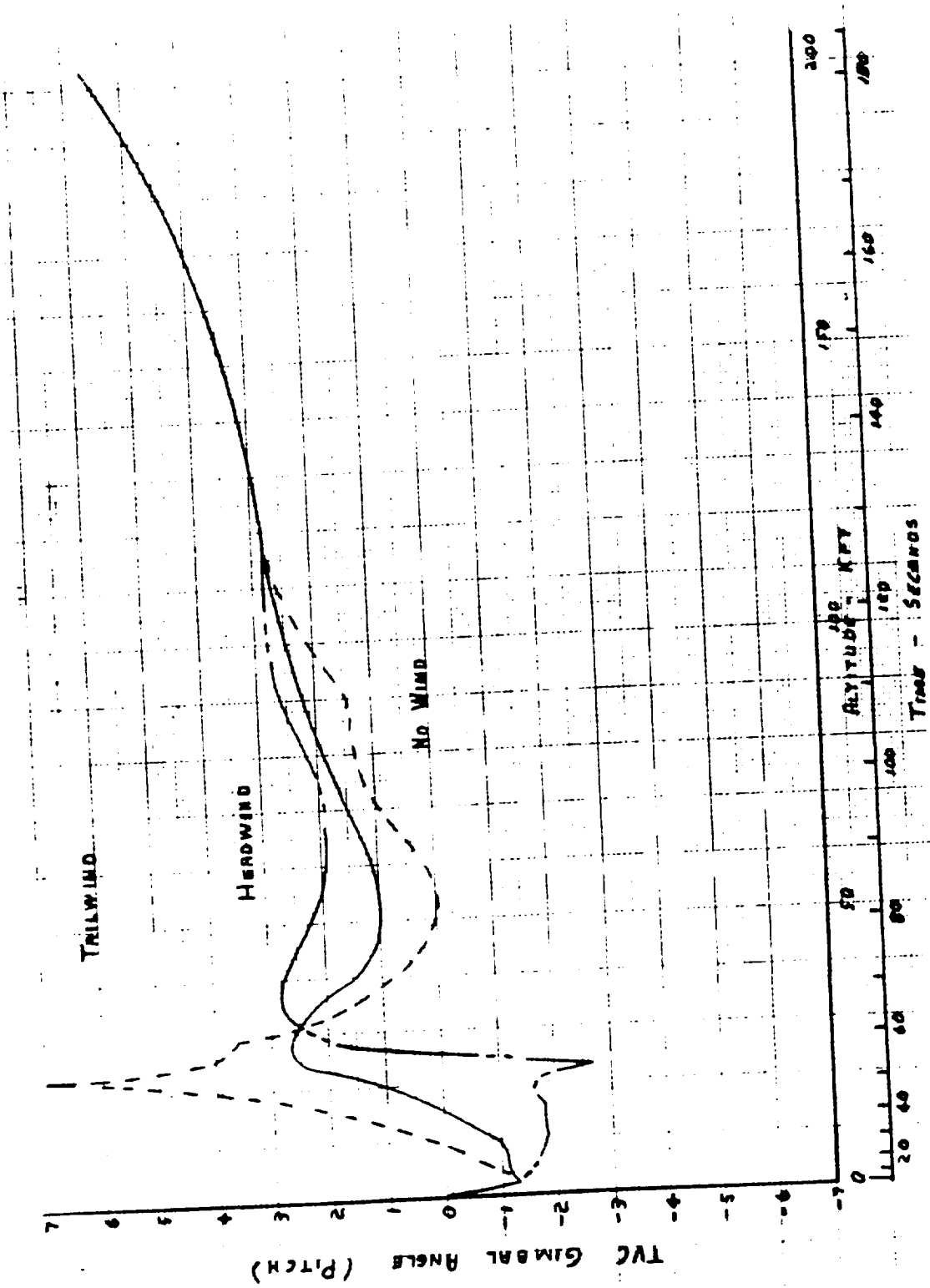


Figure A-11. Space Shuttle Pitch Program Versus Altitude and Time

R-9049

A-28

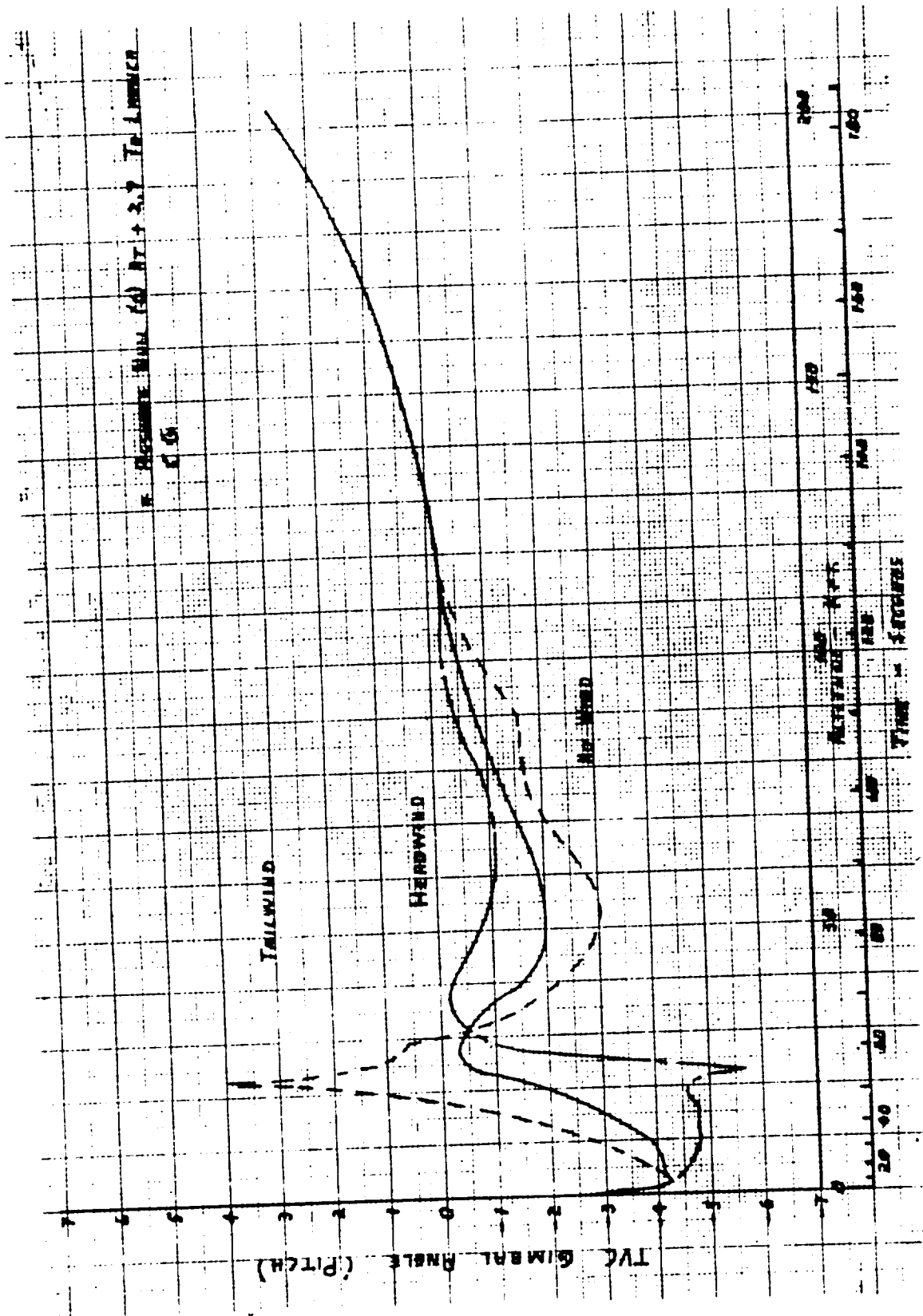


Figure A-12. Space Shuttle Pitch Program\* Versus Altitude and Time

Table A-4 Flight Profile for Checkerboard and Peripheral Systems

Time Period, seconds	Altitude, feet x 10 <sup>3</sup>	No Wind Pitch Gimbal Angle, degrees (Fig. A-12)	Checkerboard System Percent Thrust Loss (Fig. A-9)	Peripheral System Percent Thrust Loss (Fig. A-9)
0 to 10	0 to 1.8	-2.7 to -4.2	0.14	0.12
10 to 20	1.8 to 4.2	-4.1	0.13	0.11
20 to 30	4.2 to 7.9	-4.0	0.125	0.10
30 to 40	7.9 to 12.5	-3.55	0.1	0.085
40 to 50	18.6 to 2.25	-2.25	0.035	0.035
50 to 60	26.5	-0.35	0.0	0.000
60 to 70	36.0	-0.9	0.01	0.005
70 to 80	47.5	-1.9	0.025	0.095*
80 to 90	60.5	-1.8	0.02	0.085
90 to 100	74.2	-1.28	0.015	0.05
100 to 110	88.3	-0.78	0.005	0.02
110 to 120	103.2	-0.39	0.0	0.01
120 to 130	119.5	-0.1	0.0	0.00
130 to 140	135.5	+0.12	0.0	0.00
140 to 150	151	+0.58	0.005	0.01
150 to 160	165.5	+1.0	0.01	0.03
160 to 170	178.4	+1.45	0.015	0.06
170 to 180	190.5	+2.12	0.03	0.12
180 to 187	197.5	+2.7	0.05	0.195
			Σ 0.715	Σ 1.125
		Average Total	<u>0.715</u>	<u>1.125</u>
		Total Time Periods	19	19
			+0.038	+0.059
		Percent Thrust Loss	~0.04	~0.06

\*Altitude curve used from this point (Fig. A-9)

While TVC performance losses are greater with the peripheral concept, it is possible to increase system performance through altitude compensation. As mentioned earlier, the peripheral system incorporates large gimbal angle capability to combine TVC and altitude compensation. Altitude compensation for a segmented combustor engine can be divided into two regimes: aerodynamic and thrust vector. Aerodynamic altitude compensation results from exhaust stream interaction with ambient air. The exhaust stream is compressed at low altitudes and expands at high altitudes, depending on the local ambient air pressure. This interaction with atmospheric pressure causes the nozzle wall pressure ratio profile (wall pressure/chamber pressure) to vary with altitude for optimum nozzle performance. Figure A-13 (ideal wall pressures), illustrates this change in the wall pressure ratio from sea level to vacuum for various nozzle lengths. However, this variation in the nozzle pressure ratio profile causes the nozzle thrust vector angle to vary with respect to the nozzle. The thrust vector inclination angle variation with altitude is illustrated in Fig. A-14. Maximum net thrust occurs when the net thrust vector of each module is always parallel to the vehicle axis. Thus, thrust vector altitude compensation requires rotating the nozzle walls inboard from a sea level position as altitude increases to keep the thrust vector in line with the engine (vehicle) axis.

It has been estimated that thrust vector altitude compensation could effect a sea level effective thrust improvement of between 2.7 and 5 percent. The 2.7-percent value applies to the checkerboard design and is determined by taking the thrust vector altitude compensation angle, 13 degrees, and calculating the thrust vector loss (the inverse of the cosine of 13 degrees). The 5-percent value applies to the peripheral design where the angular difference may be as great as 18 to 20 degrees. The performance gain estimate assumes no changes in base area or pressure which, of course, is invalid. Rotation of the nozzle walls obviously changes the base area and, probably, the resultant base pressure. At present, base pressure variations with nozzle wall rotation are not analytically determinable. Test data are required, either wind tunnel modeling or hot fire, to determine thrust vector altitude compensation effects on base pressure and to refine analytical performance prediction techniques.

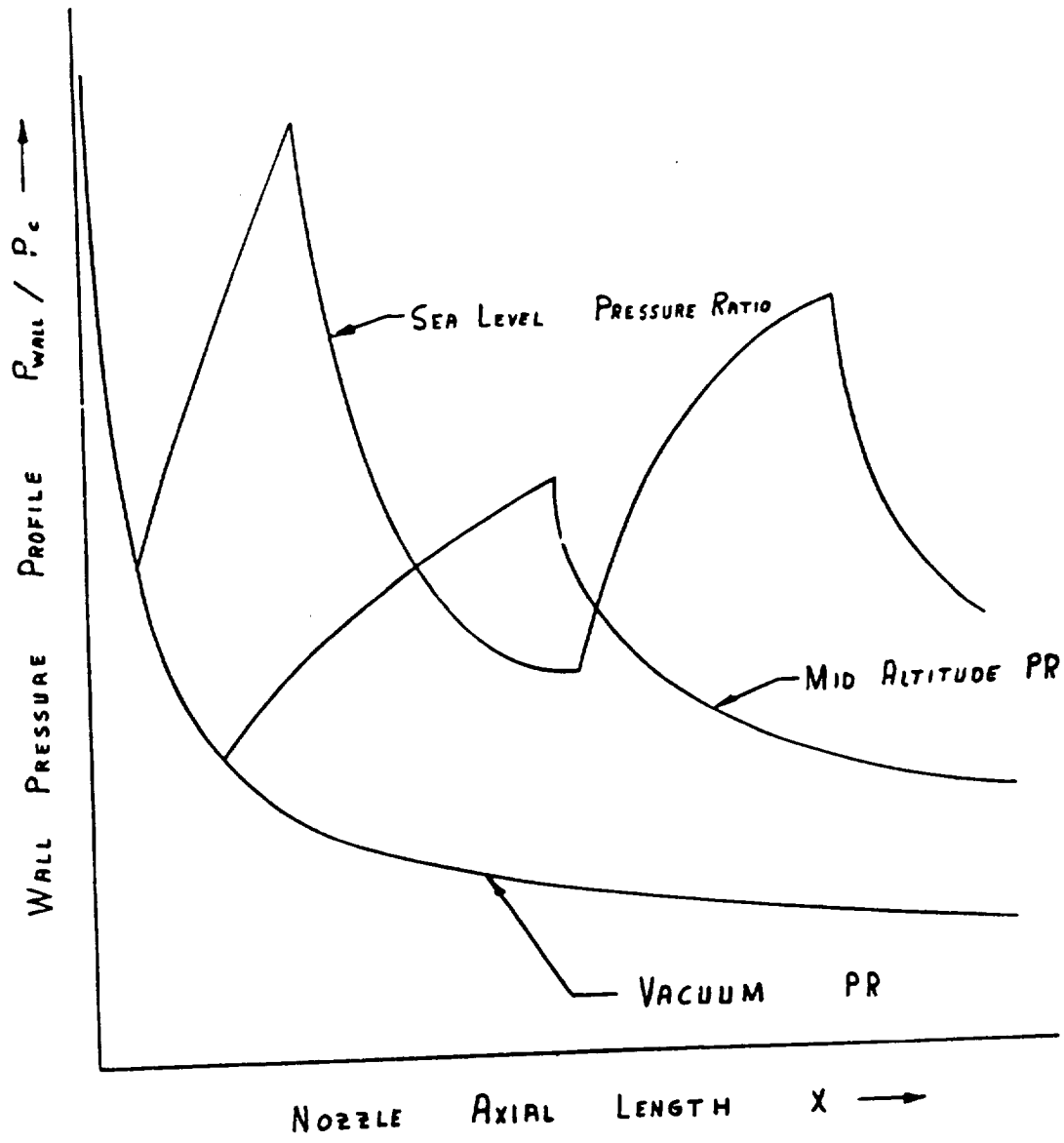


Figure A-13. Ideal Wall Pressures

R-9049

A-32

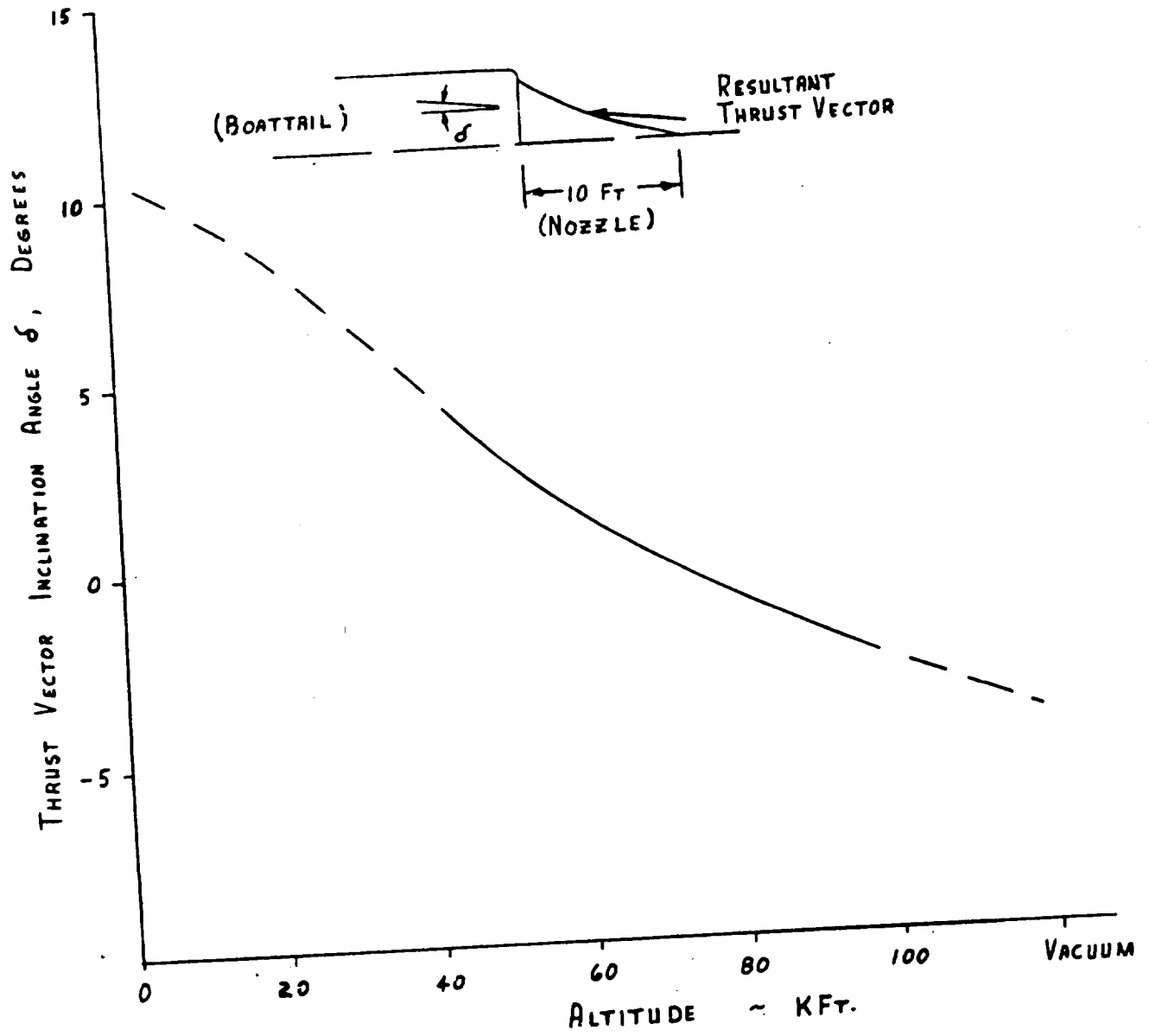


Figure A-14. Thrust Vector Inclination Angle  $\delta$  Versus Altitude

R-9049

A-33

## STRUCTURAL COMPLEXITY

Without detailed design studies, estimates of the structural complexity of differing concepts are difficult to make. However, some generalized comparisons of the two concepts are presented in Table A-5. A discussion of the features and problems associated with the designs is presented in the following sections.

### Checkerboard Design

The checkerboard concept employs readily understood design features. The thrust frame (Fig. A-5) is a welded, lightweight tubular structure of conventional construction. The thrust chambers are symmetrical about the hinge line and the resultant thrust vector passes through the hinge line. The imbalance forces are small and result only from normal thrust misalignment. This permits the use of small gimbal actuators with small actuator travel required. The thrust would be transmitted through five hinge bearings of similar design to the J-2 or F-1 gimbal bearing. The unit loading on the hinge bearing would be well within the existing state of the art.

### Peripheral Design

The peripheral concept presents more challenging structural problems (Fig. A-2 and A-3). The thrust frame is welded frame cantilever construction. The frame would be lightweight, principally because only eight combustors are required for each engine module, so the engine total width is 8 feet. The nozzle length is approximately 10 feet. The long nozzle results in large bending moments about the nozzle hinge line, which requires a high-strength nozzle backup structure with a large section modulus.

With the large hinge angle required for the peripheral engine, and the large unbalanced forces, the actuator required to effect hinging would be large with large travel distances involved. The thrust vector with relation to the nozzle, changes magnitude and direction as ambient pressure changes. An example of nozzle thrust vector location and direction variation as a function of pressure ratio ( $P_c/\text{ambient}$ )

Table A-5, Structural Complexity TVC Candidate System Comparison

Feature	Checkerboard	Peripheral
Structure	Tubular Frame Balanced Forces Welded Truss Constructed Readily Understood	Tubular Frame Unbalanced Forces Cantilever Truss Construction Large Pending Moments
Actuators	Small Forces Lightweight Less Travel	Large Forces Large Diameter Large Travel
Bearing Area Hinge Joints	5 Small Sliding Hinges	2 or 3 Large Sliding Hinges

R-9049

A-35

pressure) is shown in Fig.A-15. This changes the bending moments on the nozzle. Summation of moments about the hinge line indicates a maximum bending moment of approximately 600,000 lb-ft. These moments would be reacted by the actuator.

#### PROPELLANT FEED AND EXHAUST SYSTEM

From a TVC effects standpoint, the peripheral and checkerboard concepts show only minor differences in the propellant feed and exhaust system.

A generalized comparison of propellant feed and exhaust system features for the two candidate TVC concepts is presented in Table A-6.

The power package for either peripheral or checkerboard system engines consists of turbopumps, gas generator, main propellant valves, pneumatic control system, and associated piping, which could be mounted either rigidly above the hinge line or to the gimbaled mass below the hinge line. A rigidly mounted power package for checkerboard engines would require flexible joints in the high-pressure oxidizer and fuel ducts, and in the turbine exhaust duct. If mounted to the gimbaled mass, flexible joints would be required in the oxidizer and fuel pump inlet ducts and in the pneumatic purge and pressurant lines which cross the engine/vehicle interface. Generally speaking, flexible joints are simpler to design and fabricate with the smaller duct sizes, particularly when large hinge angles are required. When hinging is required in one direction only, the flexible joint design is simplified and can be designed for larger hinge angles.

Two flexible joint designs presently being considered for checkerboard engine application are: (1) an external gimbal ring with internal linkage (Fig.A-16), and (2) an internal tripod-mounted ball and socket joint (Fig.A-17). Both joints are fully lined with the liner remaining effective in the deflected position as well as in the neutral position. The liner shields the bellows from vibration-inducing flow forces and reduces the pressure drop. The external gimbal ring with internal linkage flexible joint would be used in high-pressure fluid lines such as pump discharge lines. The internal tripod-mounted ball and socket flexible joint would be used in exhaust system lines.

R-9049

A-36

Table A-6. Propellant Feed and Exhaust System TVC Candidate System Comparison

Feature	Checkerboard	Peripheral
With Rigidly Mounted Pumps	24 Degree Flex (Or Swivel) High Pressure Joint Required (Fuel & Oxidizer)  24 Degree Exhaust Duct Motion Required	+48 Degree Swivel High -10 Pressure Joint Required  Exhaust Duct & Oxid Turbine Bypass Dump Directly Into Plenum
With Pumps Mounted To Gimbaled Mass	Shortest Overall Engine Length  24 Degree Flex Required On Both Pump Inlets	Swivel Inlet Ducts
Base Manifold Design	With Single Hinge Engine Modules The Checkerboard Concept Does Not Have Thrust Vector Altitude Compensation.	Open

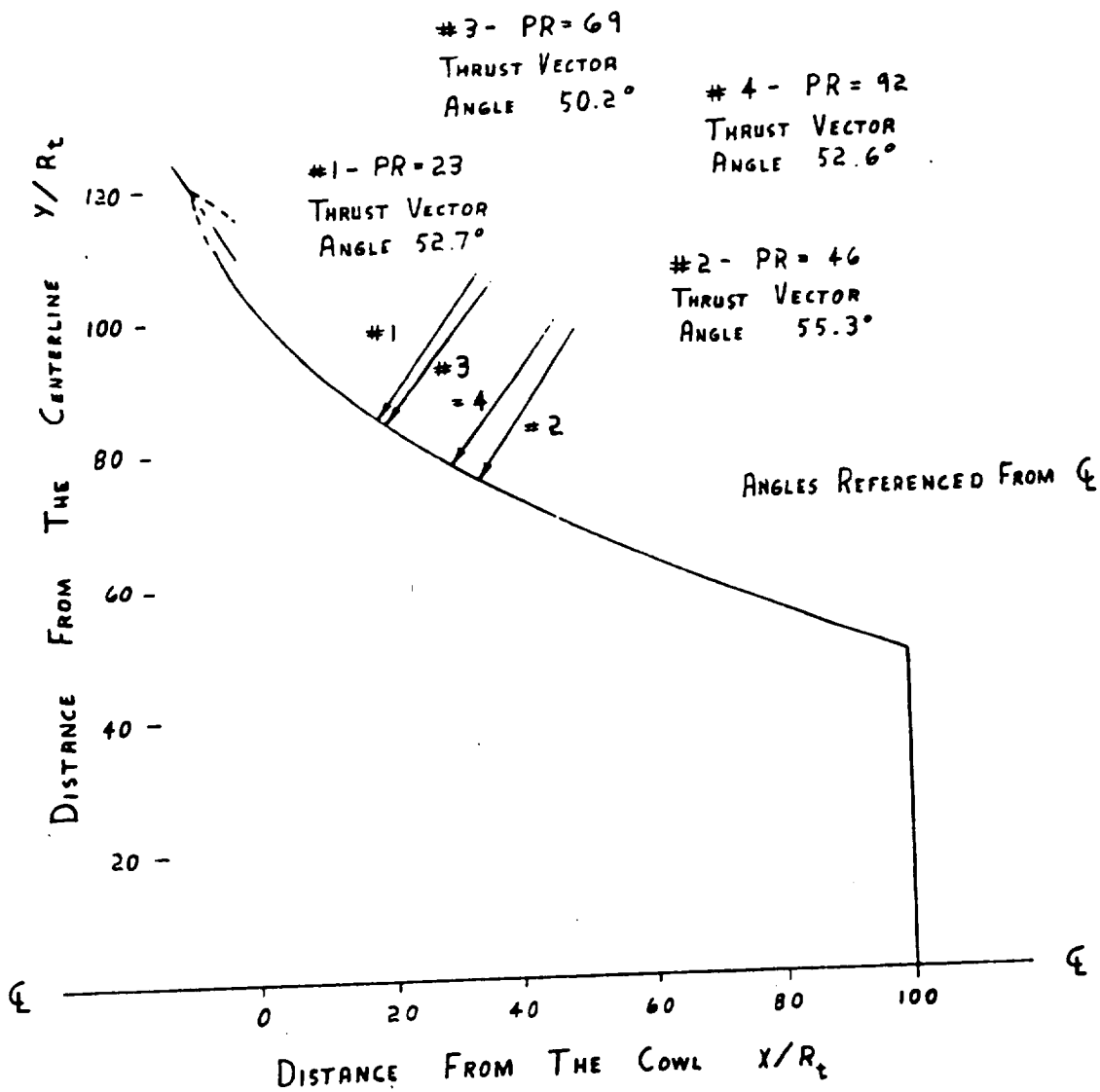
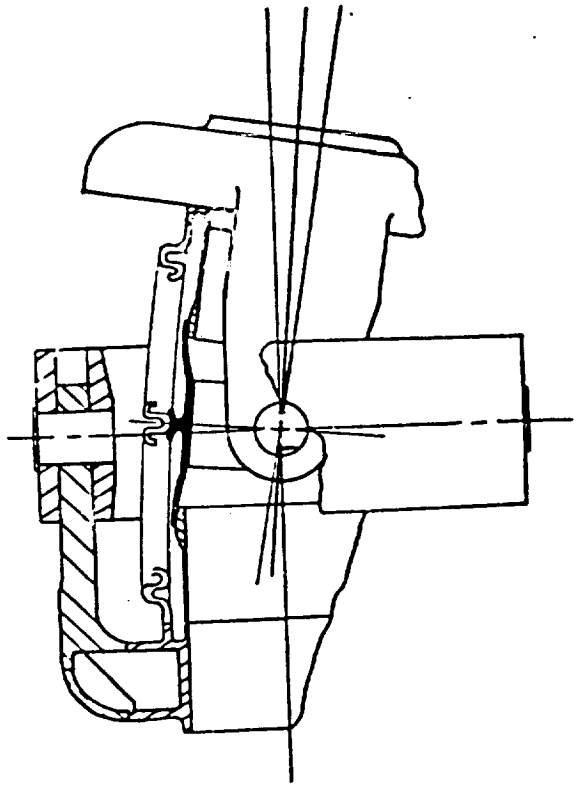


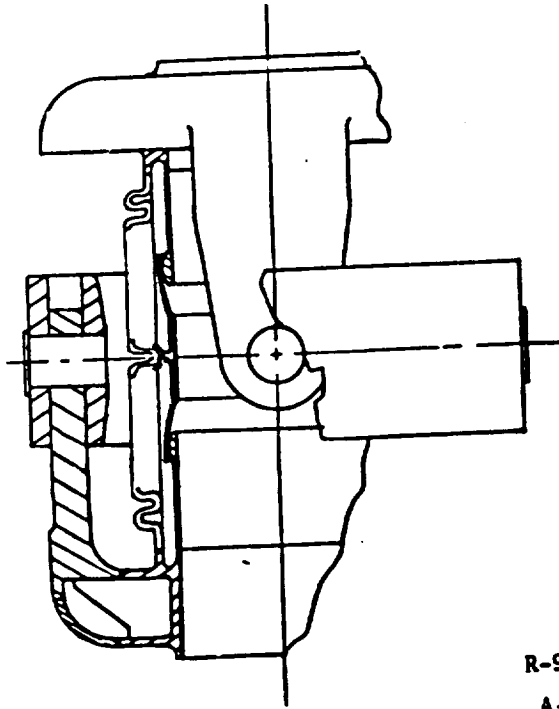
Figure A-15. Nozzle Thrust Vector Location and Direction Variation Versus Pressure Ratio ( $P_c/P_{\text{ambient}}$ )

R-9049

A-38



DEFLECTED POSITION

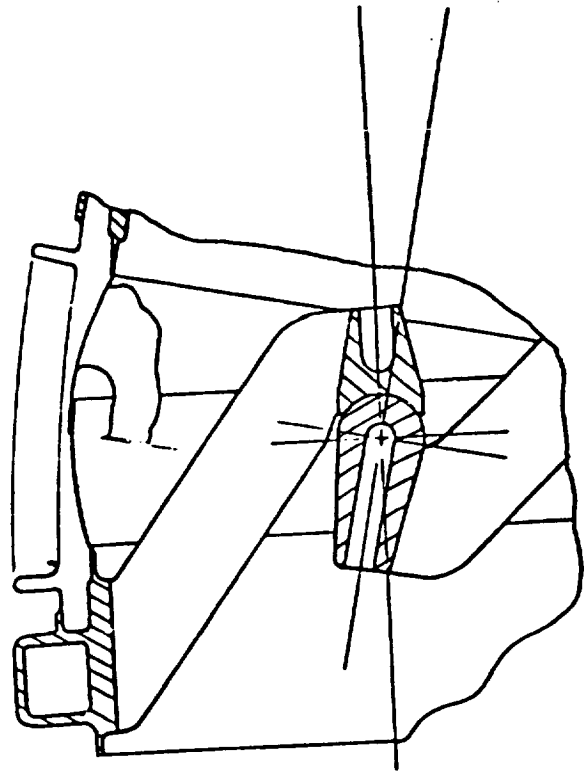


NO DEFLECTION

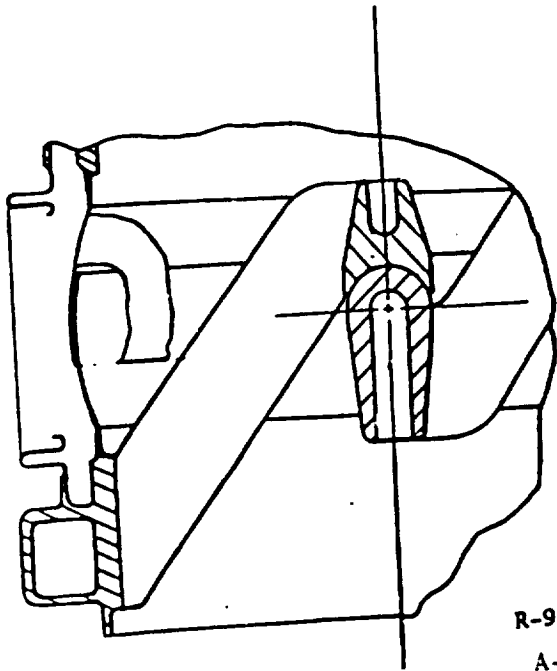
Figure A-16. External Gimbal Ring Joint With Internal Leakage

R-9049

A-39



DEFLECTED POSITION



NO DEFLECTION

R-9049  
A-40

Figure A-17. Internal Tripod Mounted Ball and Socket Joint

Both flexible or articulating joint designs consist of a flexible metal bellows, to absorb deflections and retain fluid pressures at acceptable stress levels, and a restraint linkage to resist pressure-separating forces and to position the pivot center on the bellows center. The flexible joint designs described involve known and well-understood technology, and are within the state of the art.

The peripheral system engine power package could be mounted either rigidly to the vehicle side of the hinge line or to the nozzle and hinged with the nozzle assembly. If rigidly mounted, swivel joints would be required on the fuel and oxidizer high-pressure ducts. If mounted to the nozzle, swivel joints would be required on the propellant inlet ducts. The propellant ducting presently envisioned for the peripheral engine uses a swivel design for the pump inlets (Fig.A-3). While this swivel design is more complex than that required for the checkerboard engines, the overall peripheral engine propellant ducting system is simplified because of size and single-nozzle feeding. Detailed designs of both concepts would be required to decide which is optimum and which is beyond the scope of this study. Swivel joints are feasible and have been demonstrated on other programs.

The base manifold for the checkerboard system would be a closed manifold of semi-monocoque construction similar to that used on the No. 1 breadboard test bed. The exhaust duct feeding the manifold would require flexible joints, as described earlier. If the turbopump were mounted to the hinged nozzle assembly, the flexible joint would be required only for thermal expansion. If the turbopumps were mounted rigidly above the hinge line, the exhaust duct would require flexible joints to permit hinge rotation, and would be of similar design to that of Fig.A-17.

On the checkerboard engine, the requirement for a fixed-base manifold would preclude varying the nozzle angles independently to provide thrust vector corrections for atmospheric pressure. This constraint detracts from the attractiveness of the checkerboard system. Further design effort is required to resolve this question. A flexible base manifold would eliminate these constraints and appears to be appropriate for further study.

On the peripheral system, the base would be a single, large plenum chamber fed by the exhaust from all engines. The engine exhaust would feed directly into the base for rigidly mounted turbopumps or turbopumps mounted on the hinged nozzle. Flexible joints would not be required in the exhaust duct in either case.

A flexible seal will be required between the hinged nozzle and the base plenum to preclude exhaust gas from escaping into the engine compartment. Diaphragm-type seals appear most feasible for this application.

#### ENGINE-TO-VEHICLE INTERFACE DESIGN

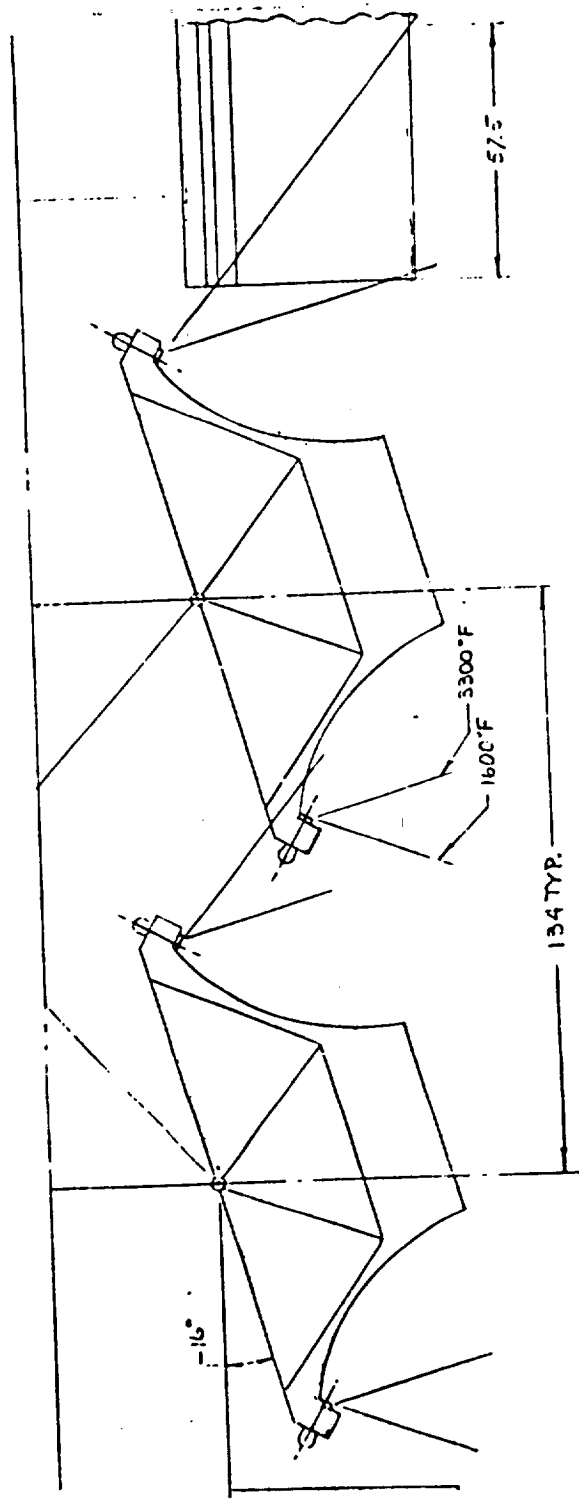
The basic engine-to-vehicle interface design requirements, with respect to TVC are to constrain and shield the vehicle and adjacent engines from combustion gases, and prevent primary combustion gas from leaking into the base region. The above is accomplished using vehicle and engine-mounted fences, flexible curtains, and sliding shields. Table A-7 presents comparative data on the engine-to-vehicle interface design.

Combustion gas impingement is not a problem with the peripheral concept; however, the larger hinge angles tend to make sealing the base from primary combustion gases a significant problem. Proposed fence locations for the peripheral concept are shown in Fig. A-2. The four vehicle-mounted fences on the peripheral system protect adjacent engines during roll maneuvers when only a portion of the pitch bank is rotated.

Combustion gas impingement is a problem with the checkerboard system engine arrangement. The impingement problem is pictorially illustrated in Fig. A-18 for a 16-degree engine pitch maneuver. For the example shown, hot combustion gases from one row of pitch engines impinge on the adjacent row of pitch engines and, also, the adjacent yaw engines. Combustion gas temperatures are lower for pitch-on-pitch engine impingement, approximately 1600 F, because of the lesser pitch engine projection into the gas stream. Similarly, yaw maneuvers result in gas impingement from one engine to another. To protect the checkerboard engine, 60 feet of uncooled, 5-foot long vehicle fences are used between the pitch and yaw

Table A-7. Engine Vehicle Interface Requirements TVC Candidate System Comparison

Feature	Checkerboard	Peripheral
Fences - Engine Mounted	16 Without Impingement 8 With Impingement (Regen. Cooled) 5 Ft. Long	16 End Fences 5 Sliding Curtains 10 Ft. Long
Base Mounted Fences - Vehicle Mounted	60 Ft. Uncooled 5 Ft. Long	4 Fences 10 Feet Long Uncooled
Shields	Flexible Curtain	Flexible Curtain Or Sliding Seals



R-9049

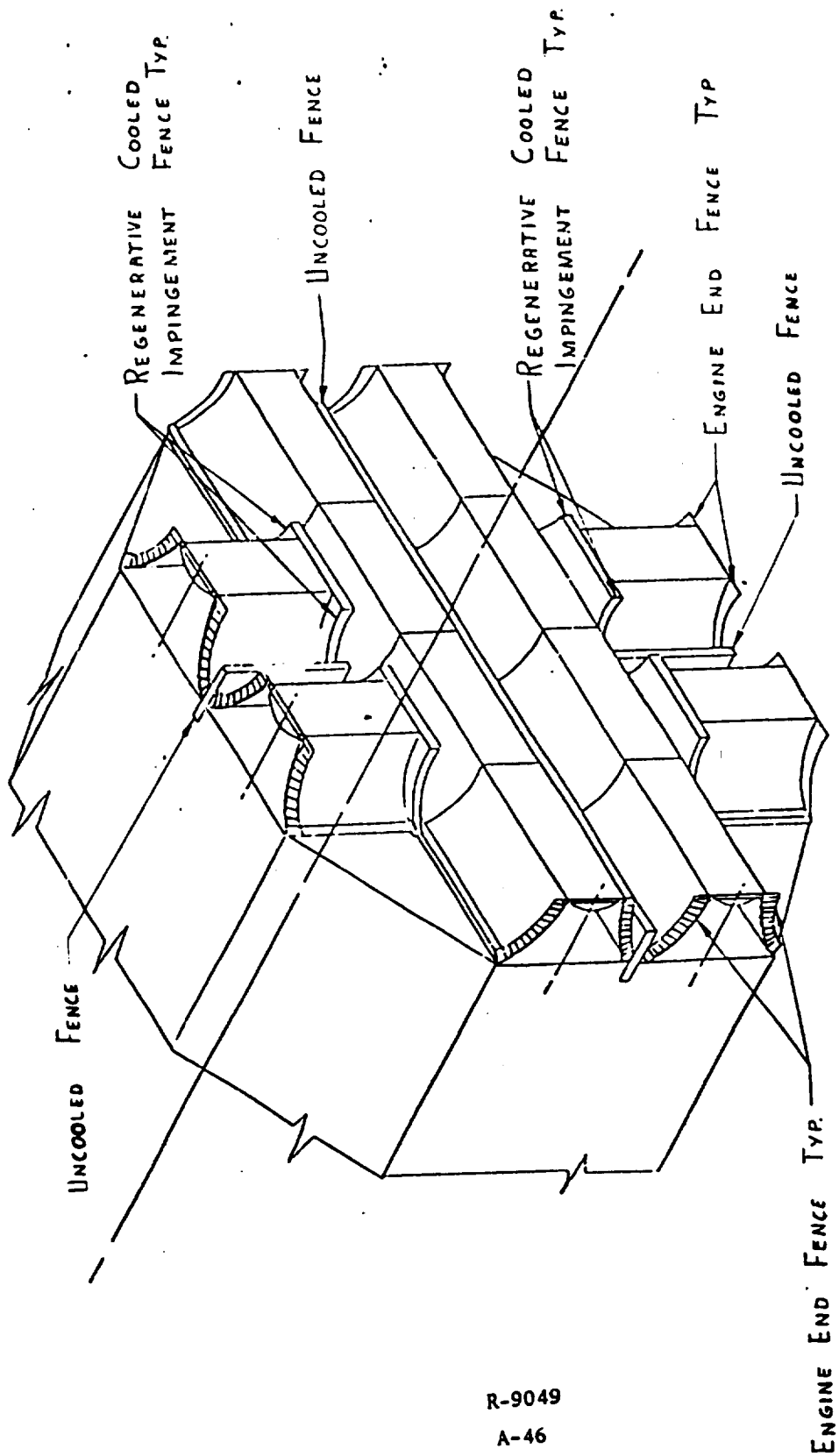
A-44

Figure A-18. Single Hinge Plume Intersection Pattern

engines. Heat transfer analysis indicates that uncooled vehicle fences are practical in this application. In addition, the yaw engine end fences facing the pitch engines must be designed to withstand direct impingement. Figure A-19 presents the checkerboard engine arrangement (shown earlier in this report) with the various combustion gas fences identified.

R-9049

A-45



R-9049  
A-46

Figure A-19. Multi-Engine Arrangement

## FUTURE STUDY AND TEST EFFORT

Additional study and test effort should be expended toward developing a double-hinge engine applicable to a checkerboard TVC system. Such a system would produce valuable data on thrust vector altitude compensation and its effects on base pressure and heat transfer. Also, base pressure and base heat transfer effects could be explored for the case of nonsymmetrical bank angulation relative to each other.

Additional questions which require resolution and/or analysis are engine-out capability, sliding curtain design (for the peripheral system), base designs for both single- and double-hinge systems, and heat transfer test data relative to fences for engine impingement protection relative to each other.

R-9049

A-47

## ENGINE SYSTEM PERFORMANCE

### ENGINE PERFORMANCE MODEL

Engine specific impulse was calculated according to the following equation:

$$I_{s_{vac}} = \left\{ \frac{\eta_{C_{fr}} (\eta_G + \eta_D + \eta_K + \eta_{baf} - 3.0) + C_{fbo}}{1 + \frac{\dot{w}_s}{\dot{w}_p}} \right\} \eta_{c^*_r} \eta_{c^*} \frac{C_{fid} c^*}{g} \quad (A-1)$$

where

- $\eta_{C_{fr}}$  = regenerative thrust coefficient recovery efficiency
- $\eta_G$  = primary nozzle geometric efficiency
- $\eta_D$  = primary nozzle drag efficiency
- $\eta_K$  = primary nozzle kinetic efficiency
- $\eta_{baf}$  = primary nozzle baffle efficiency
- $C_{fbo}$  = base thrust coefficient =  $\frac{P_B A_B}{P_C F_{fid} A_t}$
- $\dot{w}_s$  = secondary flowrate
- $\dot{w}_p$  = primary flowrate
- $\eta_{c^*_R}$  = regenerative characteristic velocity recovery efficiency
- $\eta_{c^*}$  = characteristic velocity efficiency
- $c^*$  = ideal characteristic velocity for shifting equilibrium (ft/sec)
- $C_{fid}$  = ideal nozzle thrust coefficient for shifting equilibrium
- $g$  = 32.174 (ft/sec<sup>2</sup>)
- $I_{s_{vac}}$  = engine vacuum specific impulse (seconds)

The base thrust coefficient ( $C_{fBo}$ ) was estimated to be given by:

$$C_{fBo} = K_1 (1 - \eta_G) + K_4 \left( \frac{C_{fs}^{sonic}}{C_{fid}} \right) \left( \frac{c_s^*}{c_p^*} \right) \left( \frac{w_s}{w_p} \right) + \frac{(K_2 - K_1) (1 - G) \sqrt{\frac{\dot{w}_s c_s^*}{\dot{w}_p c_p^*}}}{\sqrt{\frac{K_3}{K_4} (K_3 - K_1) \frac{C_{fid}}{C_{fs}^{sonic}} (1 - \eta_G)}} \quad (A-2)$$

where

$K_1, K_2, K_3, K_4$  = empirical constants that depend on the nature of the flow.

$C_s^{sonic}$  = sonic nozzle thrust coefficient of the secondary gas stream

$c_p^*$  = primary gas characteristic velocity

Values of the four empirical constants are given below:

Type of Flow	Plane Flow Two-dimensional	Axisymmetric Flow
$K_1$	0.69	0.58
$K_2$	0.79 (25 percent nozzle)	0.79
$K_3$	2.60	0.72
$K_4$	0.836	1.00

It is to be noted that Eq. A-1 and A-2 do not contain any provision for the effects of nozzle end fences. The addition of end fences to the nozzle will cause the nozzle thrust coefficient to be reduced. Unfortunately, the effect of using fences on linear nozzles has been defined only qualitatively. In view of this fact, the effect of fences will be disregarded for the purposes of this report. However, the reader should keep in mind that the specific impulse values quoted in the remainder of this report will be on the order of 0.5 to 1.0 percent higher than could be achieved due to the additional drag of end and base fences.

## CURRENT TVC STUDY GROUND RULES

At the present time, the basic ground rule for the TVC study linear engine is that it will be evaluated for an application similar to that planned for the Space Shuttle main engines. The rationale for selecting this application is that future vehicles are likely to be somewhat similar and that, in any event, the SSME requirements are about as severe as could be envisioned.

Two linear engine concepts appear to have sufficient merit to warrant continued study. The original and most studied concept consists of using the linear engine as a clustered engine similar to the way bell nozzles are used. The alternate concept is to build a single, large engine with the combustors arranged around the periphery of the vehicle base. The engine would then be composed of combustor-nozzle slabs, each fed by a separate pump set. These concepts are known as the checkerboard and the peripheral engines, respectively.

Detailed ground rules for the checkerboard engine have been formulated. These are summarized as follows:

1. Engine mixture ratio = 6.0
2. Optimum chamber pressure
3. Optimum specific impulse nozzle
4. Vertical thrust vector
5. SSME envelope
6. Maximum fuel pump outlet pressure = 3400 psia
7.  $\eta_{c*}$  = 99 percent minimum

Detailed ground rules for the peripheral engine have not been defined, but they are certain to include the SSME envelope requirement and the same turboachinery listed for the checkerboard. An additional ground rule for paper study purposes that the booster and orbiter versions of both checkerboard and peripheral engines should use the same combustor.

R-9049

A-50

## CHAMBER PRESSURE OPTIMIZATION

The optimum chamber pressure for an aerospike-type nozzle results from a tradeoff between available base area and the amount of secondary flow required to operate the turbopumps at a given chamber pressure level. To be able to estimate the secondary flowrate required, it is necessary to have some estimate of how the fuel-side pressure drop varies with chamber pressure. Fuel pump outlet pressure was estimated to vary as shown in Fig.A-20. However, as will be seen (Table A-8), fuel pump outlet pressure does not have a significant effect on specific impulse for the systems analyzed in this study. It is likely that a detailed analysis of specific hardware configurations would yield results considerably different than those given in Fig.A-20. Nozzle base areas for the various Mod III possibilities are fixed by the ground rule that they must be compatible with the SSME envelope. For convenience and economy of arriving at the optimum aerodynamic contour, it was decided to set the engine envelope at the SSME dimension minus 4 inches on each side, and then use this dimension as the distance between the throat centerlines. For purposes of this study, expansion area ratio was then taken to be equal to the area enclosed by the throat centerlines divided by the throat area. This introduces a slight error due to not using the distance between cowl points to calculate the nozzle exit areas. The nozzle exit areas for the various engines considered are listed below:

Configuration	Dimensions, inches	Exit Areas, (in. <sup>2</sup> )
SSME Booster	120 x 120	14,400
SSME Orbiter	220 x 220	48,400
Checkerboard Booster Engine	112 x 120	13,440
Peripheral Booster Engine	352 x 472	166,144
SSME Overall	360 x 480	172,800
Checkerboard Orbiter	212 x 220	46,640
Peripheral Orbiter	432 x 220	95,040

R-9049

A-51

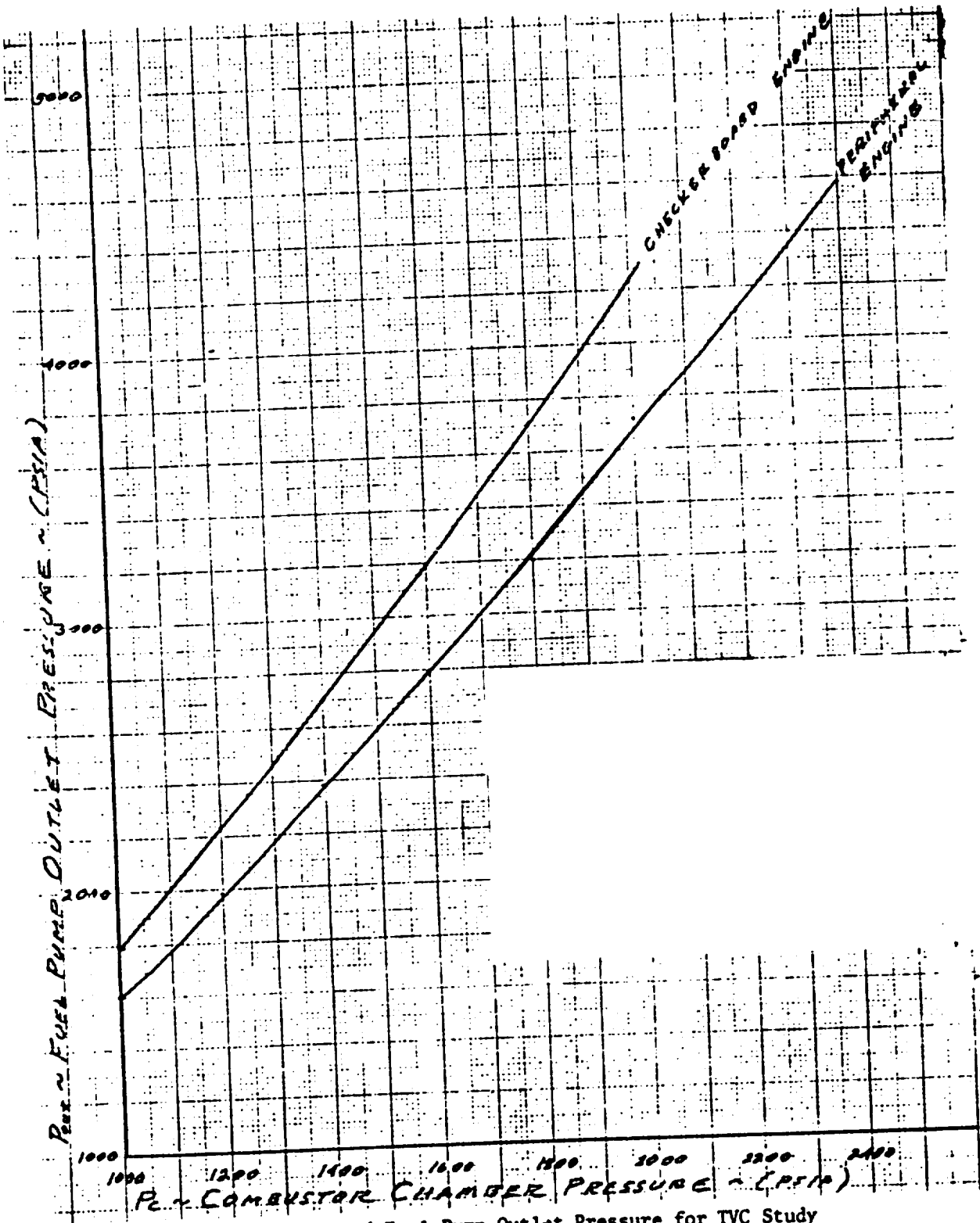


Figure A-20. Estimated Fuel Pump Outlet Pressure for TVC Study Breadboard Engine  $P_c$  Optimization Calculations (Based on Estimates for Constant Wall Temperatures of 1100 F)

R-9049

A-52

Table A-8. Performance Loss Breakdown of Various Nozzle Systems

Loss or Gain	Peripheral Booster	Checkerboard Booster	$\zeta = 79:1$ Bell Nozzle @ 1800 Pc
1. Nozzle Geometric Loss, (sec)	-18.221	-18.246	} -19.603
2. Nozzle Drag Loss (sec)	-8.340	-8.267	
3. Kinetics Loss (sec)	-0.231	-0.230	
4. Baffle Exit Loss (sec)	-0.693	-0.691	
5. C* Efficiency Loss (sec)	-4.622	-4.609	
6. Secondary Flow Loss (sec)	-13.260	-13.941	
7. Regen. Cf Gain (sec)	+2.334	+2.318	
8. Regen. C* Gain (sec)	+6.125	+6.070	
9. Base Flow Gain (sec)	+22.928	+18.779	
Theoretical Max. Isp vac (sec)	462.055	460.803	460.803
Thrust Chamber MR	6.58	6.62	6.62
Net Engine Isp (sec)	448.075	441.986	441.200
Sea Level Isp (sec)	375.517	369.294	296.900
Operating Condition			
Pc (psia)	2000.	1800.0	1800.0
Eng. MR	6.00	6.00	6.00
alt (lbs)	7,515,830	617,808.0	618,000.0
$\zeta$	87.5	79.3	79.3
*Pout (psia)	3200.0	3400.0	3400.0
Wsec (lbs/sec)	481.0	42.28	42.28
Wprimary (lbs/sec)	16,292.6	1355.52	1355.52
Ncombustors	112.	20.	1.

\*Pump outlet pressures were estimated on the basis of holding T wall gas, a constant. This would tend to over estimate delta P for decreasing chamber throat gaps.

The secondary flowrate required to operate a Mark 29F two-stage-type turbopump is shown as a function of fuel pump outlet pressure in Fig. A21 for the case where the secondary supply gas is at a temperature of 1200 F and a mixture ratio of 0.94. Figure A21 was used throughout this study. Total vehicle propellant flow was estimated to be 16,733.6 lb/sec for the booster and 2795.6 lb/sec for the orbiter, based on SSME requirements.

If the total engine flowrate, the turbopump secondary flowrate requirements, and the envelope size are set, then Eq. A-1 indicates that the engine specific impulse is a single-value function of the chamber pressure. To calculate this function for the various Mod III possibilities, Eq. A-1 and A-2 were used along with the conditions listed in Table A-9.

Table A-9. Mod III Engine Operating Conditions and Requirements

Parameter	Peripheral Booster	Peripheral Orbiter	Checkerboard Booster	Checkerboard Orbiter
Exit Area, in. <sup>2</sup>	166,144.0	95,040.0	13,440.0	46,640.0
Engine MR	6.00	6.00	6.00	6.00
Total Flowrate, lb/sec	16,773.6	2795.6	1397.8	1397.8
Estimated Altitude Thrust, pounds	7,260,000	1,210,000	605,000	605,000
Estimated Fuel Injection Turbopump, R	400	400	500	500
$\eta_{c^*}$	0.9900	0.9900	0.9900	0.9900
$\eta_{baf}$	0.9985	0.9985	0.9985	0.9985
$\eta_{kinetics}$	0.9995	0.9995	0.9995	0.9995
MR, Secondary Gas (GG out)	0.94	0.94	0.94	0.94
Temperature, Secondary Gas R	1660.0	1660.0	1660.0	1660.0
Combustor ID, inches	11.25	11.25	11.25	11.25
$N_{seg}$	112.0	32.0	20.0	32.0

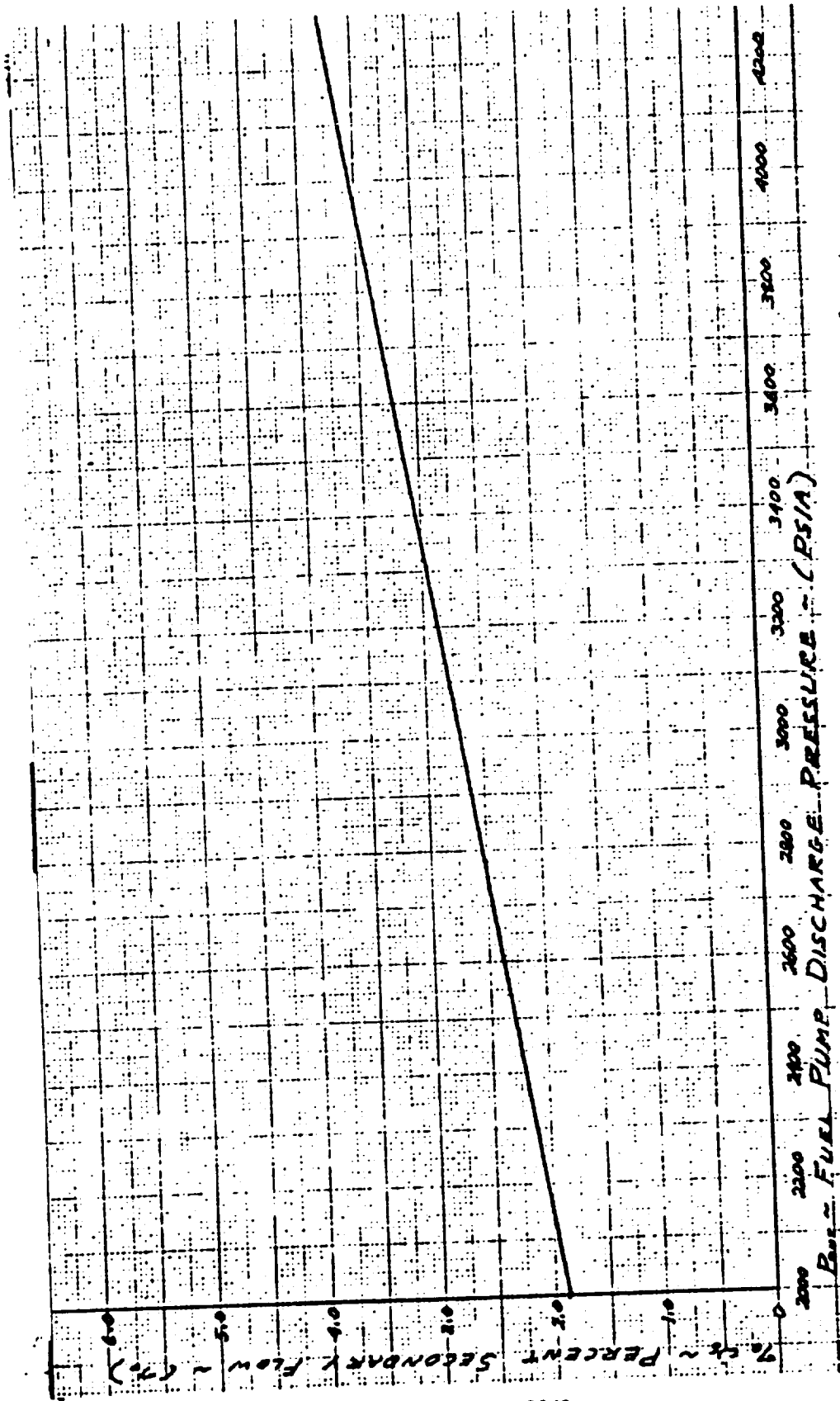


Figure A-21. TVC Study Linear Breadboard Secondary Gas Required to Operate a Mark 27F Two-Stage Type Turbopump With:  $T_{sec} = 1200 F$ ;  $MR_{sec} = 0.74$

The results of this calculation are given in Fig. A-22. Based on these results, 1800 psia is recommended as the optimum chamber pressure for the checkerboard booster engine, while 2000 psia is recommended for the peripheral booster engine.

#### SEA LEVEL-ALTITUDE PERFORMANCE SCALING

Prediction of sea level specific impulse is somewhat more complicated than is the prediction of altitude specific impulse. This is due to the formation of shocks on the nozzle surface when it is operated in the overexpanded condition and accounts for the altitude compensating properties of aerospike nozzles. In general, a method of characteristics-type analysis is required to accurately predict the sea level pressure profile and thrust of an overexpanded aerospike nozzle. However, the scheme presented in Fig. A-23 yields a fair approximation to wind tunnel data and calculations of previous nozzle shapes. Figure A-23 was constructed from a plot of  $I_s/I_{s_{vac}}$  vs  $P_c/P_{ambient}$  for various expansion ratio nozzles obtained.

#### COMPARISON WITH BELL NOZZLES

It is of interest to compare the performance of a linear engine with that for an engine of the same thrust, but using a bell nozzle. The appropriate equation for the engine specific impulse of an engine with a bell nozzle is:

$$I_{s_{vac}} = \left\{ \frac{\eta_{C_{fr}} (\eta_G + \eta_D + \eta_K - 2.0) + \frac{w_s}{w_p} C_{fs} c^*}{1 + \frac{w_s}{w_p}} \right\} \eta_{c^*_R} \eta_{c^*} \frac{C_{fid} c^*}{g} \quad (A-3)$$

where:

- $C_{fs}$  = thrust coefficient of the secondary flow
- $c^*_s$  = secondary gas characteristic velocity

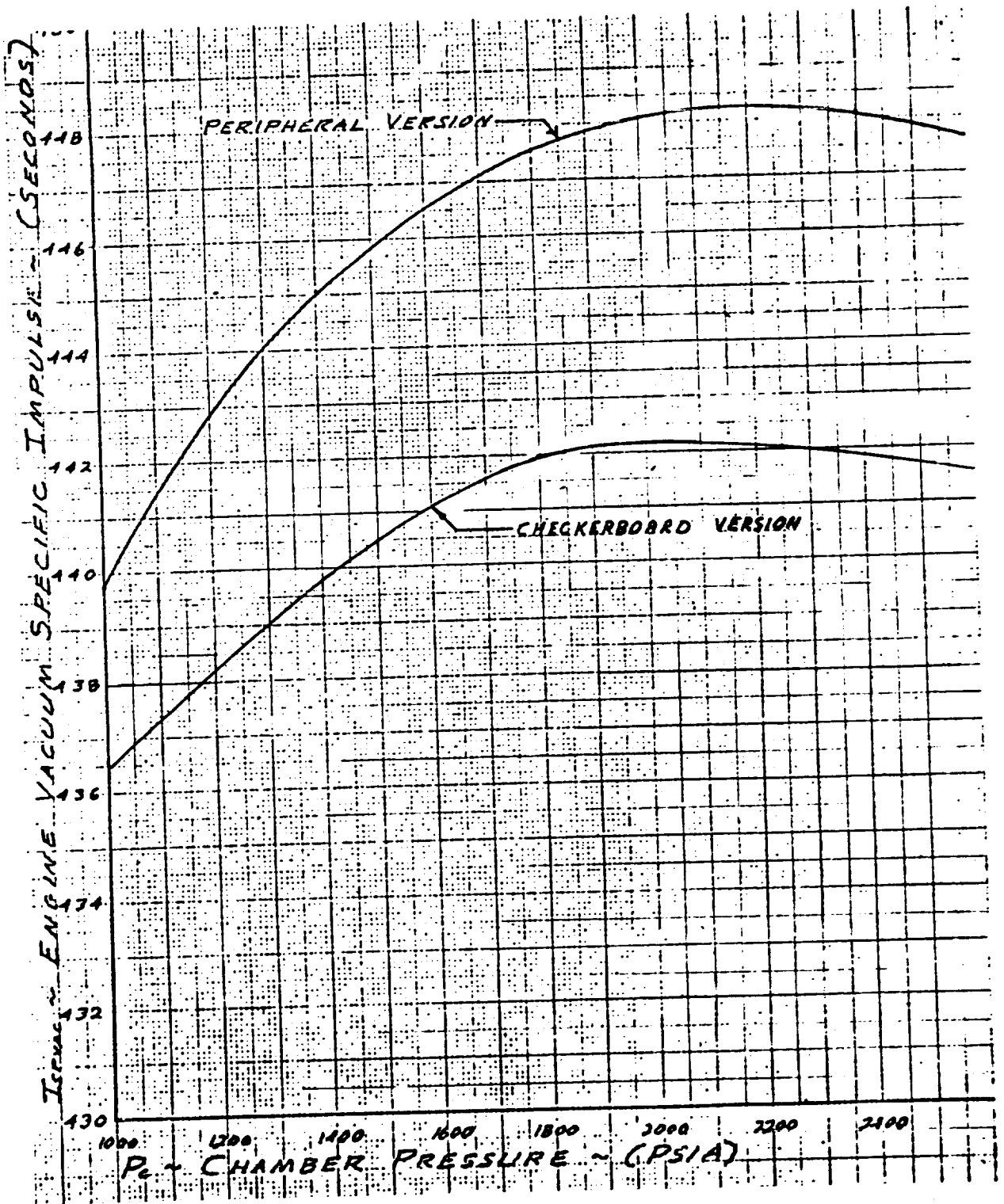


Figure A-22. TVC Study Breadboard Engine Chamber Pressure Optimization Booster Configurations

R-9049

A-57

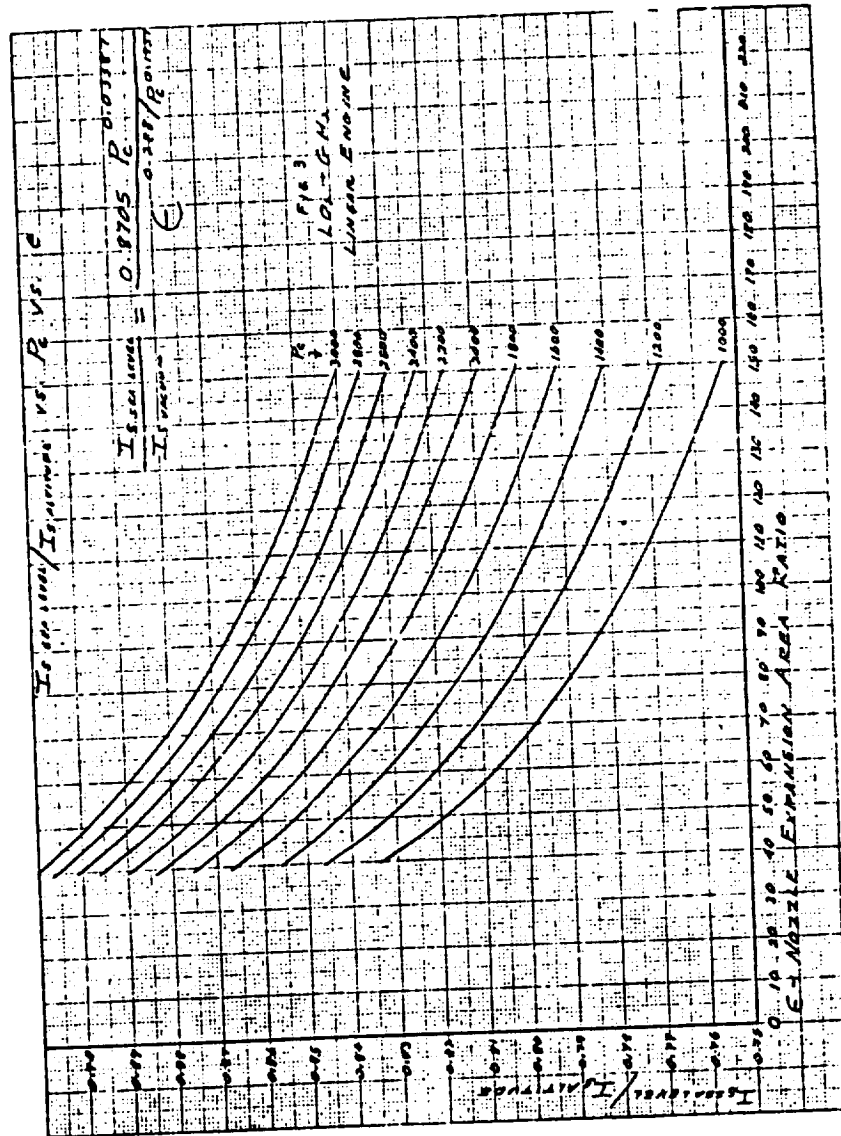


Figure A-23. LO<sub>2</sub>-GII<sub>2</sub> Linear Engine

Equation A-3 is similar to Eq. A-1 and allows for a term by term comparison of the two nozzles.

However, before such a comparison can be made, it is necessary to define the bell engine somewhat more completely. Using the results of previous bell nozzle studies, the factors in Table A-10 were estimated for an 80-percent length bell nozzle with an altitude thrust of 618,000 pounds and a  $P_c$  of 1800 psia.

Table A-10. Bell Nozzle Performance Factors

Percent length = 80,  $\epsilon = 79.3:1$ ;  $P_c = 1800$  psia:  $\tau = 618K$

$$\delta_{div} = 0.0082$$

$$\delta_{drag} = 0.0270$$

$$\delta_{kin} = 0.0005$$

Note:  $(\eta_G + \eta_D + \eta_K - 2.0) = (1 - \delta_{div} - \delta_{div} - \delta_{drag} - \delta_{kin})$

If it is assumed that the primary-secondary flow splits are equal and that the fuel injection temperatures are proportional to the respective drag losses, then the bell engine yields a specific impulse of 441.2 seconds, nearly identical to the value of 441.99 calculated for the "similar checkerboard booster. It is concluded, therefore, that there is very little difference between the nozzles if they are operating at identical conditions.

#### PERFORMANCE LOSS BREAKDOWNS

Table A-8 lists the various performance losses and gains for the nozzle systems considered in this report. From Table A-8, several interesting items emerge. The most significant point is that the base flow gain for the peripheral booster appears to be the primary source of its additional performance when compared to the checkerboard booster. This is due to the fact that the base flow was treated as being axisymmetric rather than as plane flow. Wind tunnel testing would be required to verify the adequacy of this assumption. A second item of interest

is the much higher site specific impulses obtained with aerospike nozzles when compared to the bell nozzle.

#### VEHICLE PERFORMANCE

Figure A-24 depicts the variation of specific impulse with altitude for a typical space shuttle booster flight. The net vehicle performance is represented by the areas under the respective curves. Despite lower than specified site performance, it is seen that the performance of the peripheral and checkerboard booster engines can be compatible with such an application by virtue of their higher performance at altitude.

#### ADDITIONAL EFFECTS

There are several factors that can have a significant effect on engine specific impulse but are not amenable to a simplified analysis. The most significant effect on sea level specific impulse results from rotating the entire engine contour about some point on the contour. Sea level contour thrust increases as the contour is rotated because the resultant sea level contour thrust vector is not parallel to the engine centerline if the contours are set in the optimum position for altitude operation. Unfortunately, the scheme represented by Eq. A-2 is no longer valid for this case because it is based empirically on cutoff ideal nozzle contours operating at altitude. Physical intuition would lead to the conclusion that there would have to be some decrease in base pressure if the contours are rotated outward but, at sea level, this decrease should be small. Therefore, it appears that this scheme would be promising and a more definitive answer to this question has been requested.

A consideration that is peculiar to the peripheral engine concept, with its door-like hinged sections for thrust vector control, is what happens to the base pressure when one or more of the sections is hinged outward. In this case, there is an increase in the effective base area, and physical reasoning would lead to the conclusion that there is a reduction in the base pressure at altitude (closed wake). Again, this question has been submitted for a more definitive answer.

R-9049

A-60

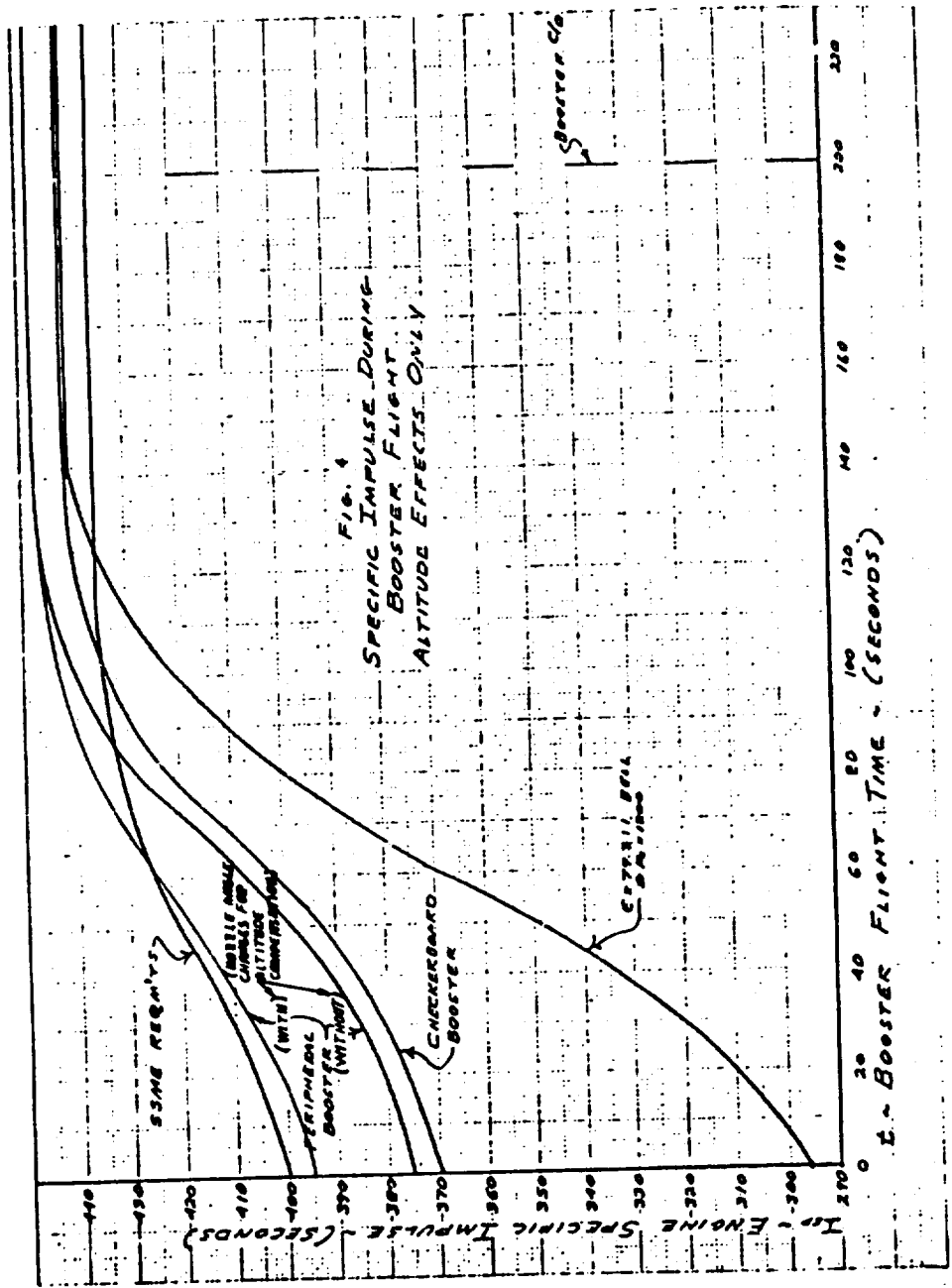


Figure A-24. Specific Impulse During Booster Flight Altitude Effects Only

